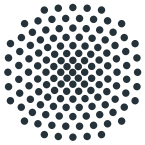

Universität Stuttgart

Development of Full Configuration Interaction Quantum Monte Carlo Methods for Strongly Correlated Electron Systems

Von der Fakultät für Chemie der Universität Stuttgart zur Erlangung der Würde eines Doktors der Naturwissenschaften (Dr. rer. nat.) genehmigte Abhandlung

Vorgelegt von

Werner Dobrautz

aus Rottenmann, Österreich

Hauptberichter:	Prof. Dr. Ali Alavi
Mitberichter:	Prof. Dr. Hans-Joachim Werner
Mitberichter:	Prof. Dr. Andreas Köhn
Prüfungsvorsitzender:	Prof. Dr. Wolfgang Kaim

Tag der mündlichen Prüfung: 26. März, 2019

Institut für Theoretische Chemie

der Universität Stuttgart

2019

An meinen Vater und Bruder...

Contents

Preface

This dissertation contains the results of my research carried out at the Max Planck Institute for Solid State Research between November 2014 and November 2018 in the group of and under supervision of Professor Ali Alavi.

Parts of **Chapter 5** are included in work that is published as:
Compact numerical solutions to the two-dimensional repulsive Hubbard model obtained via nonunitary similarity transformations. Werner Dobrautz, Hongjun Luo and Ali Alavi in Phys. Rev. B **99**, 075119 (2019)

This dissertation is a result of my own work and includes nothing which is the outcome of work done in collaboration except where specifically indicated in the text. This dissertation has not been submitted in whole or in part for any other degree or diploma at this or any other university.

Stuttgart, _____ _____

Date Werner Dobrautz

Erklärung über die Eigenständigkeit der Dissertation

Ich versichere, dass ich die vorliegende Arbeit mit dem Titel

Development of Full Configuration Interaction Quantum Monte Carlo Methods for Strongly Correlated Electron Systems

selbständig verfasst und keine anderen als die angegebenen Quellen und Hilfsmittel benutzt habe; aus fremden Quellen entnommene Passagen und Gedanken sind als solche kenntlich gemacht.

Declaration of Authorship

I hereby certify that the dissertation entitled

Development of Full Configuration Interaction Quantum Monte Carlo Methods for Strongly Correlated Electron Systems

is entirely my own work except where otherwise indicated. Passages and ideas from other sources have been clearly indicated.

Name/Name: _____

Unterschrift/Signed: _____

Datum/Date: _____

Acronyms

AFQMC	Auxiliary-field Quantum Monte Carlo
AO	Atomic Orbital
aug-cc-pVnZ	Augmented Correlation-Consistent Polarized Valence-only n-Zeta basis set
aug-cc-pwCVnZ-DK	Relativistic-contracted Augmented Correlation-Consistent Polarized Weighted Core-Valence n-Zeta Douglas-Kroll basis set
CAS	Complete Active Space
CASSCF	Complete Active Space Self-Consistent Field
CBS	Complete Basis Set
CC	Coupled Cluster
CCSD	Coupled Cluster Singles and Doubles
CCSD(T)	Coupled Cluster Singles and Doubles with perturbative Triples
cc-pVnZ	Correlation-Consistent Polarized Valence-only n-Zeta basis se
CISD	Configuration Interaction Singles and Doubles
CNDO	Complete Neglect of Differential Overlap
CP	Constrained Path
CPMC	Constrained Path Quantum Monte Carlo
CSF	Configuration State Function
DMC	Diffusion Monte Carlo
DMRG	Density Matrix Renormalization Group
DRT	Distinct Row Table
ED	Exact Diagonalization
ESC	Electronic Structure Calculation
FCI	Full Configuration Interaction
FCIQMC	Full Configuration Interaction Quantum Monte Carlo
GFMC	Green's Function Monte Carlo
GTO	Gaussian-Type Orbital
GUGA	Graphical Unitary Group Approach
HF	Hartree-Fock

HS	Hubbard-Stratonovich
i-FCIQMC	Initiator Full Configuration Interaction Quantum Monte Carlo
irrep	Irreducible Representation
KY	Kotani-Yamanouchi
LCAO	Linear Combination of Atomic Orbitals
MB	Minimal Basis
MC	Monte Carlo
MCMC	Markov Chain Monte Carlo
MCSF	Multi-Configurational Self-Consistent Field
MO	Molecular Orbital
MPn	n^{th} order Møller-Plesset
MPPT	Møller-Plesset Perturbation Theory
MPS	Matrix Product State
MRCI	Multi-Reference Configuration Interaction
OBC	Open Boundary Conditions
PBC	Periodic Boundary Conditions
PDF	Probability Distribution Function
PMC	Projector Monte Carlo
PPP	Pariser-Parr-Poble
PT	Perturbation Theory
QMC	Quantum Monte Carlo
RDM	Reduced Density Matrix
RHF	Restricted Hartree-Fock
ROHF	Restricted Open-shell Hartree-Fock
SCF	Self-Consistent Field
SD	Slater Determinant
SGA	Symmetric Group Approach
STO	Slater-Type Orbital
$SU(n)$	Special Unitary Group of order n
$U(n)$	Unitary Group of order n
UGA	Unitary Group Approach
UHF	Unrestricted Hartree-Fock
VMC	Variational Monte Carlo
ZDO	Zero Differential Overlap

Abstract

Full Configuration Interaction Quantum Monte Carlo (FCIQMC) is a prominent method to calculate the exact solution of the Schrödinger equation in a finite antisymmetric basis and gives access to physical observables through an efficient stochastic sampling of the wavefunction that describes a quantum mechanical system. Although system-agnostic (black-box-like) and numerically exact, its effectiveness depends crucially on the compactness of the wavefunction: a property that gradually decreases as correlation effects become stronger. In this work, we present two—conceptually distinct—approaches to extend the applicability of FCIQMC towards larger and more *strongly correlated* systems.

In the first part, we investigate a spin-adapted formulation of the FCIQMC algorithm, based on the *Unitary Group Approach*. Exploiting the inherent symmetries of the non-relativistic molecular Hamiltonian results in a dramatic reduction of the effective Hilbert space size of the problem. The use of a spin-pure basis explicitly resolves the different spin-sectors, even when degenerate, and the absence of spin-contamination ensures the sampled wavefunction is an eigenfunction of the total spin operator $\hat{\mathbf{S}}^2$. Moreover, targeting specific many-body states with conserved total spin allows an accurate description of chemical processes governed by the intricate interplay of them. We apply the above methodology to obtain results, not otherwise attainable with conventional approaches, for the spin-gap of the high-spin cobalt atom ground- and low-spin excited state and the electron affinity of scandium within chemical accuracy to experiment. Furthermore we establish the ordering of the scandium anion bound states, which has until now not been experimentally determined.

In the second part, we investigate a methodology to explicitly incorporate electron correlation into the initial Ansatz of the ground state wavefunction. Such an Ansatz induces a compact description of the wavefunction, which ameliorates the sampling of the configuration space of a system with FCIQMC. Within this approach, we investigate the two-dimensional Hubbard model near half-filling in the intermediate interaction regime, where such an Ansatz can be exactly incorporated by a nonunitary similarity transformation of the Hamiltonian based on a Gutzwiller correlator. This transformation generates novel three-body interactions, tractable due to the stochastic nature of FCIQMC, and leads to a non-Hermitian effective Hamiltonian with extremely compact right eigenvectors. The latter fact allows application of FCIQMC to larger lattice sizes, well beyond the reach of the method applied to the original Hubbard Hamiltonian.

Kurzfassung

„Full Configuration Interaction Quantum Monte Carlo“ (FCIQMC) ist eine prominente Methode zur Berechnung der exakten Lösung der Schrödinger Gleichung in einer finiten antisymmetrischen Basis, die den Zugang auf physikalische Observablen durch eine effiziente stochastische Stichprobennahme der Wellenfunktion eines quantenmechanischen Systems erlaubt. Obwohl diese system-agnostisch und numerisch exakt ist, hängt ihre Effektivität entscheidend von der Kompaktheit der Wellenfunktion ab: eine Eigenschaft die mit zunehmender Stärke der Korrelationseffekte graduell abnimmt. In dieser Arbeit präsentieren wir zwei, konzeptionell sehr unterschiedliche, Ansätze um die Anwendbarkeit von FCIQMC in Richtung größerer und *stärker korrelierter* Systeme zu erweitern.

Im ersten Teil dieser Arbeit untersuchen wir die Spin-adaptierte Formulierung des FCIQMC Algorithmus mit Hilfe des *Unitären Gruppen Ansatzes*. Die Nutzbarmachung der inhärenten Symmetrien des nicht-relativistischen molekularen Hamiltonoperators verursacht eine dramatische Reduktion der effektiven Hilbert Raum Größe eines Problems. Der Gebrauch einer Spin-reinen Basis löst explizit zwischen unterschiedlichen Spin Sektoren auf; auch wenn diese entartet sind. Zudem stellt das Fehlen von Spin-Kontamination sicher, dass die untersuchte Wellenfunktion eine Eigenfunktion des Gesamtspin Operators $\hat{\mathbf{S}}^2$ ist. Darüber hinaus ermöglicht die Bestimmung eines spezifischen Vielteilchen-Zustandes mit erhaltenem Gesamtspin die genaue Beschreibung chemischer Prozesse, die vom intrikaten Zusammenspiel dieser Zustände bestimmt sind. Da mit konventionellen Herangehensweisen nicht bestimmbar, verwenden wir die oben beschriebene Methode zur Bestimmung der Energiedifferenz zwischen dem Kobalt Quartett Grundzustand und angeregtem Dublett Zustand sowie der Elektronenaffinität Scandiums in Übereinstimmung mit experimentellen Ergebnissen innerhalb chemischer Genauigkeit. Außerdem etablieren wir die Ordnung der gebundenen Zustände des Scandium Anions, die bis dato experimentell noch nicht bestimmt wurde.

Im zweiten Teil dieser Arbeit untersuchen wir eine Methodik zur expliziten Einbindung von Elektronenkorrelation in den ursprünglichen Ansatz der Grundzustandswellenfunktion. Ein solcher Ansatz führt zu einer kompakten Form der Wellenfunktion. Dies wiederum erleichtert die Stichprobennahme innerhalb des Konfigurationsraumes eines Systems mit FCIQMC. Im Rahmen dessen untersuchen wir das zweidimensionale Hubbard Modell nahe Halbfüllung im mittleren Wechselwirkungsbereich. Dort ist ein solcher Ansatz, basierend auf dem Gutzwiller-Korrelator, auf exakte Weise durch eine nichtunitäre Ähnlichkeitstransformation des Hamiltonoperators umsetzbar. Diese Transforma-

tion generiert neuartige Dreikörperwechselwirkungen, die durch die stochastische Natur von FCIQMC überschaubar sind, und führt zu einem nicht-Hermiteschen effektiven Hamiltonoperator mit extrem kompakten rechten Eigenvektoren. Letztere ermöglichen die Anwendung von FCIQMC bei zunehmenden Problemgrößen, weit über die Reichweite der Methode, angewandt auf den originalen Hubbard Hamiltonoperator, hinaus.

1 Introduction

> "While it is never safe to affirm that the future of Physical Science has no marvels in store even more astonishing than those of the past, it seems probable that **most of the grand underlying principles have been firmly established** and that further advances are to be sought chiefly in the rigorous application of these principles to all the phenomena which come under our notice. It is here that the science of measurement shows its importance where quantitative work is more to be desired than qualitative work. An eminent physicist remarked that **the future truths of physical science are to be looked for in the sixth place of decimals**."
>
> –*Albert A. Michelson*, 1894

Spoken in the time of the deterministic world view of classical mechanics, the great physical discoveries in the beginning of the 20th century overthrew the above—rather unfortunate—quote of Albert A. Michelson. The great paradigm shift in physics, heralded by the quantum hypothesis of Max Planck in 1901, the discovery of the theory of special relativity and the photoelectric effect in Einstein's *annus mirabilis* of 1905, together with the formulation of quantum mechanics, by Max Born, Werner Heisenberg, Wolfgang Pauli, Paul Dirac and Erwin Schrödinger—to name a few—, spelled the end for determinism postulated by classical mechanics. The success of quantum mechanics led Dirac to the almost Icarian quote:

> "The general theory of quantum mechanics is now almost complete, the imperfections that still remain being in connection with the exact fitting in of the theory with relativity ideas. These give rise to difficulties only when high-speed particles are involved, and are therefore of no importance in the consideration of atomic and molecular structure and ordinary chemical reactions [...]. **The underlying physical laws** necessary for the mathematical theory of a large part of physics and the whole of chemistry **are thus completely known**, and the difficulty is only that the exact application of these laws leads to equations much too complicated to be soluble. It there fore becomes desirable that **approximate practical methods of applying quantum mechanics should be developed**, which can lead to an explanation of the main features of complex atomic systems without too much computation."
>
> –*Paul A. M. Dirac*, 1929

The two quotes share common features, although, I think it is safe to assume that physicists, chemists and scientists in general have nowadays realised that scientific progress happens in quite unpredictable ways. Nevertheless, Dirac's claim is certainly warranted, since quantum mechanics, especially when the effects of relativity are small enough to be neglected, is the most robust and experimentally verified theory in our hands. Indeed, we do have the basic equation, which allow us *in theory* to exactly describe any quantum mechanical system from first principles. The "only" problem is that this equation, due to the immense number of coupled degrees of freedom is impossibly hard to solve exactly, except in very rare cases.

Dirac also foreshadowed the only possible route to solve this problem: developing approximate methods that still capture the crucial physical features of the system at affordable computational cost. The advent of computers gave rise to the new branch of computational chemistry and physics, aiming to explain the underlying physical mechanisms, obtain new insights and even predict and design new materials and novel phases of matter, by *simulation* rather than experiment. The rapid growth of both computing power and resources* allows more and more complex systems to be simulated. However, the even faster exponential growth of complexity limits numerical solutions and thus necessitates the development of novel algorithms, approximations and even effective models, capturing the relevant degrees of freedom.

A historical milestone towards the (exact) numerical solution is Hartree-Fock theory, in which the troublesome interaction between particles—responsible for the coupled degrees of freedom—is approximated by an effective, *mean-field*, single-particle potential. This decoupling, while neglecting all correlation effects, † reduces the **one** *many-body* problem to **many**—readily solvable—*one-body* problems and often yields qualitatively correct results for a wide range of systems. Although, correlation effects typically act on rather small energy scales, they are in many cases still *very* relevant and—at least a major part—must be taken into account to quantitatively describe most chemical processes and physical properties.‡

While successful in studying *weakly correlated* systems, standard mean-field theories, but even perturbative approaches that go *beyond* Hartree-Fock, can become questionable or even erroneous when employed to study *strongly correlated* systems; which have drawn a lot of attention in the past couple of decades, due to their interesting macroscopic properties and microscopic structure. A different, wavefunction based, nonperturbative and system-agnostic approach to deal with the full complexity of the problem—ensuring an explicit account of correlation effects—is based on the (quantum) Monte Carlo technique, which tries to circumvent the exponential wall by attempting a stochastic, instead of a

*According to Moore's law.

†Except for the Fermi correlation, due to the Pauli- or exchange repulsion.

‡As a drastic example, HF theory is not able to correctly describe the dissociation process of H_2.

deterministic solution.* A prominent combination of using a stochastic approach to deal with the full complexity of the problem at hand is given by Full Configuration Interaction Quantum Monte Carlo (FCIQMC). Its development and application to strongly correlated systems is the main topic of this thesis.

1.1 Scope and Overview of the Thesis

All the relevant information of a quantum mechanical state is contained in the *wavefunction* of a system. Instead of describing all possible states of a system, Monte Carlo (MC) methods rely on random numbers to sample the physically most relevant and representative ones and draw conclusions from them to get an understanding of the underlying physical properties of a system. In particular, FCIQMC attempts an exact solution—in a finite basis—to an electronic problem by an efficient sampling of the wavefunction through the random walk of particles in a discrete antisymmetrised space.†

However, due to the immense number of coupled degrees of freedom, the exact wavefunction is an intractable object. An efficient sampling thereof requires various approximation to reduce the complexity and condense the most relevant features into a highly compact representation. For systems with *weakly interacting* particles the wavefunction is dominated by a single configuration (the single-reference case) and thus an efficient sampling thereof is readily possible. However, for *strongly correlated* systems a multitude of configurations are of equal importance for the characterisation of the system (the multi-reference case). Their delicate, dynamic interplay exacerbates a compact description and thus hinders a straightforward application of the MC approach to efficiently sample the most relevant physical features.

The scope of this thesis is the further development of the FCIQMC method to improve the applicability to strongly correlated electron systems of increasing size and complexity. This can only be achieved by a systematic reduction of the huge number of degrees of freedom and development of techniques to induce a more compact representation of the relevant physical features contained in the wavefunction, which in turn allows a more efficient sampling with MC methods. We live in a macroscopic world after all,‡ and this applicability to increasing system sizes is necessary to draw relevant conclusions for realistic systems by extrapolation techniques.§

This reduction of degrees of freedom—to some part—is already achieved by the stochastic approach via the Monte Carlo method. By relying on a stochastic sampling we focus only

*Which is kind of fitting for the nondeterministic world of quantum mechanics.

†To implicitly account for the antisymmetry property of fermionic wavefunctions.

‡Which seems infinitely large for our tiny studied quanta.

§Either to the complete basis set limit in the field of quantum chemistry or to the thermodynamic limit in condensed matter physics.

on the most relevant states, instead of seeking a deterministic solution to the problem. However, for strongly correlated electron systems this approach alone is not sufficient, as the antisymmetric nature of fermionic wavefunctions prohibits a straightforward application of a naive MC approach, known as the *fermion sign problem*. Thus, additional approximations and novel algorithms are necessary to further compress the information stored in the wavefunction and in turn extend the applicability of quantum Monte Carlo approaches.

In my work I studied two approaches to accomplish this feat:

I. To reduce the degrees of freedom in a simulation of a quantum mechanical system and to better understand and interpret the results, the **incorporation of the inherent symmetries** and corresponding conservation laws of the systems are of great use. For this reason, the first part of the thesis deals with the implementation of the **total** $SU(2)$ **spin symmetry** of nonrelativistic *ab-initio* Hamiltonians in the FCIQMC method. The use of a spin-adapted basis *reduces the effective Hilbert space size* of a problem by block-diagonalization of the Hamiltonian into different total spin symmetry sectors. Additionally, this allows to distinguish between distinct—even (near-)degenerate—spin states and entirely *removes spin contamination* of the sampled wavefunction, which is expected to be beneficial to the convergence behaviour of the projective FCIQMC technique. A conserved total spin quantum number also allows to *target and identify specific spin-eigenstates*, which facilitates a correct physical interpretation of calculations and description of chemical processes governed by the intricate interplay of them.

II. If symmetry alone does not suffice to reduce the vast number of degrees of freedom, we need to find a way to further efficiently *compress the most relevant physical features* in our description of a system. It is important to perform this in a controlled manner with a faithful account of the errors introduced due to this compression. However, it is possible *without loss of generality* to account for some part of the correlation between particles already in the *initial Ansatz* of the solution to the problem. The second part of the thesis is concerned with the implementation of an **explicitly correlated wavefunction Ansatz via similarity transformation** in quantum lattice systems. This Ansatz *induces* modified and novel *interactions* in the description of a system and *compresses* the relevant physical *information* encoded in the ground state wavefunction in an *extremely compact* way. This allows us to apply the FCIQMC approach to system sizes previously far out of reach for the method.

In the remainder of this chapter the basic problem we would like to solve is presented and the details prohibiting an exact solution are discussed, with an emphasis on *electron correlation effects*. A small overview of common approaches other than Monte Carlo methods to solve the problem is given. In particular, techniques we compare our FCIQMC

results against, such as the coupled cluster (CC) and density matrix renormalization group (DMRG) approaches are discussed.

In Chapter 2 the concepts of the (quantum) Monte Carlo (QMC) method and its application to quantum mechanical systems is introduced. After a brief introduction of the basic principles, the position of our method of choice, Full Configuration Interaction Quantum Monte Carlo (FCIQMC), compared to some examples of the vast plethora of QMC methods is laid out. Again with a special mention of the method providing reference results for our calculations, auxiliary-field quantum Monte Carlo (AFQMC).

In Chapter 3 the importance of symmetry in electronic structure calculations and physics and chemistry in general is discussed, with special attention to the total $SU(2)$ spin symmetry. The theoretical framework of the unitary group approach is explained in depth, as it, and its graphical extension by Shavitt, are the basis to implement the FCIQMC method purely in a spin-adapted basis, without any reference to a Slater determinant basis.

The actual computational implementation of the graphical unitary group approach to formulate FCIQMC in a spin-adapted basis is discussed in Chapter 4. The results obtained with the spin-adapted FCIQMC method (GUGA-FCIQMC) for ab-initio quantum chemical problems and the Hubbard model are presented in Section 4.4, which is followed by a conclusion and outlook of this approach in Section 4.5.

In Chapter 5 an explicitly correlated wavefunction Ansatz in FCIQMC for quantum lattice systems is presented. The Hubbard model is revisited and the Gutzwiller Ansatz as the main example of a correlated wavefunction Ansatz is presented. An explicitly correlated Ansatz in FCIQMC is incorporated via a similarity transformation of the Hamiltonian, which maps the electron correlation onto additional interaction terms in the transformed Hamiltonian. This allows an extremely compact wavefunction description of the system, which enables application of the FCIQMC method to unprecedented systems sizes. The results are presented in Section 5.5, which is followed by a conclusion and outlook of this approach in Section 5.6.

A final summary, conclusion and an outlook for future work and applications of the method presented in this work is given in Chapter 6.

1.2 Electronic Structure Theory

With relativistic effects neglected, the time evolution of a quantum mechanical system of N interacting particles is described by the *time-dependent* Schrödinger equation

$$i\hbar\frac{\partial}{\partial t}\Psi(\mathbf{x},t) = \hat{H}\Psi(\mathbf{x},t), \quad \text{with} \quad \mathbf{x} = (\mathbf{r},\sigma) \quad \text{and} \quad \mathbf{r} \in \mathbb{R}^{3N}, \tag{1.1}$$

where $\mathbf{x}$ is the combination of the $3N$ dimensional space variable $\mathbf{r}$ and spin. The Hamilton operator $\hat{H}$ in Eq. (1.1) characterizes the energy of the system and governs its dynamics. $\Psi(\mathbf{x}, t)$ is the position-space wavefunction of the quantum system, which is a function of all the space, time and spin coordinates of all N particles in the system. It contains all relevant physical information of a state. If the Hamiltonian in Eq. (1.1) does not explicitly depend on time, the *time-independent* Schrödinger equation is given by

$$\hat{H}\Psi(\mathbf{x}) = E_{ex}\Psi(\mathbf{x}), \quad \text{with} \quad \Psi(\mathbf{x}, t) = \mathrm{e}^{-iE_{ex}t}\,\Psi(\mathbf{x}), \tag{1.2}$$

with E_{ex} being the exact total energy associated with the eigenstate $\Psi(\mathbf{x})$ of the system. Since the wavefunction $\Psi(\mathbf{x})$ is a function of the continuous space variables of all N interacting particles, solving Eq. (1.2) exactly is impossible, except for rare special cases.* To solve Eq. (1.2) numerically, approximations have to be employed. For fermionic systems, to avoid the dilemma of the dependence of the wavefunction on the continuous space variables and cast Eq. (1.2) onto a finite problem, $\Psi(\mathbf{x})$ is approximated by a linear combination of antisymmetric Slater Determinants (SDs) $|D_i\rangle$

$$|\Psi\rangle = \sum_i c_i\,|D_i\rangle\,, \quad \text{with} \quad |D_i\rangle = \frac{1}{\sqrt{N!}} \begin{vmatrix} \phi_1(\mathbf{x}_1) & \phi_1(\mathbf{x}_2) & \cdots & \phi_1(\mathbf{x}_N) \\ \phi_2(\mathbf{x}_1) & \phi_2(\mathbf{x}_2) & \cdots & \phi_2(\mathbf{x}_N) \\ \vdots & \vdots & \ddots & \vdots \\ \phi_N(\mathbf{x}_N) & \phi_N(\mathbf{x}_2) & \cdots & \phi_N(\mathbf{x}_N) \end{vmatrix}, \tag{1.3}$$

formed from a set of $2n$ orthonormal *spin-orbitals* $\{\phi_m(\mathbf{x}_l)\}$. $\phi_m(\mathbf{x}_l)$ is given as a product of n spatial components $\rho_k(\mathbf{r}_l)$, with $k = 1, \ldots, n$, and a function of spin $\chi(\sigma_l)$, leading to a total of $2n$ spin-orbitals, $\{\phi_k^\sigma(\mathbf{x}_l)\}$ in short, with $\sigma = \{\uparrow, \downarrow\}$ for fermionic systems. With a finite single-particle (or one-body) basis $\{\phi_k^\sigma(\mathbf{x}_l)\}$, the SD expansion is also finite and thus $\hat{H}$ can be expressed as a square matrix in the SD basis and Eq. (1.2) can be cast in the form of an eigenvalue equation

$$\hat{H}\,|\Psi\rangle = E\,|\Psi\rangle\,, \tag{1.4}$$

with E being the approximation to the exact energy E_{ex} of Eq. (1.2) within the chosen basis set. The full spectrum of (1.4) can be obtained by exact diagonalization (ED) of the operator $\hat{H}$ constructed in the basis of all possible SDs formed from the single-particle basis, called Full Configuration Interaction (FCI), see Sec. 1.7.6, in the field of quantum chemistry. However, ED is already very expensive even for a small number of basis states. Nevertheless, since the important physical and chemical processes are in general determined by the ground state and a few low-lying excited states Eq. (1.4) can also be solved by iterative procedures, such as the Power,[110] Lanczos[176] or Davidson[63] method, with a far better scaling compared to ED. In the limit of a complete basis set (CBS) E will be identical to E_{ex}, but the SD expansion will be again infinite and thus intractable. Nevertheless, by a systematic increase in the chosen basis set size the CBS limit can be

*The one-electron hydrogen atom and H_2^+ molecule for example.

approached in a controlled manner and various extrapolation schemes exist to obtain an approximate CBS limit result at least.[133]

We have not talked about the explicit form of the Hamiltonian $\hat{H}$ yet, since the Schrödinger equation describes all nonrelativistic quantum mechanical systems in general. For *ab-initio electronic structure calculations* (ESC) in condensed matter physics and quantum chemistry $\hat{H}$, without external fields, has following form in atomic units

$$\hat{H} = \sum_{i}^{N} \left(-\frac{1}{2}\nabla_i^2 - \sum_{a}^{N_n} \frac{Z_a}{|\mathbf{r}_i - \mathbf{R}_a|} \right) + \sum_{i<j}^{N} \frac{1}{|\mathbf{r}_i - \mathbf{r}_j|} + \sum_{a<b}^{N_n} \frac{Z_a Z_b}{|\mathbf{R}_a - \mathbf{R}_b|}, \tag{1.5}$$

where the sums are over the N electrons and N_n nuclei, ∇_i^2 is the kinetic energy and $\mathbf{r}_i$ the position of electron i, Z_a are the nuclear charges and $\mathbf{R}_a$ is the position of nucleus a. The Born-Oppenheimer[31] approximation is applied, where the separation of the motion of electrons and nuclei, due to their vastly different masses, is assumed. Thus, $\hat{H}$ describes the correlated motion of electrons, $-\nabla_i^2/2 - \sum_a Z_a r_{ia}^{-1}$ with $r_{ia} = |\mathbf{r}_i - \mathbf{R}_a|$, interacting via the Coulomb force r_{ij}^{-1}, with $r_{ij} = |\mathbf{r}_i - \mathbf{r}_j|$ in a potential generated by the charges of the fixed nuclei. In this work our aim is to solve the *electronic problem*, so $|\Psi\rangle$ will from now on represent the *N-electron* wavefunction. In second quantization, the nonrelativistic *molecular electronic Hamiltonian* (1.5) in the Born-Oppenheimer approximation takes following form

$$\hat{H} = \sum_{ij}^{n} \sum_{\sigma=\uparrow,\downarrow} t_{ij} a_{i\sigma}^\dagger a_{j\sigma} + \frac{1}{2} \sum_{ijkl}^{n} \sum_{\sigma,\tau=\uparrow,\downarrow} V_{ijkl}\, a_{i\sigma}^\dagger a_{k\tau}^\dagger a_{l\tau} a_{j\sigma} + h_{nuc}, \tag{1.6}$$

with n being the number of spatial orbitals. $a_{i\sigma}^\dagger$ and $a_{i\sigma}$ are the anticommuting fermionic creation and annihilation operators, $[a_{i\sigma}^\dagger, a_{j\tau}]_+ = \delta_{ij}\delta_{\sigma\tau}$, of an electron in spin-orbital (i, σ). t_{ij} and V_{ijkl} are the *molecular one-* and *two-body integrals*[133]

$$t_{ij} = \int \phi_i^*(\mathbf{r}) \left(-\frac{1}{2}\nabla^2 - \sum_{a}^{N_n} \frac{Z_a}{|\mathbf{r} - \mathbf{r}_a|} \right) \phi_j(\mathbf{r}) d\mathbf{r} \tag{1.7}$$

$$V_{ijkl} = \int\int \frac{\phi_i^*(\mathbf{r}_1)\phi_k^*(\mathbf{r}_2)\phi_j(\mathbf{r}_1)\phi_l(\mathbf{r}_2)}{|\mathbf{r}_1 - \mathbf{r}_2|} d\mathbf{r}_1 d\mathbf{r}_2, \tag{1.8}$$

which are evaluated in the chosen spin-orbital basis $\{\phi_i\}$. The electron independent nuclear potential $h_{nuc} = \sum_{ab} Z_a Z_b r_{ab}^{-1}$ can be directly added to $\hat{H}$, since it is just an equal shift of all electronic energies. As a final note, since we deal with the *electronic* structure, the obtained solution $|\Psi\rangle$ of Eq. (1.4) must be totally antisymmetric under the exchange of two electrons $|\Psi(\mathbf{x}_1, \mathbf{x}_2)\rangle = -|\Psi(\mathbf{x}_2, \mathbf{x}_1)\rangle$ and thus obey the Pauli exclusion principle.*

*This antisymmetry property is automatically ensured in the 2nd quantized formulation with anti-commuting fermionic creation and annihilation operators and with an expansion of $|\Psi\rangle$ in antisymmetric SDs.

However, even in a finite basis the exact solution to Eq. (1.4) is a formidable—in most cases even impossible—task. The Coulomb interaction term, r_{ij}^{-1} in Eq. (1.5) and equivalently the two-body term in Eq. (1.6), correlates all electrons and thus the problem is not separable in distinct one-body systems, but a full *many-body* treatment is necessary. The space of this many-body problem, which is the number of SDs that can be created from the spin-orbital basis, the so called *Hilbert space size** increases combinatorially with the number of electrons and orbitals. This scaling makes the exact solution to (1.4) possible only up to $N = n \approx 18 - 20$.† Because of this we have to rely on approximate solutions even for the expansion in a finite single-particle basis.

Thus, in addition to the hierarchy of the single-particle basis set size, there exists a hierarchy of many-body methodologies, based on different sorts of approximations. In general, the closer a method attains the exact solution the more similar the computational cost increases. So the task of modern electronic structure theory is to find more and more elaborate approximations to come as close as possible to the exact solution of the problem at hand, while keeping the computational cost at a moderate level. Figure 1.1 sketches the relationship of the hierarchy in the one-body basis set size and level of methods, where only a combined effort can reach the exact solution to the full Schrödinger equation (1.2).

1.3 Symmetry in Electronic Structure Calculations

Symmetry is a concept of paramount importance in physics and chemistry. An observable of a physical system, represented by an operator $\hat{O}$, which is unchanged under some general transformation, represented by an operator $\hat{T}$, is said to have the symmetry related to the operation $\hat{T}$. For example if the temperature T in a room is homogeneous and thus independent of the spatial position, the continuous spatial translation $\hat{T} : \vec{r} \rightarrow \vec{r} + a$ is a symmetry of T. The operation $\hat{T}$ can be of *continuous*—e.g. rotations of a circle—or *discrete* type—i.e. the reflection along a given axis—. Continuous symmetries are described by Lie groups[75] and discrete symmetries by finite groups.[174]

The invariance of an observable $\hat{O}$ under a transformation $\hat{T}$ is equivalent to the vanishing commutator

$$[\,\hat{O}, \hat{T}\,] = 0. \tag{1.9}$$

Noether's theorem[220] proves, that every symmetry of a system is related to a conserved observable. Examples are:

*For a system of fixed number of particles. If the number of particles is variable or unknown, the even larger *Fock space* has to be considered.

†Of course for a smaller number of electrons, a larger number of orbitals feasible.

Symmetry	Transformation $\hat{T}$	Conserved quantity
Translation in time	$t \to t + a$	Energy
Translation in space	$\vec{r} \to \vec{r} + \vec{a}$	Momentum
Rotation in space	$\vec{r} \to \hat{R}\vec{r}$	Angular momentum
Coordinate inversion	$\vec{r} \to -\vec{r}$	Spatial parity
Charge conjugation	$q \to -q$	Charge parity
Time reversal	$t \to -t$	Time parity
$U(1)$ gauge transformation	$\Psi(\vec{r}, t) \to \mathrm{e}^{i\Phi}\, \Psi(\vec{r}, t)$	Electric charge

Symmetries that commute with the Hamiltonian $\hat{H}$ of a system, $[\,\hat{H}, \hat{T}\,] = 0$, are of special importance in electronic structure calculations (ESC). Since a set of commuting operators can be simultaneously diagonalized, utilising the eigenfunctions $|\Phi\rangle$ of the operator $\hat{T}$, causes $\hat{H}$ to have a block-diagonal structure. The blocks correspond to different symmetry sectors related to the "*good*", conversed quantum numbers λ, with $\hat{T}\,|\Phi\rangle = \lambda\,|\Phi\rangle$ and thus the eigenvalues λ can be used to specify the eigenstates of $\hat{H}$. The block-diagonal structure reduces the computational effort of diagonalizing $\hat{H}$. In addition, problems, due to degeneracies of energy eigenvalues of $\hat{H}$ belonging to different symmetry sectors of $\hat{T}$, can be avoided. The use of symmetry in ESCs also allows the straightforward calculation of excited states, if they belong to different symmetry sectors than the ground state of $\hat{H}$.

Common symmetries used in ESCs are:

- Discrete **translational** symmetry on a lattice, by the use of a *momentum space basis*.
- **Point group** symmetries of lattices and molecules, by the use of *symmetry-adapted* molecular orbitals (MOs).
- **Orbital angular momentum** conservation by the usage of a basis, based on the spherical harmonics Y_{lm}.
- **Conservation** of the $\hat{S}_z$ projection of the total spin, by the use of a Slater-determinant basis with *fixed* m_s eigenvalue of $\hat{S}_z$.

Concerning the last point, a Slater determinant $|D_i\rangle$ constructed from a set of single-particle spin-orbitals, given as the product of a spatial part times a spin function, $\phi_m(\mathbf{x}) = \phi_k^\sigma(\mathbf{x}) = \rho_k(\mathbf{r}) \cdot \chi_\sigma(\tau)$, with $\sigma, \tau = \{\uparrow, \downarrow\}$ and the combined spatial and spin variable $\mathbf{x} = (\mathbf{r}, \tau)$, obeys

$$\hat{S}_z \rho_k(\mathbf{r}) \chi_\sigma(\tau) = \rho_k(\mathbf{r}) \hat{S}_z \chi_\sigma(\tau) = \begin{cases} -\frac{\hbar}{2} \phi_k^\sigma(\mathbf{r}, \tau) \delta_{\sigma\tau} & \text{for} \quad \sigma = \downarrow \\ +\frac{\hbar}{2} \phi_k^\sigma(,\tau) \delta_{\sigma\tau} & \text{for} \quad \sigma = \uparrow, \end{cases} \tag{1.10}$$

is always an eigenfunction of the z-projection operator of the total spin, as $\hat{S}_z$ only acts

on the spin part $\chi_\sigma(\tau)$ of the basis state $\phi_k^\sigma(\mathbf{x})$.

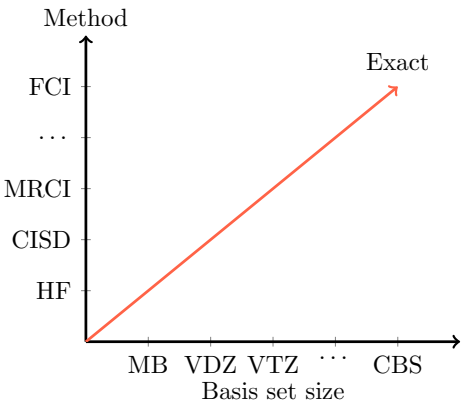

Fig. 1.1: Relationship of the hierarchy of basis set size and level of methodology with the quest to reach the exact solution to quantum mechanical system described by the Schrödinger equation (1.2).[133] The acronyms shown are explained in the text. On one hand, by improving the method, we want to reach the exact (Full Configuration Interaction) result for a given basis set. And on the other hand, by increasing the basis set size, we want to reach the Complete Basis Set (CBS) limit—desirably with FCI accuracy.

However, as one can see in Eq. (1.5), the non-relativistic, molecular Hamiltonian does not depend on spin at all, and thus, in addition to the z-projection of spin, the total spin is also a conserved quantity, indicated by the vanishing commutators

$$[\,\hat{H}, \hat{S}_z\,] = [\,\hat{H}, \hat{\mathbf{S}}^2\,] = 0. \tag{1.11}$$

The use of this total spin conservation and the accompanying total spin rotation symmetry in the FCIQMC framework is a major topic of this thesis and is more elaborated on in Chapters 3 and 4.

1.4 The Hubbard Model

In addition to the hierarchy of basis sets and methods, another route to find approximate solutions of the Schrödinger is to identify the most important degrees of freedom of a quantum mechanical system and instead of solving the full *ab-initio* Hamiltonian (1.5) derived from first principles, derive an effective *model Hamiltonian* capturing the most important physical aspects and solve for the low-energy features of the studied system.

A prime example of such a model system is the *single-band Hubbard* model, the simplest model for interacting electrons on a lattice. The Hubbard Hamiltonian in second quantization is given by

$$\hat{H} = -t \sum_{\langle i,j\rangle,\sigma=\uparrow,\downarrow} a_{i,\sigma}^\dagger a_{j,\sigma} + U \sum_i n_{i,\uparrow} n_{i,\downarrow}, \tag{1.12}$$

where $a_{i,\sigma}^{(\dagger)}$ annihilates (creates) an electron with spin $\sigma = \uparrow, \downarrow$ at a localized site i, $n_{i,\sigma} = a_{i,\sigma}^\dagger a_{i,\sigma}$ is the number operator on site i with spin σ, t is the hopping strength, U is the purely local on-site Coulomb interaction and the sum over i and j is restricted to nearest-neighbour sites indicated by $\langle i, j\rangle$. It was original introduced to study the metal-insulator transition and magnetism in narrow energy d- and f-bands.[122,142,143,154] It is however also believed that the Hubbard model captures the most important physics of the CuO_2 planes in high-temperature superconducting cuprates.[8,16,81,371] The CuO_2 planes of cuprates are

responsible for their superconducting properties and band-structure calculations[204,368] show the copper 3d and oxygen 2p orbitals are the dominant factors for their electronic properties. The half-filled antibonding molecular orbital (MOs) formed from the Cu $3d_{x^2-y^2}$ and O $2p_{x/y}$ atomic orbitals (AOs) are the only states with a significant dispersion close to the Fermi energy of the system.[88] Thus, the low energy physics of the CuO_2 planes of the cuprates can be mapped to the two-dimensional repulsive ($U > 0$) Hubbard model, which is depicted schematically in Fig. 1.2.

The Hamiltonian (1.12) has a close resemblance to the more general Pariser-Parr-Poble (PPP) Hamiltonian.[240,241,253] The PPP and Hubbard Hamiltonians are based on a similar approximation to the general *ab-initio* Hamiltonian (1.6), known as the *zero differential overlap* (ZDO) or *complete neglect of differential overlap* (CNDO).* In this approximation the differential overlap between basis states is neglected in the two-body integrals (1.8)[149] leading to $V_{ijkl} = V_{iikk}\delta_{ij}\delta_{kl}$.[252,255] The Hubbard model further employs the restriction of a uniform hopping between nearest-neighbours only and purely on-site $U = V_{iiii}\delta_{ij}\delta_{kl}\delta_{ik}$. Whereas the PPP model is the CNDO approximation applied to systems in a basis with π electrons only.

Despite its conceptual simplicity—the sum of a simple tight-binding model accounting for the kinetic energy and a purely local Coulomb interaction term—the only exact results for the Hubbard model are available for the one-dimensional case via the Bethe-Ansatz[186] and a few limiting cases in more than one dimension ($U = 0$ by Fourier transformation and $U = 0$ already diagonal in a real-space basis).† The two parameters t and U of the Hubbard model can be reduced to the relative strength of the hopping and Coulomb term U/t. The intricate dynamic interplay of the kinetic hopping term and the Coulomb on-site interaction—especially in parameter ranges where neither of them can be assumed as a small perturbation $U/t \approx 8 - 12$—make exact solutions for reasonably large systems sizes impossible and approximate numerical methods struggle to identify the different near degenerate low energy phases.

However, not only due to its physical application, the Hubbard is an interesting model to study from a theoretical point of view. As it is the simplest possible model for strongly interacting electrons, as it only accounts for the motion of electrons through lattice sites and the shortest possible, on-site interaction. The Hubbard model will be discussed more thoroughly in Sec. 4.4.4, 5.2 and 5.3.

*Strictly speaking the CNDO additional implies a treatment of valence electrons only.

†The case of infinite dimensions is also exactly solvable via an exact mapping to an impurity model[7] and consequent solution with dynamical mean-field theory.[102,211]

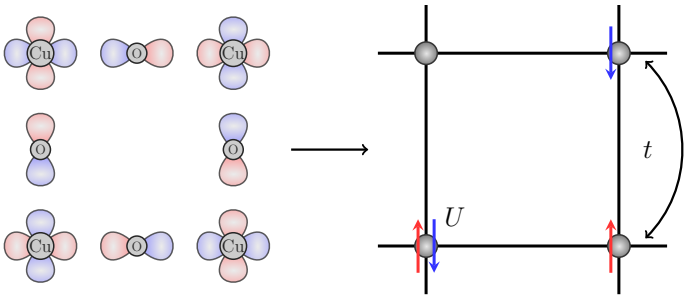

Fig. 1.2: (Left) Half-filled electronic active antibonding configuration of the copper $3d_{x^2-y^2}$ and oxygen $2p_x$ and $2p_y$ orbitals in the CuO_2 planes of cuprates. (Right) Mapping to the two-dimensional Hubbard lattice model of the CuO_2 planes with hopping t between nearest-neighbours an on-site Coulomb repulsion U.

1.5 Hartree-Fock Theory

One of the simplest approximation in *ab-initio* wavefunction theory is the Hartree-Fock (HF) method.[93,126] HF theory is usually the basis and starting point for many more elaborate methods and is historically of paramount importance in the development of electronic structure theory. In HF theory the exact N-electron wavefunction $|\Psi\rangle$ is approximated by only a *single* Slater determinant,[299] $|\Phi_{HF}\rangle$. The one-electron spin-orbitals, denoted in short as $\{\phi_k^\sigma\}$, from which $|\Phi_{HF}\rangle$ is constructed are variationally optimized to minimize the energy expectation value

$$E_{HF} = \min_{\phi_k} \langle \Phi_{HF}(\phi_k^\sigma) | \hat{H} | \Phi_{HF}(\phi_k^\sigma) \rangle \tag{1.13}$$

with $\langle \Phi_{HF} \,|\, \Phi_{HF} \rangle = 1$ and the constraint $\left\langle \phi_i^\sigma \,\middle|\, \phi_j^\tau \right\rangle = \delta_{ij}\delta_{\sigma\tau}$. The variational optimization in the space of $\{\phi_k^\sigma\}$ consists of unitary transformation within the spin-orbital basis. So $|\Phi_{HF}\rangle$ can parametrized as

$$|\Phi_{HF}\rangle = \mathrm{e}^{-\hat{\kappa}} |0\rangle\,, \qquad \text{with} \quad \hat{\kappa} = \sum_{ij,\sigma\tau} \kappa_{IJ}\, a_{i,\sigma}^\dagger a_{j,\tau}, \tag{1.14}$$

with $I = (i,\sigma)$, $J = (j,\tau)$ and $\kappa_{IJ} = -\kappa_{JI}^*$ forming an anti-Hermitian matrix of orbital rotation parameters, to ensure $\mathrm{e}^{\hat{\kappa}}$ to be unitary. $|0\rangle$ in Eq. (1.14) is an arbitrary initial Slater determinant. With the Ansatz (1.14) Eq. (1.13) is then minimized with respect to the rotation parameters κ_{IJ}. In this formulation the constraint $\left\langle \phi_i^\sigma \,\middle|\, \phi_j^\tau \right\rangle = \delta_{ij}\delta_{\sigma\tau}$ is automatically fulfilled, since unitary transformations will leave the spin-orbitals orthonormal. One can see from the form of $\hat{\kappa}$ in Eq. (1.14) orbital rotations can be formulated as single excitation operators. In the final HF solution, these single excitations will be minimized leading to the Brillouin's theorem, that the matrix elements between single excitations and the HF states are zero,[315] $\langle \Phi_I^A | \hat{H} | \Psi_{HF} \rangle = 0$, with $|\Phi_I^A\rangle = a_{a,\sigma}^\dagger a_{i,\sigma} |\Phi_{HF}\rangle$.

Physically the HF method can be understood as solving the Schrödinger equation of a single electron in the *mean-field* created by the remaining $N-1$ electrons. The correlation between electrons is treated in an averaged way and thus the single N-body problem can be separated into N one-body problems.

In the restricted Hartree-Fock (RHF) method the same set of spatial orbitals, $|\phi_i\rangle$, is used for both the ↑- and ↓-spin component of $|\phi_i^\sigma\rangle$. Thus, the one-body operator $\hat{t}$ of the original Hamiltonian (1.6) and the averaged Coulomb repulsion of the electrons, yielding the effective one-electron *Fock potential*, $\hat{V}_{eff} = \sum_k (2V_{ijkk} - V_{ikkj})$, are combined in the Fock operator

$$\hat{f} = \sum_{ij} f_{ij}\, \hat{E}_{ij}, \qquad \text{with} \quad f_{ij} = t_{ij} + \sum_{k \in \text{occ}} (2V_{ijkk} - V_{ikkj}), \tag{1.15}$$

with the spin-free excitation operators, $\hat{E}_{ij} = \sum_\sigma a_{i\sigma}^\dagger a_{j\sigma}$, and the summation over occupied spatial orbitals k. The *canonical* RHF orbitals are obtained by diagonalizing

$$\hat{f}\,|\phi_i\rangle = \epsilon_i\,|\phi_i\rangle\,, \tag{1.16}$$

yielding the *Hartree-Fock equations*, where the effective Fock potential depends on the form of the occupied orbitals k.* For canonical Hartree-Fock orbitals† ϵ_i can be interpreted as the *orbital energies*. The equivalent treatment of the spin-part in the RHF method leads to the n lowest-in-energy spatial orbitals to be doubly occupied, yielding the so called *closed-shell* HF state. However, this restriction means that RHF only works for an even number of electrons. For *open-shell* systems the *unrestricted* HF (UHF) method[19,254] optimizes the ↑- and ↓- spin-orbitals independently, which breaks the total spin symmetry of the system and thus, UHF solutions are no longer eigenfunction of the $\hat{\mathbf{S}}^2$ operator. *Restricted open-shell* HF (ROHF) theory[268] is able to treat open-shell system and the ROHF solution is at the same time an eigenstate of the total spin operator $\hat{\mathbf{S}}^2$.

In both approaches, due to nonlinear parameters κ_{IJ} in (1.13) and dependence of $\hat{f}$ on the solved for orbitals in (1.16), the solution must be found self-consistently by iteration. Due to the necessity of an iterative procedure the HF method is also called the *self-consistent field* (SCF) method.

1.6 Correlation Energy

The averaged description of the interaction between electrons in the HF method of course does not represent the physical reality. Nevertheless, for many systems the HF method yields surprisingly good results, not very far from the exact solution for a given basis set. The *correlation energy* is defined as the difference between the exact solution and the HF energy‡

$$E_{corr} = E_{exact} - E_{HF}. \tag{1.17}$$

*Which might change after optimization!

†The HF state is invariant to unitary transformations of the occupied orbitals, thus the canonical HF orbitals are not the only possible solution.

‡Strictly speaking the correlation energy is defined with both E_{exact} and E_{HF} in the CBS limit.

In *weakly correlated* systems, where the electrons barely interact, the mean-field HF model is a good description and more elaborate methods based on $|\Phi_{HF}\rangle$ will be probably sufficient to yield excellent results.
For many interesting systems however the HF method fails miserably, since the intricate correlated motion of electrons can not be described by a mean-field approach. These systems are called *strongly correlated* systems and all methods going *beyond* Hartree-Fock have the goal to determine the remaining missing correlation energy. In quantum chemistry there is a discrimination between two forms of correlation, although this distinction is arguably not completely well-defined and the two concepts are not mutually exclusive.

Static correlation is present if multiple states in the ground state wavefunction expansion of $|\Psi\rangle$ in SDs are of equal importance and/or degenerate in energy, naturally defying a single-reference description. This can be the case for systems with multiple singly occupied spatial orbitals (open-shells) or for molecules near dissociation. In general these systems can not be well described by a single Slater determinant and a *multi-reference* treatment is necessary.

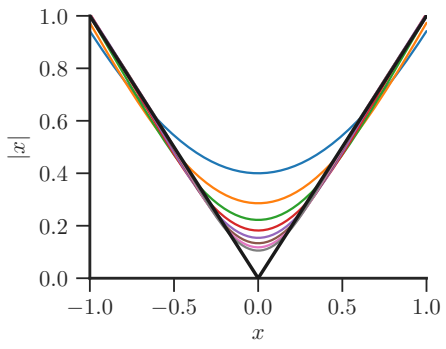

Fig. 1.3: Approximation of the nondifferentiable function $f(x) = |x|$ by even ordered polynomials up to order 20.

Dynamic correlation is associated with the actual physical repulsion of electrons due to the Coulomb force. An important consequence of this is related to the slow convergence of basis set extrapolations, due to the dynamic behaviour of electrons in close proximity. If two electrons coincide in space the electronic molecular Hamiltonian (1.5) becomes singular, while the local energy $\hat{H}\Psi(\mathbf{r})/\Psi(\mathbf{r})$ remains constant. To balance the singularity of $\hat{H}$, the exact eigenfunction $\Psi(\mathbf{r})$ must have a nondifferentiable behaviour*

$$\lim_{r_{ij}\to 0}\left(\frac{\partial\Psi}{\partial r_{ij}}\right)_{av} = \frac{1}{2}\Psi(r_{ij}=0) \tag{1.18}$$

at electron coalescence ($r_{12} = 0$) resembling a *cusp*, thus called *electronic cusp condition*[156,200] or *Kato's cusp condition*. The standard Ansatz of $\Psi(\mathbf{r})$ as a product of single-particle orbitals, i.e. Slater-type orbitals (STOs),[298] † Gaussian-type orbitals (GTOs)[37,132] or correlation consistent basis sets by Dunning,[76] struggles to capture the nondifferentiable behaviour of the exact wavefunction. This difficulty is part of the reason for the necessity of large basis set expansion sizes, and illustrated in Fig. 1.3 by the example of an approximation of the nondifferentiable function $f(x) = |x|$ by polynomials of even order. An Ansatz to take this property of $\Psi(\mathbf{r})$ explicitly into account is discussed in Sec. 1.7.7.

*Spherically averaging is assumed in Eq. (1.18).
†However STOs are able to correctly describe the related *nuclear cusp condition*.

1.7 Post-Hartree-Fock Methods

To correctly describe the interesting physics and chemical properties of system governed by *strong correlation* effects, where mean-field treatments inevitably fail, more elaborate approaches to capture the dynamic interaction between particles have to be employed. Due to the paramount importance of the HF method, theories and approaches that expand on the result obtained by the mean-field solution, thus go beyond HF, are in general categorized under the name of *post-Hartree-Fock* methods. Here only a selection of important ones —with a focus on methods used as comparison for the FCIQMC results—are briefly discussed.

1.7.1 Multi-Configurational Self-Consistent Field Method

For systems with strong static correlation, with a multitude of equally important states contributing to the ground state, the Multi-configurational Self-Consistent Field (MCSCF)[133] method is a natural and applicable extension of the HF approach. In MCSCF the wavefunction is expanded as a linear combination of *several* important SDs (configurations),

$$|\Phi_{MC}(\kappa, \mathbf{c})\rangle = \mathrm{e}^{-\hat{\kappa}} \sum_i c_i \, |D_i\rangle \tag{1.19}$$

whose expansion coefficients c_i and orbital-rotation parameter κ are simultaneously optimized to yield the lowest possible variational energy

$$E_{MC} = \min_{\kappa, \mathbf{c}} \frac{\langle \Phi_{MC}(\kappa, \mathbf{c}) | \hat{H} | \Phi_{MC}(\kappa, \mathbf{c}) \rangle}{\langle \Phi_{MC}(\kappa, \mathbf{c}) \,|\, \Psi_{MC}(\kappa, \mathbf{c}) \rangle}. \tag{1.20}$$

As in the HF method, due to the nonlinear appearance of the coefficients, this optimization has to be carried out iteratively until convergence is reached. The choice of the states to be considered, $\{D_i\}$, is the most challenging part in a MCSCF calculation.

Complete Active Space SCF

The Complete Active Space SCF (CASSCF) method[77,131,225,266] is a prominent approach to optimize the choice of configurations in MCSCF. Instead of an individual choice of SDs, a general class of configurations is chosen by partitioning the orbital space into three subspaces. The **core** or **inactive** space consists of exclusively doubly occupied orbitals, the **virtual** or **secondary** space are orbitals, which are always empty, and finally the **active** space is the set of orbitals with variably occupancies 0, 1 and 2. The *multi-configurational* space then consists of all SDs with doubly occupied core, empty virtuals and all possible distribution of electrons in the active space. The Hamiltonian (1.6) is

solved *exactly* in the space of these determinants, while orbital rotations between all spaces are optimized, as depicted in Fig. 1.4.

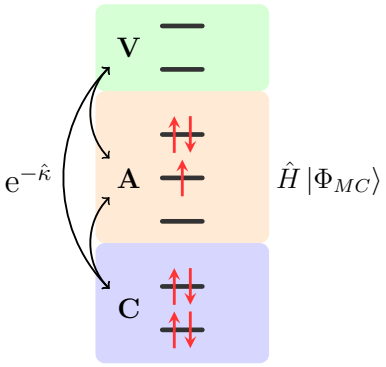

Fig. 1.4: Partitioning of the orbital space into the doubly occupied core (C), empty virtual (V) and variable occupied active (A) space. Orbital rotations $e^{-\hat{\kappa}}$ between all spaces are optimized, but only the active space is solved exactly.

Orbitals and wavefunctions optimized with the CASSCF procedure prove to be excellent starting points for more elaborate methods, as explained in Sec. 1.7.2 and with applications given in 4.4.6, as the important static correlation in the active space is captured exactly. However, the reliance on an exact solution, restricts this approach to rather small active spaces, treatable with iterative ED solvers, such as the Davidson procedure. It is however possible to use more elaborate methods, such as the density matrix renormalization group (DMRG), see Sec. 1.7.5, or the FCIQMC method[184] as the FCI solver, which enables the treatment of far active spaces. Nevertheless, the choice of the active space requires a fair amount of "chemical intuition" to correctly identify the physically important orbitals and thus this approach is definitely not a "black-box" method.

1.7.2 Configuration Interaction

The configuration interaction (CI)[291] approach approximates the eigenfunction $|\Psi\rangle$ of the molecular Hamiltonian (1.6) as a *linear* expansion of a limited set of SDs $\{|D_i^{CI}\rangle\}$. This set is obtained by considering excitations up to a certain level n_{trunc} from a given reference state, usually the HF solution $|\Phi_{HF}\rangle$. $|\Psi_{CI}\rangle$ is given by

$$|\Psi_{CI}\rangle = \sum_k c_k^{CI}\,|D_k^{CI}\rangle = \left(\mathbb{1} + \sum_{ia} c_i^a\, a_a^\dagger a_i + \sum_{ijab} c_{ij}^{ab}\, a_a^\dagger a_b^\dagger a_i a_j + \cdots\right)|\Phi_{HF}\rangle\,, \tag{1.21}$$

where $c_k^{CI} = \{c_i^a, c_{ij}^{ab}, \dots\}$ are the expansion coefficients of single, double, ... excitations up to the chosen level of truncation n_{trunc} (spin index omitted for brevity). Figure 1.5 schematically shows examples of SDs of a CI expansion up to triple excitations based on the HF determinant. The coefficients c_k^{CI} are determined by diagonalizing $\hat{H}$, fully or iteratively for the ground state, in this basis

$$\sum_l \langle D_k^{CI}|\hat{H}|D_l^{CI}\rangle c_l^{CI} = E_{CI} c_k^{CI}. \tag{1.22}$$

If the considered excitation level is lower than the maximum possible one, the CI method is neither *size-consistent* nor *size-extensive*.[13,317] Let's briefly describe these two concepts:

A method is **size consistent** if correctly describes the *additive energy separation* if a system is split into two noninteracting subsystem, e.g. due to distance in dissociation processes. Let $AB = A + B$ be a super-system consisting of two separated subsystems A and B, described by the Hamiltonians $\hat{H}_{AB} = \hat{H}_A + \hat{H}_B$ and $[\,\hat{H}_A, \hat{H}_B\,] = 0$. The total energy is additive separable, while the wavefunction of the total system $|AB\rangle$ is multiplicative separable:

$$\hat{H}_{AB}\,|AB\rangle = \left(\hat{H}_A + \hat{H}_B\right)|A\rangle\,|B\rangle = E_A\,|A\rangle\,|B\rangle + E_B\,|A\rangle\,|B\rangle = (E_A + E_B)\,|AB\rangle\,. \quad (1.23)$$

The CI method is **not** size-consistent,[177] due to the *linear* wavefunction Ansatz in (1.21), except if all levels of possible excitations are taken into account.[73]
A method is **size extensive** if it correctly describes the *linear scaling* of extensive properties, i.e. the energy, with the number of electrons. However, size-extensivity alone does not ensure that a method correctly describes fragmentation of a super-system in smaller subsystems, e.g. dissociation processes. Similar to dynamic and static correlation, size-consistency and size-extensivity are not mutually exclusive properties. In the interacting limit, size-extensivity is actually a necessary and sufficient condition for size-consistency.[13]

If the ground state solution is dominated by a single state, usually the HF state, the CI method can yield reasonably good results. Especially since lower orders of excitations, specifically doubles*, are the most important. Additionally, the CI method is systematically improvable by increasing the maximum level of excitation n_{trunc} allowed and applicable to large basis sets due to favourable scaling, if only low orders of excitations are considered, e.g. only singles and doubles (CISD). However, the CI method shows a slow convergence, due to difficulty in resolving the electronic cusp condition.[257]

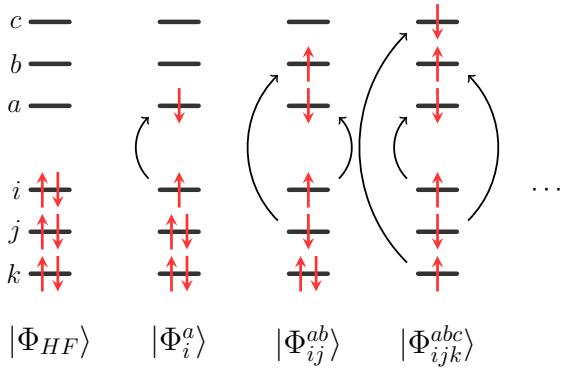

Fig. 1.5: Schematic presentation of SDs contained in a CI expansion up to triple excitation from a RHF reference determinant. Excitations are written in the form $|\Phi_i^a\rangle = a_a^\dagger a_i\,|\Phi_{HF}\rangle$ with the spin index omitted.

*Since doubles are the only one interacting directly with the HF state, as the matrix element of singles to the HF states is zero, due to Brillouin's theorem, see Sec. 1.5

Multi-Reference CI

Similar to the extension of the HF method to multi-configurational systems, via the MCSCF method, see Sec. 1.7.1, the CI approach can be extended to the Multi-Reference CI (MRCI) method.[41] In the *internally contracted* formulation of MRCI, excitations relative to a *reference space*, instead of just a single reference state*, are considered and $|\Psi_{MRCI}\rangle$ is given by

$$|\Psi_{MRCI}\rangle = \left(\mathbb{1} + \sum_{ia} c_i^a \, a_a^\dagger a_i + \sum_{ijab} c_{ij}^{ab} \, a_a^\dagger a_b^\dagger a_i a_j + \cdots\right) \sum_I d_I \, |D_I\rangle \, . \tag{1.24}$$

A suitable choice of a reference space is the solution to a CASSCF calculation, see Sec. 1.7.1. Similar to the CI method 1.7.2, MRCI suffers from the lack of size-consistency and size-extensivity, but yields better correlation energies, due to the larger wavefunction expansion. However, this comes with the price of a highly increased computational effort, which can be ameliorated with internal contraction schemes.[346]

1.7.3 Perturbation Theory

Perturbation theory attempts to find approximate solutions of a problem based on the exact solution of a related, but simpler problem. Conceptually the "hard" problem, represented by $\hat{H}$, is broken into an exactly solvable part $\hat{H}_0$, with known solutions $\hat{H}_0 \, |\Phi_n^{(0)}\rangle = E_n^{(0)} \, |\Phi_n^{(0)}\rangle$, and a perturbative correction $\hat{H}_1$:

$$\hat{H} = H_0 + \lambda \hat{H}_1, \tag{1.25}$$

with a parameter λ. This approach is known as time-independent Rayleigh-Schrödinger perturbation theory[262,278] in quantum chemistry, or just many-body perturbation theory in the physics community. If $\hat{H}_0$ is chosen as the Fock operator (1.15) and $\hat{H}_1$ as the difference of the true Coulomb interaction and the effective one-electron Fock potential $\hat{V}_{eff}$

$$\hat{H}_0 = \hat{f}, \qquad H_1 = \sum_{i<j} r_{ij}^{-1} - \hat{V}_{eff} = \hat{H} - \hat{f} = \hat{H} - \hat{H}_0 \tag{1.26}$$

the approach is known as Møller-Plesset perturbation theory (MPPT)[212] in quantum chemistry.

If we formally express the energy and eigenstates of $\hat{H}$ in a power series in λ

$$E_n = E_n^{(0)} + \lambda E_n^{(1)} + \lambda^2 E_n^{(2)} + \cdots, \qquad |\Psi_n\rangle = |\Phi_n^{(0)}\rangle + \lambda \, |\Phi_n^{(1)}\rangle + \lambda^2 \, |\Phi_n^{(2)}\rangle + \cdots, \tag{1.27}$$

*Spin-index omitted for brevity.

with $|\Phi_0^{(0)}\rangle = |\Phi_{HF}\rangle$, the first and second order energy corrections of the ground state can be obtained as

$$E_0^{(1)} = \langle\Phi_0^{(0)}|\hat{H}_1|\Phi_0^{(0)}\rangle = \langle\Phi_{HF}|\hat{H}_1|\Phi_{HF}\rangle \tag{1.28}$$

$$E_0^{(2)} = \sum_{n>0} \frac{|\langle\Phi_n^{(0)}|\hat{H}_1|\Phi_0^{(0)}\rangle|^2}{E_0^{(0)} - E_n^{(0)}} = -\sum_{a>b,i>j} \frac{|\langle\Phi_{ij}^{ab}|\hat{H}_1|\Phi_{HF}\rangle|^2}{\epsilon_a + \epsilon_b - \epsilon_i - \epsilon_j}, \tag{1.29}$$

with $\epsilon_a + \epsilon_b - \epsilon_i - \epsilon_j = E_0^{(0)} - E_n^{(0)}$ being the energy difference between two eigenstates of the Fock operator $\hat{f}$ with $|\Phi_n^{(0)}\rangle = |\Phi_{ij}^{ab}\rangle = a_a^\dagger a_b^\dagger a_i a_j |\Phi_{HF}\rangle$ (spin index omitted for brevity). It is worth noting that in the MPPT the sum of the zero and first order energy correction equals the HF energy, $E_{HF} = \langle\Phi_0^{(0)}|\hat{f} + \hat{V}_{eff}|\Phi_0^{(0)}\rangle = E_0^{(0)} + E_0^{(1)}$. The second order energy expression results form the first order wavefunction correction

$$|\Phi_n^{(1)}\rangle = \sum_{k\neq n} \frac{\langle\Phi_k^{(0)}|\hat{H}_1|\Phi_n^{(0)}\rangle}{E_n^{(0)} - E_k^{(0)}} |\Phi_k^{(0)}\rangle . \tag{1.30}$$

Since $E_0^{(0)} < E_k^{(0)}$ except for degenerate states, the second order energy correction (MP2) always lowers the total energy. In the case of equal energies Eq. (1.29) will diverge. However, it is possible to diagonalize the perturbation $\hat{H}_1$ in this degenerate subspace and obtain a new basis in which these degeneracies are—hopefully—lifted.

If the initial guess $\hat{H}_0$ is already a good description of the composite system $\hat{H}$, perturbation theory is able to obtain very accurate results, since λ is actually a small parameter. Additionally, due to the favourable scaling, energy corrections up to fourth[172] (MP4) and fifth order[261] (MP5) are feasible and PT is size-consistent and size-extensive in any expansion order.[109] Perturbation theory however is limited to single-reference systems with weak correlation, since, if $\hat{H}_0$ is far from the exact description and no small parameter λ can be found to expand the series (1.27), PT is bound to fail.

1.7.4 The Coupled Cluster Approach

In the Coupled Cluster (CC) method[237,285,337,338] the ground state wavefunction of (1.4) is expressed as an exponential Ansatz

$$|\Psi_{CC}\rangle = \mathrm{e}^{\hat{T}} |\Phi_0\rangle \tag{1.31}$$

with $|\Phi_0\rangle$ being a reference function, usually the HF solution, and $\hat{T} = \hat{T}_1 + \hat{T}_2 + \ldots$ is the cluster operator with single, double, ... excitation operators, e.g. $\hat{T}_1 = \sum_{ia} t_i^a\, a_i^\dagger a_a$ (spin index omitted). To obtain the ground states energy E_0 and amplitudes $t_i^a, t_{ij}^{ab}, \ldots$ the following set of nonlinear equations are solved

$$\langle\Phi_0|\mathrm{e}^{-\hat{T}}\,\hat{H}\,\mathrm{e}^{\hat{T}}|\Phi_0\rangle = E_0, \qquad \langle\Phi^*|\mathrm{e}^{-\hat{T}}\,\hat{H}\,\mathrm{e}^{\hat{T}}|\Phi_0\rangle = 0, \tag{1.32}$$

with $|\Phi^*\rangle$ being a certain excitation from the reference function (e.g. $|\Phi_i^a\rangle$ to obtain the singles amplitude t_i^a). In contrast to the CI method the CC approach is inherently size-consistent and size-extensive due to the exponential Ansatz (1.31), as it guarantees a multiplicative separable wavefunction.

Considering all cluster operators in $\hat{T}$ corresponds to the full solution in CC theory, but is computationally not affordable, except for systems we can solve exactly anyway. Truncating the cluster operator to only singles $\hat{T}_1$ and doubles $\hat{T}_2$ (CCSD) scales as n^6, with n being the number of spatial orbitals and is thus applicable for far larger systems. Additionally, due to the exponential Ansatz, every truncated CC scheme still contains contributions of *all* determinants of the system and it remains size-consistent.

Including triple excitations (CCSDT) already scales as n^8, which gets prohibitively hard for large systems. But it is possible to approximately include the effect of triples via perturbative corrections (CCSD(T)), scaling as n^7, with provides very accurate correlation energies and is often stated as the *gold standard* of quantum chemistry. However, due to the Ansatz (1.31) the CC method is an inherently *single reference* method and generalizing it to the multi-reference case is a very nontrivial task. Because of that CC fails for systems with strong static correlation and multiple equally important states in the ground state solution.

1.7.5 Density Matrix Renormalization Group

The density matrix renormalization group (DMRG)[354,355] approach is quite different from the methods introduced up until now. Instead of the linear or exponential expansion in Slater determinants, in DMRG the N-electron wavefunction is expanded as a *matrix product state* (MPS)[84,227,339]

$$|\Psi_{MPS}\rangle = \sum_{\{n\}} \mathrm{Tr}\left[A_1^{(n_1)} A_2^{(n_2)} \dots A_N^{(n_k)}\right] |n_1 n_2 \dots n_k\rangle \,, \tag{1.33}$$

where $A_i^{(n_i)}$ are matrices of order M and $|n_1 \dots n_k\rangle$ is the occupation number representation of a Slater determinants with $\sum_i^n n_i = N$. Hence the coefficients in the expansion are no usual c-numbers, but instead a correlated product of matrices. It is based on the idea of separating a super-system AB into two subsystems A and B and expressing $|\Psi\rangle$ as a tensor product

$$|\Psi\rangle = \sum_{i_A, j_B} \Psi_{i_A, j_B} |i\rangle_A |j\rangle_B \,, \tag{1.34}$$

where $|i\rangle_A$ and $|j\rangle_B$ are orthonormal product bases of A and B[276] and coefficients Ψ_{i_A, j_B}. The matrix dimension M of $A_i^{(n_i)}$ is truncated based on the eigenvalues ω of the reduced

density matrix

$$\hat{\rho}_A = \mathrm{Tr}_B \left|\Psi\right\rangle \left\langle\Psi\right|, \quad (\rho_A)_{ik} = \sum_{j_B} \Psi_{i_A,j_B} \Psi^*_{k_A,j_B}, \tag{1.35}$$

where the trace runs over the degrees of freedom of system B. The eigenvectors of (1.35) with an eigenvalue ω above a chosen threshold δ are used as basis function for system A, limiting the used matrix dimension M. This procedure is performed iteratively by "sweeping" over the super-system AB, separating it into variable sized subsystems A and B, optimizing the description of the system contained in the bases $\left|i\right\rangle_A$ and $\left|j\right\rangle_B$ across the boundary between A and B, until convergence is reached. This is equivalent to variationally minimizing the energy

$$E_{DMRG} = \frac{\langle\Psi_{MPS}|\hat{H}|\Psi_{MPS}\rangle}{\langle\Psi_{MPS}\,|\,\Psi_{MPS}\rangle} = \mathrm{Tr}\,\hat{\rho}\,\hat{H}, \tag{1.36}$$

in the space of matrix product states.[277] DMRG is thus able to reduce the effective degrees of freedom to the most important one by iteratively optimizing the matrices $A_i^{(n_i)}$ and truncating the matrix dimension M by keeping only states with eigenvalues of the density matrix ρ above a chosen threshold.

The success of the DMRG approach, especially in one-dimensional systems, comes from the fact that the ground state of a local, gapped Hamiltonian in 1D is in the comparable tiny Hilbert space sector with an *area law of entanglement*.[127] This means the entanglement between subsystem A and B of super-system AB given by the von Neumann entropy

$$S_A = -\,\mathrm{Tr}(\rho_A \ln_2 \rho_A) = S_B = -\,\mathrm{Tr}(\rho_B \ln_2 \rho_B) \tag{1.37}$$

grows with the *area* of the surface separating system A and B and not with the volume. It can be shown that due to the matrix structure of the coefficients in (1.33) MPS represent a state following an area law of entanglement.[80] However, the necessary size M of the matrices $A_i^{(n_i)}$ in the expansion (1.33) grows exponentially with the von Neumann entropy $M \sim \mathrm{e}^{S_{A,B}}$.

For 1D systems the area of the boundary between two subsystems is *constant*, independent of the total system size, thus the necessary M is constant and this allows DMRG to be applied to these systems for sizes unreachable with other methods. However, for dimensions larger than one the area of the boundary grows with the total system size and thus DMRG is not as readily applicable as in the 1D case. The exponential growth in the necessary matrix dimension restricts it to smaller system sizes compared to the 1D case. Additionally, since the concept of locality of correlation is an important ingredient in the optimization of the basis states $\left|i\right\rangle_A$ and $\left|j\right\rangle_B$ across the boundary of A and B, DMRG is not easily applicable for itinerant delocalized systems.

1.7.6 Full Configuration Interaction

If all levels of excitations relative to a reference determinant, e.g. $|\Phi_{HF}\rangle$, are taken into account in the CI expansion (1.21), see Sec. 1.7.2, we speak of Full Configuration Interaction (FCI).[164] FCI corresponds to the exact solution in a given single-particle basis. In contrast to a truncated CI calculation, FCI is size-consistent and size-extensive,* as it corresponds to the exact solution in a given basis set and is in addition invariant to any rotation of the spin-orbital basis $\{\phi_k^\sigma\}$.

It is the goal of almost every computational method to come as close as possible to the FCI solution in a given basis set. The major drawback of FCI, however, is its *extremely* unfavourable scaling, which is combinatorial in the number of spatial orbitals n and electrons N, since the Hilbert space size, which is the number of possible determinants—without any symmetry restrictions—, is given by all the possibilities to distribute N electrons in $2n$ orbitals

$$N_{SD} = \binom{2n}{N} = \frac{(2n)!}{N!(2n-N)!}. \tag{1.38}$$

Iterative procedures, like the Lanczos[176] or Davidson[63] method, to obtain the ground state of $\hat{H}$ (1.6) in the FCI expansion are limited to $n = N \approx 18 - 20$. The main bottleneck in these iterative schemes is the memory requirement to store at least two vectors of coefficients of the size of the Hilbert space. However, for system sizes in which the FCI solution is achievable it provides very useful benchmark results, both in accuracy and performance. By exploiting symmetries inherent to the system, mentioned in Sec. 1.3, it is possible to reduce the Hilbert space size by factors of $10 - 100$, but the combinatorial scaling remains.

The main computational method used and studied in this thesis, Full Configuration Interaction Quantum Monte Carlo (FCIQMC), attempts the FCI solution of a problem in a given single-particle basis set. FCIQMC retains the benefits of size-consistency, size-extensivity and orbital invariance of the FCI approach, while avoiding—or at least ameliorating—the unfavourable exponential scaling by a stochastic sampling of the wavefunction, expanded in a finite set of antisymmetrised Slater determinants. In contrast to other computational approaches it does not rely on perturbative techniques and thus is not restricted to single-reference systems and, as it aims for the full orbital-invariant FCI solution, there is no need for a deliberate choice of a chemical relevant active space. Additionally, its formulation does neither rely on concepts of locality nor dimensionality and thus it is also readily applicable to itinerant and multi-dimensional systems. The FCIQMC method is explained in depth in Sec. 2.3, after a general introduction to the stochastic Monte Carlo method in Sec. 2.

*Although strictly speaking size-extensivity is something that is only achieved in the thermodynamic limit.

1.7.7 Explicitly Correlated Methods

It is possible to take the nondifferentiable cusp behaviour of the exact ground state wavefunction (1.18) at electron coalescence, mentioned in Sec. 1.6, directly into account in the Ansatz for $\Psi(\mathbf{r})$. This is achieved by employing *correlating functions* of the interelectronic distance $r_{12} = |\mathbf{r}_1 - \mathbf{r}_2|$ directly in the wavefunction Ansatz. Methods using this approach are called *explicitly correlated methods*[120,129,163,294] and important examples are briefly discussed here. These methods are able to circumvent the slow convergence of the electron correlation energy with the single-particle basis expansion size, due to the poor description of the electron-electron cusp.[145,146,296] According to Kato[156] and Pack and Byers[229] the first-order singlet ($S = 0$) and triplet ($S = 1$) wavefunctions for two electrons have the form[175,294]

$$|\Psi^{(1)}_{S=0}\rangle = \left(1 + \frac{r_{12}}{2}\right)|\Phi_{HF}(r_{12} = 0)\rangle + \mathcal{O}(r_{12}^2), \quad |\Psi^{(1)}_{S=1}\rangle = \left(1 + \frac{r_{12}}{4}\right)\mathbf{r}_{12} \cdot \frac{\partial\,|\Phi_{HF}\rangle}{\partial \mathbf{r}_{12}} + \mathcal{O}(r_{12}^3) \tag{1.39}$$

near the coalescence $r_{12} = 0$. However, within a finite expansion of Slater determinants based on conventional single-particle basis sets, these conditions (1.18, 1.39) cannot be fulfilled. The first explicitly correlated method to account for the nondifferentiable behaviour (1.39) goes back to Hylleraas, who proposed the following form for a two-electron wavefunction

$$|\Psi(r_1, r_2)\rangle = \mathrm{e}^{-\zeta(r_1+r_2)} \sum_{lmn} (r_1^l r_2^m + r_1^m r_2^l)(r_1 - r_2)^n. \tag{1.40}$$

For N electrons, a general *correlator* of all pairs of N electrons

$$\hat{C} = \prod_{i<j}^{N} f(\mathbf{r}_i, \mathbf{r}_j), \quad \text{or} \quad \hat{G} = \sum_{i<j}^{N} f(\mathbf{r}_i, \mathbf{r}_j) \tag{1.41}$$

with $f(\mathbf{r}_i, \mathbf{r}_j)$ being suitable functions of the electron coordinates, can be used to express the ground state as a fully correlated wavefunction

$$|\Psi\rangle = \hat{C}\,|\Phi_0\rangle\,, \quad \text{or} \quad |\Psi\rangle = \mathrm{e}^{\hat{G}}\,|\Phi_0\rangle \tag{1.42}$$

with a suitable reference state $|\Phi_0\rangle$, usually the Hartree-Fock solution $|\Phi_{HF}\rangle$. However this introduces coupled integrals of $3N$ dimension, which restricts this approach to only the smallest of systems.[163]

The *transcorrelated* approach by Boys and Handy,[34–36] based on the work of Hirschfelder,[138] instead uses the non-Hermitian similarity transformed —the so-called transcorrelated —Hamiltonian

$$\tilde{H} = \hat{C}^{-1}\hat{H}\hat{C}, \quad \text{or} \quad \hat{\tilde{H}} = \mathrm{e}^{-\hat{G}}\,\hat{H}\,\mathrm{e}^{\hat{G}}, \tag{1.43}$$

which involves only integrals up to three electrons at most for *ab-initio* systems. Similar concepts applied to lattice systems are the basis of our explicitly correlated approach to

compress the information stored in the ground state wavefunction, which are explained in detail in Chapter 5.

The *R12*-method, introduced in the seminal work of Kutzelnigg,[175] is a hybrid scheme, which uses a conventional SD-based wavefunction expansions augmented by two-electron basis functions. For a two-electron system the R12 wavefunction is expressed as*

$$|\Psi\rangle = (1 + \lambda\, \hat{Q}_{12}\, r_{12})\, |\Phi_{HF}\rangle + \sum_{ijab} c_{ij}^{ab}\, |\Phi_{ij}^{ab}\rangle\,, \quad \text{with} \quad |\Phi_{ij}^{ab}\rangle = a_a^\dagger a_b^\dagger a_i a_j\, |\Phi_{HF}\rangle\,, \tag{1.44}$$

where λ and c_{ij}^{ab} are parameters to be optimized and $\hat{Q}_{12}$ is the *strong* orthogonality projector, which keeps $r_{12}\,|\Phi_{HF}\rangle$ orthogonal to $|\Phi_{HF}\rangle\,, |\Phi_i^a\rangle$ and $|\Phi_{ij}^{ab}\rangle$. Ten-no[320,321] introduced a modification of the R12-method, called *F12*-method, by introducing the correlating function $f(r_{12}) = -\gamma^{-1}\exp(-\gamma r_{12})$, with γ to be optimized, instead of the linear $f(r_{12}) = r_{12}$ used in the R12-method (1.44).

The general correlation function $\hat{G}$ used in the transcorrelated method (1.41) is also employed in the field of variational Monte Carlo (VMC) as the *Jastrow factor*,[148] where the functions $f(\mathbf{r}_i, \mathbf{r}_j)$ are optimized to variationally minimize the expectation value[47,91]

$$E(f) = \min_f \frac{\langle \Phi_0 | \mathrm{e}^{\hat{G}}\, \hat{H}\, \mathrm{e}^{\hat{G}} | \Phi_0 \rangle}{\langle \Phi_0 | \mathrm{e}^{2\hat{G}} | \Phi_0 \rangle}. \tag{1.45}$$

The VMC method will be explained in more detail in Sec. 2.2.1 and the use of Jastrow factors and other correlators in Chapter 5.

*Spin index omitted for brevity.

2 The (Quantum) Monte Carlo Method

The *Monte Carlo* (MC) method* is a broad class of computational algorithms that utilize *randomness* to solve problems of deterministic nature. It was invented by Ulam, von Neumann and Metropolis during their work on the Manhattan project at the Los Alamos National Laboratory.[209] It has a wide applicability in problems of optimization, numerical integration and random drawing from probability distributions[173] in the fields of physics, business, engineering and mathematics. Based on the law of large numbers the MC method is applicable to any problem that has a probabilistic interpretation.

2.1 The Monte Carlo Method

The main idea of the MC method is to use random events and their outcome as a means to study interesting phenomena and draw conclusions to solve problems, which may be too difficult to solve deterministically. An illustrative example is the determination of π by dropping random points on an unit square. Imagine a square and its inscribed quadrant, as depicted in Fig. 2.1; if points $\mathbf{r}_i = (x_i, y_i)$ are scattered at random over the square, the ratio of points inside the quadrant with $|\mathbf{r}_i| < 1$ and the total distributed points will be an estimate of the ratios of the two areas, which is $\pi/4$. This example illustrates the use of random sampling to evaluate the definite integral[153]

$$\frac{\pi}{4} = \int_0^1 \int_0^{\sqrt{1-x^2}} dxdy, \tag{2.1}$$

*The name actually refers to the famous casino in Monaco.[205, 208]

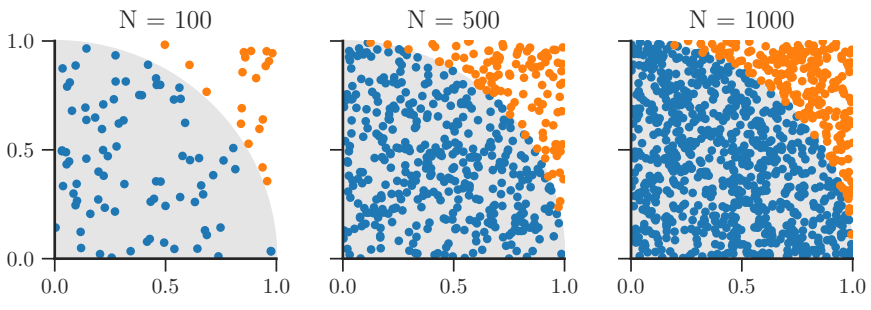

Fig. 2.1: Example of the estimation of π by measuring the ratio of M randomly scattered points inside a unit quadrant and the total number of points.

by *Monte Carlo integration*. The accuracy of the estimate of (2.1) depends on the number of random points M and usually in MC calculations a large amount of data points are necessary for a reasonable estimate. However, in contrast to deterministic integration techniques that evaluate the integrand on a regular grid, MC integration does not suffer from the *curse of dimensionality*[17,258] for multidimensional integrals, as the integrand is evaluated at randomly chosen points with a polynomial scaling computational cost with the dimension of the problem. In a naive MC approach a multidimensional finite integral

$$I = \int_\Omega f(\mathbf{r}) d\mathbf{r}, \quad \text{with volume} \quad V = \int_\Omega d\mathbf{r} \quad \text{and} \quad \Omega \subset \mathbb{R}^m \tag{2.2}$$

is evaluated at M independent, uniformly distributed, randomly chosen points $\mathbf{r}_1, \mathbf{r}_2, \ldots, \mathbf{r}_M \in \Omega$. If the chosen $\mathbf{r}_i$ are truly random and independent, $f(\mathbf{r}_i)$ can be interpreted as a random variable and its *expected* value can be estimated by the *sample mean* of independent samples

$$I \approx I_M = \frac{V}{M} \sum_i^M f(\mathbf{r}_i) = V \langle f \rangle, \quad \text{with} \quad \lim_{M\to\infty} I_M = I, \tag{2.3}$$

due to the *law of large numbers*.[18,292] According to the central limit theorem I_M is normally distributed so the variance of I_M can be estimated by the sample mean of the *sample variance* σ_M^2

$$\begin{aligned} \sigma_M^2 &= \frac{1}{M-1} \sum_i^M (f(\mathbf{r}_i) - \langle f \rangle)^2 = \frac{1}{M-1} \sum_i^M \left(f(\mathbf{r}_i)^2 - 2 f(\mathbf{r}_i) \langle f \rangle + \langle f \rangle^2 \right) \\ &= \langle f^2 \rangle - \langle f \rangle^2 \quad \rightarrow \quad \mathrm{Var}(I_M) = \frac{V^2}{M^2} \sum_i^M \sigma_M^2 = V^2 \frac{\sigma_M^2}{M}. \end{aligned} \tag{2.4}$$

Consequently the statistical *error* estimate of I_M is given by the *standard error of the mean*

$$\delta I_M \approx \sqrt{\mathrm{Var}(I_M)} = V \frac{\sigma_M}{\sqrt{M}}, \tag{2.5}$$

which decreases as $M^{-1/2}$ with the number of samples. The strength of the MC approach is that δI_M does not depend on the dimensionality m of the integral, but just on the number of samples M. So the cost of a MC integration to achieve a desired accuracy is only determined by the cost to evaluated $f(\mathbf{r}_i)$ at the randomly sampled points. Results arbitrarily close to the exact one are obtainable by an increase of the number of sampled points. The accuracy of deterministic methods on the other hand depend exponentially on m, due to the evaluation of the integrand on a regular grid, leading to the aforementioned curse of dimensionality.[153]

2.1.1 Importance Sampling

An efficient modification of the basis MC scheme to decrease the variance of the estimate I_M is the concept of *importance sampling*.[151] Instead of choosing the random sampling points $\mathbf{r}_i$ uniformly, they are drawn from a *probability distribution* $p(\mathbf{r})$, with $p(\mathbf{r}) \geq 0$ and $\int_\Omega p(\mathbf{r})d\mathbf{r} = 1$, which in the optimal case mimics the integrand $f(\mathbf{r})$ of Eq. (2.2). A naive MC approach without some sort of importance sampling in general provides very poor estimates with large variances. The idea is to draw more samples in the "important" region of $f(\mathbf{r})$ and thus increasing the efficiency and decreasing the variance of the MC sampling. With $\mathbf{r}_i \in \Omega$ randomly drawn from $p(\mathbf{r})$ the MC estimator for the integral (2.2) is given by

$$I_M = \frac{1}{M}\sum_i^M \frac{f(\mathbf{r}_i)}{p(\mathbf{r}_i)}, \quad \text{with the modified} \quad I = \int_\Omega \frac{f(\mathbf{r})}{p(\mathbf{r})} p(\mathbf{r})d\mathbf{r}, \tag{2.6}$$

where the "naive" approach is recovered for a constant $p(\mathbf{r}_i) = 1/V$. A simple example is to choose normally distributed points $\mathbf{r}_i$ for the integration of Gaussian function. In practice the choice of $p(\mathbf{r})$ is a delicate one and depends on the problem at hand. Depending on the form of $p(\mathbf{r})$, drawing random samples from the distribution can be a challenging task, since the normalization of $p(\mathbf{r})$ might be difficult to calculate, which could cause the MC approach to lose its favourable scaling, purely by the complicated sampling of $p(\mathbf{r})$.

2.1.2 Markov Chains and the Metropolis-Hastings Algorithm

A flexible and computationally cheap way to generate random samples $\mathbf{r}_i$ according to any probability distribution $p(\mathbf{r})$ is achieved by constructing a *Markov chain*[201] with a stationary distribution $\pi(\mathbf{r})$ equal to $p(\mathbf{r})$ via the *Metropolis-Hastings* algorithm[128,208] used in Markov Chain Monte Carlo (MCMC) methods. A Markov chain is a series of events, $(x_1, x_2, \dots)$ in which the probability of each subsequent event $p(x_{i+1})$ only depends on the current state x_i but not on the previous events *. A Markov chain has an asymptotic stationary distribution $\pi(\mathbf{r})$, if the transition probability between two states $p(\mathbf{r}'|\mathbf{r})$ fulfils the *detailed balance* condition[267]

$$\pi(\mathbf{r})p(\mathbf{r}'|\mathbf{r}) = \pi(\mathbf{r}')p(\mathbf{r}|\mathbf{r}'). \tag{2.7}$$

$\pi(\mathbf{r})$ is *unique*, if the Markov chain is *ergodic*, requiring aperiodicity (the same state $\mathbf{r}_i$ is not reached in fixed intervals) and that the number of steps for returning to the same state is finite, for all states $\mathbf{r}_i$. The Metropolis-Hastings algorithm ensures the detailed balance and ergodicity conditions and creates a Markov chain with the stationary distribution

*This feature is often described as the "memorylessness" of a Markov chain

$\pi(\mathbf{r}) = p(\mathbf{r})$. This is achieved by separating the transition probability into a *proposal* probability $g(\mathbf{r}'|\mathbf{r})$ of a new state $\mathbf{r}'$ given $\mathbf{r}$ and the *acceptance* probability $A(\mathbf{r}'|\mathbf{r})$ of this new state

$$p(\mathbf{r}'|\mathbf{r}) = g(\mathbf{r}'|\mathbf{r})A(\mathbf{r}'|\mathbf{r}). \tag{2.8}$$

The choice of $A(\mathbf{r}'|\mathbf{r})$ by Metropolis[208] is

$$A(\mathbf{r}'|\mathbf{r}) = \min\left(1, \frac{p(\mathbf{r}')\, g(\mathbf{r}|\mathbf{r}')}{p(\mathbf{r})\, g(\mathbf{r}'|\mathbf{r})}\right) \tag{2.9}$$

to accept state $\mathbf{r}'$ as a new state or otherwise retain $\mathbf{r}$ as the new state. The choice of the acceptance probability (2.9) ensures the detailed balance condition with $p(\mathbf{r})$ as the stationary distribution of the Markov chain

$$p(\mathbf{r})p(\mathbf{r}'|\mathbf{r}) = p(\mathbf{r}')p(\mathbf{r}|\mathbf{r}'). \tag{2.10}$$

Since only the ratio $p(\mathbf{r}')/p(\mathbf{r})$ is necessary in the evaluation of Eq. (2.9) the possibly complicated calculation of the normalization of $p(\mathbf{r})$ is avoided and thus any probability distribution can be sampled efficiently via the Metropolis-Hastings algorithm. However, everything comes with a price and the drawbacks of the Metropolis algorithm are that the stationary distribution only asymptotically reflects the targeted probability distribution and successive samples from the Markov Chain are in general *correlated*. These "auto-correlations" modify the statistical error to $\sqrt{2\tau_A + 1}\delta I_M$, with τ_A being the integrated autocorrelation time.[327] Thus, a careful equilibration and correlation length analysis must be performed to ensure correct, statistically independent samples.[153] In practice this can be done by performing e.g. a blocking analysis[92,157] on the possibly correlated samples.

The computation of a multidimensional integral with the MCMC method is realized by an ensemble of "*walkers*"* that perform a *random walk* in the m-dimensional space Ω. The integrand is evaluated at each position the walkers reach and moves to new positions are accepted according to Eq. (2.9) with a reasonable chosen proposal probability.

2.2 Bringing Quantum into Monte Carlo

The application of the MC method is by no means restricted to the evaluation of multidimensional integrals, simulating random walks and not even to the realm of classical physics. The basic notion of using repeated sampling of randomly chosen events to obtain statistical properties of a problem of interest can be readily applied to study systems of quantum-mechanical nature and lead to a multitude of different flavours of quantum

*A concept which will again be used in the Full Configuration Interaction Quantum Monte Carlo method, see Sec. 2.3.

Monte Carlo (QMC) methods. The application of a stochastic method to solve problems, which are by the very foundation of physics of nondeterministic nature, actually seems like a very natural combination.

As mentioned in Sec. 2.1 the cost of a MC simulation depends on the effort it takes to evaluate the integrand in question. In quantum mechanics the N-body wavefunction $\Psi(\mathbf{r})$ contains every information needed to describe a physical state. Thus, MC approaches to quantum systems, usually involve evaluation of $\Psi(\mathbf{r})$ at randomly chosen points $\mathbf{r}$, which in general scales as $\mathcal{O}(N^3)$, with N being the number of electrons of a system. This favourable *polynomial scaling* is the great advantage of the QMC approach.

However, especially due to the antisymmetry property of fermions or geometric frustration, there are a few caveats. The *fermion sign problem* prohibits a general polynomially scaling solution with the QMC approach applicable to all different sorts of quantum mechanical problems[327] and creative and elegant solutions have to be found to circumvent this for specific problems. The sign problem will be mentioned in the sections below and discussed in more detail in Sec. 2.2.6.

2.2.1 The Variational Monte Carlo Method

The most obvious application of the MC approach to quantum mechanical problems is the evaluation of the integral expression of the variational energy

$$E_{var} = \frac{\langle \Psi_T | \hat{H} | \Psi_T \rangle}{\langle \Psi_T \,|\, \Psi_T \rangle} = \frac{\int \Psi_T^*(\mathbf{r}) \hat{H} \Psi_T(\mathbf{r}) d\mathbf{r}}{\int |\Psi(\mathbf{r})|^2 d\mathbf{r}} \geq E_0, \tag{2.11}$$

realised in the *variational Monte Carlo* (VMC) method[49] for some trial wavefunction $|\Psi_T\rangle$ and $\hat{H}$ being the nonrelativistic Hamiltonian in the Born-Oppenheimer approximation (1.5) defined in Sec. 1.2 *. By defining the probability density $p(\mathbf{r})$ and *local energy* $E(\mathbf{r})$ as

$$p(\mathbf{r}) = \frac{|\Psi_T(\mathbf{r})|^2}{\int |\Psi(\mathbf{r})|^2 d\mathbf{r}} \quad \text{and} \quad E(\mathbf{r}) = \Psi_T(\mathbf{r})^{-1} \hat{H} \Psi_T(\mathbf{r}), \tag{2.12}$$

Eq. (2.11) can be expressed as

$$E_{var} = \int E(\mathbf{r}) p(\mathbf{r}) d\mathbf{r} = \langle E(\mathbf{r}) \rangle \geq E_0. \tag{2.13}$$

An estimate of E_{var} can be obtained by drawing independent values of $\mathbf{r}_i$ sampled from $p(\mathbf{r})$, e.g. via the Metropolis-Hastings algorithm (see Sec. 2.1.2), and evaluation of the local energy $E(\mathbf{r}_i)$. However, the quality of E_{var} strongly depends on the chosen reference function $|\Psi_T(\mathbf{a})\rangle$ that is chosen as a function of one or multiple variational parameter(s) $\mathbf{a}$, which are optimized to minimize E_{var}. The stochastic ingredient in VMC is the evaluation

*Although in principle *any* Hamiltonian can be used.

of the integral expression (2.11) via Monte Carlo integration. A popular Ansatz for the trial wavefunction is to include a so-called *Jastrow factor* $\mathrm{e}^{\hat{\tau}}$[49]

$$|\Psi_T(u)\rangle = \mathrm{e}^{\hat{\tau}} |\Phi_0\rangle = \mathrm{e}^{\sum_{i<j} u(r_{ij})} |\Phi_0\rangle \,, \tag{2.14}$$

where $|\Phi_0\rangle$ is a mean-field solution, such as the Hartree-Fock state, and $u(r_{ij})$ is the to-be-optimized function of the distance between pairs of particles. This Ansatz explicitly accounts for two-particle correlations, see Sec. 1.7.7.

An advantage in the VMC approach is the great flexibility in the choice of the trial wavefunction $|\Psi_T\rangle$, however at the same time the quality of the obtained variational energy is inherently constrained by its choice and the exact energy is only obtainable if $|\Psi_T\rangle = |\Psi_{ex}\rangle$. If fermionic particles are sampled the nodes $|\Psi_T\rangle = 0$ cause the local energy (2.12) to diverge,[48] but due to the positive definiteness of $p(\mathbf{r})$ the famous *fermion sign* problem, explained in Sec. 2.2.6 does not haunt the VMC approach.

2.2.2 The Projector Monte Carlo Method

A conceptually very different approach to the VMC method is the family of projector Monte Carlo (PMC) methods. In contrast to the reliance on a sensible choice of a trial wavefunction in the VMC approach, PMC methods aim to directly and exactly obtain the lowest energy eigenstate(s) of a quantum-mechanical system, described by the Hamiltonian $\hat{H}$. For small enough systems in a finite basis set the exact eigenfunctions of $\hat{H}$ can be obtained deterministically by iterative procedures like the Power or Lanczos method mentioned in Sec. 1.2. However, if the system becomes too big,* or we wish to obtain the solution of the Schrödinger equation in continuous space ((1.2)) deterministic approaches are bound to fail. On the other hand, stochastic implementations of the Power method are able obtain solutions of problems of larger or even *infinite* size as the time-average of random samples. The basic approach of the methods in the PMC family is the repeated application of a projector $\hat{P}(\hat{H}, \Delta\tau)$, which is a function of the Hamiltonian $\hat{H}$ of the system, in discretised intervals $\Delta\tau$ to filter out the ground state contribution from an almost arbitrary starting state $|\Psi_T\rangle$ in the asymptotic limit[332,341]

$$|\Psi_0\rangle = \lim_{n\to\infty} \hat{P}^n(\hat{H}, \Delta\tau) |\Psi_T\rangle \,. \tag{2.15}$$

Different flavours of PMC methods are based on various forms of $\hat{P}$. They are characterized by if $|\Psi_T\rangle$ and $|\Psi_0\rangle$ are expanded in a continuous or finite basis and if $\hat{H}$ is expressed in first or second quantization.[332] As long as PMC methods are applicable—i.e. the system exhibits no sign problem—they are, in theory, able to yield the exact result within

*The word "big" should be taken with a grain of salt, as already a few dozen of electrons can be too "big".

arbitrary accuracy in the asymptotic limit; in other words they are *numerically exact*. (As a side note, the power method is only applicable if the spectrum of $\hat{H}$ is bounded; a restriction that will be fulfilled for all systems studied in this thesis.)

2.2.3 The Diffusion Monte Carlo Method

The Diffusion Monte Carlo (DMC) approach is a PMC method that is similar to the Markov-chain Monte Carlo approach to solve definite integrals by random walks of particles or walkers. The equation to be solved in the DMC approach is the imaginary-time Schrödinger equation

$$\frac{\partial \Psi(\mathbf{r},\tau)}{\partial \tau} = -\hat{H}\Psi(\mathbf{r},\tau), \quad \text{with} \quad \hat{H} = \hat{T}(\mathbf{r}) + \hat{V}(\mathbf{r}), \tag{2.16}$$

with the substitution $t \to i\tau$ in Eq. (1.1) and the short handle $\hat{T}(\mathbf{r})$ for the kinetic energy term and $\hat{V}(\mathbf{r})$ for the Coulomb potential in the *ab-initio* electronic Hamiltonian (1.5).* The similarity of Eq. (2.16) to the diffusion equation[90] led Metropolis and Ulam[209] to the proposition to solve the differential equation (2.16) by an ensemble of walkers randomly diffusing in a discretised time interval $\Delta\tau$ according to the kinetic energy term ∇_i^2 and multiplying or dying governed by the potential $V(\mathbf{r})$[5] in the space of $3N$ coordinates of N particles. Integration of Eq. (2.16) yields the iterative relation

$$\Psi(\mathbf{r},\tau+\Delta\tau) = \mathrm{e}^{-\Delta\tau(\hat{H}-E_S(\tau))}\,\Psi(\mathbf{r},\tau), \tag{2.17}$$

with an adaptive estimate for the ground state energy $E_S(\tau)$. Consequently the projector used in the DMC approach is

$$\hat{P}(\hat{H},\Delta\tau) = \mathrm{e}^{-\Delta\tau(\hat{H}-E_S(\tau))} = \mathrm{e}^{-\Delta\tau(\hat{T}+\hat{V}-E_S(\tau))} \tag{2.18}$$

The short-time propagation is obtained via the convolution integral

$$\Psi(\mathbf{r},\tau+\Delta\tau) = \int G(\mathbf{r},\mathbf{r}',\Delta\tau)\Psi(\mathbf{r}',\tau)d\mathbf{r}', \tag{2.19}$$

which is evaluated by the random walks of the particles. The Green's function

$$G(\mathbf{r},\mathbf{r}',\Delta\tau) = (2\pi\Delta\tau)^{-3N/2}\exp\left(\frac{(\mathbf{r}-\mathbf{r}')^2}{2\Delta\tau}\right)\exp\left(-\frac{\Delta\tau}{2}(V(\mathbf{r})+V(\mathbf{r}')-2E_S(\tau))\right), \tag{2.20}$$

which is obtained via Trotter-Suzuki decomposition of $\mathrm{e}^{-\Delta\tau(\hat{V}+\hat{T})}$ for small timesteps $\Delta\tau$ governs the dynamic of walkers and provides the probability to move from $\mathbf{r}$ to $\mathbf{r}'$.

However, the transition probability between $\langle\mathbf{r}|\hat{P}|\mathbf{r}\rangle$ with Eq. (2.20) is always positive,

*Of course other potentials can also be solved with the DMC method.

which causes a naive DMC implementation to converge to a bosonic solution $|\Psi_0(\mathbf{r})\rangle > 0, \forall \mathbf{r}$, even for fermionic systems.*

The Fixed-node Approximation

To sample fermionic systems with DMC the fixed-node approximation is applied, where the nodal surface ($|\Psi_T(\mathbf{r}')\rangle = 0$) of a trial wavefunction $|\Psi_T(\mathbf{r})\rangle$ is imposed on the sampled wavefunction $|\Psi(\mathbf{r}, \tau)\rangle$. DMC then yields the best possible solution for the given nodal structure, by obtaining the exact solution within each area enclosed by the nodal surface subject to the boundary condition $|\Psi_T(\mathbf{r})\rangle = 0$. However, similar to VMC the quality of the estimated ground state energy then depends heavily on the form of the trial wavefunction $|\Psi_T(\mathbf{r})\rangle$ or more concretely on the nodal surface thereof.

2.2.4 The Green's Function Monte Carlo method

Similar to the DMC approach the Green's function Monte Carlo (GFMC) method yields the ground-sate solution of $\hat{H}$ by the repeated application of the "short-time" propagator[152,341]

$$\hat{P}(\hat{H}, \Delta\tau) = \frac{1}{\mathbb{1} + \Delta\tau(\hat{H} - E_S(\hat{\tau}))}, \tag{2.21}$$

which converges to the ground state of $\hat{H}$ for $\Delta\tau < (E_{max} - E_0)^{-1}$.[325] The iterative equation for the ground state solution in GFMC is given by†

$$|\Psi(\tau + \Delta\tau)\rangle = \Big[\mathbb{1} - \Delta\tau(\hat{H} - E_S(\tau))\Big] |\Psi(\tau)\rangle . \tag{2.22}$$

The GFMC approach can be applied in the continuous space of $3N$ coordinates like DMC, but the many-body wavefunction of interest can also be expanded in an appropriate finite basis set

$$|\Psi(\tau)\rangle = \sum_i c_i(\tau) |C_i\rangle . \tag{2.23}$$

In this finite basis the iterative relation (2.22) for the expansion coefficients $c_i(\tau)$ is given by

$$c_i(\tau + \Delta\tau) = \sum_j G(i, j, \Delta\tau) c_j(\tau), \tag{2.24}$$

where the Green's function G describes the propagation from the basis state i to j and is given by

$$G(i, j, \Delta\tau) = \langle C_i | \mathbb{1} - \Delta\tau(\hat{H} - E_S(\tau)) | C_j \rangle. \tag{2.25}$$

The coefficients $c_i(\tau)$ in the expansion (2.23) are assumed to be positive definite in order to be interpreted as probability densities. This restriction makes the GFMC method not applicable for fermionic systems. The concept of *branching* introduced by Trivedi and

*As the bosonic energy is always lower than the fermionic one.[332]

†We will see this equation again as the basis of the FCIQMC approach.

Ceperley[324,325] avoids configurations with low weight and thus stabilized the exponentially increasing variance in a naive GFMC implementation, which made it applicable to quantum lattice problems.

2.2.5 Auxiliary Field Quantum Monte Carlo

The auxiliary-field quantum Monte Carlo (AFQMC) method[20,48,376] is again a projector MC method to obtain the ground state (2.15), based on the same projector $\hat{P}(\hat{H}, \Delta\tau) = \exp(-\Delta\tau(\hat{H} - E_S))$ as the DMC approach. In contrast to DMC, AFQMC works in second quantized representation and in a finite antisymmetrised Slater determinant basis. As AFQMC calculations are extensively used as reference results for the Hubbard model (1.12) in this work, see Sec. 5.5, the basics of it will be briefly sketched by taking the example of the Hubbard Hamiltonian, although AFQMC is readily applicable to realistic *ab-initio* models.[1,312]

The Hubbard Hamiltonian is the sum of the one-body kinetic energy operator $\hat{T}$ and the two-body, local, on-site Coulomb interaction $\hat{V}$

$$\hat{H} = \hat{T} + \hat{V}, \quad \text{with} \quad \hat{T} = -t \sum_{\langle i,j\rangle,\sigma} a^\dagger_{i\sigma} a_{j\sigma} \quad \text{and} \quad \hat{V} = U \sum_i n_{i\uparrow} n_{i\downarrow}, \tag{2.26}$$

as explained in Sec. 1.4. For small timesteps $\Delta\tau$ the propagator $\hat{P}$ used in AFQMC can be approximated by the Trotter-Suzuki decomposition[314,326]

$$\mathrm{e}^{-\Delta\tau\hat{H}} \approx \mathrm{e}^{-\Delta\tau\hat{T}}\,\mathrm{e}^{-\Delta\tau\hat{V}}, \tag{2.27}$$

without the energy shift E_S for brevity. This approximation introduces the so-called *Trotter error* dependent on the chosen $\Delta\tau$. Since $\hat{T}$ is a one-body operator the exponential of it can be thought of as an orbital rotation, similar as in the Hartree-Fock Ansatz in Sec. 1.5.* The troublesome two-body operator $\hat{V}$ can expressed in terms of one-body operators via the so-called Hubbard-Stratonovich (HS) transformation,[135,136,311] e.g. for a single term in $\hat{V}$

$$\mathrm{e}^{-\Delta\tau U n_{i\uparrow} n_{i\downarrow}} = \mathrm{e}^{-\Delta\tau U (n_{i\uparrow}+n_{i\downarrow})/2} \sum_{x_i=\pm 1} \frac{1}{2}\,\mathrm{e}^{\gamma x_i (n_{i\uparrow}-n_{i\downarrow})}, \tag{2.28}$$

with the random *auxiliary-field* variables x_i. The HS transformation thus replaces the two-body interaction by one-body interactions, which can be thought of as replacing one interacting system by many noninteracting ones in random external auxiliary fields.[215] A two-body operator that can be written as a sum of squares of one-body operators $\hat{v}_i$, like

*However in this case this does not represent a unitary transformation, which causes the single-particle orbitals to lose orthogonality in AFQMC.

$\hat{V}$ in (2.26), can be decomposed by the HS transformation[215]

$$\hat{V} = \frac{1}{2}\sum_i \gamma_i \hat{v}_i^2 \quad \rightarrow \quad \mathrm{e}^{-\Delta\tau\gamma_i\hat{v}_i/2} = \frac{1}{\sqrt{2\pi}}\int \mathrm{e}^{-x^2/2}\,\mathrm{e}^{x\sqrt{-\Delta\tau\gamma_i}\hat{v}_i}\,dx \tag{2.29}$$

with the continuous auxiliary-field variable x, for every operator $\hat{v}_i$. If the collection of *all* auxiliary-field variables for all operator is denoted as $\mathbf{x}$ and the one-body operator $\hat{T}$ and the transformed two-body operator are combined into $\hat{B}(\mathbf{x})$, the projector used in AFQMC can be expressed as

$$\mathrm{e}^{-\Delta\tau\hat{H}} = \int \hat{B}(\mathbf{x})p(\mathbf{x})d\mathbf{x}, \tag{2.30}$$

where $p(\mathbf{x})$ is the probability density function (PDF) given by the multidimensional Gaussian from the first term in the integral of (2.29). The ground-state solution is then obtained by an iterative evaluation of

$$|\Psi(\tau+\Delta\tau)\rangle = \int d\mathbf{x}p(\mathbf{x})\hat{B}(\mathbf{x})\,|\Psi(\tau)\rangle\,, \tag{2.31}$$

where the wavefunction is approximated by a finite ensemble of walkers, randomly propagating in the space of Slater determinants

$$|\Psi(\tau)\rangle \approx \sum_i c_i(\tau)\,|\Phi_i(\tau)\rangle\,, \tag{2.32}$$

governed by Eq. (2.31) and with assigned weight $c_i(\tau)$. For a given walker on state $|\Phi_i(\tau)\rangle$, an auxiliary-field configuration $\mathbf{x}$ is drawn from the PDF $p(\mathbf{x})$, e.g. via the Metropolis-Hastings algorithm (see Sec. 2.1.2), and the walker is then propagated to a new state $|\Phi_i(\tau+\Delta\tau)\rangle = \hat{B}(\mathbf{x})\,|\Phi_i(\tau)\rangle$. Since $\hat{B}(\mathbf{x})$ is not a unitary transformation the states $\{\Phi_i\}$ can lose their orthogonality and a possible reorthogonalization is necessary.

The sign problem in AFQMC and the constrained-path approximation

The sign problem for fermionic systems in AFQMC appears due to the fundamental symmetry between the ground state $|\Psi_0\rangle$ and its negative $-|\Psi_0\rangle$.[375] For any ensemble of SDs $\{|\Phi\rangle\}$ there exists the symmetric $\{-|\Phi\rangle\}$, which is an equivalent MC representation of the ground-state $|\Psi_0\rangle$. The boundary between these degenerate halves of the Slater determinants space $\langle\Psi_0\,|\,\Phi\rangle = 0$ is in general unknown. The problem now is that, due to the random walks, it can happen for a state to land on this boundary $\langle\Psi_0\,|\,\Phi_i(\tau)\rangle = 0$ and thus this state and every further propagation of it, does not contribute to the ground-state solution any more, since

$$\langle\Psi_0\,|\,\Phi_i(\tau)\rangle = 0 \quad \Rightarrow \quad \langle\Psi_0|\mathrm{e}^{-n\Delta\tau\hat{H}}|\Phi_i(\tau)\rangle = 0 \quad \text{for any} \quad n. \tag{2.33}$$

However these walkers still get sampled in the AFQMC approach, since there is no knowl-

edge of the position of this boundary in the random walk. Instead of providing information on the ground state solution, these walkers produce noise in the MC simulation. With increasing propagation time $n\Delta\tau$, the chance for a walk to cross the boundary asymptotically reaches one, thus the ground state signal gets lost and only noise remains.

There are systems, for which the crossing of this boundary is prohibited by symmetry. The most prominent example is the repulsive Hubbard model at half-filling with no spin polarization.[137] In this case the repulsive model can be mapped to an attractive model via a particle-hole transformation with $\langle \Psi_0 \,|\, \Phi_i(\tau) \rangle > 0$ for all i and τ. For the Hubbard model off half-filling AFQMC exhibits a strong sign problem and for a general nonlocal two-body operator—with the Coulomb repulsion of the molecular Hamiltonian as a prime example—the constant γ_i in Eq. (2.29) will be negative, causing complex auxiliary field variables with an even more severe fermionic *phase* problem.[215]

Similar to the fixed-node approximation in DMC, see Sec. 2.2.3, the constrained path (CP) approximation[53,83,372,373] and phase-free formulation[376] avoids the sign/phase problem in AFQMC* by the introduction of a trial wavefunction $|\Psi_T\rangle$. The random walkers are restricted to paths where they always have a positive overlap with the chosen trial wavefunction, $\langle \Psi_T \,|\, \Phi_i(\tau) \rangle > 0$. Similar to DMC this introduces an error associated with the quality of the trial wavefunction to the otherwise numerically exact AFQMC method.† For systems without an inherent sign problem or where a suitable trial wavefunction can be chosen for the CP and phase-free approximation, AFQMC yields excellent results for the ground state energy and other observables of interest.

2.2.6 The Sign Problem in Quantum Monte Carlo

Although already mentioned in the sections above, corresponding to the specific methods, some general thoughts on the *fermionic minus sign* problem, inherent to all QMC approaches, except in a few special cases, should be mentioned. The sign problem of quantum Monte Carlo simulations of a system of fermions stems from the antisymmetry property of fermionic wavefunctions and is encountered when an integral to-be-evaluated by a MC method does not have a positive semi-definite measure.[341] The calculation of any expectation value of an operator $\hat{O}$ can be expressed as

$$\langle \hat{O} \rangle = \frac{\int d\mathbf{r}\, \hat{O}(\mathbf{r}) p(\mathbf{r})}{\int d\mathbf{r}\, p(\mathbf{r})}, \tag{2.34}$$

where we want to interpret $p(\mathbf{r})$ as a probability density function. However, for fermionic systems, due to the sign change of the wavefunction under particle exchange $p(\mathbf{r})$ can in general not be chosen positive-definite—except in a few special cases—and thus not be

*The resulting method is usually just called constrained path quantum Monte Carlo (CPQMC).

†Except the Trotter error associated with the finite timestep $\Delta\tau$, which, however, can be systematically controlled.

interpreted as a probability. A trick to circumvent this problem is to perform importance sampling based on the modified "bosonic" PDF[64]

$$\tilde{p}(\mathbf{r}) = \frac{|p(\mathbf{r})|}{\int d\mathbf{r}\, |p(\mathbf{r})|} \tag{2.35}$$

and regard the expected sign $\langle \hat{s} \rangle$ of $p(\mathbf{r})$ as part of the expectation value

$$\langle \hat{O} \rangle = \frac{\int d\mathbf{r}\, \hat{O}(\mathbf{r}) \mathrm{sign}[p(\mathbf{r})] \tilde{p}(\mathbf{r})}{\int d\mathbf{r}\, \mathrm{sign}[p(\mathbf{r})] \tilde{p}(\mathbf{r})} = \frac{\langle \hat{O}\hat{s} \rangle}{\langle \hat{s} \rangle}, \tag{2.36}$$

with $\hat{s}$ being the sign operator, with $\langle \hat{s}^2 \rangle = 1$. However it is not certain if importance sampling based on the modified bosonic PDF (2.35) captures the correct fermionic physics described by the original $p(\mathbf{r})$. Eq. (2.36) allows MC integration with importance sampling to be applied and if the average sign $\langle \hat{s} \rangle$ is close to unity, $\tilde{p}(\mathbf{r})$ in general is a good estimate of the true $p(\mathbf{r})$. However, sampling according to $\tilde{p}(\mathbf{r})$ breaks down if the average sign vanishes with $\langle \hat{s} \rangle = \epsilon \ll 1$ with a large variance $\sigma_s^2 \approx 1$ causing the relative error

$$\frac{\delta \hat{s}}{\langle \hat{s} \rangle} = \frac{\sqrt{(\langle \hat{s}^2 \rangle - \langle \hat{s} \rangle^2)/M}}{\langle \hat{s} \rangle} = \frac{\sqrt{1 - \langle \hat{s} \rangle^2}}{\sqrt{M}\, \langle \hat{s} \rangle} \approx \frac{1}{\sqrt{M}\epsilon} \tag{2.37}$$

to diverge. This causes large cancellations and statistical fluctuations with large variance in both the numerator and denominator of Eq. (2.36), making an accurate sampling of $\langle \hat{O} \rangle$ impossible in practice.[341]

In addition, according to Troyer and Wiese[327] the value of the sign operator $\langle \hat{s} \rangle$ for a general quantum mechanical system is given by the ratio of the fermionic Z_f and bosonic Z_b partition functions

$$\langle \hat{s} \rangle = \frac{Z_f}{Z_b} = \frac{\int d\mathbf{r}\, p(\mathbf{r})}{\int d\mathbf{r}\, |p(\mathbf{r})|}, \tag{2.38}$$

with Z_f and Z_b given by exponentials of the corresponding free energies f_f and f_b, particle number N and inverse temperature β, $Z_{f/b} \sim \exp(-N\beta f_{f/b})$. This causes Eq. (2.37) to scale exponentially with N and β

$$\frac{\delta \hat{s}}{\langle \hat{s} \rangle} \approx \frac{\mathrm{e}^{N\beta\Delta f}}{\sqrt{M}}, \tag{2.39}$$

with $\Delta f = f_f - f_b > 0$, as the difference of the corresponding fermionic and bosonic free energies. As a consequence the number of necessary measurements M for a desired accuracy of $\langle \hat{s} \rangle$ scales exponentially with particle number and inverse temperature. Hence, for systems with a severe sign problem the favourable polynomial scaling of the MC method is lost. Although there are elegant ways to circumvent the fermionic sign problem for *specific* systems, there is **no single** *general* solution of it applicable to all fermionic systems. This was proven by Troyer and Wiese, who have shown that the general solution of the minus

sign problem falls in the class of *nondeterministic polynomial complete decision problems* (NP-complete).[59] This implies that a general solution of the fermion sign problem in polynomial time would answer one of the millennium problems: $NP \stackrel{?}{=} P$.[58*]

2.3 The Full Configuration Interaction Quantum Monte Carlo Method (FCIQMC)

The main computational method developed, used and studied in this thesis is Full Configuration Interaction Quantum Monte Carlo (FCIQMC). It attempts the exact solution of a problem in a given single-particle basis set, by an efficient sampling of a stochastic representation of the wavefunction—expanded in a discrete antisymmetrised basis of Slater determinants—through the random walk of particles, governed by the Schrödinger equation. FCIQMC retains the benefits of size-consistency, size-extensivity and orbital invariance of the FCI approach, while avoiding—or at least ameliorating—the unfavourable exponential scaling by relying on the MC approach. In contrast to other computational approaches it does not rely on perturbative techniques and thus is not restricted to single-reference systems and, as it aims for the full orbital-invariant FCI solution, there is no need for a deliberate choice of a chemical relevant active space. Additionally, its formulation does neither rely on concepts of locality nor dimensionality and thus it is readily applicable to itinerant and multi-dimensional systems. Opposed to other QMC methods it does not rely on the use of a suitable trial wavefunction, as its formulation in the antisymmetric space of Slater determinants ensures the convergence to the correct fermionic solution. In FCIQMC, the renowned fermion sign problem, haunting QMC approaches in general, is recast to the problem of finding the correct relative sign structure of the antisymmetric basis states in the exponentially scaling Hilbert space.

With all being said, FCIQMC provides a straightforward employment of the stochastic Monte Carlo method to the quantum chemical problem in a very "black-box" manner, as its application only needs the provision of the molecular one- and two-body integrals. At the same time it is equally readily applicable to effective quantum lattice model, such as the Hubbard model, and thus it can be described as being *system-agnostic*.

2.3.1 Derivation of FCIQMC

The Full Configuration Interaction Quantum Monte-Carlo (FCIQMC) approach[30,56] is a projector Monte Carlo method, based on the imaginary-time Schrödinger equation (1.1)

$$\frac{\partial}{\partial \tau}\Psi(\mathbf{r},\tau) = -\hat{H}\Psi(\mathbf{r},\tau) \tag{2.40}$$

*Which is in general believed to be not true.

with $\tau = it$ in atomic units. To avoid the dependence on the N continuous space variables $\mathbf{r}$, the wavefunction $\Psi(\mathbf{r}, \tau)$ is expanded in a finite basis of Slater determinants

$$|\Psi(\tau)\rangle = \sum_i c_i(\tau) \, |D_i\rangle \, . \tag{2.41}$$

By formal integration of Eq. (2.40) the imaginary-time evolution of the system is given by

$$|\Psi(\tau)\rangle = \mathrm{e}^{-\tau \hat{H}} \, |\Psi(\tau = 0)\rangle \tag{2.42}$$

and for small timesteps $\Delta\tau$ the iterative relation

$$|\Psi(\tau + \Delta\tau)\rangle = \mathrm{e}^{-\Delta\tau \hat{H}} \, |\Psi(\tau)\rangle \tag{2.43}$$

holds. If $|\Psi(\tau = 0)\rangle$ is expressed in the eigenfunctions $|\phi_i\rangle$ of $\hat{H}$, with $\hat{H} \, |\phi_i\rangle = E_i \, |\phi_i\rangle$ and the Hamiltonian is shifted by the yet to be determined ground state energy E_0, with $E_0 \leq E_i, \; \forall i$, we obtain

$$|\Psi(\tau = 0)\rangle = \sum_i d_i \, |\phi_i\rangle \quad \rightarrow \quad |\Psi(\tau)\rangle = \sum_i d_i \, \mathrm{e}^{-\tau(\hat{H} - E_0)} \, |\phi_i\rangle = \sum_i d_i \, \mathrm{e}^{-\tau(E_i - E_0)} \, |\phi_i\rangle \, . \tag{2.44}$$

It is obvious that the components of all states $|\phi_i\rangle$ with $E_i > E_0$ in Eq. (2.44) decay exponentially with τ. Consequently, the ground state wavefunction can be obtained in the long time limit

$$|\Psi_0\rangle = \lim_{\tau \to \infty} \mathrm{e}^{-\tau(\hat{H} - E_0)} \, |\Phi\rangle \, , \tag{2.45}$$

with an arbitrary initial state $|\Phi\rangle$ with $\langle \Psi_0 \, | \, \Phi \rangle \neq 0$, as all excited state contributions with $E_i > E_0$ are exponentially suppressed. If the unknown E_0 is replaced with a dynamically adapted energy shift $E_S(\tau)$, the coefficient of the ground state contribution $|\phi_0\rangle$ in (2.44) stays constant as long as $E_S(\tau) = E_0$. While for $E_S(\tau) < E_0$, d_0 will decay and for $E_S(\tau) > E_0$ grow exponentially. This is a consequence of the fact that Eq. (2.42) describes a nonunitary time evolution, due to the replacement $\tau = it$, where the norm of $|\Psi(\tau)\rangle$ is not conserved. However, the observation above suggests, that if $E_S(\tau)$ is adapted to keep the norm of $|\Psi(\tau)\rangle$ constant, $E_S(\tau)$ will converge to E_0 in the long-time limit, if $|\Psi(\tau)\rangle$ is a stationary solution of (2.42).

For small timesteps $\Delta\tau$ the projector $\mathrm{e}^{-\tau(\hat{H} - E_S(\tau))}$ can be approximated by the first-order Taylor expansion and repeated application thereof

$$|\Psi_0\rangle = \lim_{n \to \infty} |\Psi(n\Delta\tau)\rangle = \lim_{n \to \infty} \left[\mathbb{1} - \Delta\tau \left(\hat{H} - E_S(\tau) \right) \right]^n |\Phi\rangle \, , \tag{2.46}$$

also yields $|\Psi_0\rangle$ for $\Delta\tau < 1/E_W$,[325] with $E_W = E_{max} - E_0$ being the spectral width of $\hat{H}$.* FCIQMC stochastically samples Eq. (2.46) in the FCI basis of Slater determinants and

*Note the similarity of the GFMC, see Sec. 2.2.4 and FCIQMC formulation presented here.

obtains a stochastic representation of the FCI wavefunction. However, the full wavefunction is never completely stored, but only sufficiently dynamically sampled to obtain an energy estimate of the ground state energy $\langle E_0 \rangle$.* It does so by introducing the concept of so called "walkers", which are positive or negative entities occupying the antisymmetrised SDs of the FCI Hilbert space, introduced in Sec. 1.7.2 an shown in Fig. 1.5. To avoid the memory bottleneck, due to the exponential scaling FCI Hilbert space size, only states $|D_i\rangle$ occupied by at least one walker $N_i > 1$ in (2.41) are kept in the simulation.† If the total number of these walkers N_w^{tot} is restricted, the maximal memory requirement can be directly controlled. This is achieved by dynamically adapting the shift energy $E_S(\tau)$ in the following way[30]

$$E_S(\tau) = E_S(\tau - A\Delta\tau) - \frac{B}{A\Delta\tau} \ln\left(\frac{N_w(\tau)}{N_w(\tau - A\Delta\tau)}\right), \tag{2.47}$$

where B is a damping parameter, A a predefined number of iteration steps between shift updates and $N_w(\tau)$ the current and $N_w(\tau - A\Delta\tau)$ the walker population A iterations ago. The form of the shift adaptation (2.47) ensure $E_S(\tau)$ does not vary too rapidly, as this can introduce biases in other energy estimators,[333] discussed in Sec. 2.3.4. Adapting $E_S(\tau)$ ensures that the L_1 norm of the wavefunction (2.41), where the coefficients $c_i \propto N_i$, are represented by the number of walkers on each state $|D_i\rangle$, is kept constant. As mentioned above, this ensures $E_S(\tau) \to E_0$ if $\Psi(\tau)$ approaches the stationary ground state (in a stochastic sense).

The formulation in the total antisymmetric space of Slater determinants ensures that a FCIQMC simulation does not converge to the incorrect "bosonic" solution. However, the NP-complete[327] fermionic sign problem is recast to the task of finding the correct relative sign structure of the basis states of the exponentially scaling Hilbert space in FCIQMC. The N_w^{tot} signed walkers follow certain dynamics, which are governed by the working equation for each expansion coefficient $c_i(\tau)$ of (2.41)

$$c_i(\tau + \Delta\tau) = \left(\mathbb{1} - \Delta\tau \left(H_{ii} - E_S(\tau)\right)\right) c_i(\tau) - \Delta\tau \sum_{j \neq i} H_{ij} c_j(\tau). \tag{2.48}$$

2.3.2 The Three Ingredients to FCIQMC

Three main *algorithmic steps* result from Eq. (2.48), which are sampled in a stochastic manner:

Walker death:
The diagonal term in Eq. (2.48) is stochastically realized by the possibility that a walker

*In principle the expectation value of any operator can be sampled to arbitrary accuracy,[310] see Sec. 2.3.5.

†This is sometimes called the *stochastic "snapshot"* of $|\Psi(\tau)\rangle$.

on state $|D_i\rangle$ dies* with the probability

$$p_d = \Delta\tau|H_{ii} - E_S(\tau)|, \quad \text{if} \quad H_{ii} - E_S(\tau) > 0. \tag{2.49}$$

If $p_d > 1$ there is a chance the walker "overdies", meaning it creates a new walker on $|D_i\rangle$ with opposite sign. This fact is detrimental to the stability of the simulation and thus additional to the restriction $\Delta\tau < 1/E_W$, the timestep $\Delta\tau$ should be chosen to restrict $p_d \leq 2$ at least. In an actual calculation this is realized by adapting $\Delta\tau(\tau)$ dynamically to ensure $\Delta\tau(\tau)|H_{ii} - E_S(\tau)| \leq 2$. The topic of dynamic timestep adaptation is explained more detailed in Sec. 2.3.7. If the quantity $H_{ii} - E_S(\tau) < 0$ the walker actually has the possibility to "give birth" to a new walker on the same state with the probability p_d. This is especially useful in the early stages of a simulation, which is generally started with a few walkers on the initial reference determinant, to allow to grow the number of walkers to the chosen N_w^{tot}.

The Spawning event:
The off-diagonal term in Eq. (2.48) is given by the sum $\Delta\tau \sum_{j\neq i} H_{ij}c_j(\tau)$. This sum is sampled stochastically by allowing each walker on a given state $|D_i\rangle$ to create or *spawn* a new walker on a state $|D_j\rangle$ connected by the Hamiltonian matrix element H_{ij}. Since there are many possible connected states $\{D_k\}$ we have to assign a definite probability $p(j|i)$ to the choice of state $|D_j\rangle$ given $|D_i\rangle$ to sample the sum *correctly*. The probability of choosing state $|D_j\rangle$ given $|D_i\rangle$, or in other words generating the excitation $(i \to j)$ is called the *generation probability*. Furthermore it is very beneficial for the *efficiency* to sample large matrix elements H_{ij} more often than smaller ones. In other words $p(j|i)$ should be proportional to $|H_{ij}|$. This makes the *spawning step* and the *excitation generation* of the FCIQMC method the most challenging conceptually and most time consuming computationally and is explained in more detail in Sec. 2.3.8 and its relation to the timestep adaptation in Sec. 2.3.7. The final probability of spawning a new walker to $|D_j\rangle$ from a walker on $|D_i\rangle$ is given by

$$p_s = \Delta\tau \frac{|H_{ij}|}{p(j|i)}. \tag{2.50}$$

The sign of the new walker on $|D_j\rangle$ is given by $-\text{sgn}(H_{ij}) \cdot \text{sgn}(N_i)$. Which leads us to the final ingredient of the FCIQMC algorithm.

The annihilation step:
At the end of an iteration, after all the spawning events from all walkers on all occupied determinants, walkers with opposite sign can end up on the same state. To converge to the correct fermionic solution of the molecular Hamiltonian (1.6),[309] walkers of opposite sign

*A harsh formulation for the rather mundane fact, that this walker gets removed from the simulation.

cancel—or more dramatically *annihilate*—each other and are removed from the simulation. In contrast to the death and spawning steps, which are both embarrassingly parallel, the annihilation step needs communication between the different computing cores if the FCIQMC method is performed in parallel. However, this can be highly optimised and currently our implementation of FCIQMC in the `NECI` code[25] formally scales linearly with the number of walkers N_w.[29] Work on an optimized parallel implementation in collaboration with F. Merz and M. Rampp from the Max Planck Computing and Data Facility (MPCDF) is in progress to scale efficiently up to 10^5 computing cores.* Determinants, which are no longer occupied by any walker, due to either death or annihilation events are not stored in the stochastic representation of $|\Psi(\tau)\rangle$. The three algorithmic steps are visualized in Fig. 2.2.

The *original* FCIQMC implementation[30] shows a very characteristic behaviour in the growth phase of walkers. If the shift is held constant and the walker number is allowed to increase and walkers explore the available Hilbert space through spawning processes, there is a steep initial exponential growth, due to the effect of the projector $\mathrm{e}^{-\tau\hat{H}}$. However, without any external influence, the growth comes to an end by itself, as more and more opposite signed walkers occupy the same states, due to incoherent spawning events, leading to an explosion of annihilation events. In this phase—termed the *annihilation plateau*—death, spawning and annihilation events almost exactly cancel each other and the total walker population stays constant. In this phase the correct sign structure of the sampled ground state wavefunction $|\Psi(\tau)\rangle$ is resolved. After this process is finished, $|\Psi(\tau)\rangle$ resembles the stationary solution of $\hat{H}$ and the further spawning events all happen in a coherent fashion, leading to a second growth phase, which, unless the shift is adapted to control the walker number, would go on forever. This behaviour is shown in Fig. 2.3 with the descriptors "non-init.", which will be explained further in Sec. 2.3.3.

The height of this annihilation plateau N_a, which varies from problem to problem, determines how difficult it is for FCIQMC to obtain correct energy estimates. For some systems it is only a tiny fraction of the Hilbert space size N_{SD},[30] while for others it can be of the same order of magnitude. If $N_w > N_a$ can be sampled, FCIQMC yields the exact FCI energy. However, if $N_w > N_a$ is not feasible, due to computational limitations, the original FCIQMC method is not applicable to these systems.

2.3.3 The Initiator Approximation

To simulate systems with a very high N_a, the initiator approximation[56] to FCIQMC (i-FCIQMC) was introduced. The annihilation plateau can be seen as a consequence of an incoherent growth of walkers, due to an incorrect sign structure of $|\Psi(\tau)\rangle$ in the early stages of a FCIQMC simulation. i-FCIQMC ensures a coherent growth of walkers, by

*Almost optimal scaling up to 10^4 cores is already provided with the current implementation.

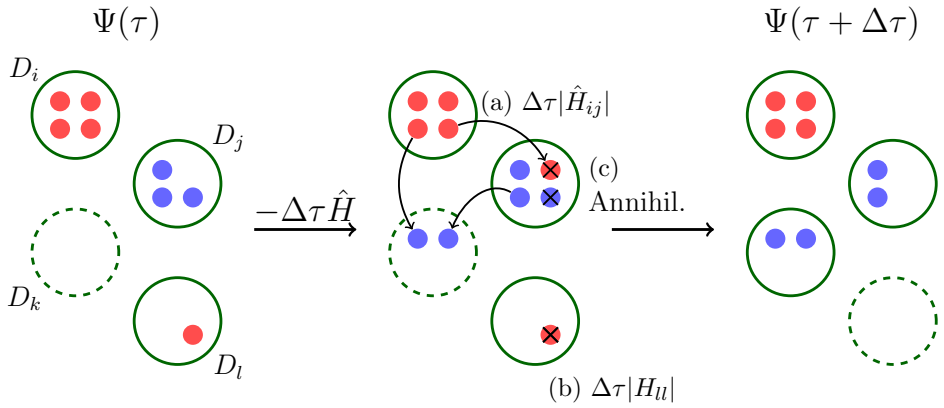

Figure 2.2: Schematic representation of the algorithmic steps in the FCIQMC method. $\Psi(\tau)$ is propagated by the increment $\Delta\tau$ via the application of $\Delta\tau(\mathbb{1} - \hat{H})$ to obtain $\Psi(\tau + \Delta\tau)$. The diagonal term $\mathbb{1}$ is omitted in the figure for brevity. Only an instantaneous representation of Ψ_0 is stored, which is indicated by the dashed circles of the unoccupied state D_k at time τ. States can be occupied by walkers with a positive (red) of negative sign (blue circles). The off-diagonal elements $\hat{H}_{ij}$ induce spawning events (a) with a probability proportional to $\Delta\tau|H_{ij}|$ and the sign of the new walker related to the sign of H_{ij}. The diagonal terms of $\hat{H}$ cause death/birth events (b) with a probability proportional to $\Delta\tau|H_{ii}|$. If walkers with opposite sign occupy the same state, due to spawning events they are annihilated (c) and removed from the simulation. States which are no longer occupied by any walker (due to death or annihilation) are no longer stored, indicated by the dashed circle at time $\tau + \Delta\tau$.

only allowing walkers from certain states $\{D_i^{init}\}$ with a walker population above a chosen threshold n_{init} to spawn new walkers on unoccupied determinants. States satisfying this condition are called *initiators*. The reasoning behind this is, that if a determinant is occupied by at least n_{init} walkers the sign of it should be correctly sampled already, thus spawns from this state are likely to be coherent with the overall sign structure of $|\Psi(\tau)\rangle$. Thus, the initiator approximation corresponds to a dynamic truncation of certain Hamiltonian matrix elements $\langle D_i|\hat{H}|D_j\rangle$ depending on the occupation of the involved determinants. The initiator approximation introduces an uncontrolled error in the FCIQMC method and since it is a projector method and thus not variational, a careful study of energy estimates obtained with i-FCIQMC has to be performed. This can be done by comparing results obtained with an increasing number of total walkers and ensuring the energy is converged, since in the limit of infinite N_w every state will fulfil $N_i > n_{init}$ and i-FCIQMC is equivalent to the original implementation.

The growth phase of the original and i-FCIQMC implementation are quite different. Due to the restriction of spawning, the growth of walkers is less steep, although still exponential, and there is no annihilation plateau phase in i-FCIQMC, as can be seen in Fig. 2.3 (non-init. corresponds to the original and init. to the i-FCIQMC method).

2.3.4 Energy Estimators

As already mentioned, if the shift energy $E_S(\tau)$ is dynamically adapted to keep the walker population constant and if $|\Psi(\tau)\rangle$ is a good estimate of the ground state, $E_S(\tau)$ is a good estimate of the ground state energy E_0. The most obvious way to obtain an energy estimate would be to sample the expectation value

$$E(\tau) = \frac{\langle \Psi(\tau)|\hat{H}|\Psi(\tau)\rangle}{\langle \Psi(\tau)\,|\,\Psi(\tau)\rangle} \tag{2.51}$$

each iteration for the current instantaneous wavefunction $|\Psi(\tau)\rangle$. Although, apart from the huge computational effort, this estimator is biased in the denominator[21] and converges more slowly to the exact result as comparable non-variational estimators.[28] In addition to the adapted shift energy $E_S(\tau)$, the *projected energy*

$$E_P(\tau) = \frac{\langle D_{ref}|\hat{H}|\Psi(\tau)\rangle}{\langle D_{ref}\,|\,\Psi(\tau)\rangle} \approx E_0, \quad \text{if} \quad |\Psi(\tau)\rangle \approx |\Psi_0\rangle\,, \quad \text{with} \quad \hat{H}\,|\Psi_0\rangle = E_0\,|\Psi_0\rangle\,, \tag{2.52}$$

with $|D_{ref}\rangle$ being the most occupied determinant in a simulation, is an estimate for the ground-state energy E_0. Essentially any state could be chosen as the reference state $|D_{ref}\rangle$, but since repeated samples of $E_P(\tau)$ yield a stochastic estimate of the energy, maximizing the denominator of (2.52) will stabilize the results and minimize stochastic fluctuations. Since $\hat{H}$ contains at most two-body operators* only double excitations of $|D_{ref}\rangle$ will contribute directly to $E_P(\tau)$. Due to possible correlations, the numerator and denominator of Eq. (2.52) should be averaged separately. It is worth noting that neither the shift energy, due to the projective nature of FCIQMC, nor the projected energy, as it does not correspond to the expectation value of $\hat{H}$, $\langle \Psi(\tau)|\hat{H}|\Psi(\tau)\rangle$†, are variational. Due to the stochastic nature of these estimators, an error analysis with the blocking algorithm[92,157] is performed on data points obtained after convergence is ensured and an equilibration time is carefully chosen to obtain the final energy estimates.

The projected energy, and FCIQMC in general, provides good estimates for systems dominated by a single configuration, usually the HF result, as the remaining small fraction of correlation energy can be obtained rather easily. However, opposed to other computational approaches, (CC 1.7.4, MPPT 1.7.3), FCIQMC is not inherently constrained to these single-reference systems.

Figure 2.3 shows an exemplary FCIQMC calculation with both the original and initiator approximated version for the neon atom in an aug-cc-pVDZ basis set. The top panel shows the total walker number and reference occupation as a function of imaginary-time τ with the maximum walker number $N_w^{tot} = 10^6$. The original (non-init.) simulation

*Except in the similarity transformed Hamiltonian introduced in Chapter 5.

†Which would be far to costly to calculate directly, but a variational estimator can be obtained via the density matrices, see Sec. 2.3.5

shows the characteristic annihilation plateau phase between $5 < \tau < 40$. The i-FCIQMC calculation, on the other hand, does not exhibit this behaviour, but rather has a constant exponential growth of walkers until $N_w^{tot} = 10^6$ is reached. Attention to the different reference occupations N_{ref} after the shift is adapted should be given. As the i-FCIQMC method restricts the occupation of determinants far out in the Hilbert space relative to $|D_{ref}\rangle$, N_{ref}^{init} is higher than the unrestrictive original implementation. The bottom panel shows the estimated correlation energy obtained via $E_S(\tau)$ and $E_P(\tau)$ for both implementations, compared to the exact FCI result E_{corr}^{ex} obtained with Molpro.[164,167,349,350] $E_S(\tau)$ is initially zero until N_w reaches N_w^{tot}, upon which it is adapted to keep $N_w \approx N_w^{tot}$ constant and converges to the correct E_{corr}^{ex} result. The projected energy agrees well with E_{corr}^{ex} already at the early stage of the calculations. Additionally it shows less statistical fluctuations—which is in general the case—than $E_S(\tau)$, due to the large reference population.

It should be noted $E_S(\tau)$ is a population wide energy estimator, since it depends on the total number of walkers. Whereas $E_P(\tau)$ is more local in character, as it is only directly determined by the reference population and up to double excitations thereof.

The Trial-space Energy

The concept the projected energy estimator can be extended for systems, which show a strong multi-reference character. This is achieved by calculating the projected energy not by projection on a single reference state, but onto a space of N_T determinants $\{D_i^T\}$, called the *trial-space*, with

$$E_T(\tau) = \frac{\langle \Phi_T | \hat{H} | \Psi(\tau) \rangle}{\langle \Phi_T \,|\, \Psi(\tau) \rangle}, \quad \text{with} \quad |\Phi_T\rangle = \sum_i^{N_T} c_i^T \, |D_i^T\rangle \,, \tag{2.53}$$

where the coefficients c_i^T are obtained by diagonalizing $\hat{H}$ in the space spanned by $\{D_i^T\}$. Here the **semi-stochastic** FCIQMC variation[23,248] is worth mentioning. In this approach a part of the Hilbert space, deemed to be of major importance, $\{D_i^{SS}\}$ is propagated deterministically by diagonalizing $\hat{H}$ exactly in this space. This space can consist e.g. of the HF determinant and single and double excitations thereof or just taking the N_{SS} most occupied states after the variable shift mode is entered. This mixed deterministic-stochastic approach—hence the name semi-stochastic—proves to greatly increase the accuracy of the FCIQMC method, as shown in the papers mentioned above. This same deterministic approach is used for the calculation of the trial-space energy, by diagonalizing $\hat{H}$ in the space spanned by $\{D_i^T\}$ to obtain $E_T^{(0)}$. The total trial-space energy is $E_T(\tau) = E_T^{(0)} + E_T^{(1)}$, with $E_T^{(1)}$ being the contributions of $|\Psi(\tau)\rangle$ outside the trial-space, but with a non-vanishing overlap $\langle \Phi_T | \hat{H} | \Psi(\tau) \rangle$.

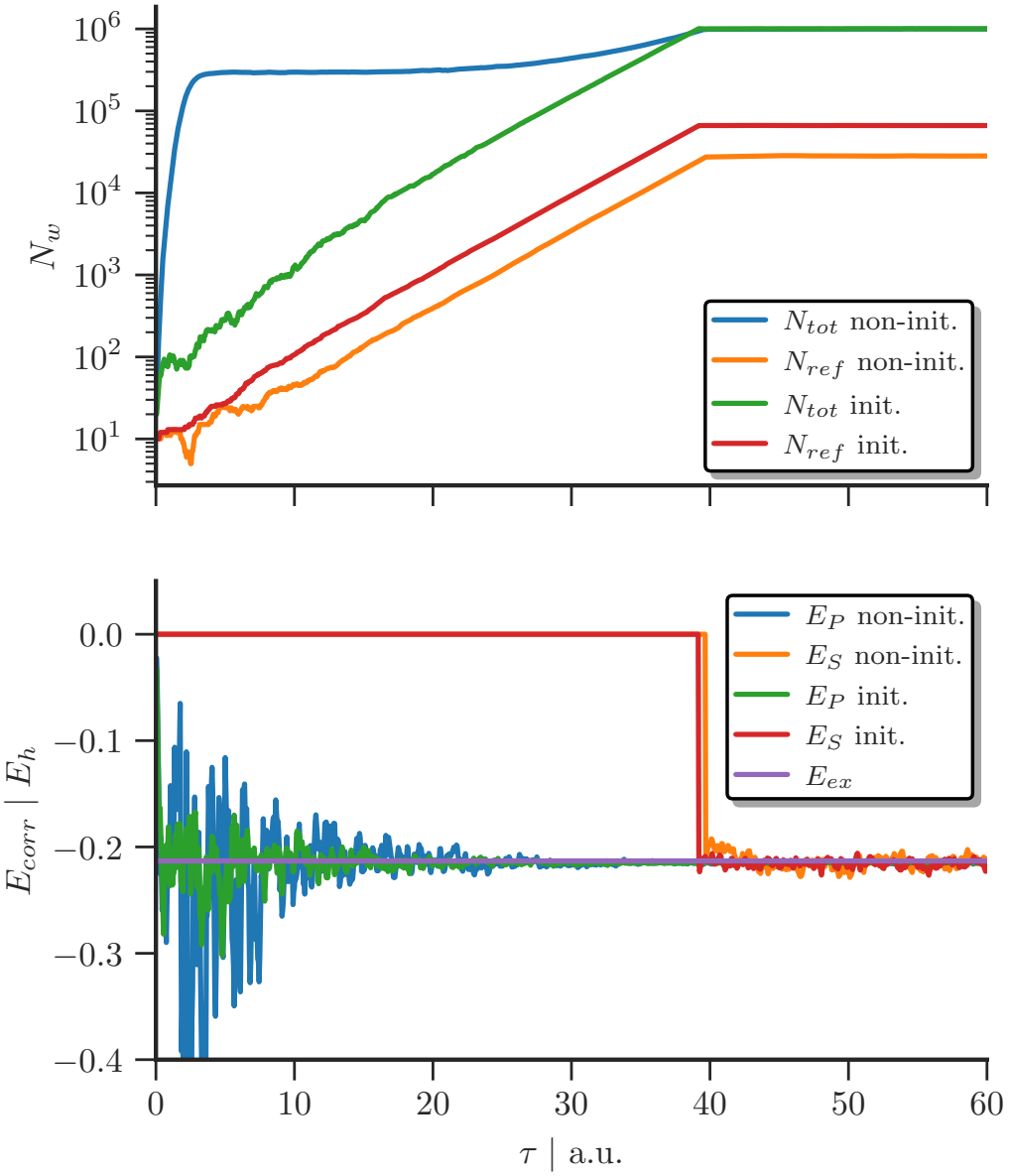

Figure 2.3: The walker dynamics and energy estimators of a non-initiator and i-FCIQMC calculation for the Ne atom in an aug-cc-pVDZ basis set. The top panel shows the total number of walkers and the reference occupation vs. imaginary time. The non-initiator walker number shows the characteristic *annihilation plateau* phase at $5 < \tau < 40$ with a constant walker population albeit constant shift $E_S(\tau)$. The bottom panel shows the projected, $E_P(\tau)$, and shift, $E_S(\tau)$, energy estimators as a function of imaginary time. After the target number of walkers $N_w = 10^6$ is reached $E_S(\tau)$ is adapted to keep N_w constant and fluctuates around the exact E_{ex}. The molecular integral files and exact result were obtained with Molpro[164,349,350]

.

2.3.5 Stochastic Sampling of Density Matrices

The expectation value of any static one- or two-body operator $\hat{Q}$ can be obtained via the one- (1-RDM) and two-body reduced density matrices (2-RDM), defined as (spin index omitted)

$$\gamma_{pq} = \langle \Psi_0 | a_p^\dagger a_q | \Psi_0 \rangle, \qquad \Gamma_{pq,rs} = \langle \Psi_0 | a_p^\dagger a_q^\dagger a_s a_r | \Psi_0 \rangle, \tag{2.54}$$

as the trace of

$$\langle \hat{Q} \rangle = \mathrm{Tr}\left[\mathbf{\Gamma} \hat{Q} \right]. \tag{2.55}$$

The density matrices (2.54) can be obtained with the stochastically sampled FCIQMC wavefunction $|\Psi(\tau)\rangle$[228]

$$\gamma_{pq} = \sum_{ij} c_i c_j \langle D_i | a_p^\dagger a_q | D_j \rangle, \qquad \Gamma_{pq,rs} = \sum_{ij} c_i c_j \langle D_i | a_p^\dagger a_q^\dagger a_s a_r | D_j \rangle, \tag{2.56}$$

by storing the product of coefficients during an excitation process $|D_i\rangle \rightarrow |D_j\rangle$ represented by the instantaneous walker populations N_i and N_j of the involved states. However, since N_i is only a stochastic representation of the "correct" coefficient c_i with an error $N_i = c_i + \delta c_i$, the statistical error of the diagonal terms of (2.54) are biased, due to the always positive $(\delta c_i)^2$. To correct for this bias, the *replica* version of FCIQMC was developed,[228] where two or more independent equivalent simulations* are ran in parallel and the diagonal contributions to (2.54) are computed from the individual calculations a and b. This removes the positive bias, since $N_i^{(a)} N_i^{(b)} = c_i^2 + c_i(\delta c_i^{(a)} + \delta c_i^{(b)}) + \delta c_i^{(a)} \delta c_i^{(b)}$ and the statistical errors of the independent simulations cancel on average. The energy obtained via the RDMs

$$E_{RDM} = \sum_{pq} t_{pq} \gamma_{pq} + \sum_{p>q, r>s} \Gamma_{pq,rs} V_{pqrd} \tag{2.57}$$

is a variational estimate for the ground state energy, $E_{RDM} \geq E_0$.

2.3.6 Excited States within FCIQMC

With the replica method, mentioned in Sec. 2.3.5, it is also possible to calculate excited states with the FCIQMC method.[22] By running n parallel simulations the n-th excited state, $|\Psi_n(\tau)\rangle$, is sampled in FCIQMC by modifying the ground state time-evolution (2.46)

$$|\Psi_n(\tau + \Delta\tau)\rangle = \hat{P}_n(\tau + \Delta\tau) \left[\mathbf{1} - \Delta\tau \left(\hat{H} - E_S^{(n)}(\tau) \right) \right] |\Psi_n(\tau)\rangle \tag{2.58}$$

*With different seeds for the random number generator of course.

with $E_S^{(n)}$ being the energy shift associated with state n and

$$\hat{P}_n(\tau) = \mathbb{1} - \sum_{m<n} \frac{|\Psi_m(\tau)\rangle \langle \Psi_m(\tau)|}{\langle \Psi_m(\tau) \,|\, \Psi_m(\tau)\rangle}, \quad E_m < E_n, \tag{2.59}$$

being the Gram-Schmidt projector,[55] which removes all contributions of lower lying states $|\Psi_m\rangle$ and orthogonalises $|\Psi_n\rangle$ to each state with $E_m < E_n$. This orthogonalization is performed at the end of each iteration step, after the annihilation step, where the calculated overlaps with lower energy states are removed from the higher energy ones. The elimination of the lower energy contribution causes $|\Psi_n(\tau)\rangle$ to converge to the next lowest energy eigenstate of $\hat{H}$.

2.3.7 Automated Timestep Optimization

There are various consideration to take into account in the choice of the timestep $\Delta\tau$ used in a FCIQMC calculation. As mentioned in Sec. 2.3.1 for the first-order Taylor expansion of the projector $\mathrm{e}^{-\Delta\tau\hat{H}}$ to correctly converge to the ground state, the timestep $\Delta\tau$ must be smaller then the inverse of the spectral width of $\hat{H}$.[325] However, this is a rather lax condition and the actual timestep usually must be chosen smaller to ensure stable dynamics of a simulation.

The death-step, see Sec. 2.3.2, places the additional restriction that $\Delta\tau$ should be chosen in such a way to ensure that the probability for a walker to die (2.49) is smaller than 2, $p_d < 2$. Otherwise a walker on a given state would continually create more and more walkers of alternating sign in each iteration and causing an unstable simulation. To avoid this situation it is possible to keep track of the largest diagonal element $|H_{ii} - E_S(\tau)|$ of all walkers and adapt $\Delta\tau$ dynamically to ensure $p_d < 2$. In the end this is in general also not the most limiting constraint on the possible timestep $\Delta\tau$.

The spawning event, see Sec. 2.3.2, especially in the initiator approximation of FCIQMC, will be the deciding limitation of the maximum possible $\Delta\tau$. A spawning probability $p_s > 1$ is realized by spawning at least $\lfloor p_s \rfloor$ walkers and one walker with probability $p_s - \lfloor p_s \rfloor$.* If the number of spawned walkers exceeds n_{init}, this would cause a possibly unoccupied state to become an initiator immediately. This could be valid, due to a large Hamiltonian matrix element H_{ij} connecting those two states, but it could be also a consequence of a poorly chosen generation probability $p(j|i)$, in the denominator of (2.50). To avoid these events it is important to choose $p(j|i)$ in a sensible way, explained in Sec. 2.3.8. As a last resort $\Delta\tau$ can be dynamically adapted to ensure $p_s < n_{init}$. This can be achieved by keeping track of the "worst-case" spawning ratio $|H_{ij}|/p(j|i)$ across all walkers and states and adapt $\Delta\tau$ to ensure $p_s < n_{init}$ similar to the death-step mentioned

*Although in nowadays FCIQMC simulation walkers are actually represented by real numbers, with a minimum occupation n_{min} and not integers any more.

above. If the excitation generation is performed in a nonoptimal way, the spawning step is usually the most limiting influence on the applicable timestep. In Section 4.3 a more flexible version of the timestep adaptation to ensure $p_s < n_{init}$ is presented.

2.3.8 Optimized Excitation Generation

The efficient stochastic realization of the off-diagonal contribution in Eq. (2.48) $c_i(\tau+\Delta\tau) \leftarrow \Delta\tau \sum_{j\neq i} H_{ij}c_j(\tau)$ via the spawning step, see Sec. 2.3.2, is the most important and most challenging part of the FCIQMC method. The sum is stochastically sampled by allowing one walker on a given state i to spawn new walkers on one connected state j, via a single application of $\hat{H}$. The challenge is to sensibly determine the *generation probability* $p(j|i)$, which in the best case scenario is proportional to the magnitude of the matrix element $|H_{ij}|$ connecting the two states. The reason is that we want to sample stronger, more important connections with a higher probability. As mentioned in Sec. 2.3.7, this has a direct impact on the maximum possible timestep $\Delta\tau$, as the spawning probability $p_s = \Delta\tau|H_{ij}|/p(j|i)$ should be lower than the initiator threshold n_{init}. For this reason a lot of work on an optimized excitation generation in FCIQMC has been expended, and in the following I will present the current implementation in our FCIQMC code `NECI`.[25*]

In the spawning step, we first choose if we want to perform a single or double excitation with dynamically adaptable probabilities p_s and $p_d = 1 - p_s$ for a walker on given state i, separating $p(j|i) = p_s + p_d$. The probabilities p_s and p_d represent the relative importance of single and double contributions in the off-diagonal sum in Eq. (2.48) and since there are usually many more double excitations possible, $p_d \gg p_s$ in general.[†]

If a **single excitation** is chosen with probability p_s, we pick an electron a from an occupied spin-orbital (a,σ) in $|D_i\rangle$ with uniform probability $p_s^e(a) = 1/N$ at random. For all symmetry allowed, see Sec. 2.3.8, unoccupied σ-spin orbitals (p',σ) in $|D_i\rangle$ the Hamiltonian matrix elements $\langle D_i|\hat{H}a^\dagger_{p',\sigma}a_{a,\sigma}|D_i\rangle$ is calculated and a specific orbital (p,σ) is chosen with the probability

$$p_s^h(p|a) = \frac{|\langle D_i|\hat{H}a^\dagger_{p,\sigma}a_{a,\sigma}|D_i\rangle|}{\sum_{p'}|\langle D_i|\hat{H}a^\dagger_{p',\sigma}a_{a,\sigma}|D_i\rangle|}. \tag{2.60}$$

Due to the loop over (p',σ) and the $\mathcal{O}(N)$ scaling of single excitation matrix elements, this choice of generation probability scales as $\mathcal{O}(nN)$, with n the number of spatial orbitals. However, since $p_s \ll p_d$ this elaborate scheme if feasible and ensures a direct proportionality $p(j|i) = p_s p_s^e(a) p_s^h(p|a) \propto |H_{ij}|$ for the rare single excitations, with $|D_j\rangle = a^\dagger_{p,\sigma}a_{a,\sigma}\,|D_i\rangle$.

*A lot of work from different people was involved in this. Most notably Simon D. Smart, George Booth, Nick Blunt, Kai Guther and myself.

†Except in a localized basis, where the molecular one-body integrals are far larger in magnitude than the two-body integrals.

If a **double excitation** is chosen with probability p_d, we further subdivide p_d into probabilities to perform spin-parallel p_p and spin-antiparallel excitations $p_a = 1 - p_p$, with $p_d = p_a + p_p$. For double excitations a pair of electrons $(p, \sigma; q, \sigma')$, with $\sigma = \sigma'$ for parallel and $\sigma = \bar{\sigma}$ for antiparallel spin excitations, is chosen randomly with uniform probability $p_d^e = 1/N_{pairs}^{p/a}$, with $N_{pairs}^{p/a}$ being the number of parallel- or antiparallel-spin pairs of electrons. For opposite spin excitations the first hole (p, σ) is chosen out of all empty spin-orbitals (p', σ) in $|D_i\rangle$ with the probability[139,300]

$$p_d^h(p|ab) = p_d^h(p|a) = \frac{\sqrt{|V_{pa,pa}|}}{\sum_p' \sqrt{|V_{p'a,p'a}|}}, \tag{2.61}$$

with p and a of same spin, since the two-body molecular integrals (1.8) fulfil the *Cauchy-Schwarz inequality*

$$|V_{ij,ab}| \leq \sqrt{|V_{ia,ia}|\,|V_{jb,jb}|}. \tag{2.62}$$

For same spin excitations the exchange contribution is additionally included in Eq. (2.61). The second hole (q, σ'), where σ' depends on the type of double excitation (spin-parallel or spin-antiparallel), is randomly chosen out of all symmetry allowed empty orbitals (q', σ') weighted with the *exact* matrix element associated with the excitation $(a, \sigma; b, \sigma' \rightarrow p, \sigma; q, \sigma')$ with probability

$$p_d^h(q|ab, p) = \frac{|\langle D_i|\hat{H}\, a_{q,\sigma'}^\dagger a_{p,\sigma}^\dagger a_{a,\sigma} a_{b,\sigma}|D_i\rangle|}{\sum_{q'} |\langle D_i|\hat{H}\, a_{q',\sigma}^\dagger a_{p,\sigma}^\dagger a_{a,\sigma} a_{b,\sigma}|D_i\rangle|}. \tag{2.63}$$

This method of calculating the generation probability for doubles scales as $\mathcal{O}(n^2)$, due to the two loops to determine the p_d^h. This can be reduced to a $\mathcal{O}(n)$ scaling, if the first empty orbital (p, σ) is just picked with uniform probability $p_d^h(p|ab) = 1/(n - N)$. However, experience has shown the full-weighted excitation generation, picking (p, σ) according to (2.61), has proven to be worth the effort. The increased timestep, due to a better relation of $p(j|i) = p_d\, p_x\, p_d^e\, p_d^h(p|ab)\, p_d^h(q|ab, p)$, with $p_x = p_p$ for parallel and $p_x = p_a$ for anti-parallel spin, and the magnitude of the matrix element $|\langle D_i|\hat{H}|D_j\rangle|$, with $|D_j\rangle = a_{q',\sigma}^\dagger a_{p,\sigma}^\dagger a_{a,\sigma} a_{b,\sigma}\,|D_i\rangle$, compensates the additional $\mathcal{O}(n)$ scaling.

In the automated timestep adaptation, it is possible to not only change $\Delta\tau$ to ensure $p_d < 2$ and $p_s < n_{init}$ but also the above mentioned probabilities, p_s, p_d, p_a and p_b. This corresponds to a dynamically adjustment of these probabilities to the importance of the corresponding types of excitations contained in the off-diagonal sum in Eq. (2.48). This means the algorithm is able to dynamically adjust these parameters to the optimal values for the specific problem at hand, represented by the Hamiltonian $\hat{H}$.

Discrete Symmetries in FCIQMC

In Section 2.3.8, "the choice of symmetry allowed orbitals" was mentioned. This refers to the *spatial* point group or translational symmetry of the studied system, explained in Sec. 1.3. The eigenfunctions of $\hat{H}$ will transform according to one of the irreducible representations (irreps) Γ_i of the point group P_G corresponding to the spatial symmetry of the problem. If the basis states $|D_i\rangle$ are constructed in such a way that they also transform according to Γ_i, $\hat{H}$ will be *block-diagonal* in this *symmetry-adapted* basis. This symmetry adaptation is implemented in the excitation generation step of FCIQMC, by only creating excitations $|D_i\rangle \rightarrow |D_j\rangle$ belonging to the same Γ_k. The point group symmetry of a Slater determinant $|D_i\rangle$ depends on the symmetry properties of the orbitals $\{\phi_l\}$ it is built from. If the orbitals $\{\phi_l\}$ transform according to the irreps of P_G (e.g. symmetry adapted molecular orbitals (MOs) created as a linear combination of atomic orbitals (LCAO)), then the symmetry Γ_i of $|D_i\rangle$ is given by

$$\Gamma_i = \bigotimes_l \Gamma_{\phi_l \in |D_i\rangle}, \tag{2.64}$$

where $\Gamma_{\phi_l \in |D_i\rangle}$ are the symmetries of the occupied orbitals ϕ_l in $|D_i\rangle$. For Abelian point groups ($\Gamma_i \otimes \Gamma_j = \Gamma_j \otimes \Gamma_i$) the symmetry adaptation in the excitation generation is ensured by:

For **single** excitations, the symmetry allowed empty spin-orbitals (p, σ) for a chosen electron (a, σ) in the excitation $|D_j\rangle = a^\dagger_{p,\sigma} a_{a,\sigma} |D_i\rangle$, are all orbitals from the same irrep $\Gamma_{a,\sigma}$.

For **double** excitations the final chosen empty orbital (q, σ') is symmetry restricted to the orbitals transforming as the irrep

$$\Gamma_{q,\sigma'} = \Gamma_{a,\sigma} \otimes \Gamma_{b,\sigma'} \otimes \Gamma_{p,\sigma}, \quad \text{to ensure} \quad \Gamma_{q,\sigma'} \otimes \Gamma_{p,\sigma} = \Gamma_{a,\sigma} \otimes \Gamma_{b,\sigma'}, \tag{2.65}$$

where (a, σ), (b, σ') and (p, σ) are the already chosen electrons and first hole in the excitation $|D_j\rangle = a^\dagger_{q,\sigma'} a^\dagger_{p,\sigma} a_{a,\sigma} a_{b,\sigma'} |D_i\rangle$ and $\Gamma^{-1}_{p,\sigma} = \Gamma_{p,\sigma}$ for Abelian point groups.

3 Spin as a Symmetry Property

As mentioned in Section 1.3, the concept of symmetry is of paramount importance in physics and chemistry. Apart from the Hilbert space size reduction by the use of a simultaneous eigenbasis of operators commuting with the Hamiltonian in question, the exploitation of symmetries inherent to the problem ensures the conservation of "good" quantum numbers and the physical correctness of calculated quantities. In addition, the use of a symmetry-adapted basis allows to target specific subspaces of the problem at hand.

Commonly used symmetries in electronic structure calculations, mentioned in Sec. 1.3, are discrete *translational* and point group symmetries, orbital angular momentum and z-projection of total spin conservation.

One often ignored symmetry is the global $SU(2)$ spin-rotation symmetry of *spin-preserving, nonrelativistic* Hamiltonians. This symmetry leads to a conservation of the total spin quantum number S and is represented by the operator $\hat{\mathbf{S}}^2$. If

$$[\,\hat{H}, \mathbf{S}^2\,] = 0 \tag{3.1}$$

the use of a spin symmetry adapted basis of $\hat{\mathbf{S}}^2$ would allow us to:

Target specific spin states with *definite* S ($S = 0$ singlet, $S = 1/2$ doublet, etc.), which allows the calculation of spin gaps between states inaccessible otherwise.

Eliminate *spin-contamination* of the sampled eigenfunctions of $\hat{H}$, which should help the FCIQMC method to converge more easily to the ground state of chosen symmetry.

Reduce the *Hilbert space size* by further block-diagonalization in (S, m_s) sectors. This reduction causes a more compact form of the wavefunction, which in turn enables a more efficient sampling by the Monte Carlo approach.

Resolve *(near-)degeneracies* of eigenstates belonging to different total spin symmetry sectors, posing a problem for the convergence of projective techniques, such as FCIQMC.

So it is obvious that the use of a spin-adapted basis would be very beneficial for electronic structure calculations and an efficient implementation thereof is a long sought-for goal

in quantum chemistry. However, a major drawback of the incorporation of the total spin symmetry is the additional computational cost associated with different flavours of implementation. Theoretically there is no problem associated with the implementation of a spin-adapted basis; but the practice begs to differ. So the question is not only, if the formulation of a method in spin-eigenfunctions has the expected benefits, but also if those advantages outweigh the additional cost. FCIQMC has been implemented in a spin-pure basis before by S. Smart[301] via different approaches than the unitary group. However, this implementation was restricted to a maximum of 16 electrons; a limitation we definitely want to exceed. In this chapter the theoretical framework to achieve this goal via the mathematically elegant unitary group approach and its graphical extension is laid out, while in the following Chapter 4 the actual computational implementation in the FCIQMC method is discussed in depth.

The remainder of this chapter is organised as follows:
In Section 3.1 a general introduction to the concept, importance and history of spin as a symmetry property is given. We present several alternative approaches to implement spin symmetry in electronic structure calculations in Section 3.2. The fundamental connection of the spin-free formulation of a general nonrelativistic Hamiltonian with the unitary group is made in Section 3.3. This relation—of utmost importance—is the basis of the Unitary Group Approach (UGA) and allows the mathematically elegant construction of a spin-adapted basis in form of the Gel'fand-Tsetlin basis with the same storage cost as a regular Slater determinant (SD) basis. In Section 3.4 the graphical extension of the UGA (GUGA) is discussed, which is the basis for an efficient implementation of the excitation generation and matrix element calculation between the spin-adapted basis states in FCIQMC. The actual computational implementation of the Gel'fand-Tsetlin basis and matrix element computation and excitation generation in the FCIQMC framework is presented in the following Chapter 4, where also results obtained with this spin-adapted formulation are presented.

3.1 A Brief History of Spin

Spin is an intrinsic property of every quantum mechanical particle and does not have a classical analogue; it is given in units $\hbar$, same as angular momentum. However, unlike orbital angular momentum, the eigenvalue of the z-projection of the total spin $\hat{S}_z$ is quantized in all negative and positive half-integer values in addition to the integer ones.[68,244] The effect of spin was first observed in the experiment of Stern and Gerlach,[103] where a quantized angular momentum of neutral silver atoms was measured. Goudsmith and Uhlenbeck[331] postulated an intrinsic angular momentum of electrons with value 1/2 to explain the even-numbered splittings —with and without external magnetic field—of spectral lines in the Bohr-Sommerfeld model of atoms[24,303] and termed this property *spin*.

Pauli proposed a 'hidden' nonclassical rotation resulting in a doubling of electron states to explain the electron shell structure of atoms and systematics of spectral lines and formulate his exclusion principle.[242]

The explanation of spin was purely phenomenological, until Dirac's Lorentz-invariant formulation of the Schrödinger equation revealed the relativistic nature of spin.[66,67] In his equation of spin-1/2 particles with mass, the spin of the electron and also the concept of *anti-matter* appear naturally from the combined treatment of special relativity and quantum mechanics. This explains also the spin-independence of the Hamiltonian and conservation of the total spin in the nonrelativistic limit. The symmetry operation associated with spin is the global $SU(2)$ spin-rotation, which is more elaborated on in Section 3.3.4. The spin s, with $S = \hbar\sqrt{s(s+1)}$, of a particle has a major influence on the statistics it obeys.[243]

Fermions with *half-integer* spin, $s = 1/2, 3/2, \ldots$, follow the Fermi-Dirac statistics[65,89] and obey the Pauli exclusion principle.[242] A fermionic wavefunction is totally antisymmetric and changes sign under the exchange of two particles $\Psi_f(x, y) = -\Psi_f(y, x)$, thus forbidding two fermions to be in the exact same quantum state.

Bosons, on the other hand, with *integer* spin, $s = 0, 1, \ldots$, follow the Bose-Einstein statistics[32] with a symmetric wavefunction under particle exchange, $\Psi_b(x, y) = \Psi_b(y, x)$. In contrast to fermions, multiple bosons are allowed to occupy the exact same quantum state at the same time. Loosely spoken, fermions are the particles which build all the "matter" of our physical world, while bosons are the particles which carry the forces between them.

3.2 The Use of Spin Symmetry in Electronic Structure Calculations

Despite the theoretical benefits, the total $SU(2)$ spin symmetry is not as widely used as other symmetries, like translational or point group symmetries, due to the usually impractical and complicated implementation thereof. There are several schemes to construct a basis of $\hat{\mathbf{S}}^2$ eigenfunctions, which will just be briefly sketched here.

Half-Projected Hartree-Fock (HPHF) functions[133,302]
are based on the fact that for an *even* number of electrons, every spin state S contains degenerate eigenfunctions with $m_s = 0$. Using *time-reversal symmetry* arguments a HPHF

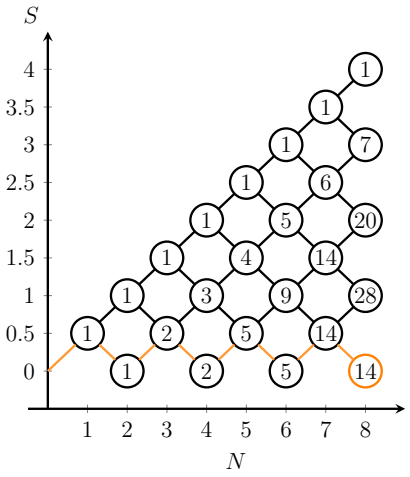

Fig. 3.1: Illustration of the sequential spin coupling in the genealogical spin eigenfunction construction. The numbers in the circles represent the number of possible pathways and thus the number of basis states belonging to the symmetry sector (N, S). Example taken and adapted from [245]. In orange on possible way to reach on the 14 states of the $N = 8, S = 0$ singlet is displayed.

function can be constructed as

$$|H_i\rangle = \begin{cases} |D_i\rangle & \text{for fully close-shell determinants} \\ \frac{1}{\sqrt{2}}\left(|D_i\rangle \pm |\overline{D_i}\rangle\right) & \text{otherwise,} \end{cases} \tag{3.2}$$

where $|\overline{D_i}\rangle$ indicates the spin-flipped version of $|D_i\rangle$. Depending on the sign of the open-shell coupled determinants, $|H_i\rangle$ are eigenfunctions of $\hat{\mathbf{S}}^2$ with odd $(-)$ or even $(+)$ eigenvalue S. HPHF functions are implemented in our FCIQMC code `NECI`,[25,27,29] but their use is restricted to systems with an even number of electrons and can only target the lowest even- and odd-S state. Thus, it can not differentiate between, e.g. a singlet $S = 0$ and quintet $S = 2$ state.

Rumer spin-paired spin eigenfunctions[270,295,301,353]

A singlet state for a two electron system in two spatial orbitals i and j is given by

$$|S = 0\rangle = \frac{1}{\sqrt{2}}\left(|i_\downarrow, j_\uparrow\rangle - |i_\uparrow, j_\downarrow\rangle\right). \tag{3.3}$$

For N electrons, Rumer spin eigenfunction are constructed by coupling g *pairs* of electrons to a singlet and the remaining $(N - 2g)$ electrons to the maximum multiplicity $S = \frac{1}{2}(N - 2g)$. Rumer type functions are connected to other flavours of spin-adapted bases, like Kotani-Yamanouchi[295] and Serber[245] type functions. The main drawback of Rumer spin-eigenfunctions is that they are not orthogonal.[263]

Kotani-Yamanouchi (KY) genealogical spin eigenfunctions[169,245,335]

KY functions are obtained by a sequential coupling of N electrons to obtain a total spin of S. A given spin eigenfunction with N electrons and total and projected spin S and m_s is related to the eigenfunctions with $N - 1$ electrons and $S \pm 1/2$ and $m_s \pm 1/2$. Furthermore, every possible eigenstate with $N + 1$ electrons and $S \pm 1/2$ and $m_s \pm 1/2$ is related to the current (N, S, m_s) spin eigenstate. The possible spin eigenstates are constructed by drawing a S vs. N diagram and every additional electron, increasing $N \to N + 1$ can

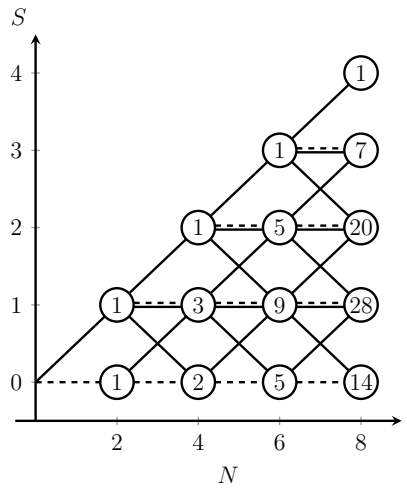

Fig. 3.2: Branching diagram of Serber spin eigenfunctions for $N = 8$ electrons. The numbers represent the number of possible routes. Dashed horizontal lines indicate singlet $\Delta S = 0$ and solid lines triplet $\Delta S = 0$ couplings. For $S = 0$ only singlet $\Delta S = 0$ is allowed. Example taken and modified from [245].

increase, $S \to S + 1/2$, or decrease , $S \to S - 1/2$, the total spin, with the restriction $S \geq 0$. All possible pathways which end up at a chosen state with definite N and S represent the basis states belonging to this symmetry sector. This is depicted in Fig. 3.1 for an 8 electron system.

Serber-type spin eigenfunctions[245,271,279]

These type of functions are obtained by the sequential coupling of *pairs* of electrons. States with N electrons and a desired total spin S are obtained from $N - 2$ electron states with $S \pm 1$ and $m_s \pm 1$. There are four ways of coupling a pair of electrons: (a) *Singlet* coupling with $S \to S$, (b) *triplet* coupling with $S \to S$ and (c) and (d) a *triplet* coupling with $S \to S \pm 1$. Similar to the KY spin eigenfunctions this can be visualized in a *branching* diagram with additional horizontal coupling paths, see Fig. 3.2. For an odd number of electrons the remaining electron can be coupled in a genealogical manner like in the KY functions.[301]

Löwdin spin-projected Slater determinants[195]

Different to the two previous *sequential coupling* schemes, it is possible to obtain a spin pure state by applying the spin-projection operator, defined by Löwdin[195] as

$$\hat{O}_S = \prod_{k \neq S} \frac{\hat{\mathbf{S}}^2 - k(k+1)}{S(S+1) - k(k+1)}, \tag{3.4}$$

on any trial state $|\Psi_T\rangle$. $\hat{O}_S$ projects out every component other than the chosen S component and thus the resulting $|\Psi_S\rangle = \hat{O}_S |\Psi_T\rangle$ will be an eigenstate of $\hat{\mathbf{S}}^2$ with total spin S. There are however issues of overcompleteness and nonorthogonality of the obtained bases, which complicates the efficient implementation of these projection based methods. However, recently there has been work using the projector 3.4 and others in the form of the Projected Coupled Cluster method[130,260,328,329] to restore spin-symmetry of a broken symmetry reference state. There has been a similar use of a projector, like Eq. 3.4, to

restore the spin-symmetry of Matrix Product States (MPS) in the Density Matrix Renormalization Group (DMRG) method.[182]

Symmetric Group Approach[74,246,269]

An approach similar to the main topic of this chapter is the Symmetric Group Approach (SGA) and as important concepts are similar in both approaches the SGA will be briefly discussed here. The symmetric group S_N is the group off all permutations of N objects. The irreducible representations (irreps) of S_N can be identified by *Young shapes*.[367] As the concept of Young shapes is helpful in understanding the Unitary Group Approach, we will briefly explain them in more detail. Those shapes are an arrangement of N boxes in rows and columns, where the number of boxes in each row is nonincreasing downwards. The components of a specific irrep of S_N are obtained by filling these boxes with distinct 'tokens' $1, 2, \ldots, N$, representing the permuted objects, which results in a so-called *Young tableau*. A *standard* Young tableau has increasing number in each row from left to right and in each column from top to bottom. An example of a Young shape representing an irrep of S_9 and an individual component is

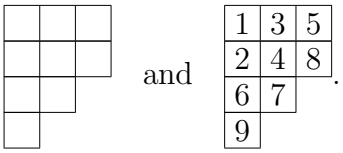

The tableau represents a linear combination of permutation operators acting on the objects represented by the tokens. For a system of three particles there are three possible Young shapes with two one-dimensional irreps and 1 two-dimensional irrep

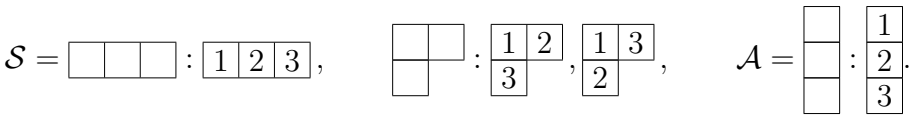

The two shapes $\mathcal{S} = \{N\}$ and $\mathcal{A} = \{1^N\}$ have a special meaning. $\mathcal{S}$ is the sum of all permutations P of the N tokens, $\mathcal{S} = \frac{1}{N!}\sum_P P$, and thus represents the 'symmetriser operator'. $\mathcal{A}$, on the other hand, is the sum of all even permutations P^e minus the sum of all odd permutations P^o, $\mathcal{A} = \frac{1}{N!}(\sum_{P^e} P^e - \sum_{P^o} P^o)$, of the N tokens and thus acts as the 'antisymmetriser'. Consider two electrons in two open shell orbitals $|\Psi_2\rangle = |\uparrow,\downarrow\rangle$. The symmetriser $\mathcal{S}$, represented by , acting on $|\uparrow,\downarrow\rangle$ yields

$$\mathcal{S}\,|\Psi_2\rangle = \frac{1}{2}\left(\mathbb{1} + P_{12}\right)|\uparrow,\downarrow\rangle = \frac{1}{2}\left(|\uparrow,\downarrow\rangle + |\downarrow,\uparrow\rangle\right),$$

with $\mathbb{1}$ being the identity operator, the symmetric spin function of the $m_s = 0$ triplet state. On the other hand $\mathcal{A} = \{1^N\} =$  acting on $|\Psi_2\rangle$ gives

$$\mathcal{A}\,|\Psi_2\rangle = \frac{1}{2}\left(\mathbb{1} - P_{12}\right)|\uparrow,\downarrow\rangle = \frac{1}{2}\left(|\uparrow,\downarrow\rangle - |\downarrow,\uparrow\rangle\right),$$

the antisymmetric singlet spin function. The spin-eigenfunction construction in the SGA relies on these Young shapes. The token in the SGA represent the singly occupied orbitals of an electronic state and thus the coupling scheme is similar to the genealogical generation of Kotani-Yamanouchi states.

The Rumer, Kotani-Yamanouchi and Serber type spin-eigenfunctions have been implemented in our FCIQMC code `NECI`[25] by Simon Smart,[301] but due to practical limitations the applications were restricted to small system sizes only.

Spin symmetry in other methods and software packages:

- The quantum chemistry software package `Molcas`,[10] which—along with `Molpro`[349,350] —is mainly used in this work to obtain the *ab-initio* Hamiltonian for the studied systems, uses the Unitary Group Approach (UGA) to conserve the total spin quantum number. However, they rely on the conversion between the Slater determinant and configuration state function bases.[125,226,284] As this conversion is used in the FCI solvers of Molcas, the spin-adapted implementation is limited to the usual limitations of the FCI method of 18 electrons in 18 spatial orbitals.

- There is a spin-adapted version of the Density Matrix Renormalization Group approach,[206,280,316,369] which uses the eigenvectors of a *quasi-density* matrix, which commutes with the $\hat{\mathbf{S}}^2$ operator, as a renormalized basis. The Wigner-Eckart theorem[359] is used to efficiently store and compute matrix elements of the irreducibly spin tensor operators with Wigner $9-j$ coefficients.[207] Recently there has also been a spin-adapted DMRG implementation based on spin-projected MPS,[182] with a projection operator similar to Eq. 3.4.

- If the chosen reference state $|\Phi_0\rangle$ in the Coupled Cluster Ansatz (1.31), see Sec. 1.7.4, is a closed-shell singlet and the cluster operators are expressed in terms of *singlet* excitation operators, e.g. the one-body operator $\hat{E}_{ia} = a^\dagger_{a\uparrow}a_{i\uparrow} + a^\dagger_{a\downarrow}a_{i\downarrow}$,* the initial spin $S = 0$ of $|\Phi_0\rangle$ is conserved. However, with unrestricted coupled cluster (UCC) methods applied to open-shell systems, where a general form of the excitation operators is used and/or the reference function $|\Phi_0\rangle$ is spin-symmetry broken, the total spin is not a conserved quantity. There exists however a symmetry-adapted cluster (SAC) approach in the CC theory,[217,218,223] where a fully spin- and symmetry-adapted form of the cluster operator is used.

- The `Columbus` program[188,190,191] deserves a special mention, as it makes direct use of the later explained *Graphical unitary group approach* (GUGA), see Sec. 3.4.

- The `GAMESS` software package[111,274] uses a CI method based on the *loop-driven* GUGA implementation of Brooks and Schaefer.[39,40]

- Based on the GUGA introduced by Shavitt,[282,283] Shepard et. al.[189,290] made exten-

*This type of operator will also play a major part in the UGA

sive use of the graphical representation of spin eigenfunctions in form of Shavitt's *distinct row table* (DRT). In the *multifacet graphically contracted method*[105,106,222,286–289] the ground state wavefunction is formulated in a nonlinear manner based on the DRT, conserving the total spin S.

3.3 The Unitary Group Approach (UGA)

The main topic of this and the following Chapter 4 is the use of the *Unitary Group Approach* (UGA)[230] to formulate the FCIQMC method in spin eigenfunctions. The UGA is used to construct a spin-adapted basis, or configuration state functions (CSFs)*, which allows to preserve the total spin quantum number S in FCIQMC calculations. With the help of the *Graphical Unitary Group Approach* (GUGA), introduced by Shavitt,[282] an efficient calculation of matrix elements entirely in the space of CSFs is possible; without the necessity to transform to a Slater determinant (SD) basis. The GUGA additionally allows the effective *excitation generation*, the cornerstone of the FCIQMC method, without reference to a non spin-pure basis and the need of storage of auxiliary information, necessary in previous spin eigenfunction formulations[301] (Serber, etc., see Sec. 3.2). Finally, opposed to the HPHF spin-symmetry implementation, it allows us to target all possible spin eigenvalues and works for odd and even numbers of electrons.

To guide through the following derivations and explanations the "roadmap" for spin eigenfunctions in FCIQMC is as follows:

(1) We concern ourselves exclusively with *spin-preserving, nonrelativistic* Hamiltonians $\hat{H}$ in the Born-Oppenheimer approximation[31] in a finite basis set.

(2) We will find a *spin-free* formulation of $\hat{H}$ in terms of singlet excitation operators, $\hat{E}_{ij}$, which fulfil the same *commutation relations* as the *generators* of the unitary group of order n, $U(n)$.

(3) We label the number of *spatial* orbitals n, which will be related to the *unitary group* of order n, $U(n)$. The resulting $2n$ *spin-orbitals* basis can be related to the unitary group of order $2n$, $U(2n)$.

(4) Our goal is to obtain the fermionic, thus totally antisymmetric, eigenfunctions of $\hat{H}$, represented by the total antisymmetric representation of $U(2n)$.

(5) $U(2n)$ can be expressed as the proper direct product $U(2n) = U^o(n) \otimes U^s(2)$, where the superscripts denote the orbital (^{o}) and spin (^{s}) character of the representation.

(6) *Mutually conjugate* representation of $U^o(n)$ and $U^s(2)$ ensure the direct product $U(2n)$ to be *totally antisymmetric*.

*See Section 3.3.5

(7) We will find a basis, which is *invariant* and *irreducible* under the action of these generators in form of the *Gel'fand-Tsetlin* (GT) basis.

(8) We will formulate the excitation generation and Hamiltonian matrix element calculation entirely in this *orthonormal* spin-adapted basis via the graphical unitary group approach.

This roadmap will lead us to an efficient formulation of FCIQMC in a spin-adapted basis. In the remainders of this chapter, the theoretical framework of the above mentioned points is laid out and the actual computational implementation in the FCIQMC method is presented in the following Chapter 4.

The basis of the unitary group approach (UGA), which goes back to Moshinsky,[213] is the spin-free formulation of the spin-independent, non-relativistic, electronic Hamiltonian in the Born-Oppenheimer approximation, see Eq. (1.6) in Sec. 1.2,

$$\hat{H} = \sum_{ij}^{n} t_{ij} \sum_{\sigma=\uparrow,\downarrow} a_{i\sigma}^{\dagger} a_{j\sigma} + \frac{1}{2} \sum_{ijkl}^{n} V_{ijkl} \sum_{\sigma,\tau=\uparrow,\downarrow} a_{i\sigma}^{\dagger} a_{k\tau}^{\dagger} a_{l\tau} a_{j\sigma}, \tag{3.5}$$

introduced in Sec. 1.2. With the reformulation

$$a_{i\sigma}^{\dagger} a_{k\tau}^{\dagger} a_{l\tau} a_{j\sigma} = a_{i\sigma}^{\dagger} a_{j\sigma} a_{k\tau}^{\dagger} a_{l\tau} - \delta_{jk} \delta_{\sigma\tau} a_{i\sigma}^{\dagger} a_{l\sigma},$$

we can define

$$\sum_{\sigma} a_{i\sigma}^{\dagger} a_{j\sigma} = \hat{E}_{ij} \tag{3.6}$$

and identify

$$\sum_{\sigma\tau} a_{i\sigma}^{\dagger} a_{k\tau}^{\dagger} a_{l\tau} a_{j\sigma} = \hat{E}_{ij} \hat{E}_{kl} - \delta_{jk} \hat{E}_{il} = \hat{e}_{ij,kl}. \tag{3.7}$$

as the *singlet* one- and two-body excitation operators.[133] (3.6) and (3.7) are called singlet operators, since acting with them on a state $|S, m_s\rangle$ with definite spin S and z-projection m_s does not change these quantum numbers of the state, see Sec. 3.3.5.
With (3.6) and (3.7) the Hamiltonian (3.5) can be expressed in terms of these spin-free excitation operators as[202]

$$\hat{H} = \sum_{ij} t_{ij} \, \hat{E}_{ij} + \frac{1}{2} \sum_{ij,kl} V_{ijkl} \, \hat{e}_{ij,kl}. \tag{3.8}$$

An elegant and efficient method to create a spin-adapted basis and calculate the Hamiltonian matrix elements in this basis is based on the important observation, that the spin-free excitation operators (3.6) and (3.7) in the non-relativistic Hamiltonian (3.8) obey the same commutation relations, as the generators of the *Unitary Group* $U(n)$,[230–232] with n being the number of spatial orbitals. The commutator of the spin-preserving excitation

operators $\hat{E}_{ij}$ can be calculated as

$$\begin{aligned}
[\,\hat{E}_{ij},\hat{E}_{kl}\,] &= \sum_{\sigma\tau} a^\dagger_{i\sigma}a_{j\sigma}a^\dagger_{k\tau}a_{l\tau} - a^\dagger_{k\tau}a_{l\tau}a^\dagger_{i\sigma}a_{j\sigma} \\
&= \sum_{\sigma\tau} a^\dagger_{i\sigma}a_{j\sigma}a^\dagger_{k\tau}a_{l\tau} - a^\dagger_{i\sigma}a^\dagger_{k\tau}a_{l\tau}a_{j\sigma} - \delta_{il}a^\dagger_{k\tau}a_{j\sigma} \\
&= \sum_{\sigma\tau} a^\dagger_{i\sigma}a_{j\sigma}a^\dagger_{k\tau}a_{l\tau} - a^\dagger_{i\sigma}a_{j\sigma}a^\dagger_{k\tau}a_{l\tau} + \delta_{jk}a^\dagger_{i\sigma}a_{l\tau} - \delta_{il}a^\dagger_{k\tau}a_{j\sigma} \\
[\,\hat{E}_{ij},\hat{E}_{kl}\,] &= \delta_{jk}\,\hat{E}_{il} - \delta_{il}\,\hat{E}_{kj},
\end{aligned} \tag{3.9}$$

which is the same as for the basic matrix units, see Eq. (3.16), and the generators of the unitary group $U(n)$, see Eq. (3.24). To give a complete overview of the concepts of the UGA we will now discuss the unitary group and its generators in more detail.

3.3.1 The Generators of $U(n)$

The Unitary Group $U(n)$ is the group of all $n \times n$ unitary matrices $\mathbf{U}$, with the property $\mathbf{U}^\dagger\mathbf{U} = \mathbb{1}$, and the ordinary matrix (Caley) product as the group operation. It is a subgroup of the *general linear group* $GL(n,\mathbb{C})$, the set of all $n \times n$ nonsingular matrices $\mathbf{A}$ with $\det A \neq 0$, over the complex numbers $\mathbb{C}$

$$U(n) = \{\mathbf{U} \in GL(n,\mathbb{C}) \mid \mathbf{U}^\dagger\mathbf{U} = \mathbb{1} = \mathbf{U}\mathbf{U}^\dagger\}. \tag{3.10}$$

The special case, $U(1)$, is the group of all complex numbers z with absolute value $|z| = 1$ and multiplication as the group operation. $U(1)$ is abelian and has a one-dimensional irreducible representation (irrep), which allows the construction of an invariant and irreducible basis of $U(n)$, see below 3.3.2. $U(n)$ is a compact, continuous, real, n^2 dimensional *Lie group*. Lie groups, in addition to algebraic operations, are also endowed with a topology (allowing the definition of concepts like neighbourhood, continuity, convergence, etc.) under which the group operations and taking the inverse are analytic functions of the group elements. The definition of $U(n)$ as the subgroup of $GL(n,\mathbb{C})$ with unitary matrices is a *nonlinear* relation. To linearise the relationship defining $U(n)$ one employs an *exponential mapping* of any square matrix $\mathbf{A}$

$$\exp(\mathbf{A}) = \sum_{n=0}^{\infty} \frac{1}{n!}\mathbf{A}^n, \tag{3.11}$$

with $\mathbf{A}^0 = \mathbb{1}$. This replaces the unitarity condition

$$\mathbf{U}\mathbf{U}^\dagger = \mathbb{1}, \quad \text{or} \quad \mathbf{U}^\dagger = \mathbf{U}^{-1} \tag{3.12}$$

with

$$\mathbf{U} = \exp \mathbf{A}, \quad \text{with} \quad \mathbf{A}^\dagger = -\mathbf{A}, \tag{3.13}$$

$$\rightarrow \mathbf{U}^\dagger = \exp \mathbf{A}^\dagger = \exp(-\mathbf{A}) = (\exp \mathbf{A})^{-1} = \mathbf{U}^{-1}, \tag{3.14}$$

where $\mathbf{A}$ is anti-Hermitian (skew-Hermitian). The set of matrices $\mathbf{A}$ is itself closed under addition and multiplication by a scalar

$$(\alpha\mathbf{A} + \beta\mathbf{B})^\dagger = -(\alpha\mathbf{A} + \beta\mathbf{B}), \tag{3.15}$$

with $\alpha, \beta \in \mathbb{R}$, and thus constitutes a n^2-dimensional vector space over $\mathbb{R}$.[234] However, instead of the matrix multiplication it is closed under the commutator operation or *Lie product* $[\,\mathbf{A}, \mathbf{B}\,] = \mathbf{AB} - \mathbf{BA}$. This vector space is the *Lie algebra* $u(n)^*$ of $n \times n$ skew-Hermitian matrices with the commutator defined as the group multiplication. Due to the vector space structure it is possible to employ the concept of a basis for the Lie algebra. A suitable basis are the $n \times n$ *matrix units* $\mathbf{e}_{ij}$ with a single nonvanishing entry in the ith row and jth column equal to 1. Any arbitrary unitary matrix can be expressed as

$$\mathbf{U} = \mathrm{e}^{\mathbf{A}}, \quad \text{with} \quad \mathbf{A} = \sum_{ij} \alpha_{ij}\, \mathbf{e}_{ij}, \quad \text{and} \quad \alpha_{ij} = -\alpha^*_{ji},$$

to ensure A is skew-Hermitian. Since a Lie algebra is closed under the commutator, so are the chosen basis states

$$[\,\mathbf{e}_{ij}, \mathbf{e}_{kl}\,] = \mathbf{e}_{ij}\mathbf{e}_{kl} - \mathbf{e}_{kl}\mathbf{e}_{ij} = \delta_{jk}\, \mathbf{e}_{il} - \delta_{il}\, \mathbf{e}_{kj}. \tag{3.16}$$

The commutation relations of $\mathbf{e}_{ij}$ are the same as for the singlet excitation operators $\hat{E}_{ij}$, see Eq. (3.9). For a mathematically rigorous comparison we have to identify the *generators* of $U(n)$. For this reason we have to define the *basic set* of *one-parameter subgroups* of $U(n)$

$$\{\mathbf{U}(t) = \exp(\mathbf{A}t) \mid t \in \mathbb{R}, \mathbf{A}^\dagger = -\mathbf{A}\} \tag{3.17}$$

with a fixed skew-Hermitian $\mathbf{A} \in u(n)$, called the *tangent matrix*, and a single real parameter t. The set of $\mathbf{U}(t)$ can be used to express any arbitrary matrix of $U(n)$ in the vicinity of $\mathbf{U}(0)$ (for mathematical rigour). $\mathbf{U}(t = 0) = \mathbb{1}$ is the identity, the inverse of $\mathbf{U}(t)$ is $\mathbf{U}(-t)$, since $[\,\mathbf{A}, \mathbf{A}\,] = 0$, and the multiplication $\mathbf{U}(t_1)\mathbf{U}(t_2)$ yields $\mathbf{U}(t_1 + t_2)$.[†] The basic set of $U(n)$ can be chosen as

$$\mathbf{U}_{ij}(t) = \exp(\epsilon_{ij}t), \quad \text{with} \quad t \in \mathbb{R}, \tag{3.18}$$

*We follow the standard terminology to term a Lie algebra corresponding to a Lie Group with a lower case letter.

[†]This rather technical explanation will be illuminated by the practical example of $U(2)$ and $SU(2)$ in Sec. 3.3.4.

where ϵ_{ij} are the skew-Hermitian matrix units

$$\epsilon_{kk} = i\mathbf{e}_{kk} \qquad \text{and} \qquad \epsilon_{kl} = \begin{cases} \frac{i}{\sqrt{2}} \left(\mathbf{e}_{kl} + \mathbf{e}_{lk}\right), & \text{for } k < l \\ \frac{1}{\sqrt{2}} \left(\mathbf{e}_{kl} - \mathbf{e}_{lk}\right), & \text{for } k > l, \end{cases} \tag{3.19}$$

with $\epsilon^\dagger = -\epsilon$. Any skew-Hermitian matrix can be expressed as linear combinations of ϵ_{kl} with real coefficients, so they can be equivalently chosen as a basis of the Lie algebra $u(n)$ instead of the basic matrix units $\mathbf{e}_{ij}$.

The final ingredient to identify the generators of $U(n)$ is to introduce the *finite-dimensional representation* Γ of a linear Lie group G. This representation is the linear action of a Lie group on a vector space V, e.g. $\Gamma : G \to U(V) : \mathbf{A} \mapsto \Gamma(\mathbf{A})$, where $\mathbf{A} \in G$ and $\Gamma(\mathbf{A}) \in U(V)$. A generator $\mathcal{A}$ of the representation Γ on V is defined for every element $\mathbf{A}$ of a Lie algebra g corresponding to a Lie Group G as[234]

$$\mathcal{A} = \left.\frac{d\Gamma(\mathbf{A}(t))}{dt}\right|_{t=0} \to \Gamma(\exp \mathbf{A}) = \exp \mathcal{A}. \tag{3.20}$$

For a compact Lie group, like $U(n)$, all finite-dimensional representations are completely reducible and all irreducible representations are finite dimensional and denumerable. The operators $\mathcal{A}$ themselves again form a Lie algebra isomorphic to g, so every representation of a Lie group induces a representation of the corresponding Lie algebra. With the one-parameter subgroups of $U(n)$ defined as $\mathbf{U}_{ij}(t) = \exp(t\epsilon_{ij})$, the representation Γ then is

$$\mathbf{U}_{ij}(t) \to \Gamma(\mathbf{U}_{ij}(t)), \tag{3.21}$$

with infinitesimal operators (or *generators*)

$$X_{ij} = \left.\frac{d\Gamma(U_{ij}(t))}{dt}\right|_{t=0}. \tag{3.22}$$

The X_{ij} have rather complicated commutation relations, but we can equivalently define the generators

$$E_{ii} = -iX_{ii} \qquad \text{and} \qquad E_{ij} = \begin{cases} \frac{-i}{\sqrt{2}} \left(X_{ij} - iX_{ji}\right) & \text{for} \quad i < j \\ \frac{1}{\sqrt{2}} \left(X_{ij} - iX_{ji}\right) & \text{for} \quad i > j, \end{cases} \tag{3.23}$$

with the same commutation relations as the basis matrix units

$$[\, E_{ij}, E_{kl} \,] = \delta_{jk} E_{il} - \delta_{il} E_{kj}. \tag{3.24}$$

This is the important relation between the generators of the unitary group $U(n)$ and the spin-free formulation of nonrelativistic quantum chemistry.* Thus, this method is

*The generators of $U(n)$ are labelled without an hat E_{ij} and the spin-free excitation *operators* with.

called the *Unitary Group Approach*(UGA) and was pioneered by Moshinsky,[213] Paldus[230] and Shavitt,[282,283] who introduced the graphical-UGA(GUGA) for practical calculation of matrix elements.

With the observation that the spin-free, nonrelativistic Hamiltonian (3.8) is expressed in terms of the generators of the unitary group, the use of a basis that is *invariant* and *irreducible* under the action of these generators is desirable. This approach to use *dynamic* symmetry to block-diagonalize the Hamiltonian is different to the case, where the Hamiltonian commutes with a symmetry operator. In the UGA $\hat{H}$ does not commute with the generators of $U(n)$, but rather is *expressed* in terms of them. Block diagonalization occurs, due to the use of an invariant and irreducible basis under the action of these generators. Hence, the UGA is an example of a *spectrum generating algebra* with dynamic symmetry.[147,304]

3.3.2 The Gel'fand-Tsetlin Basis

The so-called *Gel'fand-Tsetlin* (GT)[99–101] basis is invariant and irreducible under the action of the generators of $U(n)$. Following [304] we make the analogy to the more familiar spherical harmonics Y_{lm} to better understand the basics of the GT-basis construction.

The components, $\hat{L}_x, \hat{L}_y$ and $\hat{L}_z$, of the orbital angular momentum operator $\hat{\mathbf{L}}$ are the generators of the $SO(3)$ group of rotations in 3D space. Operators which commute with all generators of a group are called *Casimir* operators. In the case of $SO(3)$ the total orbital angular momentum operator $\hat{\mathbf{L}}^2$ has this property, $[\,\hat{\mathbf{L}}^2, \hat{L}_i\,] = 0,\ i = x, y, z$. At the same time $\hat{L}_z$ can be identified as the sole generator and Casimir operator of the rotations in 2D space, $SO(2)$. The spherical harmonics, Y_{lm}, are simultaneous eigenfunctions of the commuting Casimir operators $\hat{\mathbf{L}}^2$ of $SO(3)$ and $\hat{L}_z$ of $SO(2)$. So they are *adapted* to the group chain $SO(3) \supset SO(2)$. The values l and m, which completely label the eigenfunctions Y_{lm}, are directly related to the eigenvalues of the two Casimir operators. Additionally, there are restrictions on the possible values of m for a given l, $-l \leq m \leq l$, where l specifies the irreducible representation (irrep) of $SO(3)$. The action of the generators of $SO(3)$, $\hat{L}_x, \hat{L}_y$ and $\hat{L}_z$, on Y_{lm} results in linear combinations of spherical harmonics with differing m, but identical l quantum number. Thus, they form an *invariant* and *irreducible* basis under the action of the generators, which is exactly what we want to obtain for the generators of the unitary group $U(n)$.

The group $U(n)$ has n^2 generators, E_{ij}, and a total of n Casimir operators and similar to the Y_{lm}, which are based on the group chain $SO(3) \supset SO(2)$, the GT basis is based on the group chain

$$U(n) \supset U(n-1) \supset \cdots \supset U(2) \supset U(1), \tag{3.25}$$

where, as mentioned, $U(1)$ is Abelian and has a one-dimensional irrep. Each subgroup $U(n-1), U(n-2), \ldots, U(1)$ has $n-1, n-2, \ldots, 1$ Casimir operators, resulting in a total of $n(n+1)/2$ commuting operators, named *Gel'fand invariants*.[99] The simultaneous eigenfunctions of these invariants form the GT basis and are uniquely labelled by a set of $n(n+1)/2$ integers related to the eigenvalues of the invariants. Thus, based on the branching law of Weyl,[351] a general N-electron CSF can be represented by a *Gel'fand pattern*[101]

$$[\mathbf{m}] = \begin{bmatrix} m_{1,n} & & m_{2,n} & \cdots & m_{n-1,n} & & m_{n,n} \\ & m_{1,n-1} & & \cdots & & m_{n-1,n-1} & \\ & \ddots & & \cdots & & \ddots & \\ & & m_{1,2} & & m_{2,2} & & \\ & & & m_{1,1} & & & \end{bmatrix}. \tag{3.26}$$

The integers m_{ij} in the *top row* (and all subsequent rows) of (3.26) are nonincreasing, $m_{1n} \geq m_{2n} \geq \cdots \geq m_{nn}$, and the integers in the subsequent rows fulfil the condition

$$m_{i,j+1} \geq m_{ij} \geq m_{i+1,j+1}, \tag{3.27}$$

called the "in-between" condition.[194] This can be seen as a generalization of the restriction $-l \leq m \leq l$ for the Y_{lm}. The n non-increasing integers of the top row of Eq. (3.26), $\mathbf{m}_n = (m_{1n}, m_{2n}, \ldots, m_{nn})$, are called the *highest weight* of the representation, and specify the chosen irrep of $U(n)$, just as l does for the spherical harmonics. The following $n-1$ rows label the states belonging to the chosen irrep, similar to m in the case of Y_{lm}.

Let $\Gamma\{\mathbf{m}_n\}$ be the irreducible representation of $U(n)$, uniquely specified by the weight vector $\mathbf{m}_n$. Any representation Γ of a group G yields a representation of any of its subgroups H, $H \subset G$, *subduced* by Γ, $\Gamma \downarrow G$. $\Gamma\{\mathbf{m}_n\} \downarrow U(n-1)$ of $U(n-1)$ subduced by $\Gamma\{\mathbf{m}_n\}$ is *simply reducible*,[234] due to the *branching law of the unitary group*,[352]

$$\Gamma\{\mathbf{m}_n\} \downarrow U(n-1) = \sum \oplus \Gamma\{\mathbf{m}_{n-1}\}, \tag{3.28}$$

where the direct sum extends over all irreps $\Gamma\{\mathbf{m}_{n-1}\}$ of $U(n-1)$ for which the "in-between" condition (3.27) holds and each irrep is contained once at most.[194,353] This fact and since $U(1)$ is abelian with one-dimensional irreps, led Gel'fand and Tsetlin to the realization that the permissible highest weights of the subgroups in the chain (3.25) can be used to uniquely label the basis vectors of a general $U(n)$ irrep space.

In CI calculations one usually employs a one-particle basis of $2n$ spin-orbitals with creation $\hat{a}^\dagger_{i\sigma}$ and annihilation $\hat{a}_{j\tau}$ operators of electrons in spatial orbital i, j with spin σ, τ. The $(2n)^2$ operators

$$\hat{A}_{i\sigma,j\tau} = \hat{a}^\dagger_{i\sigma}\hat{a}_{j\tau}; \quad i,j = 1,\ldots,n; \quad \sigma,\tau = 1,2 \tag{3.29}$$

can be associated with the generators of $U(2n)$ with the commutation relation

$$[\,\hat{A}_{i\sigma,j\tau}, \hat{A}_{i'\sigma',j'\tau'}\,] = \delta_{ji'}\delta_{\tau\sigma'}\hat{A}_{i\sigma,j'\tau'} - \delta_{ij'}\delta_{\sigma\tau'}\hat{A}_{i'\sigma',j\tau} \tag{3.30}$$

While the partial sums over spin or orbital indices of these operators

$$\hat{E}_{ij} = \sum_{\sigma=\uparrow,\downarrow} \hat{A}_{i\sigma,j\sigma} \quad \text{and} \quad \hat{\mathcal{E}}_{\sigma\tau} = \sum_{i=1}^{n} \hat{A}_{i\sigma,i\tau} \tag{3.31}$$

are related to the orbital $U^o(n)$ and spin $U^s(2)$ generators. Superscript o denotes the pure orbital space and s the pure spin space. Since we deal with fermions we have to restrict ourselves to the totally antisymmetric representations of $U(2n)$, denoted as $\Gamma\{1^{2n}\}$.* Since the molecular Hamiltonian (3.8) is spin independent, we can consider the proper subgroup of the direct product of the spin-free orbital space $U^o(n)$, with n^2 generators E_{ij}, and the pure spin space $U(2)$ with the four generators $\mathcal{E}_{\sigma\tau}$,[230] given as

$$U(2n) \supset U^o(n) \otimes U^s(2). \tag{3.32}$$

With the total antisymmetric representation $\Gamma\{1^{2n}\}$ of $U(2n)$, and $\mathbf{m}_n^o$ and $\mathbf{m}_2^s$ as the highest weights representing the irreps of $U^o(n)$ and $U^s(2)$ respectively, the subduced representation $\Gamma\{1^{2n}\} \downarrow [U^o(n) \times U^s(2)]$ of $U^o(n) \times U^s(2)$ contains only those representations $\Gamma\{\mathbf{m}_n^o\} \otimes \Gamma\{\mathbf{m}_2^s\}$ of $U^o(n) \times U^s(2)$ for which $\mathbf{m}_n^o$ and $\mathbf{m}_2^s$ are *mutually conjugate*.[202,203,213,234] This can be pictorially explained by the previously introduced *Young shapes*, see Sec. 3.2 and is explained in more detail in Sec. 3.3.3 and shown in Fig. 3.3.

Plainly spoken, this means the irreps of $U^o(n)$ and $U^s(2)$ are related in a specific manner to obtain physically plausible states satisfying the Pauli exclusion principle and antisymmetry of fermionic wavefunctions. This is another aspect of the fact that in the totally antisymmetric wavefunction the totally antisymmetric orbital part must be combined with the totally symmetric spin part and vice versa. E.g. an antisymmetric spin function $(\uparrow\downarrow - \downarrow\uparrow)$ forces a symmetric spatial function (a^2 or $ab + ba$), yielding an antisymmetric singlet state. On the other hand, a symmetric spin function $(\uparrow\uparrow, \uparrow\downarrow + \downarrow\uparrow, \downarrow\downarrow)$ is combined with an antisymmetric spatial function $(ab - ba)$ to yield the antisymmetric triplet states.

Since the Hamiltonian (3.8) is spin-independent, $U^s(2)$ does not contribute to the matrix element evaluation, so we only have to concern ourselves with the irreps of the orbital $U^o(n)$ subgroup, following Matsen's spin-free approach.[202,203] Nevertheless it is illuminating to investigate the pure spin space $U^s(2)$ and its relation to the group of spin rotations $SU(2)$, which after all is the symmetry associated with the conservation of the total spin S, see Sec. 3.1.

*This corresponds to the totally antisymmetric irrep of S_N, with $N = 2n$, represented by the Young shape with only one column, see 3.2.

3.3.3 The Pure Spin Space - $U^s(2)$

The irreducible representation of the pure spin $U^s(2)$ group, appearing in the direct product (3.32), completely determines the irrep of the pure orbital $U^o(n)$ group and vice versa, to yield the totally antisymmetric representation of $U(2n)$. The operators $\hat{\mathcal{E}}_{\sigma\tau} = \sum_i^n a_{i\sigma}^\dagger a_{i\tau}$ are identified as the generators of the unitary group of order 2, $U^s(2)$. The diagonal terms, $\hat{\mathcal{E}}_{\sigma\sigma} = \sum_i^n n_{i\sigma}$, are the number operators of electrons with spin σ, $\hat{N}_\sigma$. The basis states of $U(2)$ can be uniquely labelled with the following Gel'fand pattern, corresponding to the group chain $U(2) \supset U(1)$,

$$\begin{array}{ll} U(2): & \begin{bmatrix} m_{12}^s & & m_{22}^s \end{bmatrix} \\ U(1): & \begin{bmatrix} & m_{11}^s & \end{bmatrix} \end{array}, \tag{3.33}$$

with the in-between condition $m_{12}^s \geq m_{11}^s \geq m_{22}^s$. The top row, called the *highest weight vector*, $\mathbf{m}_2^s = (m_{12}^s, m_{22}^s)$ labels the chosen irrep of $U^s(2)$. At the same time $\mathbf{m}_2^s$ mutually determines the corresponding irrep $\mathbf{m}_n^o$ of $U^o(n)$ in the direct product (3.32) to yield a totally antisymmetric representation of $U(2n)$. The top row $\mathbf{m}_2^s$ specifies the total number of electrons $N = m_{12}^s + m_{22}^s$, total spin $S = (m_{12}^s - m_{22}^s)/2$, while the entry m_{11}^s specifies the z-component of $\hat{S}_z$ of the total spin angular momentum.

The chosen irrep $\mathbf{m}_2^s$ can also be represented in a pictorial manner by the means of *Young shapes*, introduced in Sec. 3.2. The Young shape of $U^s(2)$ is an arrangement of N boxes $\square$, with m_{12}^s boxes in the first row and m_{22}^s in the second, specifying the chosen irrep of $U^s(2)$. Similar to the symmetric group approach, the basis states of $U^s(2)$ can be identified by filling the Young shape with "tokens". In the UGA, in contrast to the SGA, the token are allowed to be repeated in the same row, but not in the same column, resulting in a so-called *Weyl tableau*.* Repetition of tokens in the same column would correspond to two electrons being in the exactly same quantum state, violating the Pauli exclusion principle. In the case of $U^s(2)$ we choose the tokens $\uparrow$ and $\downarrow$, representing the eigenvectors of the $\hat{S}_z$ operator, $\hat{S}_z |\uparrow\rangle = +1/2 |\uparrow\rangle$ and $\hat{S}_z |\downarrow\rangle = -1/2 |\downarrow\rangle$ (in units of $\hbar$). The complete basis is obtained by all permissible fillings of the boxes with tokens, e.g. $\boxed{\uparrow}$. The rules to fill the Weyl tableau based on a given Gel'fand pattern are: The tokens in the first row of the Weyl Tableau are determined by the first diagonal $[m_{11}^s, m_{12}^s, \ldots, m_{1n}^s]$ of the Gelfand pattern. Starting from the bottom of the Gel'fand pattern, the first token $\uparrow$ is put m_{11} times and the second token $\downarrow$ is put $m_{12} - m_{11}$ times into the first row. In general the second diagonal determines in a similar fashion the entries of the second row of the Weyl tableau. Because there are only 2 tokens and two rows for irreps of the pure spin $U^s(2)$ group, the second token $\downarrow$ is put m_{22} times into the second row, which completely fills the second row. Consequently the entry m_{11} determines the m_s quantum number, as

$$2m_s = m_{11} - (m_{12} - m_{11}) - m_{22} = 2m_{11} - (m_{12} + m_{22}) = 2m_{11} - N, \tag{3.34}$$

*Due to the possible repetitions, tokens can also be omitted in a Weyl tableau.

Table 3.1: All permissible states of two spin-1/2 particles represented by the equivalent Gel'fand pattern, Weyl Tableau and Dirac notation.

	$S=1$			$S=0$
	$m_s=1$	$m_s=0$	$m_s=-1$	$m_s=0$
Gel'fand pattern	$\begin{bmatrix} 2 & & 0 \\ & 2 & \end{bmatrix}$	$\begin{bmatrix} 2 & & 0 \\ & 1 & \end{bmatrix}$	$\begin{bmatrix} 2 & & 0 \\ & 0 & \end{bmatrix}$	$\begin{bmatrix} 1 & & 1 \\ & 1 & \end{bmatrix}$
Weyl Tableau	$\boxed{\uparrow}\boxed{\uparrow}$	$\boxed{\uparrow}\boxed{\downarrow}$	$\boxed{\downarrow}\boxed{\downarrow}$	$\begin{array}{|c|}\hline\uparrow\\\hline\downarrow\\\hline\end{array}$
Dirac Notation	$\lvert\uparrow\uparrow\rangle$	$\frac{1}{\sqrt{2}}(\lvert\uparrow\downarrow\rangle+\lvert\downarrow\uparrow\rangle)$	$\lvert\downarrow\downarrow\rangle$	$\frac{1}{\sqrt{2}}(\lvert\uparrow\downarrow\rangle-\lvert\downarrow\uparrow\rangle)$

Table 3.2: $N=3$ particles with two possible irreps of $U(2)$, $S=1/2:\mathbf{m}_2^s=(2,1)$ and $S=3/2:\mathbf{m}_2^s=(3,0)$.

S	Gel'fand pattern	Young shape	Basis states			
			$m_{11}:$	3	2	1	0
			$m_s:$	3/2	1/2	−1/2	−3/2
1/2	$\begin{bmatrix} 2 & & 1 \\ & m_{11} & \end{bmatrix}$	$\begin{array}{|c|c|}\hline\ \ &\ \ \\\hline\ \ \\\cline{1-1}\end{array}$			$\begin{array}{|c|c|}\hline\uparrow&\uparrow\\\hline\downarrow\\\cline{1-1}\end{array}$	$\begin{array}{|c|c|}\hline\uparrow&\downarrow\\\hline\downarrow\\\cline{1-1}\end{array}$	
3/2	$\begin{bmatrix} 3 & & 0 \\ & m_{11} & \end{bmatrix}$	$\begin{array}{|c|c|c|}\hline\ \ &\ \ &\ \ \\\hline\end{array}$		$\boxed{\uparrow}\boxed{\uparrow}\boxed{\uparrow}$	$\boxed{\uparrow}\boxed{\uparrow}\boxed{\downarrow}$	$\boxed{\uparrow}\boxed{\downarrow}\boxed{\downarrow}$	$\boxed{\downarrow}\boxed{\downarrow}\boxed{\downarrow}$

with $N=m_{12}+m_{22}$ being the total number of electrons. The in-between condition $m_{12}\geq m_{11}\geq m_{22}$ ensures $|m_s|\leq S=(m_{12}-m_{22})/2$. As can be seen in the example of a single particle of spin-1/2: $\mathbf{m}_2^s=(1,0)$:

$$|\uparrow\rangle=\begin{bmatrix}1&&0\\&1&\end{bmatrix}\mathrel{\widehat{=}}\boxed{\uparrow},\qquad|\downarrow\rangle=\begin{bmatrix}1&&0\\&0&\end{bmatrix}\mathrel{\widehat{=}}\boxed{\downarrow}.$$

For two spin-1/2 particles there are two possible irreps with the highest weight $\mathbf{m}_2^S=(1,1)$ and $\mathbf{m}_2^s=(2,1)$, which correspond to singlet ($S=0$) and triplet ($S=1$) states. For the triplet there are three permissible m_{11}^s values fulfilling the in-between condition, corresponding to the $m_s=0,\pm1$ states, as can be seen in Table 3.1. An example of the doublet and quartet states of three electrons are shown in Table 3.2.

As mentioned the irreps of the orbital $U^o(n)$ and spin $U^s(2)$ space must be mutually conjugate for the irrep $\Gamma\{\mathbf{m}_n^o\otimes\mathbf{m}_2^s\}$ of the direct product subgroup $U^o(n)\otimes U^s(2)$ to obtain the totally antisymmetric representation $\Gamma\{1^{2n}\}$ of $U(2n)$. This correspondence is very clear in terms of Young shapes. To yield a totally antisymmetric representation of $U(2n)$ the Young shape of a chosen $U^s(2)$ irrep must be the *transpose* (rows and columns exchanged) of the $U^o(n)$ Young shape and vice versa, as depicted in Fig. 3.3. Since, by definition, $U^s(2)$ only corresponds to Young shapes with at most two rows, the Young

shapes representing irreps of $U^o(n)$ are restricted to have two columns at most. This is a direct correspondence to the Pauli exclusion principle that a spatial orbital i can be occupied by two electrons with different spin at most.

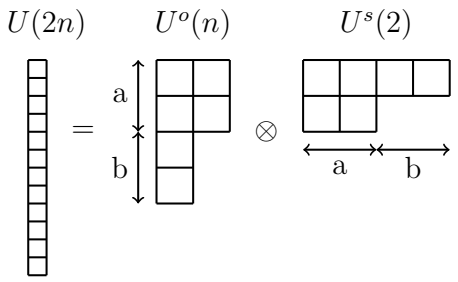

Fig. 3.3: Necessary relation of the $U^o(n)$ and $U^s(2)$ irreps represented by their Young shapes to yield the totally antisymmetric representation $\Gamma\{1^{2n}\}$ of $U(2n)$.

Denoting the number of two-row columns as a and the number of single-row columns as b for $U^s(2)$, as shown in Fig. 3.3, the total spin is given by $S = b/2$ and the number of electrons by $N = 2a + b$. The $\hat{S}_z$ operator of the z-component of the total spin can be expressed in terms of the spin operators $\mathcal{E}_{\sigma\tau}$ (in units of $\hbar$)

$$\hat{S}_z = \frac{1}{2}\left(\hat{\mathcal{E}}_{\uparrow\uparrow} - \hat{\mathcal{E}}_{\downarrow\downarrow}\right) \tag{3.35}$$

as this counts the difference of the total number of ↑- and ↓-spin electrons. For a spin-independent Hamiltonian it is unimportant which z component of the total spin is chosen, as it is block-diagonal with $2S+1$ identical blocks corresponding to the chosen multiplicity. If we choose the highest possible $S_z = S$ value and denote the chosen irrep of $U^s(2)$ by $\mathbf{m}_2^{s,max}$, it is easy to show that the chosen basis states are indeed eigenfunctions of the $\hat{\mathbf{S}}^2$ operator. This relation is most obvious if we look at the matrix representation of the $U^s(2)$ generators and their relation to the $SU(2)$ generators, expressed in terms of the more familiar Pauli matrices.

3.3.4 Matrix Representation of $U(2)$ and $SU(2)$

As a reminder, the unitary group of order 2, $U(2)$, consists of all unitary 2×2 matrices. In general every element $\mathbf{U} \in U(2)$ can be expressed as

$$\mathbf{U} = \underbrace{\mathrm{e}^{i\phi/2}}_{U(1)} \underbrace{\begin{pmatrix} \mathrm{e}^{i\phi_1}\cos\theta & \mathrm{e}^{i\phi_2}\sin\theta \\ -\mathrm{e}^{-i\phi_2}\sin\theta & \mathrm{e}^{-i\phi_1}\cos\theta \end{pmatrix}}_{SU(2)}, \tag{3.36}$$

with 4 real parameters $\phi, \phi_1, \phi_2, \theta$ and $\det \mathbf{U} = \mathrm{e}^{i\phi}$. This form highlights the relation of $U(2) = U(1) \otimes SU(2)$ as $U(1)$ is the group of all complex numbers with absolute value 1, $\mathrm{e}^{i\phi/2}$, and $SU(2)$. For the special unitary group $SU(2)$ the additional restriction of unimodularity, $\det \mathbf{U} = 1$, reduces the number of parameters to 3. Alternatively any unitary matrix can be expressed as the exponential of a skew-Hermitian matrix $\mathbf{A}$

$$\mathbf{U} = \exp \mathbf{A} \quad \text{with} \quad \mathbf{A}^\dagger = -\mathbf{A}. \tag{3.37}$$

A general skew-Hermitian matrix can be expressed as

$$\mathbf{A} = \begin{pmatrix} ia_1 & b_0 + ib_1 \\ -b_0 + ib_1 & ic_1 \end{pmatrix}, \tag{3.38}$$

with 4 real parameters a_1, b_0, b_1 and c_1. As any general 2×2 matrix, $\mathbf{A}$ can be expressed as a linear combination, $\mathbf{A} = \sum_{ij} \alpha_{ij} \mathbf{e}_{ij}$, of the four *basic matrix units* $\mathbf{e}_{ij}$

$$\mathbf{e}_{11} = \begin{pmatrix} 1 & 0 \\ 0 & 0 \end{pmatrix}, \quad \mathbf{e}_{12} = \begin{pmatrix} 0 & 1 \\ 0 & 0 \end{pmatrix}, \quad \mathbf{e}_{21} = \begin{pmatrix} 0 & 0 \\ 1 & 0 \end{pmatrix}, \quad \mathbf{e}_{22} = \begin{pmatrix} 0 & 0 \\ 0 & 1 \end{pmatrix}, \tag{3.39}$$

with complex coefficients α_{ij}. These basic matrix units fulfil the defining commutation relations of the unitary group $U(n)$

$$[\, \mathbf{e}_{ij}, \mathbf{e}_{kl} \,] = \delta_{jk} \mathbf{e}_{il} - \delta_{il} \mathbf{e}_{kj}. \tag{3.40}$$

However, to define a one-parameter subgroup of $U(2)$ it is beneficial to define the following skew-Hermitian basis set

$$\epsilon_{11} = i\mathbf{e}_{11} = \begin{pmatrix} i & 0 \\ 0 & 0 \end{pmatrix}, \qquad \epsilon_{22} = i\mathbf{e}_{22} = \begin{pmatrix} 0 & 0 \\ 0 & i \end{pmatrix} \tag{3.41}$$

$$\epsilon_{12} = \frac{i}{\sqrt{2}} (\mathbf{e}_{12} + \mathbf{e}_{21}) = \frac{i}{\sqrt{2}} \begin{pmatrix} 0 & 1 \\ 1 & 0 \end{pmatrix} \tag{3.42}$$

$$\epsilon_{21} = \frac{1}{\sqrt{2}} (\mathbf{e}_{21} - \mathbf{e}_{12}) = \frac{1}{\sqrt{2}} \begin{pmatrix} 0 & 1 \\ -1 & 0 \end{pmatrix}, \tag{3.43}$$

fulfilling $\epsilon^\dagger = -\epsilon$. ϵ_{ij} obey the slightly modified commutation relations*

$$[\, \epsilon_{ij}, \epsilon_{kl} \,] = \delta_{il} \epsilon_{jk} - \delta_{jk} \epsilon_{li} \tag{3.44}$$

in the two-dimensional matrix representation. With ϵ_{ij}, a general 2×2 skew-Hermitian matrix $\mathbf{A}$ can be expressed as $\mathbf{A} = \sum_{ij} \beta_{ij} \epsilon_{ij}$ with real parameters β_{ij}. The four one-parameter subgroups of the unitary group $U(2)$ can be expressed as

$$U_{ij}(\beta_{ij}) = \exp(\beta_{ij} \epsilon_{ij}). \tag{3.45}$$

The generators of $U(2)$ can be defined as

$$X_{ij} = \left. \frac{dU_{ij}(\beta_{ij})}{d\beta_{ij}} \right|_{\beta_{ij}=0}. \tag{3.46}$$

*Note the different indices!

These generators X_{ij} are just the skew-Hermitian basic matrix units ϵ_{ij}. By redefining a different set of generators as

$$\mathcal{E}_{ii} = -i\mathcal{E}_{ii}, \quad \mathcal{E}_{12} = -\frac{i}{\sqrt{2}}\left(X_{12} - iX_{21}\right) \quad \text{and} \quad \mathcal{E}_{21} = \frac{1}{\sqrt{2}}\left(X_{21} - iX_{12}\right) \tag{3.47}$$

we end up again with generators fulfilling the same commutation relations as the basic matrix units $\mathbf{e}_{ij}$

$$[\,\mathcal{E}_{ij}, \mathcal{E}_{kl}\,] = \delta_{jk}\mathcal{E}_{il} - \delta_{il}\mathcal{E}_{kj} \tag{3.48}$$

and the Hermitian property $\mathcal{E}_{ij}^{\dagger} = \mathcal{E}_{ji}$. The cumbersome route over defining skew-Hermitian matrix units was necessary for a mathematically sound definition of the one-parameter subgroups $U_{ij}(\beta_{ij})$ of $U(2)$ as mentioned in Sec. 3.3.1.

Matrix representation of $SU(2)$

The special unitary group $SU(2)$ is a subgroup of $U(2)$ consisting of all unitary 2×2 matrices $\mathbf{S}$ with $\det \mathbf{S} = 1$. They can be expressed as*

$$\mathbf{S} = \begin{pmatrix} a & b \\ -b^* & a* \end{pmatrix} = \begin{pmatrix} a_0 + ia_1 & b_0 + ib_1 \\ -b_0 + ib_1 & a_0 - ia_1 \end{pmatrix} = \begin{pmatrix} \mathrm{e}^{i\phi_1}\cos\theta & \mathrm{e}^{i\phi_2}\sin\theta \\ -\mathrm{e}^{-i\phi_2}\sin\theta & \mathrm{e}^{-i\phi_1}\cos\theta \end{pmatrix} \tag{3.49}$$

with $\det = |a|^2 + |b|^2 = a_0^2 + a_1^2 + b_0^2 + b_1^2 = 1$; a real three-parameter Lie Group. $\mathbf{S}$ can also be expressed in terms of the 2×2 identity $\mathbf{I}_2$ and the Pauli spin matrices

$$\hat{\sigma}_x = \begin{pmatrix} 0 & 1 \\ 1 & 0 \end{pmatrix}, \quad \hat{\sigma}_y = \begin{pmatrix} 0 & -i \\ i & 0 \end{pmatrix}, \quad \hat{\sigma}_z = \begin{pmatrix} 1 & 0 \\ 0 & -1 \end{pmatrix} \tag{3.50}$$

in the following way

$$\mathbf{S} = a_0 I_2 + ia_1\hat{\sigma}_x + ia_2\hat{\sigma}_y + ia_3\hat{\sigma}_z. \tag{3.51}$$

Or more concise as $\mathbf{S} = a_0\mathbf{I}_2 + i\vec{a}\cdot\vec{\hat{\sigma}}$, with $\vec{a} = (a_1, a_2, a_3)$ and $\vec{\sigma} = (\hat{\sigma}_x, \hat{\sigma}_y, \hat{\sigma}_z)$. Since $\hat{\sigma}_i^2 = \mathbf{I}_2$ there are 3 one-parameter subgroups of $SU(2)$

$$g_j(a_j) = \exp(ia_j\hat{\sigma}_j) \tag{3.52}$$

and the infinitesimal generators are given by the Pauli matrices

$$\sigma_j = \left.\frac{dg_j(a_j)}{da_j}\right|_{a_j=0} = \frac{1}{2}\hat{\sigma}_j, \tag{3.53}$$

with the commutation relations

$$[\,\hat{\sigma}_i, \hat{\sigma}_j\,] = 2i\epsilon_{ijk}\hat{\sigma}_k, \tag{3.54}$$

with ϵ_{ijk} being the totally antisymmetric Levi-Civita tensor. Equivalently the spin-angular

*Notice the equivalence to the second term in Eq. (3.36).

momentum operators $\hat{S}_j = 1/2\sigma_j$ which fulfil the $SU(2)$ (and $SO(3)$) commutation relations

$$[\,\hat{S}_i, \hat{S}_j\,] = i\epsilon_{ijk}\hat{S}_k \tag{3.55}$$

can be chosen as generators. This shows the connection of the $SU(2)$ group to the $SO(3)$ group of proper rotations in 3D space. However, the definition of $\hat{S}_j = 1/2\,\hat{\sigma}_j$ implies that for the one-parameter subgroups of $SU(2)$

$$g_j(a_j) = \exp(i\frac{a_j}{2}\hat{S}_j) \tag{3.56}$$

an angle of a_j and $a_j + 2\pi$ map to two distinct elements of $SU(2)$. However, a rotation of 2π in 3D space maps to the same element of $SO(3)$. This is the distinct property of spin-1/2 particles obtaining a phase of -1 after rotation of 2π and only mapping to the same element after a 4π rotation.*

3.3.5 Connection of $U(2)$ and $SU(2)$

With these results it is easy to see the connection between the generators of $U(2)$, $\mathcal{E}_{ij}$ and $SU(2)$, $\hat{S}_i$, given by[235]

$$\hat{S}_x = \frac{1}{2}\hat{\sigma}_x = \frac{1}{2}\begin{pmatrix}0 & 1\\ 1 & 0\end{pmatrix} = \frac{1}{2}\left(\mathcal{E}_{12} + \mathcal{E}_{21}\right) = \frac{1}{2}\left(\hat{\mathcal{E}}_{\uparrow\downarrow} + \hat{\mathcal{E}}_{\downarrow\uparrow}\right) \tag{3.57}$$

$$\hat{S}_y = \frac{1}{2}\hat{\sigma}_y = \frac{1}{2}\begin{pmatrix}0 & -i\\ i & 0\end{pmatrix} = -\frac{i}{2}\left(\mathcal{E}_{12} - \mathcal{E}_{21}\right) = -\frac{i}{2}\left(\hat{\mathcal{E}}_{\uparrow\downarrow} - \hat{\mathcal{E}}_{\downarrow\uparrow}\right) \tag{3.58}$$

$$\hat{S}_z = \frac{1}{2}\hat{\sigma}_z = \frac{1}{2}\begin{pmatrix}1 & 0\\ 0 & -1\end{pmatrix} = \frac{1}{2}\left(\mathcal{E}_{11} - \mathcal{E}_{22}\right) = \frac{1}{2}\left(\hat{\mathcal{E}}_{\uparrow\uparrow} - \hat{\mathcal{E}}_{\downarrow\downarrow}\right), \tag{3.59}$$

where the last relation comes from the choice of the eigenbasis of $\hat{S}_z$, $|\uparrow\rangle = (1,0)$ and $|\downarrow\rangle = (0,1)$. And conversely

$$\mathcal{E}_{11} = \hat{\mathcal{E}}_{\uparrow\uparrow} = \hat{S}_z + \frac{1}{2}\mathbb{1}, \qquad \mathcal{E}_{22} = \hat{\mathcal{E}}_{\downarrow\downarrow} = \hat{S}_z - \frac{1}{2}\mathbb{1} \tag{3.60}$$

$$\mathcal{E}_{12} = \hat{\mathcal{E}}_{\uparrow\downarrow} = \hat{S}_x + i\hat{S}_y = \hat{S}_+, \qquad \mathcal{E}_{21} = \hat{\mathcal{E}}_{\downarrow\uparrow} = \hat{S}_x - i\hat{S}_y = \hat{S}_-, \tag{3.61}$$

with the known ladder operators $\hat{S}_+$ and $\hat{S}_-$. With these relations the total spin operator $\hat{\mathbf{S}}^2$ can be expressed in terms of $\mathcal{E}_{\sigma\tau}$[234] as

$$\hat{\mathbf{S}}^2 = \hat{S}_z\left(\hat{S}_z + \mathbb{1}\right) + \hat{S}_-\hat{S}_+ = \frac{1}{4}\left(\hat{\mathcal{E}}_{\uparrow\uparrow} - \hat{\mathcal{E}}_{\downarrow\downarrow}\right)\left(\hat{\mathcal{E}}_{\uparrow\uparrow} - \hat{\mathcal{E}}_{\downarrow\downarrow} + 2\mathbb{1}\right) + \hat{\mathcal{E}}_{\downarrow\uparrow}\hat{\mathcal{E}}_{\uparrow\downarrow}. \tag{3.62}$$

As mentioned above the choice of the S_z quantum number is arbitrary for a spin-independent Hamiltonian. If we denote the direct product basis of $U^o(n) \times U^s(2)$ as $|\mathbf{m}^o\rangle \otimes |\mathbf{m}^{s,max}\rangle$

*This is the reason $SU(2)$ is said to be twice the size of $SO(3)$.

with maximum possible $S_z = S$, the action of the $\hat{S}_+$ operator on a basis state yields

$$\hat{S}_+ |\mathbf{m}^o\rangle \otimes |\mathbf{m}^{s,max}\rangle = \hat{\mathcal{E}}_{\uparrow\downarrow} |\mathbf{m}^o\rangle \otimes |\mathbf{m}^{s,max}\rangle = |\mathbf{m}^o\rangle \otimes \hat{\mathcal{E}}_{\uparrow\downarrow} |\mathbf{m}^{s,max}\rangle = 0, \tag{3.63}$$

since $\hat{\mathcal{E}}_{\uparrow\downarrow}$ only affects the spin part and $\hat{S}_+$ acting on a state with already maximal S_z^{max} yields zero. As already seen the chosen basis functions are eigenfunction of the remaining $\hat{S}_z = \frac{1}{2}\left(\hat{\mathcal{E}}_{\uparrow\uparrow} - \hat{\mathcal{E}}_{\downarrow\downarrow}\right)$ operators with eigenvalue $S_z^{max} = S$. So the composite basis states $|\mathbf{m} \otimes \mathbf{m}^{s,max}\rangle$ are eigenfunctions of $\hat{\mathbf{S}}^2$ with eigenvalue $S(S+1)$ with $S = S_z^{max}$. This can also be shown for a general S_z value, but is not necessary here, since we only wanted to demonstrate that the chosen basis functions are eigenfunction of the total spin operator and the choice of the S_z value is arbitrary for a spin-independent Hamiltonian.

The fact that the *singlet* excitation operators $\hat{E}_{ij}$ commute with $\hat{S}_z$ and $\hat{\mathbf{S}}^2$,

$$[\,\hat{S}_z, \hat{E}_{ij}\,] = [\,\hat{\mathbf{S}}^2, \hat{E}_{ij}\,] = 0 \tag{3.64}$$

and consequently do not change the spin of a state, mentioned in Sec. 3.3, is easy to show with the relations (3.57-3.59). Since

$$[\,\hat{E}_{ij}, \hat{\mathcal{E}}_{\sigma\tau}\,] = 0, \tag{3.65}$$

because $\hat{E}_{ij}$ are spin-independent and $\hat{\mathcal{E}}_{\sigma\tau}$ are orbital independent,[233] Eq. (3.64) is easy to show with $\hat{S}_z$ and $\hat{\mathbf{S}}^2$ expressed in terms of $\hat{\mathcal{E}}_{\sigma\tau}$ (3.57-3.59). Furthermore, since the spin-free Hamiltonian (3.8) is expressed solely in terms of the singlet excitation operators $\hat{E}_{ij}$,

$$[\,\hat{H}, \hat{\mathbf{S}}^2\,] = [\,\hat{H}, \hat{S}_z\,] = 0 \tag{3.66}$$

follows directly from (3.64).
The special case of the diagonal spin-independent occupation number operators of spatial orbital i, $\hat{E}_{ii} = n_{i\uparrow} + n_{i\downarrow} = \hat{N}_i$, of course also commutes with $\hat{\mathbf{S}}^2$ and $\hat{S}_z$

$$[\,\hat{S}_z, \hat{N}_{i\uparrow} + \hat{N}_{i\downarrow}\,] = [\,\hat{\mathbf{S}}^2, \hat{N}_{i\uparrow} + \hat{N}_{i\downarrow}\,] = 0. \tag{3.67}$$

This means we can set up spin-eigenfunctions which are simultaneous eigenfunctions of the operator $\hat{N}_i$. Singly occupied orbitals of these eigenfunctions of $\hat{N}_i$ are degenerate independent from the fact if they are filled with an $\uparrow$- or a $\downarrow$-spin electron, as only the orbital occupation matters. The set of all states with the same orbital occupation number is called an *orbital configuration*[133] and if all those degenerate states are combined in the construction of a spin-eigenbasis the resulting states are called *configuration state functions* (CSFs). Spin-eigenfunctions based on the UGA fall in the category of CSFs and thus we will refer to them as CSFs from now on. As an example there are four possible SDs for two electrons in two spatial orbitals with the orbital configuration $n_1 = n_2 = 1$ and z-projection of spin $m_s = 0, \pm 1$. These four states can be combined to CSFs to yield

the singlet $S = 0$ and three possible $S = 1$ triplet spin eigenfunctions:

Orbital configuration	Spin-orbit representation	m_s	Configuration state functions	S
$\|1,1\rangle$	$\|\uparrow,\downarrow\rangle$	0	$\frac{1}{\sqrt{2}}(\|\uparrow,\downarrow\rangle - \|\downarrow,\uparrow\rangle)$	0
	$\|\downarrow,\uparrow\rangle$	0	$\frac{1}{\sqrt{2}}(\|\uparrow,\downarrow\rangle + \|\downarrow,\uparrow\rangle)$	1
	$\|\uparrow,\uparrow\rangle$	1	$\|\uparrow,\uparrow\rangle$	1
	$\|\downarrow,\downarrow\rangle$	-1	$\|\downarrow,\downarrow\rangle$	1

3.3.6 The Pure Orbital Space - $U^o(n)$

After this in-depth discussion of the properties of the pure-spin group $U^s(2)$, we turn our focus now on the pure orbital space, associated with the unitary group of order n, $U(n)$, where we will soon drop the superscript ^{o} for brevity. The consequence of the mutually conjugate relationship between $U^o(n)$ and $U^s(2)$ irreps for electronic structure calculations is that the integers m_{ij} in a Gel'fand pattern for $U^o(n)$ are related to occupation numbers of spatial orbitals. This means they are restricted to $0 \leq m_{ij} \leq 2$, due to the Pauli exclusion principle. The highest weight, $\mathbf{m}_n^o$, indicates the chosen electronic state with the conditions

$$\sum_{i=1}^{n} m_{in} = N \quad \text{and} \quad \frac{1}{2}\sum_{i=1}^{n} \delta_{1,m_{in}} = S, \tag{3.68}$$

with N being the total number of electrons and the number of singly occupied orbitals, $\delta_{1,m_{ij}}$ is equal to twice the total spin value S.

Therefore a top row of $\mathbf{m}_3 = (2,1,0)$ specifies an electronic state with 3 electrons (the sum of the top row entries is equal to three) in 3 spatial orbitals with a total spin of $S = 1/2$ (the sum of the singly occupied orbitals is equal to one). All the CSFs belonging to this irrep are obtained by filling the Gel'fand pattern with integers m_{ij} in all possible ways, fulfilling the *in-between* condition (3.27). The 8 possible ways to do that are:

$$\begin{bmatrix} 2 & & 1 & & 0 \\ & 2 & & 1 & \\ & & 2 & & \end{bmatrix} \quad \begin{bmatrix} 2 & & 1 & & 0 \\ & 2 & & 1 & \\ & & 1 & & \end{bmatrix} \quad \begin{bmatrix} 2 & & 1 & & 0 \\ & 2 & & 0 & \\ & & 2 & & \end{bmatrix} \quad \begin{bmatrix} 2 & & 1 & & 0 \\ & 2 & & 0 & \\ & & 1 & & \end{bmatrix}$$

$$\begin{bmatrix} 2 & & 1 & & 0 \\ & 2 & & 0 & \\ & & 0 & & \end{bmatrix} \quad \begin{bmatrix} 2 & & 1 & & 0 \\ & 1 & & 1 & \\ & & 1 & & \end{bmatrix} \quad \begin{bmatrix} 2 & & 1 & & 0 \\ & 1 & & 0 & \\ & & 1 & & \end{bmatrix} \quad \begin{bmatrix} 2 & & 1 & & 0 \\ & 1 & & 0 & \\ & & 0 & & \end{bmatrix}$$

3.3.7 The Paldus tableau

The restriction of $0 \leq m_{ij} \leq 2$ in *electronic* Gel'fand patterns led Paldus[230] to the more compact formulation by a table of $3n$ integers. It is sufficient to count the appearances $2's$, $1's$ and $0's$ in each row i of a Gel'fand pattern and store this information, denoted by a_i, b_i and c_i in a table, named a *Paldus tableau*. Eq. (3.69) shows the equivalent representation

of a state with 6 electrons in 8 orbitals and total spin $S = 2$ in the Gel'fand pattern and Paldus tableau format.

$$\begin{bmatrix} 2 & 2 & 1 & 1 & 0 & 0 & 0 & 0 \\ & 2 & 2 & 1 & 1 & 0 & 0 & 0 \\ & & 2 & 1 & 1 & 0 & 0 & 0 \\ & & & 2 & 1 & 1 & 0 & 0 \\ & & & & 2 & 1 & 0 & 0 \\ & & & & & 1 & 1 & 0 \\ & & & & & & 1 & 0 \\ & & & & & & & 1 \end{bmatrix} \equiv \begin{bmatrix} a_i & b_i & c_i \\ \hline 2 & 2 & 4 \\ 2 & 2 & 3 \\ 1 & 2 & 3 \\ 1 & 2 & 2 \\ 1 & 1 & 2 \\ 0 & 2 & 1 \\ 0 & 1 & 1 \\ 0 & 1 & 0 \end{bmatrix} \tag{3.69}$$

The first column, a_i, contains the number of doubly occupied orbitals, the second column, b_i, the number of singly occupied and the last one, c_i, the number of empty orbitals. And for each row the condition

$$a_i + b_i + c_i = i, \quad (i = 1, \ldots, n) \tag{3.70}$$

holds, so any two columns are sufficient to uniquely determine the state. The top row satisfies the following properties

$$a = a_n = \frac{1}{2}N - S, \quad b = b_n = 2S, \quad c = c_n = n - a - b = n - \frac{1}{2}N - S, \tag{3.71}$$

completely specifying the chosen electronic state as an irrep of $U(n)$*. The total number of CSFs for a given number of orbitals n, electrons N and total spin S is given by the Weyl-Paldus[230,352] dimension formula

$$N_{CSF} = \frac{b+1}{n+1}\binom{n+1}{a}\binom{n+1}{c} = \frac{2S+1}{n+1}\binom{n+1}{\frac{N}{2}-S}\binom{n+1}{n-\frac{N}{2}-S}. \tag{3.72}$$

As it can be seen from Eq (3.72), the number of possible CSFs—of course—still scales combinatorially with the number of electrons and orbitals, as seen in Fig. 3.4 with a comparison to the total number of possible SDs (1.38). However, the ratio of the total number of SDs (without any symmetry restriction) and CSFs for $N = n$ can be estimated by Stirling's formula (for sufficiently large n and N) as

$$\frac{N_{SD}}{N_{CSF}} \approx \frac{\sqrt{\pi\, n} n}{2(2S+1)}, \tag{3.73}$$

which shows orbital dependent, $\sim n^{3/2}$, decrease of the efficient Hilbert space size for a spin-adapted basis. The Paldus tableau also emphasizes the cumulative aspects of the coupling between electrons, with the i-th row providing information on number of electrons, N_i (up to i-th level) and the spin, S_i, by

$$N_i = 2a_i + b_i, \qquad S_i = \frac{1}{2}b_i. \tag{3.74}$$

*From now on we drop the superscript o as we exclusively deal with the orbital group $U(n)$.

Table 3.4: Conjugate irreps of the spatial $U(3)$ and spin $U(2)$ group for the singlet, $S = 0$, and triplet, $S = 1$, state of 2 electrons in 3 spatial orbitals. The spatial U(n) irreps are determined by the spin-state states. All the CSFs belonging to this irrep are obtained by filling orbital "tokens" (1,2,3) with no repetitions in same column in the Weyl tableau representation. The correspondence to Gel'fand patterns is also shown.

$S = 0$: $U(3) \otimes U(2)$				$S = 1$: $U(3) \otimes U(2)$	
$\begin{bmatrix} 2 & 0 & 0 \\ 2 & 0 \\ & 2 \end{bmatrix}$	$\begin{array}{\|c\|c\|}\hline 1&1\\\hline\end{array}$	$\begin{bmatrix} 2 & 0 & 0 \\ 1 & 0 \\ & 1 \end{bmatrix}$	$\begin{array}{\|c\|c\|}\hline 1&3\\\hline\end{array}$	$\begin{bmatrix} 1 & 1 & 0 \\ 1 & 1 \\ & 1 \end{bmatrix}$	$\begin{array}{\|c\|}\hline 1\\\hline 2\\\hline\end{array}$
$\begin{bmatrix} 2 & 0 & 0 \\ 2 & 0 \\ & 1 \end{bmatrix}$	$\begin{array}{\|c\|c\|}\hline 1&2\\\hline\end{array}$	$\begin{bmatrix} 2 & 0 & 0 \\ 1 & 0 \\ & 0 \end{bmatrix}$	$\begin{array}{\|c\|c\|}\hline 2&3\\\hline\end{array}$	$\begin{bmatrix} 1 & 1 & 0 \\ 1 & 1 \\ & 1 \end{bmatrix}$	$\begin{array}{\|c\|}\hline 1\\\hline 3\\\hline\end{array}$
$\begin{bmatrix} 2 & 0 & 0 \\ 2 & 0 \\ & 0 \end{bmatrix}$	$\begin{array}{\|c\|c\|}\hline 2&2\\\hline\end{array}$	$\begin{bmatrix} 2 & 0 & 0 \\ 0 & 0 \\ & 0 \end{bmatrix}$	$\begin{array}{\|c\|c\|}\hline 3&3\\\hline\end{array}$	$\begin{bmatrix} 1 & 1 & 0 \\ 1 & 0 \\ & 0 \end{bmatrix}$	$\begin{array}{\|c\|}\hline 2\\\hline 3\\\hline\end{array}$

Of course, like a Gel'fand pattern, a Paldus tableau can also be represented by a *Weyl tableau*.[162] As mention in Sec. 3.3.3, the permissible Young shapes for $U(n)$ irreps have 2 columns at most, due to the Pauli exclusion principle. The top row of the Gel'fand pattern, $[m]_n$, with $0 \leq m_{in} \leq 2$, specifies how many boxes are in each row, i.e. m_{1n} boxes in the first row, m_{2n} boxes in the second row and so on, while the same information is provided by the a_n and b_n values of the Paldus tableau, i.e. a_n rows with two boxes and b_n rows with 1 box, see Table 3.3. For components of the $U(n)$ irrep this shape is then filled with *tokens* $1, 2, \ldots, n$, representing the *occupied spatial orbitals*. Starting from the first spatial orbital $i = 1$ in a consecutive way, empty spatial orbital are omitted, doubly occupied orbitals are put in the first and second column of the Weyl tableau. Orbitals which is coupled in a way to increase the incremental total spin, $\Delta S_i = S_i - S_{i-1} = 1/2$, are inserted in the first column, while orbitals, which decrease the incremental total spin, $\Delta S_i = -1/2$, are collected in the second column, with the restriction $S_i \geq 0, \forall i$. An example of this correspondence is shown in Tables 3.4 and 3.3 for a system of 2 electrons in 3 spatial orbitals for $S = 0$ and $S = 1$.

Table 3.3: Correspondence of Paldus tableau, step-vector and Weyl tableau representation of a CSF belonging to the $N = 8$, $n = 7$ and $S = 2$ irrep of $U(n)$.

a
b

1	1
2	5
4	7
6	
7	

orbital (i)	a_i	b_i	N_i	S_i	d_i
7	3	2	8	1	3
6	2	2	6	1	1
5	2	1	5	1/2	2
4	1	2	4	1	1
3	1	1	3	1/2	0
2	1	1	3	1/2	1
1	1	0	2	0	3
0	0	0	0	0	

As indicated above, starting from the "vacuum" 0'th row $i = 0$, there are *four* possible ways of coupling a spatial orbital based on the group chain (3.25). Paldus identified the different possibilities in terms of the difference vectors $\Delta x_i = x_i - x_{i-1}$, with $x = a, b, c$ and the four possible ways are shown in Table 3.5, where the same restriction $S_i \geq 0$, $\forall i$ applies.

Table 3.5: Four possible ways of coupling an orbital i.

d_i	Δa_i	Δb_i	Δc_i	ΔN_i	ΔS_i
0	0	0	1	0	0
1	0	1	0	1	1/2
2	1	-1	1	1	-1/2
3	1	0	0	2	0

The *step-value* d_i in Tab. 3.5 is given by $d_i = 2\Delta a_i - \Delta c_i + 1$ and the collection of all d_i into the **step-vector d** representation is the *most compact* form of representing a CSF, with the same storage cost as a Slater determinant. One can create all basis function of a chosen irrep of $U(n)$ by constructing all possible distinct step-vectors $|\mathbf{d}\rangle$ which lead to the same top-row of the Paldus tableau (3.71) with the restriction $S_i \geq 0$, $\forall i$.

As mentioned in Sec. 3.3.5, this choice of basis does not fix the value of the m_s quantum number.[284] However, the Hamiltonian matrix elements are independent of m_s, and thus any allowed value of m_s can be assumed. However, the value of m_s can be fixed by a permissible choice of an irrep of the spin unitary group, $U^s(2)$.[233]

3.4 The Graphical Unitary Group Approach (GUGA)

The graphical unitary group approach (GUGA) of Shavitt[282,284] is based on this step-vector representation and the observation that there is a lot of repetition of possible rows in the Paldus tableaux specifying the CSFs of a chosen irrep of $U(n)$. So, instead of all possible Paldus tableaux, Shavitt suggested to just list the possible sets of rows in a table, called the *distinct row table* (DRT). The number of possible elements of this table is given by[282]

$$\begin{aligned} N_{DRT} &= (a+1)(c+1)\left(b+1+\frac{d}{2}\right) - \frac{d(d+1)(d+2)}{6} \\ &= \left(\frac{N}{2}-S+1\right)\left(n-\frac{N}{2}-S+1\right)\left(2S+1+\frac{d}{2}\right) - \frac{d(d+1)(d+2)}{6}, \end{aligned} \tag{3.75}$$

with $d = \min(a, c) = \min(N/2-S, n-N/2-S)$, which is drastically smaller than the total number of possible CSFs (3.72) and Slater determinants (1.38) (without any symmetry restrictions) as seen in Fig. 3.4. Each row is identified by a pair of indices (i, j), with $i = a_{ij} + b_{ij} + c_{ij}$ being the *level index*, related to the orbital index* and j being the *lexical row index* such that $j < j'$ if $a_{ij} > a'_{ij}$ or if $a_{ij} = a'_{ij}$ and $b_{ij} > b'_{ij}$. A simple example of the

*Remember that for n orbitals we will have tables with n rows.

Table 3.6: Distinct row table for $n = 3$, $N = 4$ and $S = 0$.

a	b	c	i	j	d_0	d_1	d_2	d_3	u_0	u_1	u_2	u_3
2	0	1	3	1	2	0	3	4	-	-	-	-
2	0	0	2	2	0	0	0	5	1	0	0	0
1	1	0	2	3	0	5	0	6	0	0	1	0
1	0	1	2	4	5	0	6	7	0	0	0	1
1	0	0	1	5	0	0	0	8	4	3	0	2
0	1	0	1	6	0	8	0	0	0	0	4	3
0	0	1	1	7	8	0	0	0	0	0	0	4
0	0	0	0	8	-	-	-	-	7	6	0	5

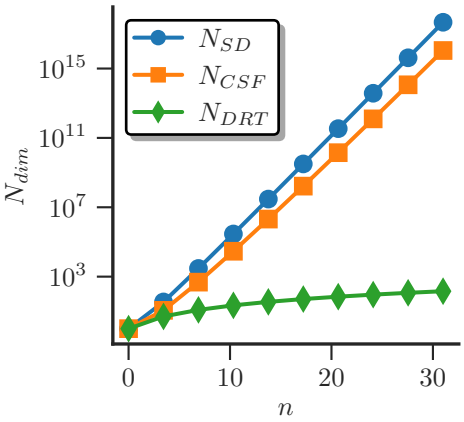

Figure 3.4: Number of total SDs (without any symmetry restrictions), CSFs and entries of the distinct row table (DRT) for $S = 0$ and $N = n$ as a function of n.

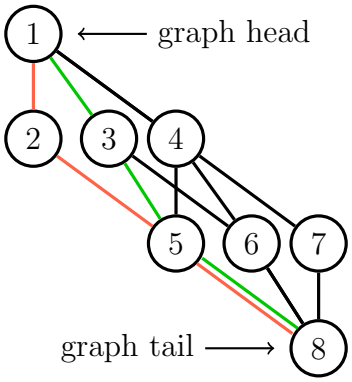

Figure 3.5: Graph representing the DRT of Table 3.6. The orange line corresponds to the CSF $|d\rangle_1 = |3, 3, 0\rangle$ and the green line to $|d\rangle_2 = |3, 1, 2\rangle$ in the step-vector representation.

DRT of a system with $n = 3$, $N = 4$ and $S = 0$ is shown in Table 3.6. Relations between elements of the DRT belonging to two neighbouring levels k and $k - 1$ are indicated by the so called *downward*, d_{d_k}, and *upward*, u_{d_k}, *chaining indices*, with $d_k = 0, 1, 2, 3$. These indices indicate the connection to a lexical row index in a neighbouring level by a step-value d_k, where a zero entry indicates an invalid connection associated with this step-value. Given a DRT table any of the possible CSFs can be generated by connecting distinct rows linked by the chaining indices.

This DRT table can be represented as a graph, see Fig. 3.5, where each distinct row is represented by a *vertex* (node) and nonzero chaining indices are indicated by an *arc* (directed edge). The vertices are labelled according to the lexical row index j, starting at the unique *head* node at the top, which corresponds to the highest row (a, b, c). It ends at the second unique null row $(0, 0, 0)$, which is called the *tail* of the graph. Vertices with the same i-value of Table 3.6 are at the same level on this grid. The highest i-value is on top and the lowest at the bottom. Vertices also have left-right order with respect to their a_i value and vertices that share the same a_i value are further ordered—still horizontally—with respect to their b_i value. With the above mentioned ordering of the

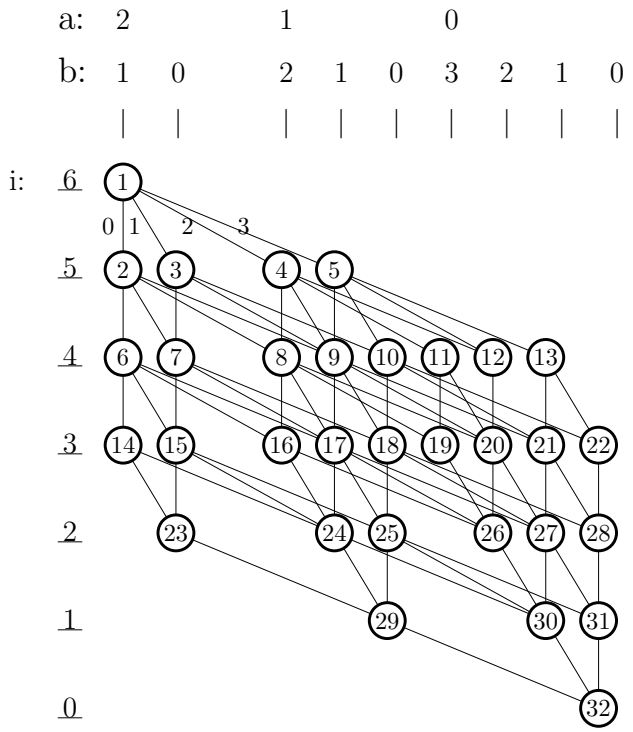

Fig. 3.6: Graph representing the DRT for a $n = 6$, $N = 5$ and $S = \frac{1}{2}$ state. The a and b values indicating the ordering in the graph are shown at the top and the level index i is indicated at the left. The different step-values d connecting the nodes are shown for the node 1 at the top.

vertices according to their a_i and b_i values, the slope of each arc is in direct correspondence to the step-value d_i, connecting two vertices. $d = 0$ corresponds to vertical lines, and the tilt of the other arcs increases with the step-value d_i.

Each CSFs in the chosen irrep of $U(n)$, is represented by a *directed walk* through the graph starting from the tail and ending at the head, e.g. the green and orange lines in Fig. 3.5, representing the states $|\mathbf{d}_1\rangle = |3, 3, 0\rangle$ and $|\mathbf{d}_2\rangle = |3, 1, 2\rangle$. Such a walk spans n arcs (number of orbitals) and visit one node at each hierarchical level. There is a direct correspondence between the Paldus tableau, Gel'fand patterns and directed walks on *Shavitt graphs* for representing all possible CSFs in a chosen irrep of $U(n)$.

A lengthy example. Consider a system with $n = 6$, $N = 5$ and $S = \frac{1}{2}$. The DRT of this state has 32 distinct rows (omitted for brevity), while the total number of CSFs is $N_{CSF} = 210$. The graph representing this state is shown in Fig. 3.6, where the vertical ordering according to the index i and the horizontal ordering according to the a_i and b_i values is indicated.

3.4.1 Evaluation of Nonvanishing Hamiltonian Matrix Elements

Given the expression of the nonrelativistic spin-free Hamiltonian in (3.8) a matrix element between two CSFs, $|m'\rangle$ and $|m\rangle$, is given by:

$$\langle m'|\hat{H}|m\rangle = \sum_{ij} t_{ij}\langle m'|\hat{E}_{ij}|m\rangle + \frac{1}{2}\sum_{ij,kl} V_{ijkl}\langle m'|\hat{e}_{ij,kl}|m\rangle. \tag{3.76}$$

The matrix elements, $\langle m'|\hat{E}_{ij}|m\rangle$ and $\langle m'|\hat{e}_{ij,kl}|m\rangle$, provide the *coupling coefficients* between two given CSFs and t_{ij} and V_{ijkl} are the *integral contributions*. They are independent of the orbital shape and depend only on the actual coupling between the CSFs, $|m'\rangle$ and $|m\rangle$, involved. Therefore, for a given set of integrals the problem of computing Hamiltonian matrix elements is reduced to the evaluation of these coupling coefficients. The graphical representation of CSFs has been proven a powerful tool to evaluate these coupling coefficients thanks to the formidable contribution of Paldus, Boyle, Shavitt and others.[71,236,283]

The great strength of the graphical approach is the identification and evaluation of non-vanishing matrix elements of the excitation operators (generators) $\hat{E}_{ij}$, between two GT states (CSFs), $\langle m'|\hat{E}_{ij}|m\rangle$. The generators are classified according to their indices, with $\hat{E}_{ii}$ being diagonal *weight* (W) and $\hat{E}_{ij}$ with $i < j$ being *raising* (R) and $i > j$ *lowering* (L) operators (or generators). In contrast to Slater determinants, $\hat{E}_{ij}$ applied to $|m\rangle$ yields a *linear combination* of CSFs $|m'\rangle$,

$$\hat{E}_{ij}\,|m\rangle = \sum_{m'} |m'\rangle\,\langle m'|\hat{E}_{ij}|m\rangle, \tag{3.77}$$

with an electron moved from spatial orbital j to orbital i without changing the spin of the resulting states $|m'\rangle$. They are called raising(lowering) operators since the resulting $|m'\rangle$ will have a higher(lower) lexical order than the starting CSF $|m\rangle$.

The distance, S_0, from $\min(i,j)-1$ to $\max(i,j)$, is an important quantity and is called the *range of the generator* $\hat{E}_{ij}$. For the one-body term in (3.8) Shavitt[282] was able to show that the walks on the graph, representing the CSFs $|m\rangle$ and $|m'\rangle$, must coincide outside of this range S_0 to yield a non-zero matrix element. The two vertices in the DRT graph, related to orbital $i-1$ and j (with $i < j$) represent the points of separation of the walks and they are named *loop head* and *loop tail*. And the matrix element $\langle m'|\hat{E}_{ij}|m\rangle$ only depends on the *shape of the loop* formed by the two graphs in the range S_0, shown in fig 3.7. Shavitt[283] showed that for a raising generator the relations

$$N'_k = N_k + 1, \quad b'_k = b_k \pm 1 \quad \text{and} \quad S'_k = S_k \pm \frac{1}{2} \quad \text{for} \quad k \in S_0, \tag{3.78}$$

between $|m\rangle$ and $|m'\rangle$ must be fulfilled to yield a nonzero matrix element. While for a *lowering* generator (L) $N'_k = N_k - 1$ must be fulfilled. This allows *two* possible relations between the vertices at each level in terms of Paldus array quantities depending on the type of generator (R,L).
For *raising generators* R:

$$a'_k = a_k, \quad b'_k = b_k + 1, \quad c'_k = c_k - 1, \quad \rightarrow \underline{\Delta b_k = -1}, \tag{3.79}$$

$$a'_k = a_k + 1, \quad b'_k = b_k - 1, \quad c'_k = c_k \quad \rightarrow \underline{\Delta b_k = +1}, \tag{3.80}$$

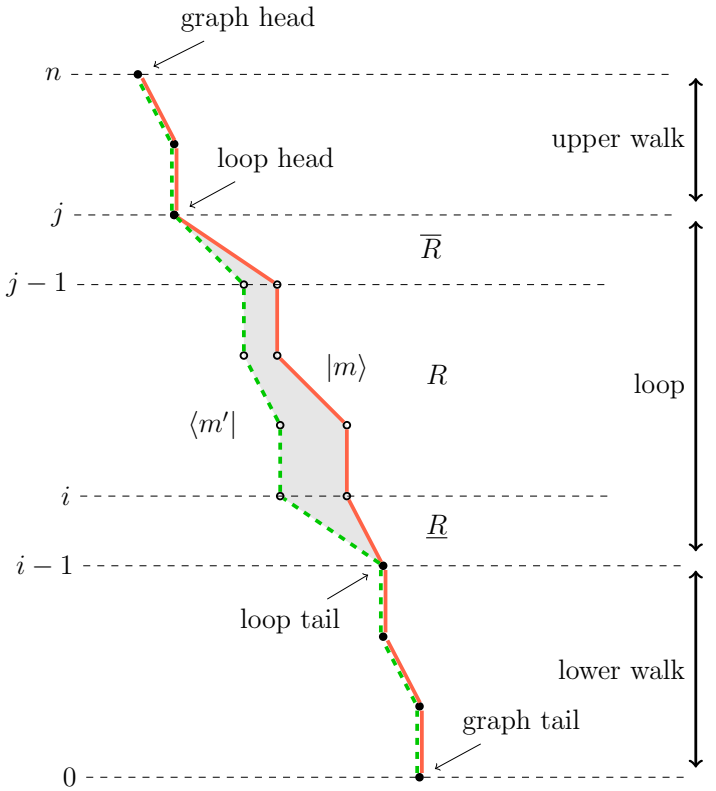

Fig. 3.7: Graphical representation of a matrix element $\langle m'|\hat{E}_{ij}|m\rangle$ as a loop shape created by two CSFs $|m'\rangle$ and $|m\rangle$ on a Shavitt graph.

where $\Delta b_k = b_k - b'_k$. And for *lowering generators* L:

$$a'_k = a_k - 1, \quad b'_k = b_k + 1, \quad c'_k = c_k \quad \rightarrow \underline{\Delta b_k = -1}, \tag{3.81}$$

$$a'_k = a_k, \quad b'_k = b_k - 1, \quad c'_k = c_k + 1 \quad \rightarrow \underline{\Delta b_k = +1}. \tag{3.82}$$

At each vertex of the loop in range k one of the relations (3.79-3.82) must be fulfilled for the one-body matrix element to be non-zero.

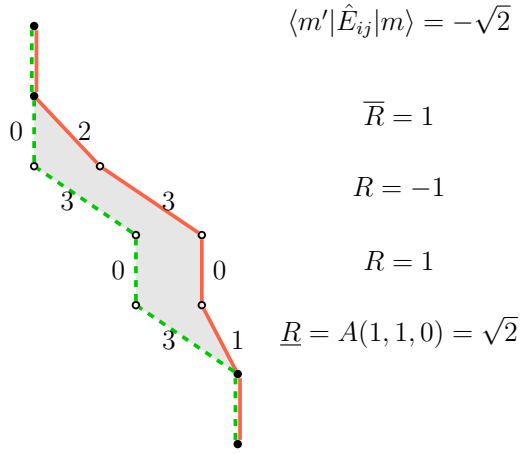

$\langle m'|\hat{E}_{ij}|m\rangle = -\sqrt{2}$

$\overline{R} = 1$

$R = -1$

$R = 1$

$\underline{R} = A(1,1,0) = \sqrt{2}$

Fig. 3.8: Graphical representation of the matrix element $\langle 030300|\hat{E}_{25}|010320\rangle = -\sqrt{2}$.

Based on the graphical approach, Shavitt[283] showed that the matrix elements of the generators $\hat{E}_{ij}$ can be factorized in a product, where each term corresponds to a segment of the loop in the range S_0 and is given by

$$\langle m'|\hat{E}_{ij}|m\rangle = \prod_{k=i}^{j} W(Q_k; d'_k, d_k, \Delta b_k, b_k), \tag{3.83}$$

where b_k is the b value of state $|m\rangle$ at level k. $W(Q_k; d'_k, d_k, \Delta b_k, b_k)$ additionally depends on the *segment shape* of the loop at level k, determined by the type of the generator $Q_k = W, R, L$, the step values d'_k

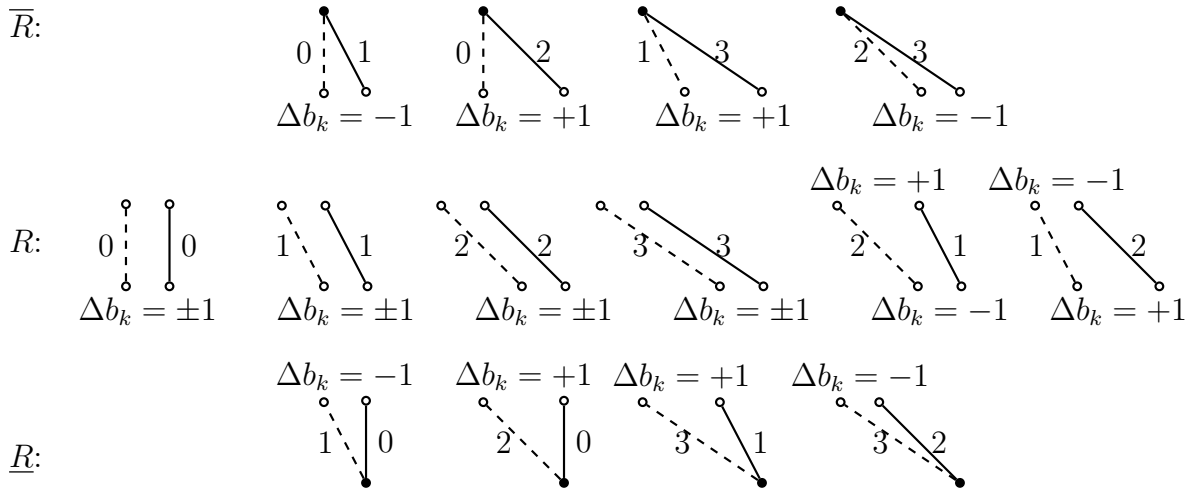

Figure 3.9: Nonzero segment shapes of a raising generator $\hat{E}_{ij}$. The numbers next to the lines indicate the step-values d' and d. $\underline{R}(\overline{R})$ correspond to the loop tail (head) segments and R to shapes inside the generator range S_0. Δb_k indicates the possible difference of b'_k and b_k leading to nonzero matrix elements.

and d_k and $\Delta b_k = b_k - b'_k$. The nonzero segment shapes for a raising (R) generator are shown in Fig. 3.9. In Table 3.7 the nonzero matrix elements of the one-electron operator $\hat{E}_{ij}$ depending on the segment shape symbol, the step-values and the b-value are given in terms of the auxiliary functions

$$A(b,x,y) = \sqrt{\frac{b+x}{b+y}}, \quad C(b,x) = \frac{\sqrt{(b+x-1)(b+x+1)}}{b+x}. \tag{3.84}$$

As an example, Fig. 3.8 shows the graphical representation of the matrix element $\langle 030300|\hat{E}_{25}|010320\rangle$, with $|m'\rangle$ and $|m\rangle$ in their step-vector representation. Each segment shape is obtained from Fig. 3.9 with the corresponding value from Table 3.7 and the resulting matrix element is given as the product of them.

3.4.2 Two-Body Matrix Elements

The matrix elements of the two-body operators $\hat{e}_{ij,kl}$ are more involved than the one-body operators, especially the product of singlet excitation generators, $\hat{E}_{ij}\hat{E}_{kl}$. Similar to the one-electron operators, the GT states $|m\rangle$ and $|m'\rangle$ must coincide outside the total range $\min(i,j,k,l)$ to $\max(i,j,k,l)$ for $\langle m'|\hat{e}_{ij,kl}|m\rangle$ to be nonzero. The form of the matrix element depends on the *overlap range* of the two ranges

$$S_1 = (i,j) \cap (k,l). \tag{3.85}$$

Table 3.7: Nonzero matrix elements of the one-body operator $\hat{E}_{ij}$ in terms of the auxiliary functions (3.84.

$d'd$	W
00	0
11	1
22	1
33	2

$d'd$	$\overline{R}$	$\underline{L}$
01	1	1
02	1	1
13	$A(b,0,1)$	$A(b,2,1)$
23	$A(b,2,1)$	$A(b,0,1)$

$d'd$	$\underline{R}$	$\overline{L}$
10	1	1
20	1	1
31	$A(b,1,0)$	$A(b,0,1)$
32	$A(b,1,2)$	$A(b,2,1)$

	R		L	
$d'd$	$\Delta b=-1$	$\Delta b=+1$	$\Delta b=-1$	$\Delta b=+1$
00	1	1	1	1
11	-1	$C(b,0)$	$C(b,1)$	-1
12	$-1/(b+2)$	-	$1/(b+1)$	-
21	-	$1/b$	-	$-1/(b+1)$
22	$C(b,2)$	-1	-1	$C(b,1)$
33	-1	-1	-1	-1

One possibility to calculate the matrix element would be to sum over all possible intermediate states, $|m''\rangle$,

$$\langle m'|\hat{E}_{ij}\hat{E}_{kl}|m\rangle = \sum_{m''}\langle m'|\hat{E}_{ij}|m''\rangle\langle m''|\hat{E}_{kl}|m\rangle, \tag{3.86}$$

but in practice this is very inefficient. For non-overlapping ranges $S_1 = \emptyset$ the matrix element just reduces to the product

$$\langle m'|\hat{e}_{ij,kl}|m\rangle = \langle m'|\hat{E}_{ij}\hat{E}_{kl}|m\rangle = \langle m'|\,\hat{E}_{ij}\,|m''\rangle\,\langle m''|\,\hat{E}_{kl}\,|m\rangle\,, \tag{3.87}$$

where $|m''\rangle$ must coincide with $|m\rangle$ in the range (i,j) and with $|m'\rangle$ in range (k,l). The same rules and matrix elements as for one-body operators apply in this case. An example of this is shown in the left panel of Fig. 3.10.
For $S_1 \neq \emptyset$, we define the *non-overlap range*

$$S_2 = (i,j) \cup (k,l) - S_1, \tag{3.88}$$

where the same restrictions and matrix elements as for one-body operators apply. In the overlap range, S_1, different restrictions for the visited Paldus tableau vertices p apply for the matrix element to be nonzero. This depends on the type of the two generators involved and were worked out by Shavitt.[284] For two raising generators (RR) the following

conditions apply

$$a'_p = a_p, \quad b'_p = b_p + 2, \quad c'_p = c_p - 2 \quad \rightarrow \underline{\Delta b_p = -2} \tag{3.89}$$

$$a'_p = a_p + 2, \quad b'_p = b_p + 2, \quad c'_p = c_p \quad \rightarrow \underline{\Delta b_p = +2} \tag{3.90}$$

$$a'_p = a_p + 1, \quad b'_p = b_p, \quad c'_p = c_p - 1 \quad \rightarrow \underline{\Delta b_p = 0}. \tag{3.91}$$

For two lowering generators (LL):

$$a'_p = a_p + 2, \quad b'_p = b_p + 2, \quad c'_p = c_p, \quad \rightarrow \underline{\Delta b_p = -2} \tag{3.92}$$

$$a'_p = a_p, \quad b'_p = b_p - 2, \quad c'_p = c_p + 2 \quad \rightarrow \underline{\Delta b_p = +2} \tag{3.93}$$

$$a'_p = a_p - 1, \quad b'_p = b_p, \quad c'_p = c_p + 2 \quad \rightarrow \underline{\Delta b_p = 0}. \tag{3.94}$$

And for a mixed combination of raising and lowering generators (RL)

$$a'_p = a_p - 1, \quad b'_p = b_p + 2, \quad c'_p = c_p - 1, \quad \rightarrow \underline{\Delta b_p = -2} \tag{3.95}$$

$$a'_p = a_p + 1, \quad b'_p = b_p - 2, \quad c'_p = c_p + 1 \quad \rightarrow \underline{\Delta b_p = +2} \tag{3.96}$$

$$a'_p = a_p, \quad b'_p = b_p, \quad c'_p = c_p \quad \rightarrow \underline{\Delta b_p = 0}. \tag{3.97}$$

Drake and Schlesinger,[72] Paldus and Boyle,[236] Payne[247] and Shavitt and Paldus[284] were able to derive a scheme, where the two-body matrix elements can be computed as a product of *segment values* similar to the one-body case (3.83)

$$\langle m'|\hat{e}_{ij,kl}|m\rangle = \prod_{p\in S_2} W(Q_p; d'_p, d_p, \Delta b_p, b_p) \times \sum_{x=0,1} \prod_{p\in S_1} W_x(Q_p; d'_p, d_p, \Delta b_p, b_p), \tag{3.98}$$

where S_1 and S_2 are the overlap (3.85) and non-overlap (3.88) ranges defined above. $W(Q_p; d'_p, d_p, \Delta b_p, b_p)$ are the already defined single operator segment values in Table 3.7 and $W_x(Q_p; d'_p, d_p, \Delta b_p, b_p)$ are new segment values of the overlap range (their comprehensive listing can be found in [284] or in the Tables A.4 and A.5 in the Appendix A.2). There is a sum over two products in S_1, $x = 0$ corresponding to *singlet coupled* intermediate states, with a nonzero contribution if $\Delta b_p = 0, \forall p \in S_1$ and $x = 1$, corresponding to a *triplet intermediate coupling*. Examples of some of the new segment shapes W_x is given in Fig. 3.11.

This product formulation of the two-body matrix elements in a spin-adapted basis is the great strength of the graphical unitary group approach, which allows an efficient implementation of the GT basis in the FCIQMC algorithm. The detail of the matrix element calculation in this basis are, however, tedious and will be omitted here for brevity and clarity. More details on the matrix element calculation, especially the contribution of the two-body term to diagonal and one-body matrix elements can be found in Appendix A.2.

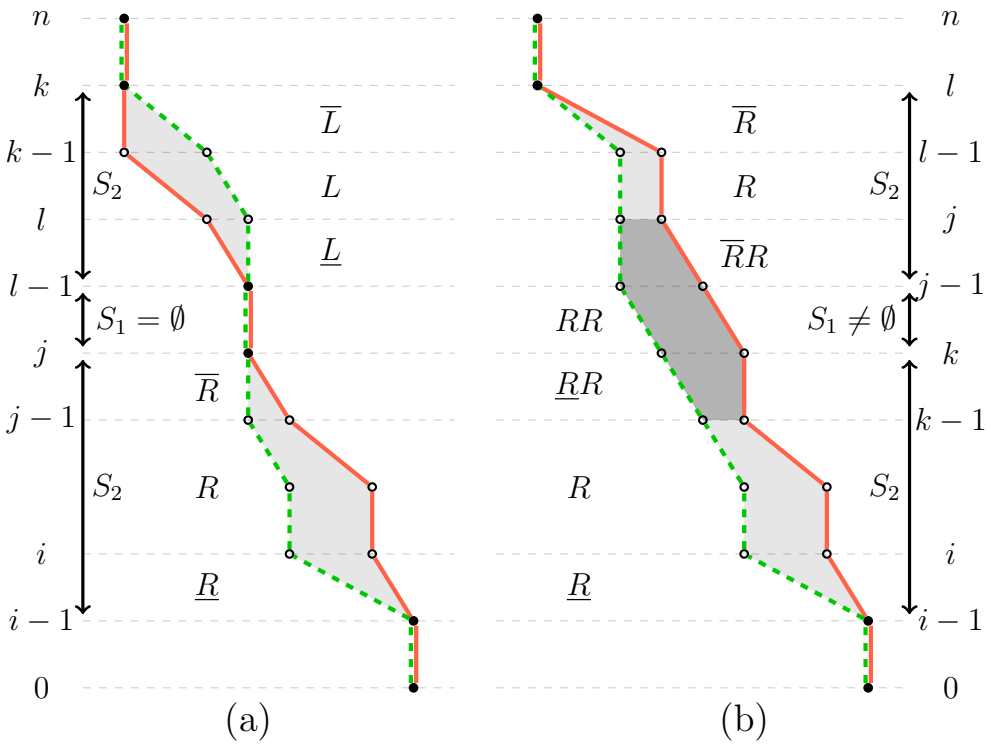

Figure 3.10: Two examples of nonzero two-body matrix elements. (a) shows a non-overlapping ($i < j < l < k$) raising-lowering (RL) example and (b) shows a overlapping ($i < k < j < l$) loop with two raising generators (RR).

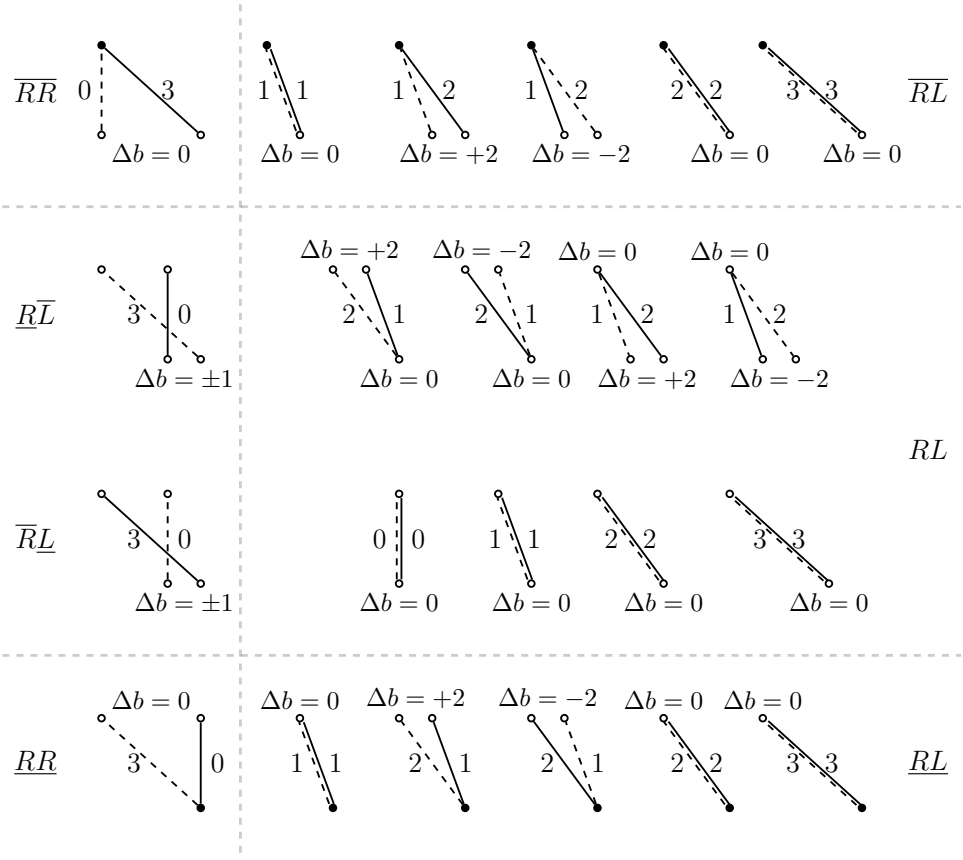

Fig. 3.11: Some of the new two-body segment shapes with the focus on the mixed generator RL combination.

We are now at the end of the roadmap laid out in the Sec. 3.3 and the final missing piece for a spin-adapted formulation of FCIQMC is the efficient implementation of these ideas and a spin-conserving formulation of the excitation generation process, which will be discussed in the following chapter.

4

Spin-Adapted Full Configuration Interaction Quantum Monte Carlo

Having introduced the theoretical basis of the unitary group approach (UGA) and its graphical extension (GUGA) to permit a mathematically elegant and computationally efficient incorporation of the total spin symmetry in form of the Gel'fand-Tsetlin basis, here we will present the actual implementation of these ideas in the FCIQMC framework, termed GUGA-FCIQMC As mention in Chapter 3, a successful spin-adapted implementation will come with the benefits of *Hilbert space size reduction*—leading to a more efficiently sampled compact wavefunction—, *elimination of spin-contamination*—improving convergence of the projective FCIQMC technique—and the possibility to *target states with a specific total spin*—resolving (near-)degeneracies of different spin sectors–and thus allowing the sampling of states, which may not accessible for the SD-based FCIQMC method, due to the projective nature of the algorithm.*

Fundamentally, the three necessary ingredients for an efficient spin-adapted formulation of FCIQMC are:

(i) Efficient storage of the spin-adapted basis

(ii) Efficient excitation identification and matrix element computation

(iii) Symmetry adapted excitation generation with manageable computational cost

The first point is guaranteed with the UGA, since storing CSFs and SDs amounts to the same memory requirement with CSFs represented in the step-vector representation. The efficient excitation identification is rather technical and explained in the Appendix A.1. All that we need to know here is, although the determination if two CSFs are connected by a single application of $\hat{H}$ is more involved than for SDs, it is possible to do it efficiently. The matrix element computation is based on the product structure of the one- (3.83) and two-body (3.98) matrix elements derived by Shavitt[283] explained in Sec. 3.4.1 and presented in more detail in Appendix A.2. Concerning point (iii), as mentioned in Sec. 2.3.8, symmetry adaptation in FCIQMC is most efficiently implemented at the excitation generation step, by only creating symmetry allowed excitations. For

*For example, if a high spin state is the true ground state of system, this precludes the calculation of lower spin states on the normal FCIQMC algorithm, since any long-time projection leads to the high-spin ground state solution.

the continuous $SU(2)$ spin symmetry this is based on Shavitt's DRT and the restriction for nonzero matrix elements in the GUGA derived in Sec. 3.4.1. This, in addition to the formulation in a spin-pure GT basis, ensures the total spin quantum number S is conserved in a FCIQMC calculation.

The remainder of this chapter is organized as follows:
In Section 4.1 the spin-conserving excitation generation based on the GUGA in FCIQMC in discussed, using the example of *single excitations*. The concepts of the *branching tree* and *weights* to ensure nonzero spin-conserving excitation with a favourable generation probability is introduced. In addition the possibility of *on-the-fly* matrix element calculation during the excitation process is highlighted; a feature of utmost importance for the efficient spin-adapted formulation. The extension of these concept for *double excitations* is discussed in Section 4.2 and the important modification of the automated timestep adaptation based on histograms, which in the end allows the application of GUGA-FCIQMC to realistic systems, is presented in Sec. 4.3. Section 4.4 is concerned with the results obtained with the spin-adapted implementation. We present benchmark results and scaling analysis for the nitrogen atom and dimer, the one-dimensional hydrogen chain and the Hubbard model in real- and momentum-space formulation. These studies demonstrate the applicability of GUGA-FCIQMC far beyond the previously possible 16 electrons and to highly multireference systems with up to 30 open-shell orbitals. At last results—not obtainable prior to this implementation—for the spin gap of the cobalt atom and the electron affinity of scandium are presented. Section 4.5 contains a conclusion of the major findings and gives an outlook for further work on this method.

4.1 Excitation Generation: Singles

The concept of efficient excitation generation in the spin-adapted GT basis via the GUGA will be explained in detail by the example of single excitations. Although more complex, the same concepts apply for generation of double excitation, explained in Sec. 4.2.

In contrast to excitation generation for SDs, there are now two steps involved for a CSF basis. The first, being the same as in a formulation of FCIQMC in Slater determinants, is the choice of the two spatial orbitals i and j, with probability $p(i)\,p(j|i)$. As mentioned in Sec. 2.3.8, this should be done in a way to ensure the generation probability to be proportional to the Hamiltonian matrix element involved. However, here comes the first difference of a CSF based implementation compared to a SD-based one. For Slater determinants the choice of an electron in spin-orbital (i,σ) and an empty spin-orbital (j,σ) is sufficient to uniquely specify the excitation $|D_j\rangle = a^\dagger_{j,\sigma} a_{i,\sigma}\,|D_i\rangle$ and calculate the involved matrix element $\langle D_j|\hat{H}|D_i\rangle$. However, in a CSF basis, the choice of an occupied *spatial* orbital j and empty or singly occupied *spatial* orbital i, only determines the type of excitation generator $\hat{E}_{ij}$ acting on an CSF basis state $|m\rangle$ and the involved *integral*

contributions t_{ij}, V_{ikjk} and V_{ikkj} of the matrix element $\langle n|\hat{H}|m\rangle$, see Eq. (3.76). To ensure $p(i|j) \propto |t_{ij} + \frac{1}{2}\sum_{k\in\mathrm{occ}}(V_{ikjk} - V_{ikkj})|$ the occupied orbital j and (partially) empty i are picked in the same way as for SD, see Sec. 2.3.8, but with an additional restriction to ensure $\hat{E}_{ij}\,|m\rangle \neq 0$ explained in Appendix A.3.
However, the choice of (i, j) does not uniquely determine the excited CSF as there are multiple possible ones, since the action of $\hat{E}_{ij}$ yields a linear combination of connected $|m'\rangle$,

$$\hat{E}_{ij}\,|m\rangle = \sum_{m'} \langle m'|\hat{E}_{ij}|m\rangle\,|m'\rangle\,.$$

As a consequence, the choice of spatial orbitals i and j does not determine the *coupling coefficient* $\langle m'|\hat{E}_{ij}|m\rangle$ of the matrix element $H_{m'm}$. Optimally, for a given $|m\rangle$ and generator $\hat{E}_{ij}$, the connected CSF $|n\rangle$ has to be created with a probability $p(m'|m)$ proportional to the coupling coefficient $\langle m'|\hat{E}_{ij}|m\rangle$. By ensuring $p(j|i)$ is proportional to the integral contributions and $p(m'|m)$ to the coupling coefficients, the total spawning probability

$$p_s(m'|m) = p(i)\,p(j|i)\,p(m'|m) \tag{4.1}$$

will be proportional to the magnitude of Hamiltonian matrix element $|H_{m'm}|$. As mentioned in Sec. 2.3.8, the efficiency of the FCIQMC algorithm depends on the ratio of the Hamiltonian matrix element $|H_{m'm}|$ between two connected states and the probability $p_s(m'|m)$ to choose the excitation $|m\rangle \to |m'\rangle$, as the imaginary timestep $\Delta\tau$ of the simulation is adapted to faithfully account for all excitations

$$\Delta\tau^{-1} \propto \frac{|H_{m'm}|}{p_s(m'|m)}. \tag{4.2}$$

In a primitive implementation, $\Delta\tau$ is determined by the "worst-case" $\max|H_{m'm}/p_s(m'|m)|$ ratio during a simulation. A less strict approach to this problem is discussed in Section 4.3. Only choosing nonzero $\hat{E}_{ij}\,|m\rangle \neq 0$ and ensuring $p(m'|m)$ is achieved by a *branching tree* approach, to obtain one of the different possible walks on the Shavitt graph with nonzero loop contributions with the starting CSF $|m\rangle$.

4.1.1 The Branching Tree

In the spin-adapted excitation generation, after a certain generator $\hat{E}_{ij}$ is picked with a probability $p(i|j)$ based on the integral contributions of the Hamiltonian matrix element, the type of generator is determined, raising (R) if $i < j$ and lowering (L) if $i > j$. One connecting single excitation is then chosen by looping from starting orbital $\min(i, j)$ to $\max(i, j)$ and stochastically choosing a valid nonzero Shavitt graph, based on the restrictions 3.79-3.82, mentioned in Sec. 3.4.1. As an example let's have a closer look at a chosen *raising* generator. As can be seen in the single segment value tables 3.7 there are 4 possible nonzero $\underline{R}$ matrix elements. Which can even reduce to 3, if $b_i = 0$

Table 4.1: Nonzero starting segments for $\underline{R}$ with the number of electrons $N_i' = N_i + 1$ in all cases.

$\underline{R}$				$\overline{R}$			$\underline{L}$				$\overline{L}$		
d_i	d_i'	ΔS_i	Δb_i	d_j	d_j'	Δb_{j-1}[a]	d_i	d_i'	ΔS_i	Δb_i	d_j	d_j'	Δb_{j-1}[a]
0	1	$+1/2$	-1	1	0	-1	1	0	$-1/2$	$+1$[b]	0	1	$+1$
0	2	$-1/2$	$+1$[c]	2	0	$+1$	2	0	$+1/2$	-1	0	2	-1
1	3	$-1/2$	$+1$[b]	3	1	$+1$	3	1	$+1/2$	-1	1	3	-1
2	3	$+1/2$	-1	3	2	-1	3	2	$-1/2$	-1[c]	2	3	$+1$

[a] Necessary Δb value for a valid CSF.
[b] Here $b_i > 0$ is ensured, due to $d_i = 1$.
[c] Only for $b_i > 0$ otherwise $S_i' < 0$ would be a non-valid CSF.

at the start of the loop, since then a $d_i' = 2$ value would lead to a forbidden $S_i' < 0$ value. These starting segments are associated with a relative difference of the total spin $\Delta S_i = S_i(m') - S_i(m)$ and $\Delta b_i = b_i(m') - b_i(m)$ between the two CSFs $|m\rangle$ and $|m'\rangle$ at level i, as shown in Table 4.1. For certain step-values ($d_i = 0$ for raising and $d_i = 3$ for lowering generators) two possible excited CSFs with different Δb_i are possible. This can be represented pictorially as elements of a branching tree, as seen in Fig. 4.1 for raising generator, where the number in the boxes represent the step-value d_i of $|m\rangle$ and the direction of the outgoing lines the Δb_i value to possible excited CSFs $|m'\rangle$. Left going lines correspond to $\Delta b_i = -1$ and right going ones $\Delta b_i = +1$. The number above the small dots represent the associated d_i' value of $|m'\rangle$.

The intermediate contributions to the coupling coefficients R/L, see Table 3.7, have similar properties. Depending on the current Δb_k value of the excitation $|m'\rangle$ relative to $|m\rangle$ there are *branching* possibilities for singly occupied spatial orbitals in $|m\rangle$, corresponding to possible spin-recouplings in the *excitation range* of $\hat{E}_{ij}$. An excitation with $\Delta b_{k-1} = -1$ can branch at $d_k = 1$ values, into $d_k' = 1$ with $\Delta b_{k-1} = \Delta b_k = -1$ or change the spin-coupling to $d_k' = 2$ accompanied by a change to $\Delta b_k = +1$. At empty or doubly occupied orbitals only $d_k' = d_k$ and $\Delta b_k = \Delta_{k-1}$ leads to nonzero excitations. These relations are tabulated in Table 4.2 and pictorially represented in Fig. 4.1.

The possible single excitations of a given CSF can be represented by a branching diagram, where each node is a successive element of d_k and a left going branch represents a $\Delta b_k = -1$ value and a right going branch $\Delta b_k = +1$. The end value $d_j = 1$ requires an incoming $\Delta b_{j-1} = -1$ value, whereas $d_j = 2$ requires $\Delta b_{j-1} = +1$ to ensure $\Delta b_j = 0$ at the end of the excitation, indicated by the directions of the ingoing lines of the elements at the bottom of Fig. 4.1. For a raising generator both Δb_{j-1} values are possible for $d_j = 3$. The restrictions on the end segments $\overline{R}/\overline{L}$ are listed in Table 4.1 and pictorially represented in Fig. 4.1. These restrictions are a direct consequence of the conservation of the total spin quantum number S.

A very simple implementation to create a single excitation $|m'\rangle$ would be to loop from

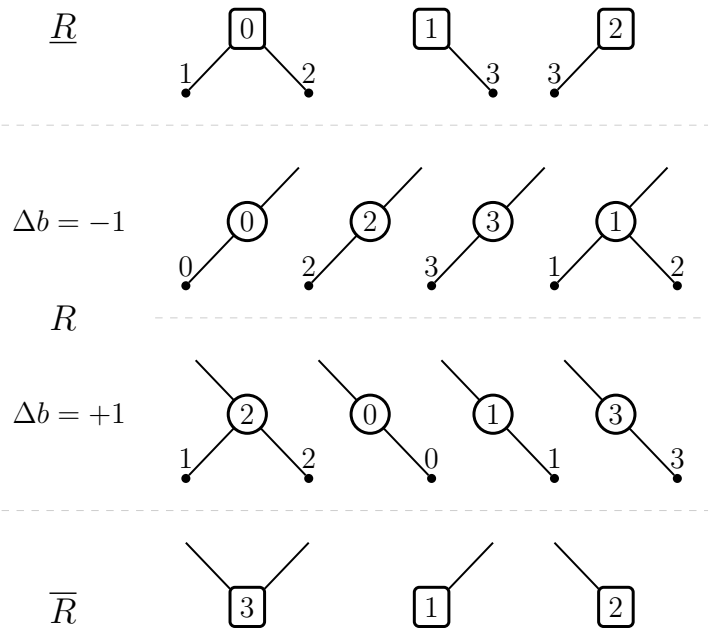

Figure 4.1: Branching tree elements of a one-body operator $\hat{E}_{ij}$.

orbital i to j and depending on the step-value d_k of $|m\rangle$, at each orbital $k \in (i, j)$ choose one possible Δb_k path at random if there are multiple possible ones. However, this would totally neglect that there are certain branching choices which would lead to a dead end, due to incompatible end-segments $\overline{R}, \overline{L}$ and would not relate the probability to create a certain CSF $|m'\rangle$ to the magnitude of the generator matrix element. The restrictions on the end segments $\overline{R}/\overline{L}$ are listed in Table 4.1 and pictorially represented in Fig. 4.1. An example of the excitation generation based on the *branching tree* is given in Fig. 4.2, for the raising generator $\hat{E}_{26}$ acting on the CSF $|m\rangle = |1, 0, 1, 2, 0, 1, 0\rangle$, moving an electron from spatial orbital 6 to 2. The left panel of Fig. 4.2 shows this excitation in the Shavitt graph form based on the DRT. The right panel shows the branching tree representation,* with ± 1 indicating the Δb_k value associated to the possible branches. The orange path in both the Shavitt graph and branching tree representation show one valid single excitation $|m'\rangle$ of $\hat{E}_{26}\,|m\rangle$. The above mentioned dead ends are indicated with dashed lines and crossed out vertices in the right panel of Fig. 4.2.

As one can see the number of connected CSFs $n_{m'}$ to $|m\rangle$ by a generator $\hat{E}_{ij}$ depends on the number of singly occupied orbitals n_s within the excitation range (i, j) and grows approximately as $n_{m'} \approx 1.6^{n_s+2}$. The highest number of possible connected CSFs is given for a starting segment $\underline{R}/\underline{L}$ with two possible branches, exclusively alternating singly occupied orbitals $d_k = \{1, 2\}$ in the excitation range with $b_k > 0$ and an end-segment $\overline{R}/\overline{L}$ with nonzero contributions for both $\Delta b_k = \pm 1$. In this case the number of connected

*With the orbitals from top to bottom now, as this is the usual representation of trees.

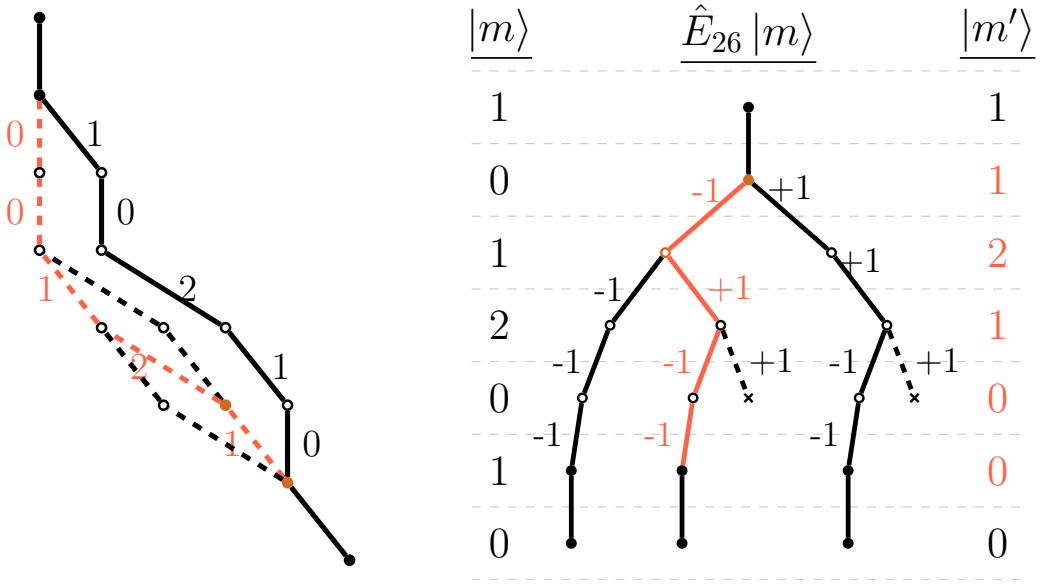

Figure 4.2: (left) Example of different branching possibilities for a raising single excitation $\hat{E}_{26}\,|1,0,1,2,0,1,0\rangle$. (right) Branching tree form of the possible single excitation of $\hat{E}_{2,6}\,|1,0,1,2,0,1,0\rangle$.

CSFs is related to the Fibonacci series and given by the Fibonacci number

$$N_S^{max} = F_{n+2} = \sum_{k=0}^{\lfloor \frac{n-1}{2} \rfloor} \binom{n-k-1}{k}. \tag{4.3}$$

Calculating all of them would lead to an exponential wall for highly open-shell CSFs $|m\rangle$, but since we only need to obtain **one** connected CSF in the excitation generation of FCIQMC, this exponential scaling is not an immediate problem. However, since the overall generation probability $\sum_{m'} p(m'|m)$ is normalized to unity, a specific $p(m'|m)$ will be negligibly small for numerous possible excitations. Since the timestep is directly related to this probability (4.2), a small $p(m'|m)$ directly causes a lowering in the usable $\Delta\tau$ in a FCIQMC calculation.

Since this is a consequence of the inherent *high connectivity* of a spin-adapted basis, systems with many open-shell orbitals are difficult to treat in such a basis. In general this restricts common implementations of spin-eigenfunctions to a maximum of 18 open-shell orbitals. However, similar to the avoidance of the exponential wall associated with the FCI solution to a system, the stochastic implementation of the CSF excitation generation in FCIQMC, avoids the exponential bottle-neck, caused by the high connectivity of a CSF basis. In general, however, we do not have to deal with these large number of open-shell orbitals in most quantum chemistry problems, since they are usually associated with high-order excitations from the HF state. However, for systems in which a localised basis is preferable the number of open-shell orbitals can be quite large, but due to the stochastic nature of the spin-adapted FCIQMC, we are able to obtain results for the low-spin eigenstates of systems with important low-energy states with up to 30 open-shell orbitals, see Sec. 4.4.3 and 4.4.4.

4.1.2 Remaining Switches

To avoid ending up in incompatible dead-end excitations it is convenient, for a given excitation range (i, j), to determine the vector of remaining switch possibilities $s_k(\Delta b_k)$ for the $\Delta b_k = \pm 1$ branches. $s_k(\Delta b_k)$ is the number of $d_{k'} = 1$ for $\Delta b_k = -1$ and $d_{k'} = 2$ for $\Delta b_k = +1$ to come in $k' = k+1, \dots j-1$ (with the already mentioned restriction of $b_{k'} > 1$ for $d_{k'} = 2$ to be a valid $\Delta b_k = +1$ switch)

$$s_k(\Delta b_k) = \begin{cases} \sum_{l=k+1}^{j-1} \delta_{d_l,1} & \text{for} \quad \Delta b_k = -1 \\ \sum_{l=k+1}^{j-1} \delta_{d_l,2} & \text{for} \quad \Delta b_k = +1. \end{cases} \tag{4.4}$$

The quantity $s_k(\Delta b_k)$ can be used to decide if a possible Δb_k branch is taken or not, depending on if it will end up in a dead-end of the branching tree.

Table 4.2: Nonzero intermediate R and L segments.

d_k	d'_k	$\Delta b_{k-1} = -1$	$\Delta b_{k-1} = +1$
		Δb_k	Δb_k
0	0	-1	$+1$
1	1	-1	$+1$
1	2	-1[a]	-[c]
2	1	-[c]	-1
2	2	-1	-1[b]
3	3	-1	$+1$

[a] $b_k > 0$ is ensured due to $d_k = 1$.
[b] Only possible if $b_k > 1$.
[c] Not possible otherwise $|\Delta b_k| > 1$.

4.1.3 On-The-Fly Matrix Element Calculation

To pick the connecting CSF $|m'\rangle$ with a probability $p(m'|m)$ relative to the magnitude of the generator matrix element $|\langle m'| \hat{E}_{ij} |m\rangle|$ we have to investigate the matrix element between a given CSF $|m\rangle$ and an excitation $\langle m'| \hat{E}_{ij} |m\rangle$. As mentioned in Sec. 3.4.1, the coupling coefficient is calculable as a product of terms, which depend on the type of excitation (lowering, raising) and is determined by the step-vector values d_k, d'_k, the b_k and the Δb_k associated to each level of the excitation

$$\langle m'| \hat{E}_{ij} |m\rangle = \prod_{k=(i,j)} W(Q_k; d'_k, d_k, \Delta b_k, b_k). \tag{4.5}$$

One of the major advantages of the GUGA in FCIQMC is that this matrix element can be calculated **on-the-fly** during the creation of the excitation. As one can see in Table 3.7 in Sec. 3.4.1, there is a relation between the matrix element amplitude and the number of direction switches of Δb_k in the excitation range. Most product contributions are of order $\mathcal{O}(1)$, except the elements related to a switch of $\Delta b_{k+1} \leftarrow -\Delta b_k$, which are of order $\mathcal{O}(1/b_k)$

$$W(Q_k; d'_k, d_k, \Delta b_k, b_k) = \begin{cases} \mathcal{O}(1) & \text{for } d_k = d'_k \\ \mathcal{O}(b_k^{-1}) & \text{for } d_k \neq d'_k. \end{cases} \tag{4.6}$$

So for a higher intermediate value of b_k, which in the end also means more possibly pathways, it should be less favourable to change the current Δb_k value. In order to create an excitation $|m'\rangle$ with a probability proportional to the coupling coefficient $|\langle m'|\,\hat{E}_{ij}\,|m\rangle|$ this fact should be included in the decision of the chosen branch and is achieved by the use of *branch weights.*

4.1.4 Branch Weights

It is possible to take into account the "probabilistic weight" of each tree branches at a possible branching decision. As one can see in the left panel of Fig. 4.3, the starting $\Delta b_i = \pm 1$ branches each have on contribution of order $\mathcal{O}(1)$. For each branching possibility there is a resulting branch with opposite Δb and weight of order $\mathcal{O}(b^{-1})$. However, it also depends on the end-segment determined by d_j, if a given branch can be chosen. The following branch weights

$$\zeta_- = f(d_j) + \frac{s_k(-1)}{b} g(d_j) + \mathcal{O}(\frac{1}{b^2}), \qquad \zeta_+ = g(d_j) + \frac{s_k(+1)}{b} f(d_j) + \mathcal{O}(\frac{1}{b^2}) \tag{4.7}$$

with

$$f(d_j) = \begin{cases} 0 & \text{if } d_j = 2 \\ 1 & \text{else} \end{cases}, \qquad g(d_j) = \begin{cases} 0 & \text{if } d_j = 1 \\ 1 & \text{else} \end{cases} \tag{4.8}$$

where $s_k(\pm 1)$ is the number of remaining switches (4.4), can be used to determine the probability of each Δb branch to be chosen. The right panel of Fig. 4.3 shows the influence of the matrix element on the branching probabilities in the excitation range. By choosing the $\Delta b = -1$ with a probability $p_- = \frac{\zeta_-}{\zeta_- + \zeta_+}$ at the start of an excitation and in the excitation region choose to *stay* on the current Δb branch according to

$$p_s^{\pm} = \frac{b\zeta_{\pm}}{b\zeta_{\pm} + \zeta_{\mp}}, \tag{4.9}$$

the overall probability to choose the specific excitation $|m'\rangle$ is given by

$$p(m'|m) = p_-(i) \prod_{k=i+1}^{j-1} p_s^{\pm}(k). \tag{4.10}$$

With this choice of branching probabilities it is possible to retain an *almost linear* ratio between $p(m'|m)$ and generator matrix elements $\langle m'|\hat{E}_{ij}|m\rangle$. Additionally, because of the $f(d_j)$ and $g(d_j)$ functions and inclusion of the remaining switches (4.4) in Eq. (4.7), this approach avoids coming to a dead-end and choosing invalid excitations.

An important note on the matrix element calculation of single excitations: there are of course contractions of the two-body operator in Eq. (3.76), which contribute to the matrix element of a single excitation $\langle m'|\hat{H}|m\rangle$. These contractions have to be taken into

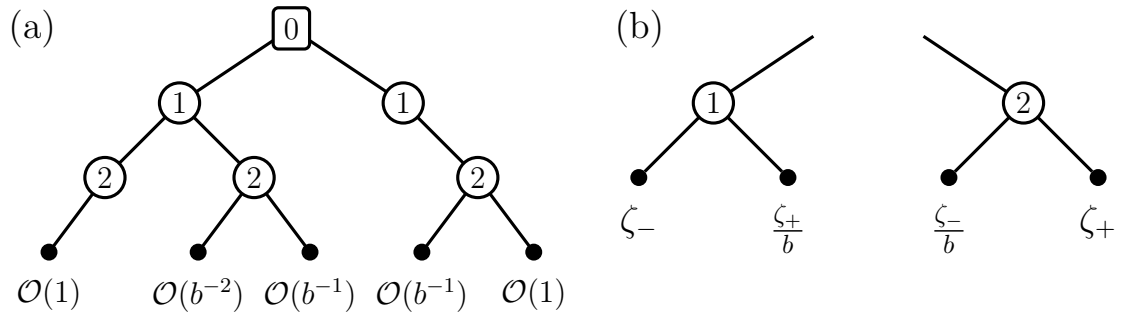

Figure 4.3: (a) Scaling of one-body coupling coefficients with changes in Δb along the branching tree. (b) Future branch weights at branching possibility.

account in the "on-the-fly matrix element computation" and are explained in more detail in Appendix A.2.2.

4.2 Excitation Generation: Doubles

The generation of double excitation in the GUGA formalism is more involved than single excitations and the detailed background on matrix element computation and weighted orbital choice is found in the Appendix A.2.2 and A.3.2 for conciseness of this manuscript. Nevertheless, the general ideas, which are very similar to single excitations, see Sec. 4.1, and also involve the concepts of the branching tree and weight and remaining switches, are presented here.

Depending on the ordering of the involved spatial orbitals of the one- and two-body generators, $\hat{E}_{ij}$ and $\hat{e}_{ij,kl}$, 30 different excitation types, involving different combinations of lowering (L) and raising (R) generators, can be identified and are listed in Table 4.3. Some of them are equivalent, in the sense that they lead to the same excitations, such the 7 single excitation (0a-0g) in Table 4.3, which reduce to the two distinct raising $\underline{R} \rightarrow \overline{R}$ and lowering $\underline{L} \rightarrow \overline{L}$ generators. The pictorial representation of these generators are shown in Fig. 4.4, where the ordering of orbitals is from bottom to top and arrows indicate the replacement of electrons. The two-body operators $\hat{e}_{ij,kl}$, which contribute to single excitations, (0c-0g) in Table 4.3, are already taken into single excitation matrix element calculation, see Sec. 4.1 and Appendix A.2.2. These also include the single overlap excitation (0b) and (0e) with two alike generator types.

Double excitation with a single overlapping index j but two different generators (1a) and (1b) can be treated very similar to single excitations, with the same weighting functions (4.7) and classification of remaining switches (4.4), but with a change of generator type at the overlap site, $L \leftrightarrow R$. Double excitations with an empty overlap range S_1 (3.85) ($3c_0$, $3d_0$, $3e_0$ and $3f_0$) can be calculated as the product of two single excitations (3.87), see Sec. 3.4.2. However, e.g. for excitation ($3c_0$), the two-body operators $\hat{e}_{ij,kl}$ and $\hat{e}_{kj,il}$ contribute to the same Hamiltonian matrix element. We made the decision to treat these

Table 4.3: Distinct types of double excitations. $i < j < k < l$ in all cases and $e_{ij,kl} = e_{kl,ij}$ in mind.

Label	Generator order	Operator
0a	$\underline{R}(i) \to \overline{R}(j)$	$\hat{E}_{ij}$
0b	$\underline{R}(i) \to \overline{R}\underline{R}(j) \to \overline{R}(k)$	$\hat{e}_{ij,jk}$
0c	$W\underline{R}(i) \to \overline{R}(j)$	$\hat{e}_{ii,ij}$
0d	$\underline{L}(i) \to \overline{L}(j)$	$\hat{E}_{ji}$
0e	$\underline{L}(i) \to \overline{L}\underline{L}(j) \to \overline{L}(k)$	$\hat{e}_{ji,kj}$
0f	$\underline{L}(i) \to W\overline{L}(j)$	$\hat{e}_{ji,jj}$
0g	$\underline{L}(i) \to W(j) \to \overline{L}(k)$	$\hat{e}_{ki,jj}$
1a	$\underline{L}(i) \to \overline{L}\underline{R}(j) \to \overline{R}(k)$	$\hat{e}_{ji,jk}$
1b	$\underline{R}(i) \to \overline{R}\underline{L}(j) \to \overline{L}(k)$	$\hat{e}_{ij,kj}$
1c	$\underline{R}(i) \to \underline{R}R(j) \to \overline{RR}(k)$	$\hat{e}_{jk,ik}$
1d	$\underline{L}(i) \to L\underline{L}(j) \to \overline{LL}(k)$	$\hat{e}_{ki,kj}$
1e	$\underline{L}(i) \to \underline{R}L(j) \to \overline{RL}(k)$	$\hat{e}_{jk,ki}$
1f	$\underline{R}(i) \to \underline{L}R(j) \to \overline{RL}(k)$	$\hat{e}_{kj,ik}$
1g	$\underline{RR}(i) \to R\overline{R}(j) \to \overline{R}(k)$	$\hat{e}_{ik,ij}$
1h	$\underline{LL}(i) \to \overline{L}L(j) \to \overline{L}(k)$	$\hat{e}_{ji,ki}$
1i	$\underline{RL}(i) \to \overline{R}L(j) \to \overline{L}(k)$	$\hat{e}_{ij,ki}$
1j	$\underline{RL}(i) \to \overline{L}R(j) \to \overline{R}(k)$	$\hat{e}_{ji,ik}$
2a	$\underline{RR}(i) \to \overline{RR}(j)$	$\hat{e}_{ij,ij}$
2b	$\underline{LL}(i) \to \overline{LL}(j)$	$\hat{e}_{ji,ji}$
2c	$\underline{RL}(i) \to \overline{RL}(j)$	$\hat{e}_{ij,ji}$
3a	$\underline{R}(i) \to \underline{R}R(j) \to R\overline{R}(k) \to \overline{R}(l)$	$\hat{e}_{jl,ik}/\hat{e}_{jk,il}$
3b	$\underline{L}(i) \to L\underline{L}(j) \to \overline{L}L(k) \to \overline{L}(l)$	$\hat{e}_{ki,lj}/\hat{e}_{li,kj}$
$3c_0$	$\underline{R}(i) \to \overline{R}(j) \to \underline{R}(k) \to \overline{R}(l)$	$\hat{e}_{ij,kl}$
$3c_1$	$\underline{R}(i) \to \underline{L}R(j) \to \overline{L}R(k) \to \overline{R}(l)$	$\hat{e}_{kj,il}$
$3d_0$	$\underline{L}(i) \to \overline{L}(j) \to \underline{L}(k) \to \overline{L}(l)$	$\hat{e}_{ji,lk}$
$3d_1$	$\underline{L}(i) \to \underline{R}L(j) \to \overline{R}L(k) \to \overline{L}(l)$	$\hat{e}_{jk,li}$
$3e_0$	$\underline{R}(i) \to \overline{R}(j) \to \underline{L}(k) \to \overline{L}(l)$	$\hat{e}_{ij,lk}$
$3e_1$	$\underline{R}(i) \to \underline{L}R(j) \to \overline{R}L(k) \to \overline{L}(l)$	$\hat{e}_{ik,lj}$
$3f_0$	$\underline{L}(i) \to \overline{L}(j) \to \underline{R}(k) \to \overline{R}(l)$	$\hat{e}_{ji,kl}$
$3f_1$	$\underline{L}(i) \to \underline{R}L(j) \to R\overline{L}(k) \to \overline{R}(l)$	$\hat{e}_{jl,ki}$

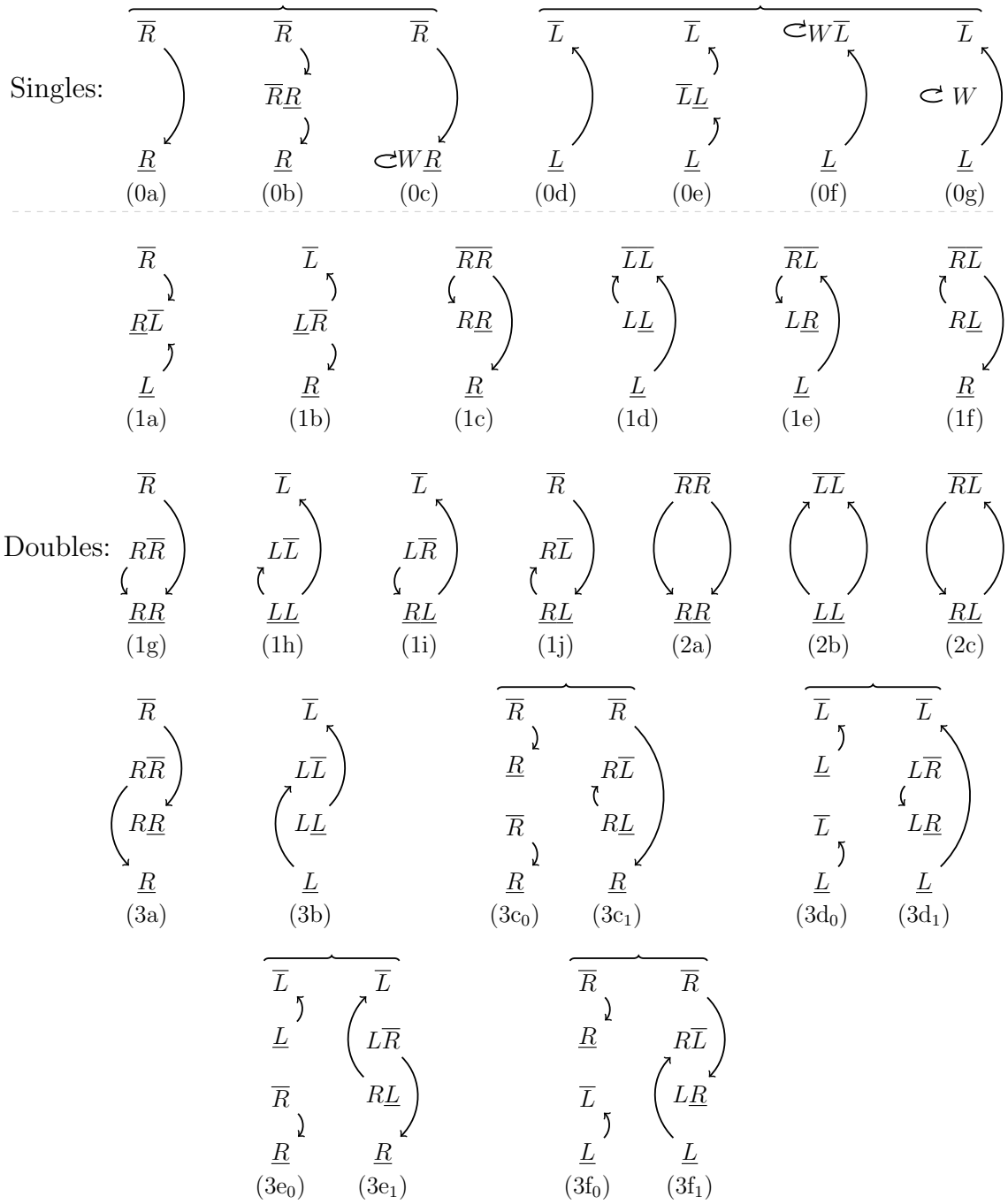

Figure 4.4: The 30 different types of single and double excitations, where the equivalent excitations are grouped together and reduce the number of distinct types to 21. The indices correspond to the entries in Table 4.3.

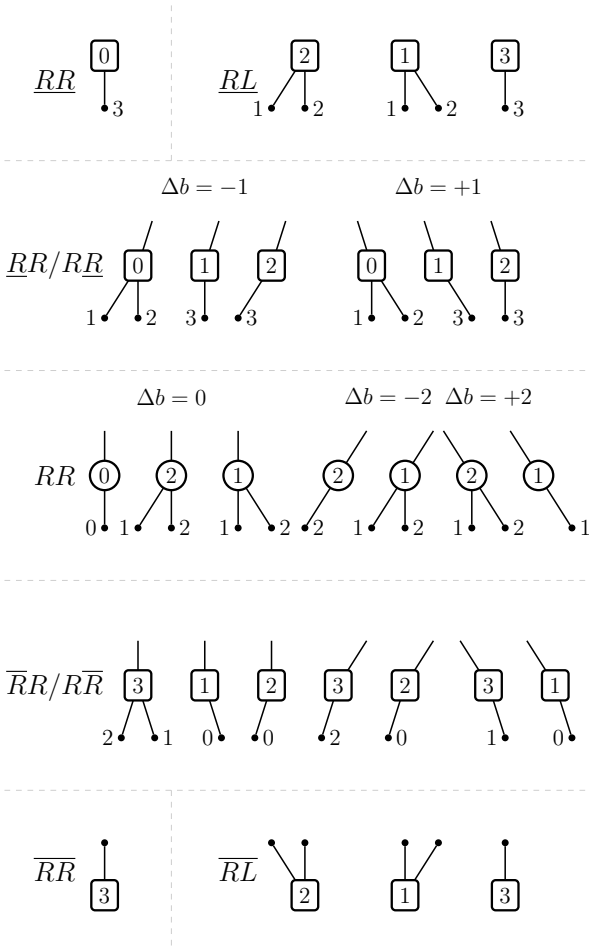

Fig. 4.5: An example of possible new branching tree elements for double excitations. Vertical lines now indicate the $\Delta b = 0$ branch, while left going lines in the overlap range correspond to $\Delta b = -2$ and right going ones to $\Delta b = +2$.

non-overlap excitations by using the corresponding two-body generators with a nonzero overlap range S_1, see Appendix A.1 and A.2.2 for more details.

For "proper" double excitations, we separate the excitation range $\min(i,j,k,l) \rightarrow \max(i,j,k,l)$ into the lower non-overlap range S_2 below the overlap range S_1 and the upper non-overlap range S_2' above S_1, as depicted in Fig. 3.10 in Sec. 3.4.2. We introduce the terminology of a *full-start* of mixed generators $\underline{RL}$ and alike generators $\underline{RR}/\underline{LL}$, a *semi-start* corresponds to the segment types like $R\underline{R}$ or $R\underline{L}$, a *semi-stop* indicates generator combination like $L\overline{L}$ or $L\overline{R}$ and a *full-stop* is where both generators end on the same orbital, e.g. $\overline{LL}$ or $\overline{RL}$.

The excitation generation for doubles is again performed by choosing a valid path in a branching tree with modified rules in the overlap range S_1 of the double excitation. As can be seen by the restrictions for nonzero two-body matrix elements, Eq. (3.89-3.97) in Sec. 3.4.2, the allowed Δb values in S_1 are now ± 2 and 0. This leads to new elements of the branching tree in S_1, which are shown by the example of alike raising and mixed generators in Fig. 4.5, where vertical lines indicate the new $\Delta b = 0$ branch, and left (right) going lines in S_1 correspond to $\Delta b = \pm 2$. The rules for the intermediate elements RR, LL and RL are the same for all combinations of generators. Only a short explanation on the double excitation generation is given here, the interested reader can find a comprehensive explanation in Appendix A.3.2.

The calculation of the remaining switch possibilities (4.4) essentially are the same as for single excitations, except they are calculated for each segment, S_2, S_1 and S_2' of the excitation separately. In S_1 a $\Delta b_k = -2$ branch can switch at $d_k = 1$, a $\Delta b_k = +2$ at $d_k = 2$ and the $\Delta b_k = 0$ branch at both open-shell step-values

$$s_k(\Delta b_k) = \begin{cases} \sum_{l>k\in S_1} \delta_{d_l,1} & \text{for} \quad \Delta b_k = -2 \\ \sum_{l>k\in S_1} \delta_{d_l,2} & \text{for} \quad \Delta b_k = +2 \\ \sum_{l>k\in S_1} \delta_{d_l,1} + \delta_{d_l,2} = s_k(-2) + s_k(+2) & \text{for} \quad \Delta b_k = 0. \end{cases} \tag{4.11}$$

The remaining switches in S_2 are calculated up until the index of the start of S_1, as, similar to single end segments, e.g. $\overline{R}$, there are the restrictions for nonzero matrix elements for semi-start segments, e.g. $R\underline{L}$, to guarantee the total spin is conserved. Similarly, for the end of the overlap range, depending on the step-value at e.g. $L\overline{L}$, the mentioned restrictions apply so the remaining switches (4.11) are calculated until the start of S_2'.

As a side note: We do not take into account the b-value restriction for the switch possibilities, since it does not influence the possible branches in a straight forward way. It would be too complicated to take this effect into account thoroughly and since it only influences low spin intermediate segments, $S_k = b_k/2 \approx 0$, and these are not the most complicated type of excitations.

To relate $p(m'|m)$ to the generator matrix element $\langle m'|\hat{e}_{ij,kl}|m\rangle$ we again use branching weights to determine which paths of the tree are chosen. For a full-start $\underline{RL}(i)$ into full-stop $\overline{RL}(j)$ excitation the weights of the different Δb branches in terms of the intermediate b-values and remaining switch possibilities are

$$\Sigma_{-2}^{(k)} = f(d_j) + \frac{s_k(-2)}{b_k} + \mathcal{O}(b_k^{-2}), \tag{4.12}$$

$$\Sigma_{+2}^{(k)} = g(d_j) + \frac{s_k(+2)}{b_k} + \mathcal{O}(b_k^{-2}), \tag{4.13}$$

$$\Sigma_0 = 1 + \frac{1}{b_k}\left(s_k(-2)g(d_j) + s_k(+2)f(d_j)\right) + \mathcal{O}(b_k^{-2}), \tag{4.14}$$

with $f(d_j)$ and $g(d_j)$ given by Eq. (4.8). We bias towards the $\Delta b_k = 0$ branch at the start of the excitation range

$$p_0 = \frac{\Sigma_0}{\Sigma_0 + \Sigma_{\pm 2}}, \tag{4.15}$$

depending if $d_i = \{1, 2\}$ and weight to stay on the current Δb_k excitation branch in S_1 with

$$p_{\Delta b} = \frac{b_k \Sigma_{\Delta b}}{b_k \Sigma_{\Delta b} + \Sigma_{\Delta b}}. \tag{4.16}$$

For a full-start into semi-stop excitation, e.g. $\underline{RL} \to \overline{L}R \to \overline{R}$, the weights of the branches

in the overlap region S_1 are given by

$$\Sigma_{-2}^{(k)} = f(d_j)\zeta_{-1}(j) + \frac{s_k(-2)}{b_k}\left[g(d_j)\zeta_{+1}(j) + f(d_j)\zeta_{+1}(j)\right] + \mathcal{O}(b_k^{-2}), \tag{4.17}$$

$$\Sigma_{+2}^{(k)} = g(d_j)\zeta_{+1}(j) + \frac{s_k(+2)}{b_k}\left[g(d_j)\zeta_{-1}(j) + f(d_j)\zeta_{+1}(j)\right] + \mathcal{O}(b_k^{-2}), \tag{4.18}$$

$$\Sigma_{0}^{(k)} = f(d_j)\zeta_{+1}(j) + g(d_j)\zeta_{-1}(j) + \frac{1}{b_k}\left[s_k(-2)g(d_j)\zeta_{+1}(j) + s_k(+2)f(d_j)\zeta_{-1}(j)\right] + \mathcal{O}(b_k^{-2}), \tag{4.19}$$

where $\zeta_{\pm1}(j)$ are the single weights (4.7) for the non-overlap region S_2' at the end of the excitation, evaluated with the b_j and $s_j(\pm2)$ values at the semi-stop. The biasing function towards a certain branch at the beginning of an excitation and to stay at a chosen Δb branch are the same as (4.15) and (4.16) and in the non-overlap region S_2' the single excitation weights and biasing factors (4.7, 4.9) apply.

The weighting functions in the non-overlap region S_2 for a semi-start into full-stop excitation, e.g. $\underline{R}(i) \to \underline{L}R(j) \to \overline{RL}(k)$, are given by

$$\sigma_{-1}^{(k)} = f(d_j)\Sigma_0(j) + g(d_j)\Sigma_{-2}(j) + \frac{s_k(-2)}{b_k}\left[f(d_j)\Sigma_{+2}(j) + g(d_j)\Sigma_0(j)\right] + \mathcal{O}(b_k^{-2}), \tag{4.20}$$

$$\sigma_{+1}^{(k)} = g(d_j)\Sigma_0(j) + f(d_j)\Sigma_{+2}(j) + \frac{s_k(+2)}{b_k}\left[g(d_j)\Sigma_{+2}(j) + f(d_j)\Sigma_0(j)\right] + \mathcal{O}(b_k^{-2}), \tag{4.21}$$

with Σ_x being the weights of the full-stop excitation (4.12) evaluated with the b_j and $s_j(\pm2)$ values at the start of the overlap region j. The biasing function for the start and staying probabilities are the same as in the single excitation case (4.9) evaluated with $\sigma_{\pm1}$ instead of $\zeta_{\pm1}$.

For a "full" double excitation, e.g. $\underline{R}(i) \to \underline{R}R(j) \to \overline{R}R(k) \to \overline{R}(l)$, the weights and biasing functions for the first non-overlap S_2 region $i \to j-1$ are the same as for the semi-start into full-stop excitation (4.20), but evaluated with the full-start into semi-stop weights Σ_x(4.17). In the overlap region S_1, $j \to k-1$, the weights and biasing functions are the same as for full-start into semi-stop excitations (4.17), where the $f(d_k), g(d_k)$ and $\zeta_{\pm1}$ functions are evaluated at the semi-stop index k now. And finally for the final non-overlap region S_2', $k \to l-1$, the weights and biasing functions for single excitations (4.7, 4.9) apply.

By using this biasing we ensure to create a valid *spin conserving* excitation, avoid ending up in a dead-end of the branching tree and create excitations with a probability $p(m'|m)$ proportional to the coupling coefficient magnitude $|\langle m'|\hat{e}_{ij,kl}|m\rangle|$. The used weight functions are set up before an excitation in terms of the b_k and remaining switch possibilities with, if necessary, the precomputed switch possibilities for the remaining overlap and non-overlap contributions and Δb conditions. So it is not necessary to recompute the whole setup at each step of the excitation. The computational effort to set up this weight objects, as it needs the information of the remaining switches is $\mathcal{O}(n)$, in the worst case of

an excitation spanning the whole orbital range. Results on the increase in computational effort of the GUGA-FCIQMC method compared to the SD based implementation can be found in Sec. 4.4.5.

4.3 Histogram based Timestep Optimization

Due to the increased connectivity of CSFs compared to SDs the generation probability, p_{ij}, to spawn a new walker on state $|D_j\rangle$ from an occupied CSF $|D_i\rangle$ is in general much lower in the GUGA-FCIQMC method compared to the original method. An efficient sampling of the off-diagonal Hamiltonian matrix elements and stable dynamics of a simulation demand the quantity $\Delta\tau^{-1}|H_{ij}|/p_{ij}$ to be close to unity. In the original determinant-based FCIQMC algorithm this is ensured by a dynamically adapted timestep $\Delta\tau(t)$, taking on the value of the "worst-case" $p_{ij}/|H_{ij}|$ ratio encountered during a simulation.

However, due to the large amount of possible connections between CSFs, this causes the timestep to drop dramatically, if we chose this approach for the GUGA-FCIQMC. At the same time a tiny spawning probability p_{ij} means, these problematic excitation only happen a minuscule fraction of times compared to more "well-behaved" excitations. However, through the timestep, the global dynamics of all the walkers are affected by possibly only one ill-sampled excitation with a large $|H_{ij}|/p_{ij}$ ratio. The optimized excitation generation mentioned in the sections above, ameliorates this issue, but still cannot avoid the inherent "connectivity problem" of a CSF based implementation. If we store all $|H_{ij}|/p_{ij}$ of all successful excitation attempts in a histogram of certain bin width, we can see that the majority of excitations are well represented by the optimized generation probability, see Fig. 4.6.

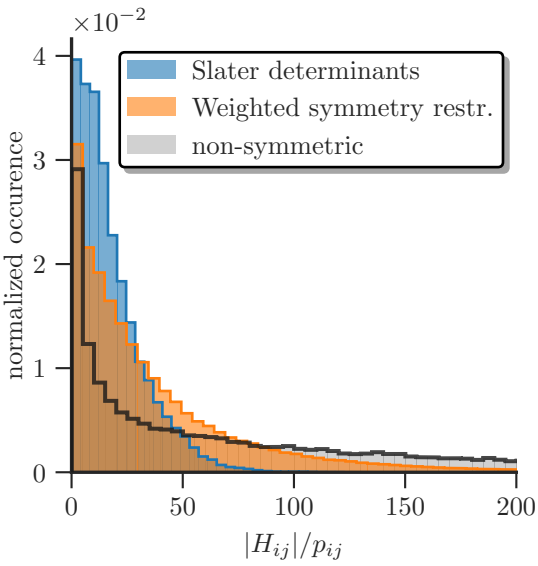

Fig. 4.6: Histogram of $|H_{ij}|/p_{ij}$ for the determinant- and CSF-based FCIQMC method for N_2 at the equilibrium geometry in a cc-pVDZ basis set. Both the optimized (orange) and unoptimized GUGA (black) results are shown.

The SD based method has a fast exponential decaying tail. This is the reason the "worst-case" timestep adaptation did not cause any problems for the original FCIQMC implementation. The GUGA implementation on the other hand, especially in the unoptimized version, has a very slow decay and much larger maximum $|H_{ij}|/p_{ij}$ ratios, over 10000 in the N_2 example shown in Fig. 4.6 (not displayed for clarity). The optimized CSF excitation scheme, explained above, greatly improves the p_{ij} to $|H_{ij}|$ relation, but expectedly

Table 4.4: Automatically obtained timesteps for an SD- and GUGA-based (optimized and vanilla) simulation of N_2 at equilibrium distance in a cc-pVDZ basis. Results for the "worst-case" optimization $\Delta\tau_w$ and for the integrated histogram based optimization $\Delta\tau_h$ covering 99.99% of all excitations.

	$\Delta\tau_w$	$\Delta\tau_h$	$\Delta\tau_h/\Delta\tau_w$
SD	$5.59 \cdot 10^{-3}$	$6.20 \cdot 10^{-3}$	1.11
GUGA vanilla	$4.78 \cdot 10^{-5}$	$8.62 \cdot 10^{-5}$	1.80
GUGA optimized	$5.20 \cdot 10^{-5}$	$1.12 \cdot 10^{-3}$	21.50
GUGA van. / GUGA opt.	0.92	0.08	
SD / GUGA opt.	107.51	5.55	

behaves worse than the SD based method. The timestep obtained with the "worst-case" optimization are given in Table 4.4.

To avoid this hampering of the global dynamics by a few ill-behaved excitations, we implemented a new automated timestep adaptation by storing the $|H_{ij}|/p_{ij}$ ratios off all successful excitation attempts in a histogram, and setting the timestep $\Delta\tau$ to ensure $\Delta\tau|H_{ij}|/p_{ij} \leq 1$ for a certain percentage of all excitations. The results of this "histogram-tau-search" are listed in Table 4.4 for a SD based and unoptimized (vanilla) and optimized GUGA-FCIQMC implementation for simulations of the nitrogen dimer at equilibrium geometry in a cc-pVDZ basis. For an SD-based implementation there is not much difference between the two approaches. Similar, for the vanilla GUGA implementation, due to the slow decaying tail in the histograms, see Fig. 4.6. There is a two order of magnitude difference between the SD-based and the unoptimized GUGA-based timestep, which in practice would make the GUGA-FCIQMC implementation useless. However, with the optimized CSF excitation generation, the histogram-based $\Delta\tau_h$-adaptation yields a timestep two orders of magnitude larger than the "worst-case" $\Delta\tau_w$-optimization. The obtained $\Delta\tau_h$ is still twice as large as in the SD-based FCIQMC, but due to a smaller Hilbert space size, and possibly faster convergence for spin-degenerate systems, this makes the GUGA-FCIQMC applicable for real systems.

4.4 Results from the Spin-Adapted FCIQMC Approach

We tested and benchmarked the applicability of the spin-adapted FCIQMC approach via the graphical unitary group approach against other quantum chemistry methods on the nitrogen atom, the nitrogen dimer, a one-dimensional hydrogen chain and the Hubbard lattice model in a real- and momentum-space basis. The scaling of the implementation is analysed for these systems and compared against the original, Slater determinant based FCIQMC method. Finally, the spin-adapted approach is used to calculate the spin gap of the cobalt atom and the electron affinity of scandium, both of which are not obtainable with the original determinant based FCIQMC approach.

4.4.1 Nitrogen Atom

The dissociation energy of the nitrogen molecule N_2 for a long time has been a test case for the capabilities of quantum chemical methods.[2,51,348] There is a large change in the correlation energy as the triple bond of N≡N is stretched and finally broken. This is accompanied by a change of the electronic structure from single-reference-like to highly multiconfigurational.

We first investigated the problem of the constituent nitrogen atom N. The ground state configuration of N is $1s^2 2s^2 2p^3$ with the 3 electrons in the p-shell forming a $S = 3/2$ quartet ${}^4S^o$ state. The first excited state is the $S = 1/2$ ${}^2D^o$ doublet, 2.384 eV above the ground state,[95,171] with spin-orbit effects neglected. This setup of a half-integer high-spin ground state with low-spin excited state is the prime playground of the GUGA-FCIQMC method. Previous spin-adapted implementations in FCIQMC, using half-projected and projected Hartree-Fock (HPHF) states,[302] are only applicable to an even number of electrons. At the same time, restricting the total m_s quantum number to target an excited state only works if the low-spin state is the ground state with excited states being high-spin, since the high-spin ground state also contains contributions of energetically lower m_s states, causing the projective FCIQMC to converge to the latter one.

We prepared all-electron ab-initio Hamiltonians with Molpro[349,350] for N in a cc-pVnZ basis set, with n = D, T, Q, 5 and 6. The maximal symmetry point group in Molpro is D_{2h} and thus the much larger SO(3) symmetry of N gets reduced to degenerate sets of irreps of D_{2h}. The $S = 3/2$ quartet with singly occupied 2p orbitals belongs to the irrep A_u. While the $S = 1/2$ doublet splits into one A_u state with three open-shell 2p orbitals and three states belonging to B_{1u}, B_{2u} and B_{3u} with one doubly occupied and one open-shell 2p orbital, see Fig. 4.7.

We calculated the quartet-doublet, ${}^4S^o - {}^2D^o$, spin-gap with the spin-adapted i-FCIQMC

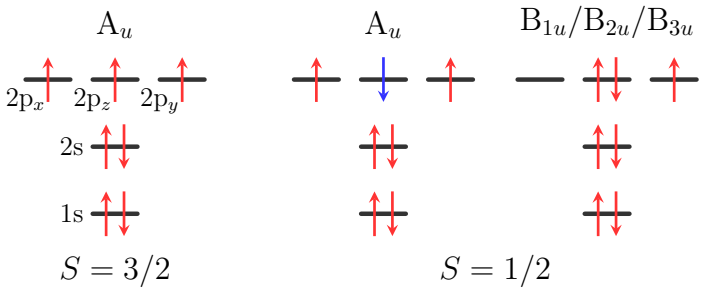

Fig. 4.7: Schematic orbital diagram of nitrogen $1s^2 2s^2 2p^3$ for the doublet ($S = 1/2$) and quartet ($S = 3/2$) states. A_u and B_{iu}, $i = 1, 2, 3$, represent the irrep of D_{2h} from the reduction of SO(3) symmetry.

method (GUGA-FCIQMC) for basis sets up to cc-pV6Z and compared our results to unrestricted coupled cluster singles and doubles with perturbative triples ((U)CCSD(T)) and FCI calculations up to cc-pVTZ obtained with Molpro[164–167] and experimental results.[95,171] The CCSD(T) calculations are based on restricted open-shell Hartree-Fock[268] (ROHF) orbitals, which for the $S = 1/2$ state are only possible to be done for the B_{iu}, $i = 1, 2, 3$, states. Although GUGA-FCIQMC calculations for the B_{iu} irreps yield the same results as for the $S = 1/2$ A_u state, the CCSD(T) results are far off the FCI results and the experimental gap, due to the multi-reference character of these states.

The results are given in Table 4.5 with a complete basis set (CBS) extrapolation given by a two-parameter inverse cube fit

$$E(n) = E_{CBS} + \frac{A}{n^3} \tag{4.22}$$

using $n =$ T, Q and 5. The GUGA-FCIQMC CBS results shows excellent agreement with the experimental value within chemical accuracy. Fig. 4.8 shows the energy of the $^4S^o$ and $^2D^o$ state versus the cardinal number n of the basis set cc-pVnZ (left) and versus n^{-3} (right). The solid lines represent the fit (4.22) to the data and the FCI results up to cc-pVTZ show perfect agreement with the i-FCIQMC results. Fig. 4.9 shows the difference of the calculated spin gap of the nitrogen $^4S^o$ and $^2D^o$ state, obtained with GUGA-FCIQMC and CCSD(T), to the experimental value[95,171] as a function of the cardinal number of the basis set n (left) and the inverse cube n^{-3} (right). The solid lines are the inverse cube fit to the $n = T, Q, 5$ data points. The GUGA-FCIQMC results converge to the correct experimental value, while the CCSD(T) calculations are not able to obtain the correct result, due to the multiconfigurational character of the $^2D^o$ excited state.

We also calculated the ionization potential (IP) of the nitrogen atom in the CBS limit with GUGA-FCIQMC and compared our results to CCSD(T) calculations and experimental data. The ground state of the N^+ cation is the $S = 1$ triplet $^3P_0$ state. The results from GUGA-FCIQMC and CCSD(T) calculations up to cc-pV6Z basis set are shown in Table 4.5. Since CCSD(T)[164–167] can treat both the $^4S^o$ and $^3P_0$ well, coupled cluster results and GUGA-FCIQMC CBS limit values, using $n =$ Q, 5 and 6, agree within *chemical accuracy* with experimental values.

Table 4.5: Spin gap $^2D^o - {}^4S^o$ and ionization potential (IP) $^3P_0 - {}^4S^o$ of the nitrogen atom obtained with all-electron GUGA-FCIQMC and CCSD(T)[165,166] calculations for different basis set sizes cc-pVnZ, $n = 2, 3, 4, 5, 6$ (2 = D, 3 = T, 4 = Q) and CBS limit extrapolations (4.22) compared with experimental results.[82,95,171] Energies are given in atomic units.

	$^2D^o - {}^4S^o$ spin gap		$N^+ {}^3P_0$ - N $^4S^o$ IP	
n	CCSD(T)	GUGA-FCIQMC	CCSD(T)	GUGA-FCIQMC
2	0.1061699	0.099951(11)	0.5216483	0.5215711(23)
3	0.1013301	0.0923719(90)	0.5310023	0.5310210(83)
4	0.0994312	0.0896661(73)	0.5333069	0.5333855(25)
5	0.0986498	0.0885878(67)	0.5341573	0.534204(12)
6	0.0983705	0.0881762(69)	0.5344735	0.5345070(62)
CBS	0.097950(35)	0.0875830(80)	0.534987(43)	0.534971(13)
Experiment	0.08746(37)		0.5341192(15)	
ΔE	0.01034(40)	0.00003(38)	0.000868(46)	0.000852(16)

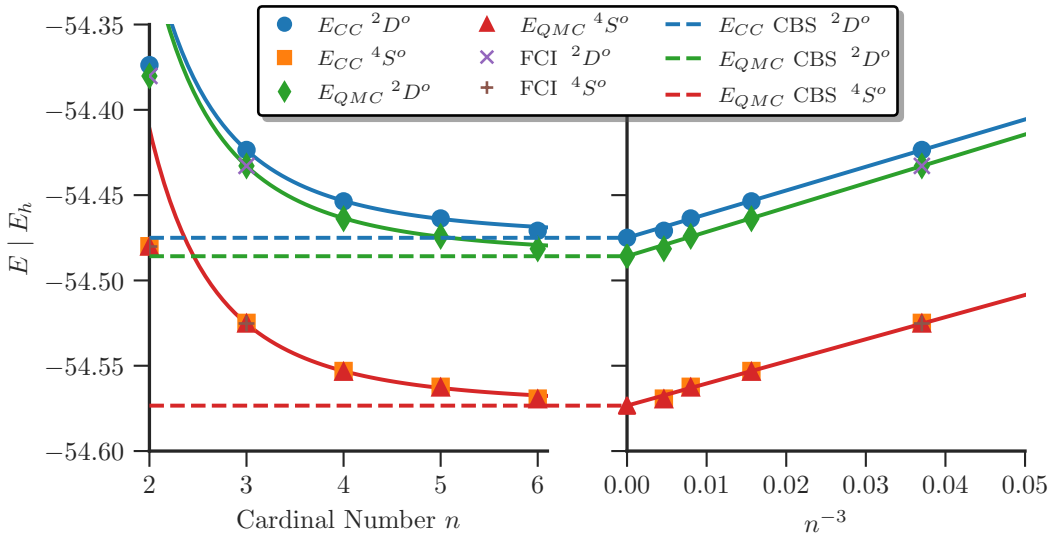

Figure 4.8: Energy of the $^4S^o$ and $^2D^o$ state of the nitrogen atom versus cardinal number of the basis set cc-pVnZ obtained with GUGA-FCIQMC compared with CCSD(T)[165,166] and FCI[164,167,349,350] results. The solid lines represent the inverse cube fit, Eq. (4.22) to n = T, Q and 5 and the dashes lines show the CBS limit results.

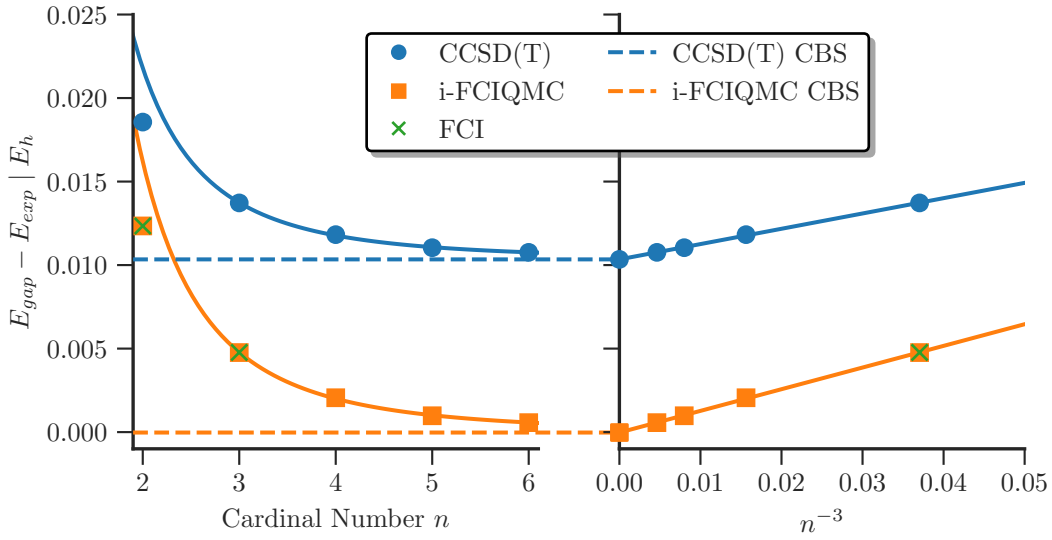

Figure 4.9: GUGA-FCIQMC and CCSD(T)[165,166,349,350] energy difference of the nitrogen ${}^4S^o$ and ${}^2D^o$ state to the experimental value[95,171] vs. the cardinal number (left) and inverse cube (right) of the cardinal number n of the basis set obtained. The solid lines are the inverse cube fit to the $n = T, Q, 5$ data points. The dashed lines and $n^{-3} = 0$ point indicate the CBS limit result. FCI results are obtained with Molpro.[164,167]

4.4.2 Nitrogen Dimer Binding Curve

The breaking of the strong triple bond of N_2 is accompanied by a change of single-reference to multiconfigurational character of the electronic structure and the concomitant strong electron correlation effects pose a difficult problem for quantum chemical methods. The ground state of the nitrogen molecule at equilibrium bond distance, $r_0 \approx 2.1a_0$, is a singlet ${}^1\Sigma_g^+$. All bonding molecular orbitals (MOs) formed from the 2p atomic orbitals (AOs) of the constituent N atoms are doubly occupied, see Fig. 4.10.

At large bond distances the ground states of the $S = 0, 1, 2$ and 3 states are degenerate, since the coupling of the independent nitrogen atoms A and B, ${}^4S_A^o \otimes {}^4S_B^o$, are all degenerate. We calculated the dissociation energy of N_2 as the difference of the ${}^1\Sigma_g^+$ N_2 ground state at equilibrium geometry $r_0 = 2.074a_0$ and the ${}^7\Sigma_u^+$ state at $r = 30a_0$ up to cc-pV5Z basis set with four core electrons frozen and performed a CBS limit extrapolation using Eq. (4.22) with the n = T, Q and 5 results. The results are shown in Table 4.6 with CCSD(T) results obtained with Molpro[165,166,349,350] and compared with experimental results,[144] which are corrected to remove scalar relativistic, spin-orbit and core correlation effects according to.[43,87] We also checked the convergence of the $r = 30a_0$ results with the independent atom calculations with a frozen core and found excellent agreement and the CCSD(T) and GUGA-FCIQMC results for the dissociation energy of N_2 agree with experimental values within chemical accuracy.

The energy as function of the bond length of the ${}^1\Sigma_g^+$ ground state of N_2 in the cc-pVDZ basis with a frozen core and comparison with available FCI and all-electron DMRG

n	N_2 Dissociation energy | E_h	
	CCSD(T)	GUGA-FCIQMC
2	0.3184752	0.3198257(42)
3	0.3448342	0.345412(26)
4	0.3551440	0.355565(55)
5	0.3587423	0.358984(49)
CBS(TQ5)	0.362603(47)	0.362797(53)
Experiment	0.362700(10)	
ΔE	-0.000097(57)	0.000097(63)

Tab. 4.6: Frozen-core GUGA-FCIQMC N_2 dissociation energy for increasing cardinal number n of the cc-pVnZ basis set compared to CCSD(T)[165,166,349,350] and experimental results,[43,87,144] corrected for scalar relativistic, spin-orbit and core correlation effects. The CBS limit is obtained with Eq. (4.22) for the n = T, Q and 5 data points.

Table 4.7: N_2 ground state energy with frozen core compared to FCI and all-electron DMRG results[51] for various bond distances in a cc-pVDZ basis set. Energies in atomic units.

r | a_0	E_{FCI}	GUGA-FCIQMC	ΔE_{FCI}	DMRG all-e^-	ΔE_{DMRG}
2.118	-109.278339	-109.278301(32)	0.000038(32)	-109.282157	0.0038553(13)
2.4	-109.238397	-109.238354(40)	0.000043(40)	-109.241886	0.0035321(14)
2.7	-109.160305	-109.160273(26)	0.000032(26)	-109.163572	0.0032993(13)
3.0	-109.086209	-109.086181(37)	0.000028(37)	-109.089375	0.0031937(14)
3.6	-108.994906	-108.99486(16)	0.00005(16)	-108.998052	0.0031928(26)
4.2	-108.966950	-108.966913(79)	0.000037(79)	-108.97009	0.0031768(18)

results[51] is shown in Table 4.7. There is excellent agreement with FCI results and a consistent energy difference of $\Delta E_{fc} \approx 0.0034\,E_h$ to the all-electron calculations.

The spin-resolved binding curves in a cc-pVDZ basis of all degenerate states at dissociation are shown in Fig. 4.11. Those are the ground state $^1\Sigma_g^+$, and the excited triplet $^3\Sigma_u^+$, quintet $^5\Sigma_g^+$ and septet $^7\Sigma_u^+$. At $r = 6a_0$ the 4 states are degenerate within chemical accuracy, < 1 kcal/mol. The right panel of Fig. 4.12 shows the lowest singlet and triplet states between r = 1.0Å and r = 2.25Å, compared with the experimental binding curve shown on the left. The "tower of states" at the $^1\Sigma_g^+$ equilibrium geom-

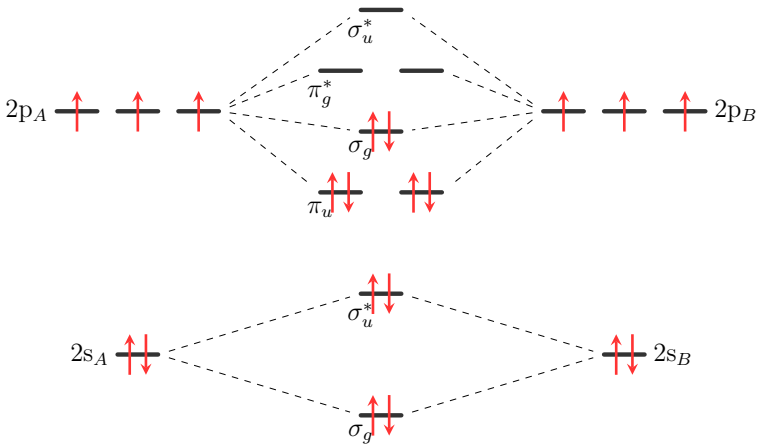

Fig. 4.10: Schematic energy diagram of the N_2 atomic and molecular orbitals. Note, due to *sp*-mixing, the σ_g MO formed from the 2p atomic orbitals is higher in energy than the π_u orbital at equilibrium.

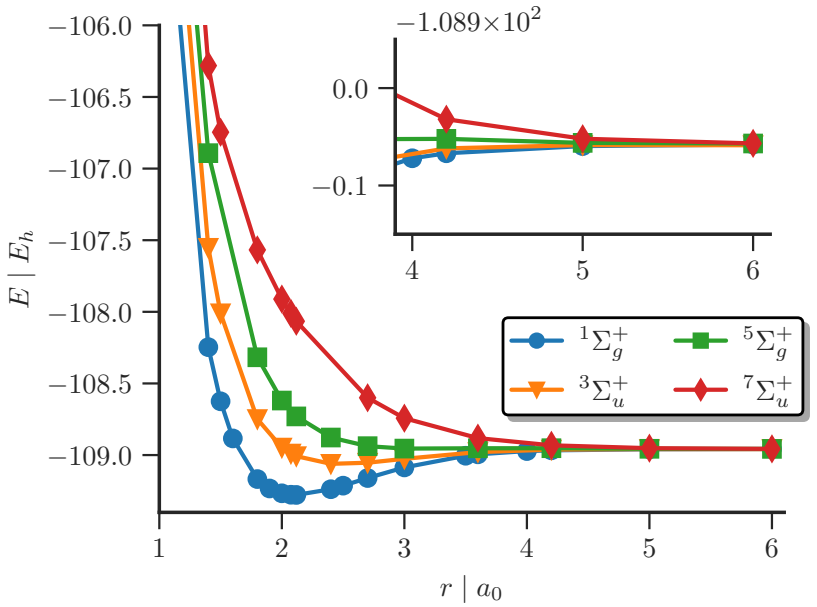

Fig. 4.11: Energy vs. bond distance of the degenerate states of N_2 at dissociation in a cc-pVDZ basis set. Integrals were created with Molpro.[349,350]

etry $r_0 = 1.121$Å at the cc-pVDZ basis level compared with the experimental order (see[107,108,193,216]) is

$$r = 2.118a_0 : {}^1\Sigma_g^+ < {}^3\Sigma_u^+ < {}^3\Pi_g < {}^3\Delta_u < {}^1\Pi_g < {}^3\Sigma_u^- < {}^1\Delta_u < {}^1\Sigma_u^- < {}^3\Pi_u,$$
$$\text{Exp.} : {}^1\Sigma_g^+ < {}^3\Sigma_u^+ < {}^3\Pi_g < {}^3\Delta_u < {}^1\Pi_g < {}^3\Sigma_u^- < {}^1\Sigma_u^- < {}^1\Delta_u < {}^3\Pi_u,$$

with excellent agreement with the experimentally observed ordering, except for the high-lying ${}^1\Delta_u$ and ${}^1\Sigma_u^-$ states, which are in reversed order. At other bond distances the correct term ordering is not completely captured within a cc-pVDZ basis set, but the general structure closely resembles the experimental results, as can be seen in Fig. 4.12.

Another benefit of the spin-adapted FCIQMC method is the possibility to calculate excited states belonging to the same total spin symmetry sector with the approach explained in Sec. 2.3.6. Although this is not necessary for the spin resolved nitrogen binding curve, since the states of same spin belong to different point group symmetry sectors. Thus, utilizing the discrete spatial symmetry, explained in Sec. 2.3.8, suffices to resolve excited states within the same spin symmetry sector in this case.

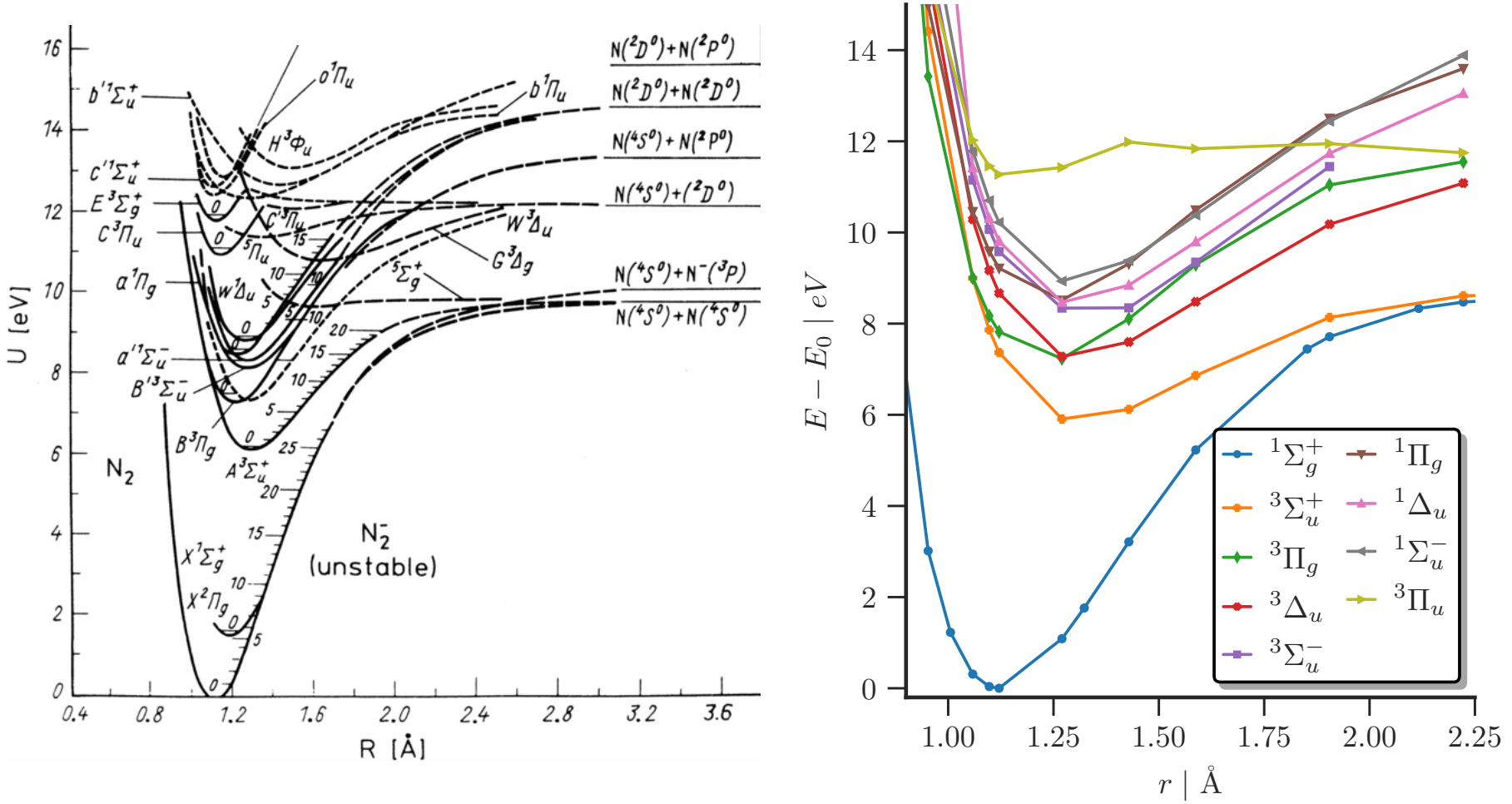

Figure 4.12: Experimental binding curve, taken and modified from [107, 193, 199] of N_2 compared with the spin-resolved results obtained with the spin-adapted FCIQMC in a cc-pVDZ basis set. (Permission to reproduce this figure has been granted by Elsevier and AIP Publishing.)

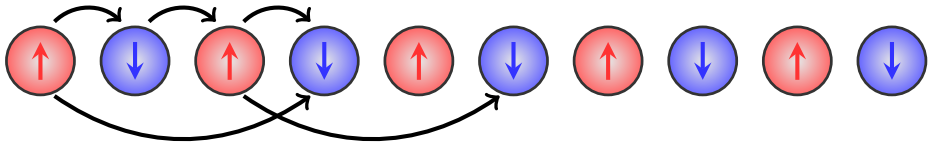

Figure 4.13: Level diagram of the hydrogen chain. Dominant excitation in an ordered basis are indicated with arrows above and in an unordered basis with arrows below.

4.4.3 One-Dimensional Hydrogen Chain

To further benchmark the GUGA-FCIQMC method we applied it to a linear chain of L equidistant hydrogen atoms[124] recently studied to test a variety of quantum chemical methods.[214] Using a minimal STO-6G basis there is only one orbital per H atom and the systems resembles a one-dimensional Hubbard model[122,142,240,241] with long-range interaction. By employing larger basis sets more features of real materials are captured. Studying a system of hydrogen atoms removes complexities like core electrons or relativistic effects and thus is an optimal benchmark system for quantum chemical methods.

For large equidistant separation of the H atoms a localized basis with singly occupied orbitals centred at each hydrogen is more appropriate than a HF orbital basis. Thus, this is an optimal difficult benchmark system of the GUGA-FCIQMC method, since the complexity of a spin-adapted basis depends on the number of open-shell orbitals, which is maximal for this system. Particularly targeting the low-spin eigenstates of such highly open-shell systems poses a difficult challenge within a spin-adapted formulation. This situation is depicted schematically in Fig. 4.13.

We calculated the $S = 0, 1$ and 2 (only $S = 0$ for $L = 30$) energy per atom up to $L = 30$ H atoms in a minimal STO-6G and cc-pVDZ basis (only for $L = 10$) at the equilibrium bond distance $r_0 = 1.8\,a_0$[214] and at the stretched $r = 3.6\,a_0$ geometry and compared it with DMRG[50,52,280,354] and MRCI+Q[214] results. The results are shown in Table 4.8, where we see excellent agreement within chemical accuracy with the reference results. At the equilibrium bond distance, $r_0 = 1.8\,a_0$, the use of HF orbitals is beneficial, since the electronic structure has a strong single-reference character. At the stretched, $r = 3.6\,a_0$, geometry, however, the use of a localized basis, obtained with the default Boys-localization in Molpro's `LOCALI` routine for the STO-6G basis set, is more suitable than an HF orbital basis. However, this represents the "worst-case" scenario of a spin-adapted implementation, especially when targeting the low-spin solutions of such highly open-shell systems, as the possible spin-recouplings, and thus the computational effort in general, depend strongly on the number of singly occupied orbitals in the wavefunction expansion. We studied this system to show that we are able to treat systems with up tp 30 open-shell orbitals. Due to the stochastic nature of the FCIQMC excitation generation we are able to correctly calculate the ground state energy of the $S = 0, 1$ and 2 spin states. An important fact is the order of the orbitals though. Similar to the DMRG method it is most beneficial to order the or-

Table 4.8: Energy per site E for an hydrogen chain for different number L of H atoms, bond lengths r and total spin S in a STO-6G basis set compared with DMRG[50,280] and MRCI+Q reference results.[214] For $L = 10$ also cc-pVDZ results are shown.

L	$r \mid a_0$	S	Basis	$E_{ref} \mid E_h$	GUGA-FCIQMC	$\Delta E \mid E_h$
10	1.8	0	sto-6g	-0.54243854	-0.54243629(87)	-0.00000225(87)
10	1.8	1	sto-6g	-0.52970810	-0.52970356(53)	-0.00000454(53)
10	1.8	2	sto-6g	-0.49001220	-0.49001410(35)	0.00000190(35)
10	1.8	0	cc-pVDZ	-0.56141048	-0.5613849(21)	-0.0000256(21)
10	1.8	0	cc-pVDZ	-0.561486[a]	-0.5613849(21)	-0.000101(10)
10	1.8	1	cc-pVDZ	-0.55131875	-0.5512561(42)	-0.0000627(42)
10	1.8	2	cc-pVDZ	-0.52065930	-0.520620(13)	-0.000039(13)
10	3.6	0	sto-6g	-0.48187008	-0.48186924(88)	-0.00000084(88)
10	3.6	1	sto-6g	-0.48079321	-0.4807873(10)	-0.0000059(10)
10	3.6	2	sto-6g	-0.47755076	-0.47755056(95)	-0.00000020(95)
10	3.6	0	cc-pVDZ	-0.51239171	-0.5123632(21)	-0.0000285(21)
10	3.6	1	cc-pVDZ	-0.51117613	-0.5111597(69)	-0.0000164(69)
10	3.6	2	cc-pVDZ	-0.50747105	-0.5074480(58)	-0.0000231(58)
20	1.8	0	sto-6g	-0.54129388	-0.5412255(14)	-0.0000684(14)
20	1.8	1	sto-6g	-0.53781131	-0.5376748(88)	-0.0001365(14)
20	1.8	2	sto-6g	-0.52702418	-0.5269256(90)	-0.0000986(90)
20	3.6	0	sto-6g	-0.48197897	-0.48194178(35)	-0.00003719(35)
20	3.6	1	sto-6g	-0.48168308	-0.4816776(22)	-0.0000055(22)
20	3.6	2	sto-6g	-0.48076572	-0.4807632(15)	-0.0000026(15)
30	1.8	0	sto-6g	-0.54098959	-0.5402611(63)	-0.0007285(63)
30	3.6	0	sto-6g	-0.48202026	-0.4808580(43)	-0.0011623(43)

[a] MRCI+Q reference result.[214]

bitals according to their overlap, since the number of possible spin recouplings depends on the number of open shell orbitals in the excitation range. If we make a poor choice in the ordering of orbitals, excitations between physically adjacent and thus strongly overlapping orbitals are accompanied by a large number of possible spin-recouplings in the excitation range, if stored far apart in the list of orbitals. This situation is depicted in Fig. 4.13.

This is also reflected in the ground state wavefunction expansion, where an optimal ordering of the orbitals is reflected by a stronger single reference character, see Fig. 4.14. The localized cc-pVDZ basis corresponds to orthogonalized atomic orbitals and all one- and two-electron integrals were computed with Molpro.[349,350]

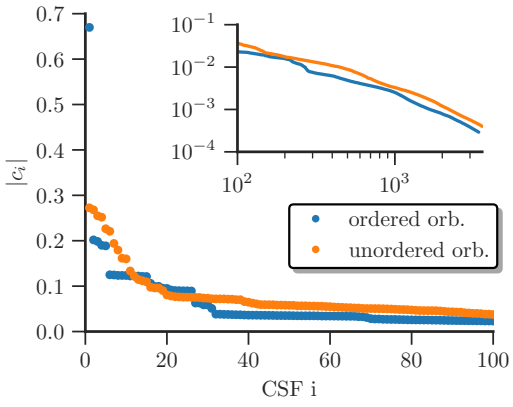

Fig. 4.14: $S = 0$ ground state wavefunction coefficients $|c_i|$ of the $L = 10$, $r = 3.6a_0$ H-chain with ordered and unordered localized orbitals.

4.4.4 The Hubbard Model

In this section results for the Hubbard model, introduced in Sec. 1.4, obtained by the spin-adapted FCIQMC method via the unitary group approach are presented. There are two important formulations of the Hubbard model. In general the hopping strength t is chosen as the energy scale of the system and only the relative strength of the kinetic hopping and on-site Coulomb term U/t is the defining parameter of the model. For small ratios of U/t the Hubbard model shows a metallic behaviour and thus a formulation in a momentum space basis via a Fourier transformation is beneficial. For large on-site repulsion U compared to the hopping strength t, $U/t \gg 1$, a real-space basis is more appropriate. Both cases are discussed in this section.

The Hubbard model in the real-space basis

As a reminder, the single-band Hubbard model[122,142,143,154] with nearest-neighbour hopping t and on-site repulsion U is given by

$$\hat{H} = -t \sum_{\langle i,j\rangle,\sigma} a^\dagger_{i\sigma} a_{j\sigma} + U \sum_i n_{i,\uparrow} n_{i,\downarrow}, \tag{4.23}$$

in the real-space formulation. Electrons can hop between nearest-neighbour sites $\langle i,j\rangle$ with strength t and interact purely locally if they are on the same site via the Coulomb interaction U. This is shown schematically for a 2D 18-site system in Fig. 4.15. The sign of U determines, if we look at the repulsive ($U > 0$) or attractive ($U < 0$) model. In terms of the unitary group generators Eq. (4.23) takes the very simple form

$$\hat{H} = -t \sum_{<i,j>} \hat{E}_{ij} + \frac{U}{2} \sum_i \hat{e}_{ii,ii}. \tag{4.24}$$

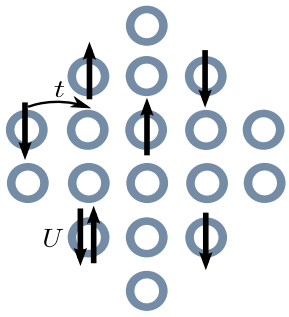

Fig. 4.15: Schematic representation of a two-dimensional 18-site Hubbard model with nearest neighbour hopping t and on-site repulsion U.

This means only the action and matrix elements for single generator $\hat{E}_{ij}$ for nearest neighbours $\langle i,j\rangle$ have to be considered, which greatly simplifies the application of the GUGA-FCIQMC method when applied to the real-space Hubbard model, as there are no double excitations and also no contribution to singles coming from the two-body operator. However, the efficiency of the GUGA implementation is tested to its limit, since for systems with high on-site repulsion $U \gtrapprox 12$, where it is beneficial to use a real-space basis, almost all sites are singly occupied in the most important CSF contributions to the ground state wavefunction.

The Hubbard model in a real-space basis with large on-site repulsion U/t can be compared to the stretched geometry of

the hydrogen chain in a minimal basis, see Sec. 4.4.3. Similar to the H-chain, and highly open-shell systems in general, the calculation of the low-spin eigenstates pose a challenge, due to the vast amount of possible spin-recouplings within a spin-adapted basis. Additionally, the ordering of the orbitals also plays an important role in the Hubbard model, where orbitals should be stored next to their neighbours. In one dimension this is easily doable, but already fails in the two-dimensional case.

If periodic boundary conditions and more than one dimensional systems are studied, even the nearest neighbour hopping terms, correspond to excitations with large ranges $|i-j|$, similar to problems DMRG[277] faces for systems of higher dimension than one. For this reason and to make analogies to the one-dimensional hydrogen chain we focused on the 1D Hubbard chain to study the applicability of the spin-adapted FCIQMC approach, but also compare our results to the exactly diagonalizable two-dimensional 4×4 lattice.

The Hubbard model in the momentum-space basis

With a Fourier transformation of the operators

$$a^\dagger_{\mathbf{l},\sigma} = \frac{1}{\sqrt{L}} \sum_{\mathbf{k}} \mathrm{e}^{-i\mathbf{k}\cdot\mathbf{l}}\, c^\dagger_{\mathbf{k},\sigma} \rightarrow \hat{E}_{\mathbf{lm}} = \frac{1}{L} \sum_{\mathbf{k},\mathbf{k}'} \mathrm{e}^{-i(\mathbf{l}\cdot\mathbf{k}-\mathbf{m}\cdot\mathbf{k}')}\, \hat{E}_{\mathbf{kk}'}, \tag{4.25}$$

with system size L and the fermionic annihilation(creation) operators, $c^{(\dagger)}_{\mathbf{k},\sigma}$, of an electron in a state with momentum $\mathbf{k}$ and spin σ, the spin-free Hubbard Hamiltonian (4.24) can be transformed to the momentum-space basis as

$$\hat{H} = \sum_{\mathbf{k}} \epsilon_{\mathbf{k}} \hat{E}_{\mathbf{kk}} + \frac{U}{2L} \sum_{\mathbf{k},\mathbf{k}',\mathbf{q}} \hat{e}_{\mathbf{k}+\mathbf{q},\mathbf{k};\mathbf{k}'-\mathbf{q},\mathbf{k}'}, \tag{4.26}$$

with the dispersion relation $\epsilon(\mathbf{k}) = -2t\cos\mathbf{k}$. In the momentum space Hubbard model (4.26) the one-body operator is diagonal and only double excitations have to be considered. Due to *momentum conservation* certain excitation types of the GUGA formalism are symmetry forbidden. The type 2a and 2b excitations listed in Table 4.3 are not possible since this would imply $\mathbf{k}+\mathbf{q} = \mathbf{k}'-\mathbf{q}$ and $\mathbf{k} = \mathbf{k}'$, which is only possible if $\mathbf{q} = 0$, which would be a diagonal contribution. Additionally the type 1e, 1f 1i and 1j excitations in Table 4.3 are not possible, since applying the momentum conservation criteria would lead to a contradiction for the necessary different indices, e.g. type 1e: $\hat{e}_{jk,ki}$ would imply $\mathbf{k}' = \mathbf{k}+\mathbf{q}$ with momentum conservation, which would imply $j = i$. So the only possible exchange term is the fully symmetric type 2c excitation $\hat{e}_{ij,ji} = \hat{e}_{\mathbf{k}+\mathbf{q},\mathbf{k};\mathbf{k},\mathbf{k}+\mathbf{q}}$, with $\mathbf{q} \neq 0$. The momentum space Hubbard model with low interaction strength U/t can be compared to the equilibrium geometry hydrogen chain in a minimal basis using HF orbitals, see Sec. 4.4.3.

Table 4.9: Energy per site E of the half-filled 1D-Hubbard chain for $U/t = 2$ in a momentum-space basis and $U/t = 12$ in a real-space basis with periodic (PBC) and open (OBC) boundary conditions and different total spin S values. Energies are given in units of the hopping strength t and comparison with DMRG[50,280] results are given

L	U/t	S	BC	$E_{ref} \mid t$	i-FCIQMC	$\Delta E \mid t$
10	2	0	PBC	-0.86384156	-0.8638376(32)	-0.0000040(32)
10	2	1	PBC	-0.78699638	-0.787004(11)	0.0000073(110)
10	2	2	PBC	-0.68347569	-0.6834803(43)	0.0000046(43)
10	12	0	PBC	-0.22779184	-0.22778308(21)	0.00000876(21)
10	12	1	PBC	-0.21409173	-0.2140549(10)	-0.0000368(10)
10	12	2	PBC	-0.17785459	-0.1778427(11)	-0.0000119(11)
10	12	0	OBC	-0.21130895	-0.2113058(10)	-0.0000031(10)
10	12	1	OBC	-0.20070058	-0.2006914(32)	-0.0000092(32)
10	12	2	OBC	-0.16892931	-0.1689216(31)	-0.0000077(31)
20	2	0	PBC	-0.84299369	-0.842875(47)	-0.000119(47)
20	2	1	PBC	-0.83684320	-0.836635(29)	-0.000208(29)
20	2	2	PBC	-0.79716782	-0.797168(75)	0.000055(75)
20	12	0	PBC	-0.22575066	-0.2257440(40)	-0.0000067(40)
20	12	1	PBC	-0.22222905	-0.222187(12)	-0.000042(12)
20	12	2	PBC	-0.21228724	-0.212233(12)	-0.000054(12)
20	12	0	OBC	-0.21808186	-0.21807886(32)	-0.00000300(32)
20	12	1	OBC	-0.21516665	-0.2151468(11)	-0.0000198(11)
20	12	2	OBC	-0.20614436	-0.2061172(20)	-0.0000271(20)

Results on the Hubbard model

We calculated the energy per site of the half-filled $L = 10$ and $L = 20$ site Hubbard chain for $U/t = 2$ in a momentum-space basis with periodic boundary conditions (PBC) and $U/t = 12$ in a real-space basis with PBC and open boundary conditions (OBC) for a total spin of $S = 0, 1$ and 2. The results are given in Table 4.9 with comparison to DMRG reference results, obtained with the spin-adapted `BLOCK`[50,280] DMRG code. There is excellent agreement with the reference results and as expected the OBC results are in better agreement than the corresponding PBC calculations for $L = 10$ and 20 for $U/t = 12$, due to the problematic large excitation range excitation occurring with PBC.

We also calculated the energy per site of the off half-filling two-dimensional 4×4 Hubbard model with PBC at $U/t = 16$ with 15 electrons for $S = 1/2, \ldots, 13/2$. The calculations were performed with the original FCIQMC framework[30] without the initiator approximation[56] in a spin-adapted basis, since it has proven to perform well in the large U/t regime of the real-space Hubbard model. The results are shown in Fig. 4.16 with comparison the exact diagonalization (ED) results obtained with the Lanczos[176] method.[121] There is good agreement of the GUGA-FCIQMC with the ED results.

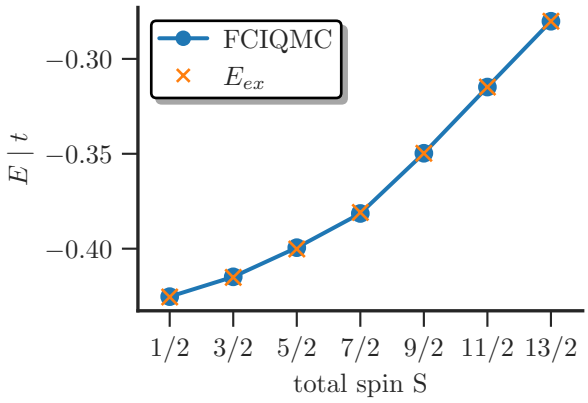

Fig. 4.16: Energy per site of the off half-filling $N = 15$ 4×4 Hubbard models with periodic boundary conditions at $U/t = 16$ versus the total spin S. Comparisons with exact diagonalization results are given.[121]

4.4.5 Computational Effort and Scaling of GUGA-FCIQMC

To analyse the additional computational cost associated with the GUGA-based CSF implementation in FCIQMC, we compare the time per iteration, t_{iter}, and timestep, $\Delta\tau$, with the original SD-based FCIQMC method for the systems (N, N_2, hydrogen chain and the Hubbard model in the real- and momentum space basis) mentioned above. Since FCIQMC is formally linear-scaling with the walker number N_w[29] we removed the bias of walker number differences by comparing the time per iteration and per walker.

The left panel of Fig. 4.17 shows the timestep $\Delta\tau$ obtained with the histogram based optimization, see Sec. 4.3, for N_2 at $r = 4.2\,a_0$ vs. the cardinal number n of the cc-pVnZ basis set. As expected the usable timestep in the SD-based simulation is higher compared to the CSF-based calculation, with roughly twice the possible $\Delta\tau$. However, rather surprisingly the difference of the two decreases with increasing basis set size. The right panel of Fig. 4.17 shows the time per iteration and walker for the same simulations. The additional computational cost of the GUGA implementation roughly doubles the time per iteration compared to the original FCIQMC method. While there seems to be a steeper increase with increasing basis set size for the CSF-based implementation, it is nowhere near the formally $\mathcal{O}(n)$ cost, with n being the number of orbitals, mentioned in Section 4.2. So in total, with twice the timestep and twice the time per iteration, the spin-pure GUGA implementation amounts to a fourfold increase in computational cost compared to the original SD-based FCIQMC method. *

To examine the scaling in more detail, a least-squares fit to the polynomial $f(n) = a + b \cdot n^c$, with 3 parameters a, b and c, was performed on the available data points with n being the cardinal number of the basis set. The lines in Fig. 4.17 represent this fit for the timestep $\Delta\tau(n)$ and time per iteration $t_{iter}(n)$, as a function of the cardinal number n of the basis set. The results for the determinant- and CSF-based calculations are

*All simulations for this comparison were performed on identical 20 core Intel Xeon E5-2680 nodes with 2.8GHz clock rate, 20MB cache and 128GB memory.

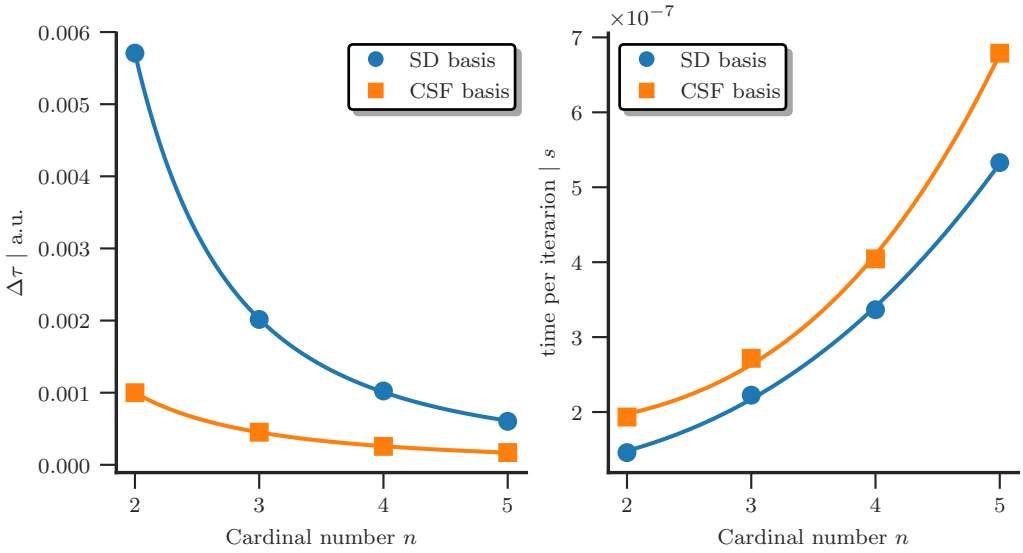

Figure 4.17: SD- and CSF-based results for N_2 at $r = 4.2a_0$ for cc-pVnZ basis sets, n = D, T, Q, 5. (left) Time-step $\Delta\tau$ adapted with the histogram-based optimization with an integration threshold of 0.9999 and (right) time per iteration vs. the cardinal number of the basis set. The results were obtained on identical 20 core Intel Xeon E5-2680 nodes with 2.8GHz clock rate and with $N_w^{tot} = 100k$. The lines are fits to the data explained in the main text.

		a	b	c	δa	δb	δc
$\Delta\tau$	SD:	$1.25 \cdot 10^{-4}$	$3.53 \cdot 10^{-2}$	-2.66	$4.4 \cdot 10^{-5}$	$1.2 \cdot 10^{-3}$	0.06
	CSF:	$1.05 \cdot 10^{-5}$	$3.95 \cdot 10^{-3}$	-2.00	$9.9 \cdot 10^{-6}$	$8.9 \cdot 10^{-5}$	0.04
t_{iter}	SD:	$1.14 \cdot 10^{-7}$	$5.04 \cdot 10^{-9}$	2.74	$1.4 \cdot 10^{-8}$	$2.0 \cdot 10^{-9}$	0.23
	CSF:	$1.75 \cdot 10^{-7}$	$2.08 \cdot 10^{-9}$	3.41	$1.6 \cdot 10^{-8}$	$1.1 \cdot 10^{-9}$	0.31

with one standard deviation errors of the fit parameters given. The scaling of the decrease in the possible timestep $\Delta\tau$ is almost less than a factor of n smaller in the CSF based implementation and the increase of the time per iteration t_{iter} less than n larger compared to the determinant based implementation. However, the combination of these two effects causes the spin-adapted FCIQMC implementation to scale by an additional factor of $\approx \mathcal{O}(n^{1.3})$ for this specific system, compared to the original SD-based FCIQMC method.

Table 4.10 shows the averaged timestep and time per iteration ratios between GUGA- and SD-based simulations on the systems mentioned until now. Compared to the CSF-based FCIQMC the maximum possible timestep in the original determinant based implementation is larger by a factor of 2.31 to 3.87 and the time per iteration is smaller by a factor of 0.36 to 0.90. Although the timings for the nitrogen dimer indicated by the footnote a in Table 4.10 should be taken with a grain of salt, as they are results from an older, less optimized version of the spin-adapted implementation. The combination of these effects result in a slow down by a factor of 2.8 to 5.2 of the spin-adapted FCIQMC method.

System	$n_{samples}$	$\Delta\tau_{SD}/\Delta\tau_{CSF}$	$\delta\Delta\tau$	t_{SD}/t_{CSF}	δt
N	10	2.55	0.12	0.90	0.08
N_2	9	3.87	0.48	0.75	0.05
N_2[a]	23	2.31	0.10	0.36	0.03
H-chain	8	-[b]	-[b]	0.63	0.05
Hubbard[a]	34	-[b]	-[b]	0.20	0.03
Hubbard	18	-[b]	-[b]	0.67	0.10

[a] Older, less optimized version of the GUGA implementation

[b] No data available

Tab. 4.10: Averaged timestep $\Delta\tau$ and time per iteration t ratios of CSF- and SD-based FCIQMC calculations for various systems and sample sizes $n_{samples}$. The standard errors δt and $\delta\Delta\tau$ are also given.

4.4.6 3d Transition Metal Atoms

All the previous systems were studied to show the applicability of the spin-adapted FCIQMC implementation based on the graphical unitary group approach and benchmark it against the original determinant based formulation, exact results and other quantum chemical methods. However, except for the CBS limit results of the nitrogen atom, all results could have been obtained with the original determinant based FCIQMC method.

In this section we study the two transition metal atoms cobalt and scandium, and calculate the spin gap of the ground state and low-lying excited states and electron affinities. Both atoms have an odd number of electrons and thus the HPHF approach in the original FCIQMC can not be applied. Additionally, as most open-shell transition metals, the cobalt atom has a high-spin ground state, due to Hund's rule. This prohibits the calculation of the spin-gap to low-spin excited states by restriction of the m_s quantum number, as inevitably these excited state calculations will converge to the high-spin ground state in the projective procedure of FCIQMC. These systems are therefore the perfect playground to show the capability of the spin-adapted FCIQMC approach, to calculate quantities not obtainable with the original (spin-unprojected) method. We compare our results to coupled cluster calculations, which are not so easily applicable, due to the multireference character of the excited states of these systems.

Cobalt

The ground state electronic configuration of the neutral cobalt atom is $[\mathrm{Ar}]3s^2 3p^6 3d^7 4s^2$ and is a quartet ${}^4F$ state. We calculated the spin gap to the first doublet excited state ${}^2F$ with the $[\mathrm{Ar}]3s^2 3p^6 3d^8 4s$ configuration with the GUGA-FCIQMC method. We employed an ANO basis set[3] with primitive contractions corresponding to a comparable VnZP basis with n = D, T and Q and the *full* and completely uncontracted *primitive* ANO basis set. The ANO molecular integral files were computed with Molcas.[10] We also prepared ab-

initio integrals with an augmented correlation consistent core-valence basis set with 2nd order Douglas-Kroll scalar relativistic corrections[264] aug-cc-pwCVnZ-DK (denoted as cc-basis in Table 4.11) up to n = Q. The cc-basis molecular integrals were computed with Molpro.[349,350] We also performed 2nd order complete active space perturbation theory[9,198] (CASPT2) calculation on the ANO basis set with Molcas and CCSD(T) calculation in the cc-basis with Molpro.

Similar to the nitrogen atom, see Sec. 4.4.1, the odd number of electrons and high-spin ground state to low-spin excited state setup makes previous spin-pure methods implemented in FCIQMC not applicable. However, as the results in Table 4.11 show, the GUGA-FCIQMC implementation is able to provide energies within chemical accuracy close to the experimental result.[171,249,313] At least the CBS limit extrapolation of the two-point (VTZP and VQZP) inverse cube fitted (4.22) ANO-basis results are below 1 kcal/mol away from the experimental result. However, the good agreement with experiment must be attributed to some beneficial error cancellation, due to both neglected scalar relativistic and spin-orbit coupling effects. The CBS limit results using n = D, T and Q from the cc-basis are approx. $0.003\,E_h \approx 1.88$ kcal/mol above the experimental results, where the remaining error can be attributed to the neglected spin-orbit coupling effects.

Similar to the spin gap of nitrogen 4.4.1 CCSD(T) is not able to provide correct results of the doublet ^2F state of cobalt. The CCSD(T) calculations are based on ROHF orbitals and the valence electronic configuration of the ^2F state, $3d^8 4s$, enforces the $4s$ orbital to be singly occupied with all the d-electrons being in a closed shell conformation. This obviously violates Hund's rule and thus the CCSD(T) results give a too high energy for the ^2F state, as can be seen in Fig. 4.18.

The starting orbitals for the Co ^2F and ^4F calculation with FCIQMC were CASSCF[131,225] orbitals with the $1s^2 2s^2 2p^6 3s^2 3p^6$ orbitals frozen, 9 active electrons in the active space of $4s, 3d, 4p, 5s$ and $4d$, CAS(9,15) and further orbitals being virtuals, see the left panel of Fig. 4.19. The CASSCF calculations were performed with Molcas[10] and Molpro.[168,345] Similar to the nitrogen atom the SO(3) symmetry of Co is reduced to the D_{2h} symmetry implemented in Molpro and Molcas. We chose the B_{1g} irrep for the ^2F- and the A_g irrep for the ^4F-state.

Scandium

The electronic configuration of the neutral scandium doublet ^2D ground state is [Ar]$3s^2 3p^6 3d 4s^2$. The electron affinity of scandium is an interesting problem, as the electronic configuration of the ground state of the Sc^- anion was experimentally—as a surprise—determined[86] to be [Ar]$3s^2 3p^6 3d 4s^2 4p$, with the additional electron occupying the $4p$ shell instead of the expected $3d^2$. Two bound states, a singlet $^1D^o$ and triplet $^3D^o$,

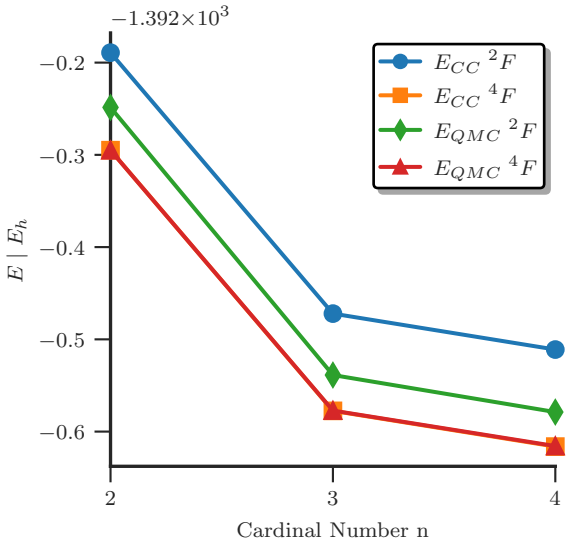

Fig. 4.18: Energy of the ^4F and ^2F states of Co versus the cardinal number n of the cc-basis, calculated with GUGA-FCIQMC and CCSD(T)[165,166] based on ROHF orbitals.

Table 4.11: GUGA-FCIQMC, CASPT2[10] and CCSD(T)[349,350] results for the $^2F - {}^4F$ spin gap of Co in an ANO[10] and cc-basis set[349,350] compared with the experimental values.[171,249,313] CBS limit extrapolations were obtains with Eq. (4.22) with the data points of basis sets in parentheses.

		Co $^2F - {}^4F$ spin gap | E_h		
	Basis set	i-FCIQMC	CASPT2	CCSD(T)
ANO-basis	VDZP	0.04895(32)	0.04667	
	VTZP	0.04326(14)	0.04373	
	VQZP	0.03775(54)	0.03675	
	Full	0.03626(21)	0.03565	
	Primitive		0.03565	
	CBS(TQ)	0.03373(94)	0.03448(16)	
cc-basis	n = D	0.046448(88)		0.1057278
	n = T	0.03855(22)		0.1054354
	n = Q	0.03685(27)		0.1052032
	CBS(DTQ)	0.03535(22)		0.1051967(92)
	Experiment		0.032285183	
	ΔE_{ANO}	0.00144(94)	0.00220(16)	
	ΔE_{CC}	0.00306(22)		0.0729115(92)

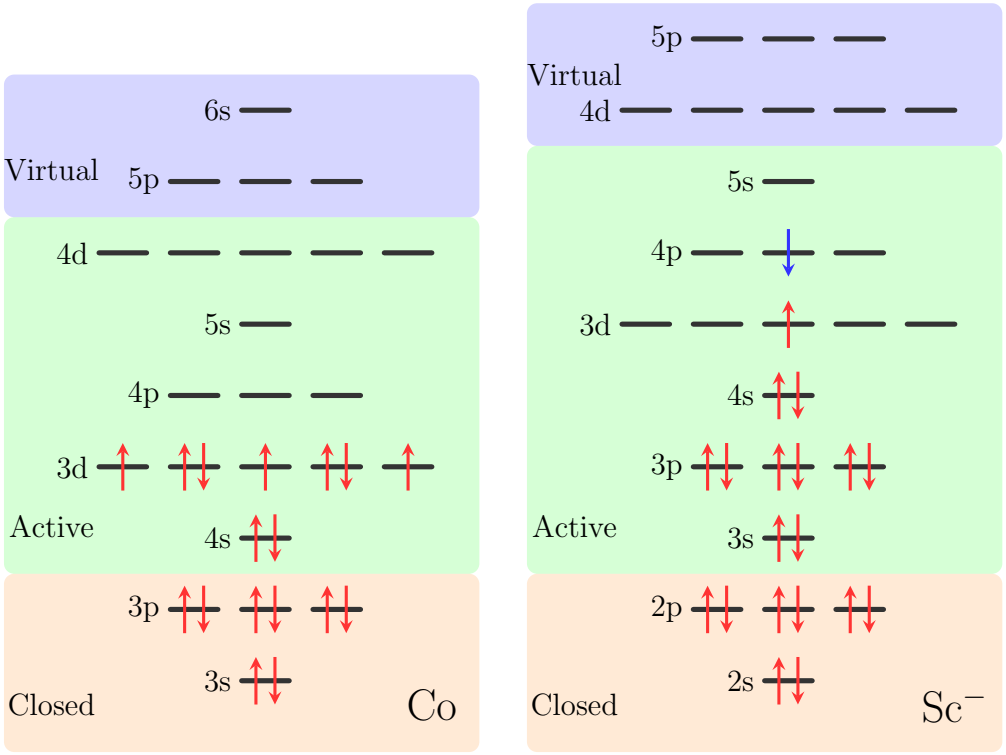

Figure 4.19: Schematic orbital energy diagram of and ground state electron configuration of the ^4F state of cobalt (left) and the ^1D state of the scandium anion (right). The chosen active spaces for the CASSCF calculation are shown in orange (closed), green (active) and blue (virtual).

were identified with no clear experimental consensus which one of the two is the ground state of Sc^-. Subsequent theoretical studies[14,150] identified the singlet $^1D^o$ state as the ground state of Sc^-. However, more recent coupled cluster (CC) studies of the ionization potentials and electron affinities (EA) of the $3d$ transition metals[11,12,322] left out the EA of scandium, due to the multiconfigurational character of the anion ground state. Nevertheless, in [12] EA results of Sc obtained with the internally contracted multireference averaged coupled pair functional (MR-ACPF) method[96,347] in excellent agreement with experiment were reported.

Similar to the already mentioned problems of the coupled cluster method for the $^2D^o$ state of nitrogen and ^4F state of cobalt, see Sec. 4.4.1 and 4.4.6 respectively, the $^1D^o$ state of Sc^- has two open-shell $3d$ and $4p$ orbitals coupled to a singlet. This makes the applicability of ROHF based CCSD(T) problematic and combined with the multiconfigurational character of the ground state causes CC to yield non satisfactory results.

We performed spin-adapted i-FCIQMC calculations for the ^2D state of Sc and for the $^1D^o$ and $^3D^o$ state of Sc^- in an aug-cc-pwCVnZ-DK basis, n = D, T and Q, with CASSCF orbitals. The $1s, 2s$ and $2p$ orbitals were closed, with an active space of 11 (for Sc) and 12 (for Sc^-) electrons in the $3s, 3p, 3d, 4s, 4p$ and $5s$ orbitals, yielding a CAS(11,14) for Sc and CAS(12,14) for Sc^-, and the remaining orbitals as virtuals. The $^1D^o$ electronic configuration, the orbital energy diagram and the chosen active space conformation is

Table 4.12: Electron affinity (EA) of scandium and spin gap of the two bound states of Sc^- $^1D^o$ and $^3D^o$ obtained with GUGA-FCIQMC in an aug-cc-pwCVnZ basis compared with experimental results[86] (Exp.). The CBS limit result is obtained with Eq. (4.22) using the n = T and Q results. The experimental $^3D^o$ values are not corrected for spin-orbit effects. Energies are given in atomic units.

n	$^2D - {}^1D^o$ EA	$^2D - {}^3D^o$ EA	Sc^- $^1D^o - {}^3D^o$
2	0.007740(75)	0.000380(77)	0.007341(76)
3	0.00734(54)	0.002572(77)	0.00499(33)
4	0.00667(75)	0.002381(65)	0.00480(42)
CBS	0.0062(14)	0.00224(13)	0.00466(76)
Exp.	0.00695(74)	0.00154(74)	0.00540(147)
ΔE	0.0008(21)	-0.00070(86)	0.0007(22)

shown in the right panel of Fig. 4.19. Similar to the nitrogen 4.4.1 and cobalt 4.4.6 atom the SO(3) symmetry is reduced to the available D_{2h} point group symmetry in Molpro[349,350] with which the integrals were produced. We chose the B_{1g} irrep for the ^2D scandium ground state and the B_{1u} irrep for the $^1D^o$ and $^3D^o$ state of Sc^-. Although a recent we found*, using state-averaged orbitals of the degenerate set of $2A_u$, and B_{iu}, $i = 1, 2, 3$, irreps yields a more compact wavefunction expansion and faster convergence rates.

The EA of Sc relative to the $^1D^o$ and $^3D^o$ state of Sc^- and the gap between the latter two states, obtained with GUGA-FCIQMC is shown in Table 4.12. There is agreement within 1 kcal/mol with the experimental values and in accordance to previous theoretical studies[12,14,150] we can definitely identify the singlet $^1D^o$ as the ground state of Sc^-.

*Too late to include in this manuscript.

4.5 Conclusion and Outlook

In this chapter the implementation of a spin-adapted basis in form of the Gel'fand-Tsetlin basis based on the unitary group approach in the FCIQMC method was presented. The efficient excitation generation and matrix element evaluation directly in this basis, without any reference to a Slater determinant formulation, is possible with the help of the graphical unitary group approach. Utilising this basis the conservation of the total spin quantum number in FCIQMC simulations is ensured, with the accompanying benefits of Hilbert space size reduction, resolution of different—even degenerate—spin eigenstates and easy calculations of spin gaps, otherwise not accessible.

The motivation behind this approach was to reduce the effective degrees of freedom and allow a more compact description of problems with inherent total spin symmetry and enabling the application of the FCIQMC method to more complex systems. Furthermore, as many chemical and physical processes depend on the delicate interplay of near-degenerate—or at least close in energy—states of different spin symmetry, the possibility to target specific spin states and obtain solutions without contamination of different symmetry sectors, is highly desirable. However, to be competitive compared to conventional approaches, a very efficient implementation is necessary, due to the additional computational cost associated with the more complex internal structure of this basis compared to Slater determinants.

The method was tested and benchmarked for the nitrogen atom, nitrogen dimer, one-dimensional hydrogen chains and the single band Hubbard model. Excellent agreement with exact results, where available, and other quantum chemical methods was observed.

We found that the additional computational cost associated with the more complicated and highly connected Hilbert space of CSFs is manageable and applications of this approach for systems with up to 30 open-shell orbitals was demonstrated; eradicating the severe limitations of previous spin-adapted approaches in general and in FCIQMC in particular. Even more so, the problematic calculation of the low-spin eigenstates of highly open-shell systems is affordable with this stochastic approach.

The validity of the approach was proven and the direct targeting of specific spin states is possible; enabling to obtain results previously not accessible to the FCIQMC method. These are gaps of high-spin ground and low-spin excited state systems with an odd number of electrons and the excitation energies within an explicit spin symmetry sector. However, although the scaling is manageable, we did not observe the—initially expected—acceleration of convergence compared to the original SD based FCIQMC implementation. In this regard, it seems the benefits and drawbacks of this approach mutually compensate each other.

The method does not allow us to simulate larger systems. On the contrary, the additional scaling with the number of spatial orbitals, starts to become relevant for large basis set expansions, limiting the applicability, where the SD based implementation remains preferable. The increased connectivity of a spin-pure basis reduces the generation probabilities in the spawning step of the FCIQMC method and thus limits the possible timestep of a simulation and causing stability issues in the sampling process.

In this regard, the scope of application of this method is rather to target specific, interesting spin states, which allows a clearer chemical and physical interpretation of results. As a consequence, more insight in chemical processes governed by the interplay of different spin states is possible.

Along this line, we calculated, within chemical accuracy to experimental results, the spin gap between the cobalt quartet ^{4}F ground state and first doublet ^{2}F excited state. Due to the high-spin ground- and low-spin excited-state configuration, these results are not obtainable by the conventional SD-based FCIQMC implementation. Additionally, the electron affinity of scandium with agreement to experimental results within chemical accuracy was determined, and the experimentally undetermined ordering of the scandium anion singlet ^{1}D^o and triplet ^{3}D^o bound states was investigated. In agreement with previous theoretical studies, our results indicate that the singlet is the ground state of Sc^- with a spin-gap energy of $\Delta E_{S-T} = 2.92 \pm 0.48$ kcal/mol to the triplet bound state, compared to the experimental value of $\Delta E_{exp} = 3.39 \pm 0.92$ kcal/mol, with undetermined ordering of the states however.

Outlook

The spin-adapted FCIQMC method has also been applied to far larger systems as mention in this manuscript. In collaboration with G. Li Manni, we studied the spin-gap of iron-porphyrin (Fe(II)-Porphyrin) and iron-sulphur clusters with up to 32 electrons in a CASSCF active space of 34 orbitals. Excellent agreement with previous theoretical studies[183] were obtained for the Fe(II)-Porphyrin system, but due to time limitations these results were omitted from this manuscript and are subject of future work.

Another great benefit of the spin-adapted formulation of FCIQMC is the possibility to calculate excited states within a given spin symmetry sector with the approach in FCIQMC, explained in Sec. 2.3.6. An association of a definite total spin S to an excited state result is not possible in the determinant based FCIQMC implementation, neither by using HPHF functions, see Sec. 3.2, nor by restricting the $\hat{S}_z$ eigenvalue. However, this advantageous property of the spin-adapted FCIQMC formulation still needs further investigation.

The sampling of reduced density matrices (RDMs), see Sec. 2.3.5, in the spin-adapted formulation based on the GUGA is unfortunately a highly non-trivial task. Although there is no theoretical problem of density matrices in the unitary group formalism,[115,238,251,287] from a practical standpoint there is. Due to the increased connectivity within a CSF basis

and the possibility of generators with different spatial indices contributing to the same density matrix element, see Sec. 3.4.1 and appendix A.2, there is a large overhead involved in sampling RDMs in the spin-adapted FCIQMC method. However, we are optimistic to solve these problems in due time, which would allow us to use GUGA-FCIQMC as a spin-pure FCI solver in the stochastic CASSCF method.[184] This would enable us to solve active spaces of unprecedented size in a spin-pure fashion, extending even further the applicability of the method.

Furthermore, the unitary group formalism is extendable to spin-dependent operators,[72,112–114,158–160,180,360] and an extension of the spin-adapted FCIQMC method to this approach is currently investigated to enable us to study systems with spin-orbit coupling and explicit spin dependence.

Along this line, another interesting problem to be investigated is the application of GUGA-FCIQMC to the two-dimensional t-J model

$$\hat{H}_{t-J} = -t \sum_{\langle i,j\rangle,\sigma} a^\dagger_{i,\sigma} a_{j,\sigma} + J \sum_{\langle i,j\rangle} \left(\hat{\mathbf{S}}_i \cdot \hat{\mathbf{S}}_j - \frac{n_i n_j}{4} \right) \tag{4.27}$$

and the Heisenberg lattice model

$$\hat{H}_H = J \sum_{\langle i,j\rangle} \hat{\mathbf{S}}_i \cdot \hat{\mathbf{S}}_j + h \sum_i \hat{S}^z_i, \tag{4.28}$$

with the vector of spin operators acting on site i, $\hat{\mathbf{S}}_i$ and $n_i = n_{i\uparrow} + n_{i\downarrow}$. Both can be derived as effective low-energy models of Hubbard model (4.23) in the large U/t limit with a suppression of doubly occupied sites. As the Coulomb repulsion U increases with fixed hopping strength t, doubly occupied sites become very unfavourable energetically and thus the important states in the ground state wavefunction have exclusively singly occupied sites. In the limit of infinite U/t only hopping processes to empty nearest neighbour sites and second order virtual hopping processes, resulting in spin-flips of nearest-neighbour sites remain. The Heisenberg model is the special case of the t-J model at half-filling. Since doubly occupied sites are projected out for these models, every site in the Heisenberg model is either occupied by an ↑- or ↓-spin, which interact via nearest-neighbour spin flip processes of strength J. In the less than half-filled t-J model, the spins are additionally allowed to hop to empty nearest neighbour sites with the hopping strength t. The spin operator components in (4.27) and (4.28) can be expressed as[235]

$$\hat{S}^{(k)}_i = \frac{1}{2} \sum_{\mu,\nu=\uparrow,\downarrow} \hat{\sigma}^{(k)}_{\mu,\nu} a^\dagger_{i,\mu} a_{i,\nu} \tag{4.29}$$

in terms of the Pauli spin matrices $\hat{\sigma}^k$ and fermionic creation and annihilation operators. Especially the Heisenberg model, which contains only the vector of spin operators on site i, $\hat{\mathbf{S}}_i$, should be an interesting system to be studied with a spin-adapted approach. With

Eq. (4.29) the product $\hat{\mathbf{S}}_i \cdot \hat{\mathbf{S}}_j$ can be expressed as

$$\hat{\mathbf{S}}_i \cdot \hat{\mathbf{S}}_j = \underbrace{\frac{1}{4}(n_{i\uparrow} - n_{i\downarrow})(n_{j\uparrow} - n_{j\downarrow})}_{\hat{S}_i^z \cdot \hat{S}_j^z} - \underbrace{\frac{1}{2}\sum_\sigma a_{i\sigma}^\dagger a_{j\sigma} a_{j\bar{\sigma}}^\dagger a_{i\bar{\sigma}}}_{\hat{S}_i^x \cdot \hat{S}_j^x + \hat{S}_i^y \cdot \hat{S}_j^y}, \tag{4.30}$$

where the first term is diagonal in an $\hat{S}^z$ eigenbasis and the second term corresponds to second order spin-flip processes between nearest-neighbour sites i and j. With the observation

$$\hat{E}_{ij}\hat{E}_{ji} = \left(\sum_\sigma a_{i\sigma}^\dagger a_{j\sigma}\right) \cdot \left(\sum_\tau a_{j\tau}^\dagger a_{i\tau}\right) = \sum_\sigma a_{i\sigma}^\dagger a_{j\sigma} a_{j\bar{\sigma}}^\dagger a_{i\bar{\sigma}} + \sum_\sigma \underbrace{a_{i\sigma}^\dagger a_{j\sigma} a_{j\sigma}^\dagger a_{i\sigma}}_{=n_{i\sigma}(1-n_{j\sigma})} \tag{4.31}$$

Eq. (4.30) can be expressed as

$$\hat{\mathbf{S}}_i \cdot \hat{\mathbf{S}}_j = \hat{S}_i^z \cdot \hat{S}_j^z - \frac{1}{2}\hat{E}_{ij}\hat{E}_{ji} + \sum_\sigma n_{i\sigma}(1 - n_{j\sigma}) \tag{4.32}$$

in terms of unitary group generators and spin-dependent, but diagonal, operators $\hat{S}_i^z$ and $n_{i\sigma}$. With Eq. (4.32) the t-J and Heisenberg model can be expressed as

$$\hat{H}_{t-J} = \sum_{\langle i,j \rangle} \left[-t\hat{E}_{ij} + J\left(\hat{S}_i^z \cdot S_j^z - \frac{1}{2}\hat{E}_{ij}\hat{E}_{ji} + \sum_\sigma n_{i\sigma}(1 - n_{j\sigma}) - \frac{\hat{E}_{ii}\hat{E}_{jj}}{4} \right) \right] \tag{4.33}$$

$$\hat{H}_H = J \sum_{\langle i,j \rangle} \left(\hat{S}_i^z \cdot S_j^z - \frac{1}{2}\hat{E}_{ij}\hat{E}_{ji} + \sum_\sigma n_{i\sigma}(1 - n_{j\sigma}) \right) + h \sum_i \hat{S}_i^z. \tag{4.34}$$

Both the t-J and Heisenberg model have been implemented in our FCIQMC code `NECI`,[25] but application of the spin-adapted approach to them has to be further investigated.

5 Explicitly Correlated Ansatz in FCIQMC

To simulate larger and more complex systems, we need to find means to compress the relevant physical information stored in the wavefunction to allow a more efficient sampling of it with the FCIQMC method. Various approaches exist to achieve this reduction of degrees of freedom by explicitly taking into account some part of the correlation already in the initial Ansatz for the ground state wavefunction. Particularly for *ab-initio* systems the huge many-body wavefunction expansions are to some part an artefact of deficiencies of the underlying single-particle basis set in capturing the dynamic correlation of electrons in close proximity. As mentioned in Sec. 1.6, the exact wavefunction has a nondifferentiable behaviour, Kato's cusp condition (1.18),[156,229] at electron coalescence $r_{12} = 0$. The struggle of basis sets, i.e. based on Gaussian type orbitals,* describing this feature is one of the main reasons for the slow convergence of the correlation energy with the basis set expansion size. Additionally, most high-level post-Hartree-Fock methods, such as FCIQMC, have an unfavourable scaling with the basis set size, hence utilizing extrapolation techniques is difficult and reaching the complete basis set limit is prohibitively hard.

In Sec. 1.7.7 multiple quantum chemical approaches to ameliorate the unfavourable scaling with the basis set size, by including explicit dependence on the interelectronic coordinate r_{12} in the wavefunction Ansatz,[145,146,296] were presented. The goal of each of these approaches is to obtain a highly compact form for the short-ranged wavefunction by explicit inclusion of the interelectronic distance r_{12}, which naturally describes the dynamic correlation problem. Several of these approaches for *ab-initio* systems were implemented and studied with the FCIQMC method.[26,161,281]

However, in this chapter we take a different approach and leave quantum chemistry momentarily aside. We exclusively focus on an explicitly correlated wavefunction Ansatz for the two-dimensional, repulsive Hubbard lattice model, introduced in Sections 1.4 and 4.4.4.

*Albeit their immense benefits of efficient integral evaluation.

5.1 Nonunitary Similarity Transformations

Our goal is to perform an exact similarity transformation of the Hubbard model based on the Gutzwiller Ansatz,[38,122] where the correlation captured in the Ansatz introduces novel three-body interaction terms in the transformed Hamiltonian. Due to the nonunitarity of the transformation the resulting operator is not Hermitian any more, causing the left- and right eigenvector to differ, which, however, induces a very compact form of the right eigenvector, due to the suppression of energetically unfavourable double occupancies.

This compression of the essential physical features of the wavefunction is especially desirable for stochastic approaches, where a compact description of the system facilitates the sampling and thus allows the simulation of system sizes unreachable otherwise. Due to its projective nature, the FCIQMC method is able to sample the right eigenvector even of non-Hermitian problems and the stochastic approach enables an exact treatment of the novel 3-body interaction without undue increase in computational cost.

The Hubbard model, introduced in Sec. 1.4 and presented in both the real- and momentum-space formulation in Sec. 4.4.4 is revisited and discussed in more detail here.

The results in this chapter were obtained in collaboration with Hongjun Luo and Ali Alavi and parts of the remaining chapter are included in the published article:[69]
Compact numerical solutions to the two-dimensional repulsive Hubbard model obtained via nonunitary similarity transformations. Werner Dobrautz, Hongjun Luo and Ali Alavi, Phys. Rev. B **99**, 075119 (2019)

5.2 Introduction

The Fermionic two-dimensional Hubbard model[122,142,154] with repulsive interactions is a minimal model of itinerant strongly correlated electrons that is believed to exhibit extraordinarily rich physical behaviour. Especially in the past thirty years, it has been intensively studied as a model to understand the physics of high-temperature superconductivity observed in layered cuprates[371] . Its phase diagram as a function of temperature, interaction strength and filling includes antiferromagnetism, Mott metal-insulator transition, unconventional high T_C superconductivity[61] with d-wave pairing off half-filling, striped phases, a pseudo gap regime, charge and spin density waves.[272] Confronted with such a plethora of physical phenomena, accurate numerical results are indispensable in resolving various competing theoretical scenarios.
Unfortunately the numerical study of the 2D Hubbard model has proven extraordinarily challenging, particularly in the off-half-filling regime with intermediate-to-strong interaction strengths $U/t = 4 - 12$. Major difficulties include severe sign problems for

quantum Monte Carlo (QMC) methods, whilst the 2D nature of the problem causes convergence difficulties for density matrix renormalization group (DMRG)[273,356,357] based methodologies which have otherwise proven extremely powerful in 1D systems. Nevertheless, extensive numerical studies have been performed with a variety of methods, such as variational,[79,104,323,361,365] fixed-node,[15,60,334] constrained-path auxiliary field[53,54,373] and determinental[336] QMC, dynamical[134,134] and variational[62,256] cluster approximations (DCA/VCA), dynamical mean-field theory (DMFT)[170,185] and density matrix renormalization group (DMRG). Thermodynamic limit extrapolations have been carried out with the aim of assessing the accuracy of the methodologies in various regimes of interaction, filling factor and temperature.[178,259,377] On the other hand each of these methods incur systematic errors which are extremely difficult to quantify and there is an urgent need to develop methods in which convergence behaviour can be quantified internally.

In chapter we present the idea instead of attempting a direct numerical attack on the 2D Hubbard Hamiltonian with a given technique, we ask if there is an alternative *exact* reformulation of the problem, the solution of which is easier to approximate than that of the original problem. If this is the case (and this is obviously highly desirable), it should be demonstrable within the framework of a given technique, without reference to any other method. The physical basis for any observed simplification should be transparent. Such an approach turns out to be possible, at least for intermediate interactions strengths based, on a Gutzwiller nonunitary similarity transformation of the Hubbard Hamiltonian.

The Gutzwiller Ansatz[38,122] and Gutzwiller approximation[123,221,340,370] are intensively studied methods to solve the Hubbard model. The parameter of the Ansatz is usually optimised to minimize the energy expectation value by variational Monte Carlo schemes[118,140] based on a single Fermi-sea reference state. It has been long realized that the simple Gutzwiller Ansatz misses important correlations,[97,155,210] especially in the strong interaction regime of the Hubbard model. More general, Jastrow-like,[148] correlators, including density-density[44] and holon-doublon,[192,344] have been proposed to capture more physical features within the Ansatz. In addition, the Fermi-sea reference function have been extended to HF spin-density waves[181] and BCS[8] wavefunctions[6,78,116,117,239,365,366] including antiferromagnetic[104,179] and charge order.[141]
An alternative strategy is to use a Gutzwiller correlator to perform a non-unitary similarity transformation of the Hubbard Hamiltonian, whose solution can be well approximated using a Slater determinant. Such an approach is reminiscent of the quantum chemical *transcorrelated* method of Boys and Handy,[34,35] as well as Hirschfelder,[138] in which a non-Hermitian Hamiltonian is derived on the basis of a Jastrow factorisation of the wavefunction.
This idea was applied by Tsuneyuki[330] to the Hubbard model by minimizing the variance of the energy based on projection on the HF determinant. Scuseria and coworkers[342] and Chan *et al.*[219] have recently generalized to general two-body correlators and more sophisticated reference states, where the correlator optimisation was not performed in a

stochastic VMC manner, but in the spirit of coupled-cluster theory, by projecting the transformed Hamiltonian in the important subspace spanned by the correlators.
These methods have in common that they are based on a single reference optimisation of the correlation parameters and thus the energy obtained is on a mean-field level. We instead would like to fully solve the similarity transformed Hamiltonian in a complete momentum space basis. We will use a single reference optimisation, based on projection,[219,342] to generate a similarity-transformed Hamiltonian (non-Hermitian with 3-body interactions), whose ground state solution (right eigenvector) will be using the projective FCIQMC[56] method.

The remainder of this chapter is organized as follows:
In 5.3 the derivation of the Gutzwiller similarity transformed Hubbard Hamiltonian is recapped and the projective solution based on the restricted Hartree-Fock determinant is presented. Additionally, analytic and exact diagonalization results, to illustrate the influence of the transformation on the energies and eigenvectors are provided. In 5.4 the necessary adaptations of the FCIQMC method for its application to the similarity transformed Hubbard Hamiltonian in a momentum-space basis, named similarity transformed FCIQMC(ST-FCIQMC) are discussed. In addition, the implications of the approach to excited states calculation is expanded on. In 5.5 the ST-FCIQMC method is benchmarked for the exact diagonalizable 18-site Hubbard model and ground- and excited-state energies are presented. A huge increase in compactness of the right eigenvector of the non-Hermitian transformed Hamiltonian is observed. Finally, results obtained with the similarity transformed Hamiltonian for nontrivial 36- and 50-site lattices, at and off half-filling with interaction strengths up to $U/t = 4$ are shown. In 5.6 a conclusion of our findings is given and future applications for observables other than the energy and correct calculation of left and right excited state eigenvectors are discussed. Additionally, the application of the method to other lattice models, especially the t-J and Heisenberg model is discussed.

5.3 The Similarity Transformed Hamiltonian

We would like to solve for the ground state energy of the two-dimensional, single-band Hubbard model[122,142,154] with the Hamiltonian in a real-space basis

$$\hat{H} = -t \sum_{\langle ij \rangle, \sigma} a^{\dagger}_{i,\sigma} a_{j,\sigma} + U \sum_{l} n_{l,\uparrow} n_{l,\downarrow}. \tag{5.1}$$

$a^{(\dagger)}_{i,\sigma}$ being the fermionic annihilation(creation) operator for site i and spin σ, $n_{l,\sigma}$ the number operator, t the nearest neighbour hopping amplitude and $U \geq 0$ the on-site Coulomb repulsion. We employ a Gutzwiller-type Ansatz[42,122,221] for the ground state

wavefunction

$$|\Psi\rangle = g^{\hat{D}}\,|\Phi\rangle = \mathrm{e}^{\hat{\tau}}\,|\Phi\rangle\,, \quad \text{with} \tag{5.2}$$

$$\hat{\tau} = \ln g\hat{D} = J\sum_{l} n_{l,\uparrow}n_{l,\downarrow} \quad \text{and} \quad 0 \leq g \leq 1, \tag{5.3}$$

where $\hat{D}$ is the sum of all double occupancies in $|\Phi\rangle$, which are repressed with $0 \leq g \leq 1 \rightarrow -\infty < J \leq 0$.
In the Gutzwiller Ansatz, $|\Phi\rangle$ is usually chosen to be a single-particle product wavefunction,[98,122] $|\Phi_0\rangle$, such as the Fermi-sea solution of the non-interacting $U = 0$ system, or other similar forms such as unrestricted Hartree-Fock spin-density waves,[181] or superconducting BCS wavefunctions.[78] The parameter J is usually optimised via Variational Monte Carlo(VMC),[370] minimizing the expectation value

$$E_{VMC} = \min_{J} \frac{\langle\Phi_0|\mathrm{e}^{\hat{\tau}}\,\hat{H}\,\mathrm{e}^{\hat{\tau}}|\Phi_0\rangle}{\langle\Phi_0|\mathrm{e}^{2\hat{\tau}}|\Phi_0\rangle}, \tag{5.4}$$

see Sec. 2.2.1. In this work, however, $|\Phi\rangle$ is taken to be a full CI expansion in terms of Slater determinants

$$|\Phi\rangle = \sum_{i} c_i\,|D_i\rangle \tag{5.5}$$

with which we aim to solve an equivalent exact eigenvalue equation

$$\mathrm{e}^{-\hat{\tau}}\,\hat{H}\,\mathrm{e}^{\hat{\tau}}\,|\Phi\rangle = \bar{H}\,|\Phi\rangle = E\,|\Phi\rangle\,, \quad \text{with} \tag{5.6}$$

$$\bar{H} = -t\sum_{<ij>,\sigma} \mathrm{e}^{-\hat{\tau}}\,a^{\dagger}_{i,\sigma}a_{j,\sigma}\,\mathrm{e}^{\hat{\tau}} + U\sum_{l} n_{l,\uparrow}n_{l,\downarrow}, \tag{5.7}$$

$\bar{H}$ denotes a similarity-transformed Hamiltonian. Eq.(5.6) is obtained by substituting Eq. (5.2) as an eigenfunction Ansatz into Eq. (5.1) and multiplying with $e^{-\hat{\tau}}$ from the left, and due to $[n_{i,\sigma}, \hat{\tau}] = 0$. The similarity transformation of Eq. (5.1) moves the complexity of the correlated Ansatz for the wavefunction $|\Psi\rangle$ into the Hamiltonian, without changing its spectrum. It is a nonunitary transformation, and the resulting Hamiltonian is not Hermitian. Such similarity transformations have been introduced in quantum chemistry[35,36,138] in the context of a *Slater*-Jastrow Ansatz, where it is known as the *transcorrelated*-method of Boys and Handy. It was first applied to the Hubbard model by Tsuneyuki.[330] The transcorrelated method has been quite widely applied in combination with explicitly correlated methods in quantum chemistry,[196,197,281,364] with approximations being employed to terminate the commutator series arising from the evaluation of $\mathrm{e}^{-\hat{\tau}}\,\hat{H}\,\mathrm{e}^{\hat{\tau}}$.[318,319] The explicit similarity transformation of the Hubbard Hamiltonian(5.1) with a Gutzwiller(5.2)[330,343] or more general correlator,[219,342] which can be obtained without approximations due to a terminating commutator series, has been solved on a mean-field level.[330] In the present work, we will not restrict ourselves to a mean-field solution, but solve for the exact ground state of $\bar{H}$ with the FCIQMC method.[30,56]

5.3.1 Recap of the Derivation of $\bar{H}$

Tsuneyuki[330] and Scuseria *et al.*[342] have provided a derivation of the similarity transformed Hubbard Hamiltonian, based on the Gutzwiller and more general two-body correlators, respectively. Their derivations result in a Hamiltonian expressed in real-space. Here we go one step further and obtain an exact *momentum space* representation of the similarity transformed Hamiltonian, which is advantageous in the numerical study of the intermediate correlation regime. In this representation, the total momentum is an exact quantum number, resulting in a block diagonalised Hamiltonian. This is computationally useful in projective schemes, especially where there are near-degeneracies in the exact spectrum close to the ground state, which can lead to very long projection times and be problematic to resolve. Additionally, it turns out that even in the intermediate strength regime, the ground state right eigenvector is dominated by a single Fermi determinant for the half-filled system. This is in stark contrast with the ground state eigenvector of the original Hubbard Hamiltonian, which is highly multiconfigurational in this regime.

As seen in Eq. (5.7) we need to compute the following transformation

$$\hat{F}(x) = \mathrm{e}^{-x\hat{\tau}}\, a^\dagger_{i,\sigma} a_{j,\sigma}\, \mathrm{e}^{x\hat{\tau}} \tag{5.8}$$

which can be done by introducing a formal variable x and performing a Taylor expansion (cf. the Baker-Campbell-Hausdorff expansion). The derivatives of (5.8) can be calculated as

$$\begin{aligned}
\hat{F}'(0) &= [\, a^\dagger_{i,\sigma} a_{j,\sigma}, \hat{\tau}\,] = J \sum_l [\, a^\dagger_{i,\sigma} a_{j,\sigma}, a^\dagger_{l,\sigma} a_{l,\sigma}\,]\, n_{l,\bar{\sigma}} = J a^\dagger_{i,\sigma} a_{j,\sigma}\, (n_{j,\bar{\sigma}} - n_{i,\bar{\sigma}})\,, \\
\hat{F}''(0) &= [\,[\, a^\dagger_{i,\sigma} a_{j,\sigma}, \hat{\tau}\,], \hat{\tau}\,] = J\,[\, a^\dagger_{i,\sigma} a_{j,\sigma} (n_{j,\bar{\sigma}} - n_{i,\bar{\sigma}}), \hat{\tau}\,] = J^2 a_{i,\sigma} a_{j,\sigma}\, (n_{j,\bar{\sigma}} - n_{i,\bar{\sigma}})^2\,, \\
\hat{F}^{(n)}(0) &= [\,[\, a^\dagger_{i,\sigma} a_{j,\sigma}, \hat{\tau}\,], \ldots, \hat{\tau}\,] = J^n a_{i,\sigma} a_{j,\sigma}\, (n_{j,\bar{\sigma}} - n_{i,\bar{\sigma}})^n\,,
\end{aligned} \tag{5.9}$$

where $\bar{\sigma}$ indicates the opposite spin of σ. With this closed form (5.9) the Taylor expansion can be summed up as $\hat{F}(1) = a^\dagger_{i,\sigma} a_{j,\sigma}\, \mathrm{e}^{J(n_{j,\bar{\sigma}} - n_{i,\bar{\sigma}})}$ and Eq. (5.6) takes the final form of[330,342,343]

$$\bar{H} = -t \sum_{<ij>,\sigma} a^\dagger_{i,\sigma} a_{j,\sigma}\, \mathrm{e}^{J(n_{j,\bar{\sigma}} - n_{i,\bar{\sigma}})} + U \sum_l n_{l,\uparrow} n_{l,\downarrow} \tag{5.10}$$

Due to the idempotency of the (Fermionic) number operators, $n^2_{i,\sigma} = n_{i,\sigma}$, we have for $m \geq 1$:

$$(n_{j,\sigma} - n_{i,\sigma})^{2m-1} = n_{j,\sigma} - n_{i,\sigma}, \quad \text{and} \quad (n_{j,\sigma} - n_{i,\sigma})^{2m} = n_{j,\sigma} + n_{i,\sigma} - 2n_{i,\sigma} n_{j,\sigma}. \tag{5.11}$$

With Eq. (5.11) the exponential factor in Eq. (5.10) can be calculated as

$$\begin{aligned}\mathrm{e}^{J(n_{i,\sigma}-n_{j,\sigma})} =& 1+\sum_{m=1}^{\infty}\frac{J^{2m-1}}{(2m-1)!}\left(n_{j,\sigma}-n_{i,\sigma}\right)+\sum_{m=1}^{\infty}\frac{J^{2m}}{(2m)!}\left(n_{j,\sigma}+n_{i,\sigma}-2n_{i,\sigma}n_{j,\sigma}\right)\\ =& 1+\sinh(J)\left(n_{j,\sigma}-n_{i,\sigma}\right)+\left(\cosh(J)-1\right)\left(n_{j,\sigma}+n_{i,\sigma}-2n_{i,\sigma}n_{j,\sigma}\right)\\ =& 1+\left(\mathrm{e}^{J}-1\right)n_{j,\sigma}+\left(\mathrm{e}^{-J}-1\right)n_{i,\sigma}-2\left(\cosh(J)-1\right)n_{i,\sigma}n_{j,\sigma}. \end{aligned} \tag{5.12}$$

With Eq. (5.12) we can write the final similarity transformed Hamiltonian as

$$\bar{H}=\hat{H}-t\sum_{<ij>,\sigma}a_{i,\sigma}^{\dagger}a_{j,\sigma}\Big[\left(\mathrm{e}^{J}-1\right)n_{j,\bar{\sigma}}+\left(\mathrm{e}^{-J}-1\right)n_{i,\bar{\sigma}}-2\left(\cosh(J)-1\right)n_{i,\bar{\sigma}}n_{j,\bar{\sigma}}\Big]. \tag{5.13}$$

Formulated in a real-space basis the additional factor in Eq. (5.13) is simply a nearest-neighbour density dependent renormalization of the hopping amplitude. For large interaction $U/t \gg 1$, as already pointed out by Fulde *et al.*,[155] the simple Ansatz (5.2) shows the incorrect asymptotic energy behaviour, $E \sim -t^2/(U \ln U)$ instead of $E \sim -t^2/U$,[97,210] proportional to the magnetic coupling of the Heisenberg model for $U/t \gg 1$, due to the missing correlation between nearest-neighbour doubly occupied and empty sites. The Gutzwiller Ansatz does however provide a good energy estimate in the low to intermediate U/t regime. For these values of U/t the momentum space formulation is a better suited choice of basis, due to a dominant Fermi-sea determinant and thus a single reference character of the ground state wavefunction. Thus, we transform Eq. (5.13) into a momentum space representation with

$$a_{\mathbf{l},\sigma}^{\dagger}=\frac{1}{\sqrt{M}}\sum_{\mathbf{k}}\mathrm{e}^{-i\mathbf{k}\cdot\mathbf{l}}\,c_{\mathbf{k},\sigma}^{\dagger}, \tag{5.14}$$

where M is the size of the system and $c_{\mathbf{k},\sigma}^{(\dagger)}$ the annihilation (creation) operator of a state with momentum $\mathbf{k}$ and spin σ. The terms of Eq. (5.13) become

$$\sum_{<ij>,\sigma}a_{i,\sigma}^{\dagger}a_{j,\sigma}n_{j,\bar{\sigma}} = \frac{1}{M}\sum_{\mathbf{pqk},\sigma}\epsilon_{\mathbf{p}-\mathbf{k}}\,c_{\mathbf{p}-\mathbf{k},\sigma}^{\dagger}c_{\mathbf{q}+\mathbf{k},\bar{\sigma}}^{\dagger}c_{\mathbf{q},\bar{\sigma}}c_{\mathbf{p},\sigma}, \tag{5.15}$$

$$\sum_{<ij>,\sigma}a_{i,\sigma}^{\dagger}a_{j,\sigma}n_{i,\bar{\sigma}} = \frac{1}{M}\sum_{\mathbf{pqk},\sigma}\epsilon_{\mathbf{p}}\,c_{\mathbf{p}-\mathbf{k},\sigma}^{\dagger}c_{\mathbf{q}+\mathbf{k},\bar{\sigma}}^{\dagger}c_{\mathbf{q},\bar{\sigma}}c_{\mathbf{p},\sigma} \tag{5.16}$$

$$\sum_{<ij>,\sigma}a_{i,\sigma}^{\dagger}a_{j,\sigma}n_{i,\bar{\sigma}}n_{j,\bar{\sigma}} = \frac{1}{M^2}\sum_{\mathbf{pqskk'},\sigma}\epsilon_{\mathbf{p}-\mathbf{k}+\mathbf{k'}}\,c_{\mathbf{p}-\mathbf{k},\sigma}^{\dagger}c_{\mathbf{q}+\mathbf{k'},\bar{\sigma}}^{\dagger}c_{\mathbf{s}+\mathbf{k}-\mathbf{k'},\bar{\sigma}}^{\dagger}c_{\mathbf{s},\bar{\sigma}}c_{\mathbf{q},\bar{\sigma}}c_{\mathbf{p},\sigma}, \tag{5.17}$$

with $\epsilon_{\mathbf{k}}$ being the dispersion relation of the lattice. The original Hubbard Hamiltonian in k-space is

$$\hat{H}=-t\sum_{\mathbf{k},\sigma}\epsilon_{\mathbf{k}}n_{\mathbf{k},\sigma}+\frac{U}{2M}\sum_{\mathbf{pqk},\sigma}c_{\mathbf{p}-\mathbf{k},\sigma}^{\dagger}c_{\mathbf{q}+\mathbf{k},\bar{\sigma}}^{\dagger}c_{\mathbf{q},\bar{\sigma}}c_{\mathbf{p},\sigma}. \tag{5.18}$$

while the similarity transformed Hamiltonian in k-space is a function of the correlation

parameter J

$$\begin{aligned}\bar{H}(J) = &- t\sum_{\mathbf{k},\sigma}\epsilon_{\mathbf{k}}n_{\mathbf{k},\sigma} + \frac{1}{M}\sum_{\mathbf{pqk},\sigma}\omega(J,\mathbf{p},\mathbf{k})c^{\dagger}_{\mathbf{p}-\mathbf{k},\sigma}c^{\dagger}_{\mathbf{q}+\mathbf{k},\bar{\sigma}}c_{\mathbf{q},\bar{\sigma}}c_{\mathbf{p},\sigma} \\ &+ 2t\frac{\cosh(J)-1}{M^2}\sum_{\mathbf{pqskk'},\sigma}\epsilon_{\mathbf{p}-\mathbf{k}+\mathbf{k'}}c^{\dagger}_{\mathbf{p}-\mathbf{k},\sigma}c^{\dagger}_{\mathbf{q}+\mathbf{k'},\bar{\sigma}}c^{\dagger}_{\mathbf{s}+\mathbf{k}-\mathbf{k'},\bar{\sigma}}c_{\mathbf{s},\bar{\sigma}}c_{\mathbf{q},\bar{\sigma}}c_{\mathbf{p},\sigma}, \qquad (5.19)\end{aligned}$$

$$\omega(J,\mathbf{p},\mathbf{k}) = \frac{U}{2} - t\left[\left(\mathrm{e}^{J}-1\right)\epsilon_{\mathbf{p}-\mathbf{k}} + \left(\mathrm{e}^{-J}-1\right)\epsilon_{\mathbf{p}}\right]. \qquad (5.20)$$

Comparing to the original Hubbard Hamiltonian in k-space (5.18), $\bar{H}$ (5.19) has a modified 2-body term and contains an additional 3-body interaction, which for $\mathbf{k} = 0$ gives rise to parallel-spin double excitations. These are not present in the original Hamiltonian. As mentioned above, in contrast to other explicitly correlated approaches[224] this is an *exact* similarity transformation of the original Hamiltonian and does not depend on any approximations. Hence, the spectrum of this Hamiltonian is the same as that of (5.1). Unlike the canonical transcorrelation Ansatz of Yanai and Shiozaki[364] which employ a unitary similarity transformation, the resulting Hamiltonian (5.19) is not Hermitian (the non-Hermiticity arising in the two-body terms), and hence its spectrum is not bounded from below. Variational minimization approaches are not applicable. The left and right eigenvectors differ, and form a biorthogonal basis $\left\langle \Psi_i^L \middle| \Psi_j^R \right\rangle = 0$ for $i \neq j$. Tsuneyuki circumvented the lack of a lower bound by minimizing the variance of $\bar{H}$

$$\min\langle\Phi_{HF}|\left(\bar{H} - \left\langle\bar{H}\right\rangle\right)^2|\Phi_{HF}\rangle \qquad (5.21)$$

to determine the optimal J_{var}.

Projective methods such as the Power method,[110] or a stochastic variant such as FCIQMC,[30] can converge the right/left eigenvectors by multiple application of a suitable propagator, without recourse to a variational optimisation procedure, and this is the technique we shall use here. Since the matrix elements of (5.19) can be calculated analytically and on-the-fly, the additional cost of the 3-body term is no hindrance in our calculations, and we do not need to apply additional approximations, unlike other explicitly correlated approaches.[362,363] While complicating the calculation of observables other than the energy, due to the need to have both the left and right eigenvector of the now non-Hermitian Hamiltonian (5.19), the difference between the left and right eigenvectors actually proves to be beneficial for the sampling of the ground state wavefunction in the FCIQMC method. This will be numerically demonstrated below in 5.3.3. As a side note, the use of more elaborate correlators, like density-density[44] or holon-doublon[85,192,344] is no hindrance in the real-space formulation of the Hubbard model and is currently being investigated,[70] but in the momentum-space basis would lead to even higher order interactions and have not been further explored.

5.3.2 Optimisation of J and Analytic Results for the Hubbard Model

As a starting point we optimise the strength of the correlation factor, controlled by the single parameter J from the Ansatz (5.2) by projection. Projecting the Ansatz (5.2) on the Hartree-Fock state $\langle\Phi_{HF}|$ would yield us the energy E_J^{HF}

$$\langle\Phi_{HF}|\underbrace{\mathrm{e}^{-\hat{\tau}}\,\hat{H}\,\mathrm{e}^{\hat{\tau}}}_{\bar{H}}|\Phi_{HF}\rangle = E_J, \tag{5.22}$$

where as usual HF denotes the state with all orbitals with $|\mathbf{k}| \leq k_F$ being doubly occupied and k_F being the Fermi surface. And projecting onto the single basis of the correlation factor[219,342,343] $\langle\Phi_{HF}|\,\hat{\tau}^\dagger$ yields

$$\langle\Phi_{HF}|\,\hat{\tau}^\dagger\bar{H}\,|\Phi_{HF}\rangle = E_J^{HF}\langle\Phi_{HF}|\hat{\tau}^\dagger|\Phi_{HF}\rangle, \tag{5.23}$$

where $\left\langle\hat{\tau}^\dagger\right\rangle_{HF} \neq 0$ only for $\mathbf{k} = 0$ terms in the momentum space representation of $\hat{\tau}$

$$\hat{\tau} = \frac{J}{M}\sum_{\mathbf{p},\mathbf{q},\mathbf{k},\sigma} c^\dagger_{\mathbf{p}-\mathbf{k},\sigma}c^\dagger_{\mathbf{q}+\mathbf{k},\bar{\sigma}}c_{\mathbf{q},\bar{\sigma}}c_{\mathbf{p},\sigma}. \tag{5.24}$$

Combining Eq. (5.22) and (5.23) yields

$$\left\langle(\hat{\tau} - \langle\hat{\tau}\rangle)^\dagger\,\bar{H}\right\rangle_{HF} = 0, \tag{5.25}$$

where the diagonal, $\mathbf{k} = 0$, terms cancel*. Eq. (5.25) needs to be solved to optimise J based on a single determinant $|\Phi_{HF}\rangle$. Eq.(5.25) is similar to the optimisation of coupled cluster amplitudes.[317] Eq. (5.25) can also be seen as a projection of the eigenvalue equation $(\bar{H} - E)\,|\Phi_{HF}\rangle = 0$ on the single basis of the correlation factor $\hat{\tau}$. The remaining contributing contractions ($\mathbf{k} \neq 0$) of (5.25) of $\bar{H}$ are

$$\begin{aligned}\left\langle\hat{\tau}^\dagger\bar{H}\right\rangle_c = \frac{1}{M^2}\sum_{\mathbf{pqk},\sigma} n_{\mathbf{p},\sigma}n_{\mathbf{q},\bar{\sigma}}(1-n_{\mathbf{p}-\mathbf{k},\sigma})(1-n_{\mathbf{q}+\mathbf{k},\bar{\sigma}})\\ \times\left\{\underbrace{\omega_2(J,\mathbf{p},\mathbf{k})}_{\text{2-body}} + 2t\frac{\cosh J - 1}{M}\times\left[\underbrace{N_{\bar{\sigma}}\left(\epsilon_{\mathbf{p}}+\epsilon_{\mathbf{p}-\mathbf{k}}\right)}_{\text{3-body RPA}} - \underbrace{\sum_{\mathbf{s}}\left(\epsilon_{\mathbf{p}+\mathbf{q}-\mathbf{s}}+\epsilon_{\mathbf{p}-\mathbf{q}-\mathbf{k}+\mathbf{s}}\right)n_{\mathbf{s},\bar{\sigma}}}_{\text{3-body exchange}}\right]\right\}.\end{aligned} \tag{5.26}$$

Equation (5.26) can be evaluated directly, or since $\hat{\tau}\,|\Phi_{HF}\rangle = c_{HF}\,|\Phi_{HF}\rangle + \sum_i c_i\,|D_i\rangle$ corresponds to all the double excitation on top of the Hartree-Fock determinant, it is the sum of all the double excitation matrix elements with the Hartree-Fock determinant.

*In the language of the coupled cluster approach an equivalent expression to Eq. (5.25) is $\langle\hat{\tau}^\dagger H\rangle_c = 0$, where $\langle\ldots\rangle_c$ denotes a cumulant expression over linked diagrams[94] only.

Table 5.1: J_{opt} obtained by solving Eq. (5.25) for the specific lattice sizes, fillings and U/t values used in this manuscript. J_{ex} is the value, which sets set the J-dependent Hartree-Fock energy, E_J^{HF}, to the exact energy, if available, or to the AFQMC reference energies[178,259,293,342] for larger systems.[69]

M	U/t	n_{el}	J_{opt}	J_{ex}	e_{ex}	e_J	$e_J/e_{ex}[\%]$
6	4	6	-0.67769	-0.74282	-0.61145	-0.56306	92.1
18	2	18	-0.27053	-0.28536	-1.32141	-1.31697	99.7
18	4	18	-0.52345	-0.57472	-0.95847	-0.92697	96.7
18	4	14	-0.55794	-0.62474	-1.13644	-1.09786	96.7
36	2	36	-0.30485	-0.45423	-1.15158	-1.09840	95.4
36*	2	36	-0.28683	-0.31783	-1.20831	-1.19904	99.3
36	4	36	-0.58521	-0.79141	-0.85736	-0.71675	83.6
36*	4	36	-0.55295	-0.65181	-0.87306	-0.81145	92.9
36*	4	24	-0.53570			-1.13399	-
36†	4	24	-0.52372	-0.57014	-1.18530	-1.16457	98.3
50	1	50	-0.14290	-0.15357	-1.43718	-1.43561	99.9
50	2	50	-0.28298	-0.30852	-1.22278	-1.21523	99.4
50	3	50	-0.41788	-0.46639	-1.03460	-1.01278	97.9
50	4	50	-0.54600	-0.63177	-0.87966	-0.82601	93.9
50	4	48	-0.54945	-0.62810	-0.93720	-0.88954	94.9
50	4	46	-0.55208	-0.62227	-0.99114	-0.95008	95.9
50	4	44	-0.54772	-0.61530	-1.03788	-1.00016	96.4
50	4	42	-0.54324	-0.60263	-1.08002	-1.04765	97.0
50	4	26	-0.51076	-0.56162	-1.11564	-1.09946	98.6

The diagonal contribution again cancels with the $\langle\hat{\tau}\rangle$ term in (5.25). The specific optimal J values for the lattice sizes, fillings and U/t values used in this study are listed in Table 5.1.

For an infinite system at half-filling, and only considering the two-body contribution Eq. (5.25) can be solved analytically, see Appendix B.1. The optimal J which fulfils Eq. (5.25), and the corresponding total energy per site, as (see B.1) can be expressed as

$$J_{opt}^{TDL} = \sinh^{-1}\left(-\frac{5U\pi^6}{288t\,(16+\pi^4)}\right), \tag{5.27}$$

$$E_J^{TDL} = -t\frac{64}{4\pi^2} + \frac{U}{4} - tJ_{opt}^{TDL2}\left(\frac{16}{4\pi^2} + \frac{64}{\pi^6}\right). \tag{5.28}$$

The results of Eq. (5.25) and (5.27-5.28) compared with AFQMC results[259] on a 16×16 half-filled square lattice are shown in Table 5.2, for various values of U/t. The superscript (TDL) denotes thermodynamic limit results from Eq. (5.27-5.28) for both the energy and J parameter, and an absent superscript refers to the solution of Eq. (5.25) for the actual finite lattices. At half-filling AFQMC does not suffer from a sign problem[137] and is numerically exact. One can see that the results obtained from Eq. (5.25) and (5.27-5.28) capture most of the correlation energy for low values of U/t. For larger U/t, due to the

Table 5.2: Ground state energy per site for the half-filled 16×16 square lattice with periodic (PBC) and mixed (anti-)periodic (ABPC) boundary conditions along the (y-)x-axis.[69] Thermodynamic limit extrapolations (TDL) for various values of U/t obtained with AFQMC[259] are denoted as $E_{Ref}^{(TDL)}$. Results obtained by evaluating Eq. (5.25) and Eq. (5.27-5.28) are noted as $E_J^{(TDL)}$. The optimal value of J is also shown. All energies are in units of t.

	$U/t=2$		$U/t=4$		$U/t=6$		$U/t=8$	
	PBC	APBC	PBC	APBC	PBC	APBC	PBC	APBC
E_{ref}	-1.174203(23)	-1.177977(20)	-0.86051(16)	-0.86055(16)	-0.65699(12)	-0.65707(20)	-0.52434(12)	-0.52441(12)
E_J	-1.151280	-1.166370	-0.76354	-0.77769	-0.42855	-0.44160	-0.12848	-0.14051
$E_J/E_{ref}\%$	98.0	99.0	88.7	90.4	65.3	67.2	24.5	26.8
J_{opt}	-0.29233	-0.28957	-0.56284	-0.55787	-0.80107	-0.79460	-1.00701	-0.99956
E_{ref}^{TDL}	-1.1760(2)		-0.8603(2)		-0.6567(3)		-0.5243(2)	
E_J^{TDL}	-1.1609		-0.7686		-0.4203		-0.0943	
$E_J^{TDL}/E_{ref}\%$	98.7		89.4		64.0		18.0	
J_{opt}^{TDL}	-0.29025		-0.55911		-0.79621		-1.00142	

missing correlation between empty and doubly occupied sites in the Ansatz (5.2), the energies progressively deteriorate compared to the reference results. The optimal value J_{opt} is also displayed in Table 5.2. We use the values of J obtained by solving Eq. (5.25) as a starting point for our FCIQMC calculations to capture the remaining missing correlation energy.

To compare this most basic combination of an on-site Gutzwiller correlator and a single restricted Hartree-Fock determinant as a reference in Eq. (5.25) we show in Table 5.3 the percentage of the energy obtained with this method to more elaborate correlators and reference states, for different system sizes M, number of electrons n_{el} and interaction strengths U/t. $E_{(S)UGST}$ in 5.3 denotes an on-site Gutzwiller correlator with a (symmetry-projected) unrestricted Hartree-Fock reference state.[343] At half filling and $U/t \leq 4$ we can capture more than 80% of the energy obtained with a more elaborate reference determinant. Off half-filling the recovered energy is above 90% up to $U/t = 4$. For a more dilute filling of $\langle n \rangle = 0.8$, for $M = 100$ and $U/t = 2$, the energies agree to better than 99%. Although the absolute error in energy increases off half-filling, as already mentioned in Ref. [342,343] the relative error actually decreases,[118,119,365] as can be seen in the comparison with the AFQMC reference results,[178,259,293,342] E_{ref} in Table 5.3. As expected, for $U/t > 4$ the results from Eq. (5.25) drastically deteriorate compared to $E_{(S)UGST}$.
$E_{R/UJ}$ in Table 5.3 refer to energies obtained with restricted/unrestricted Hartree-Fock reference states with a general two-body correlator,[342] which includes all possible density-density correlations in addition to the on-site Gutzwiller factor. The comparison with E_{RJ} shows that, as already found in Ref. [342], the Gutzwiller factor is by far the most important term in a general two-body correlator for low to intermediate values of $U/t \leq 4$, with an agreement of over 98% with E_{RJ}. Off half-filling, as can be seen in the $N = 36, n_{el} = 24$ and $U/t = 8$ case, the relative error remains small even for large interaction. The comparison with the available AFQMC reference results,[178,259,293,342] E_{ref}, shows that the solution of Eq. (5.25) with a on-site Gutzwiller correlator and a restricted Hartree-Fock

Table 5.3: Fraction of the total energy obtained with the Gutzwiller Ansatz(5.2) based on the Hartree-Fock determinant(5.25) compared with a Gutzwiller correlator with an unrestricted Hartree-Fock reference E_{UGST} and subsequent symmetry projection E_{SUGST}[343] and a general two-body correlator with a Hartree-Fock reference E_{RJ} and unrestricted Hartree-Fock reference E_{UJ}[342] and numerically exact AFQMC reference results[178,259,293,342] for different number of sites M, number of electrons n_{el} and interaction strengths U/t.[69]

M	n_{el}	U/t	$\%E_{UGST}$	$\%E_{SUGST}$	$\%E_{RJ}$	$\%E_{UJ}$	$\%E_{ref}$
16	14	2	97.34	97.03	99.69	97.30	96.79
16	14	4	92.81	91.70	99.02	93.07	90.75
16	14	8	72.68	70.16	92.28	73.84	66.60
16	16	2	80.85	80.75	99.82	93.77	93.16
16	16	4	81.84	80.18	98.57	82.61	80.24
16	16	8	21.37	20.19	47.54	21.81	20.08
36	24	4			99.67		98.26
36	24	8			98.72		93.53
64	28	4			99.74		99.19
64	44	4			99.77		98.38
100	80	2	100.00	99.98			99.84
100	80	4	99.85	99.61			97.43
100	100	2	97.69	97.56			97.27
100	100	4	88.50	88.08			87.39
100	100	6	65.70	65.19			64.04
100	100	8	25.01	24.76			23.89

reference, retrieves above 80% of the energy for $U/t \leq 4$. This gives us confidence that the optimal J obtained by this method is appropriate in the context of the Gutzwiller similarity transformed Hamiltonian, which we further solve with the FCIQMC method.

5.3.3 Exact Diagonalization Study

Due to the non Hermitian nature of $\bar{H}$ (5.19) the left and right ground state eigenvectors $|\Phi_0^{L/R}\rangle$ differ and depending on the strength of the correlation parameter J they can have a very different form. The most important characteristic for the projective FCIQMC method is the *compactness* of the sampled wavefunction. As a measure of this compactness we chose the L^2 norm of the exact $|\Phi_0^{L/R}\rangle$ contained in the leading HF-determinant $|\Phi_{HF}\rangle$ and double excitations $|\Phi_{ij}^{ab}\rangle = c_a^\dagger c_b^\dagger c_i c_j |\Phi_{HF}\rangle$(spin-index omitted) thereof, i.e. the sum over the squares of the coefficients of these determinants: $L^2_{(0,2)} = c_0^2 + \sum_{i<j,a<b} c_{ijab}^2$.

As a simple example, in the top panel of Figure 5.1 we show $L^2_{(0,2)}$ for the 1D half-filled 6-site Hubbard model with periodic boundary conditions at $U/t = 4$ and $\mathbf{k} = 0$, as a function of the correlation parameter J. $J = 0$ corresponds to the original Hamiltonian (5.18). In the bottom panel of Fig. 5.1 the Hartree-Fock energy E_{HF} and results of minimizing the variance of the energy E_{var} by Tsuneyuki,[330] $E_{HF}(J_{opt})$ with J_{opt} obtained

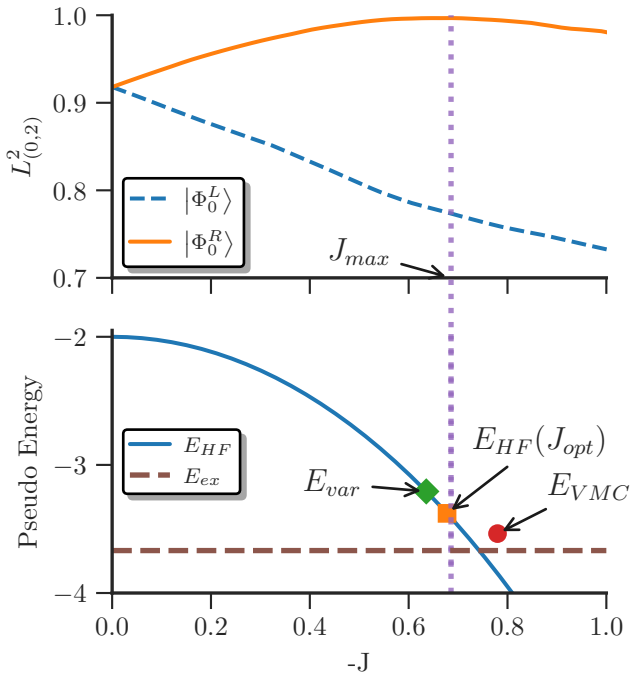

Fig. 5.1: Top: L^2 norm within the HF determinant and double excitations, $L^2_{(0,2)}$, for a half-filled 6-site Hubbard chain with periodic boundary conditions at $U/t = 4$ and $\mathbf{k} = 0$ for the left $|\Phi_0^L\rangle$ and right $|\Phi_0^R\rangle$ ground state eigenvector of $\bar{H}$ as a function of $-J$.[69] Bottom: The Hartree-Fock energy $E_{HF}(J) = \langle\Phi_{HF}|\bar{H}(J)|\Phi_{HF}\rangle$ as a function of $-J$. The dotted line indicates the exact ground state energy E_{ex} for this system, and since $\bar{H}$ is not Hermitian E_{HF} can drop below the exact energy. Also indicated are the results of minimizing the variance of the energy of the similarity transformed Hamiltonian E_{var} by Tsuneyuki,[330] the result of solving Eq. (5.25) $E_{HF}(J_{opt})$ and the result from a VMC optimisation E_{VMC}.[265] The vertical dotted line indicates J_{max} where $L^2_{(0,2)}$ of $|\Phi_0^R\rangle$ is maximal. All energies are in units of t and the two panels share the x-axis.

by solving Eq. (5.25) and Variational Monte Carlo(VMC) results[265] E_{VMC} are shown. Due to the fact that $\bar{H}$ is not Hermitian any more, and hence not bounded by below, E_{HF} can drop below the exact ground state energy E_{ex}, also displayed in Fig. 5.1, so following Tsuneyuki[330] we termed the energy axis "pseudo energy". There is a huge increase in the $L^2_{(0,2)}$ norm of the $|\Phi_0^R\rangle$ until an optimal value of J_{max}, close to the J_{opt} obtained by solving Eq. (5.25), see Tab. 5.1, where $L^2_{(0,2)} \approx 1$, followed by subsequent decrease. The result obtained by minimizing the energy variance E_{var} is higher in energy and farther from J_{max} than J_{opt}. And, although E_{VMC} is closer to E_{ex}, the optimised correlation parameter obtained by VMC is also farther from J_{max} than J_{opt}. At the same time $L^2_{(0,2)}$ of $|\Phi_0^L\rangle$ shows a monotonic decrease with increasing $-J$. This shows that the amount of relevant information contained within the HF determinant and double excitations thereof can be drastically increased in the right eigenvector, whilst decreased in the left one. For the calculation of the energy, where only the right eigenvector is necessary, a more efficient sampling with the stochastic FCIQMC method should be possible.

5.4 The Similarity Transformed FCIQMC Method

In this section the necessary adaptations of the FCIQMC method, see Sec. 2.3, sample the non-Hermitian similarity transformed Hamiltonian (5.19) with 3-body interactions are discussed. Additionally, the arguments why the shift energy $E_S(\Delta\tau)$ (2.47) remains a valid energy estimator for excited states calculation via Gram-Schmidt orthogonalisation,

see Sec. 2.3.6, even for the nonorthogonal set of right eigenvectors of a non-Hermitian operator are presented.

In variational approaches the lack of a lower bound of the energy due to the non-Hermiticity of the similarity transformed Hamiltonian poses a severe problem. As a projective technique the FCIQMC method has no inherent problem sampling the right ground state eigenvector, obtaining the corresponding eigenvalue by repetitive application of the projector (2.46). Additionally, the increased compactness of $|\Phi_0^R\rangle$ observed in Section 5.3.3, due to the suppressed double occupations via the Gutzwiller Ansatz, tremendously benefits the sampling dynamics of i-FCIQMC. On the other hand, the implementation of the additional 3-body term in (5.19) necessitate major technical changes to the FCIQMC algorithm. We changed the `NECI`[25] code to enable triple excitations. Due to momentum conservation and the specific spin relations ($\sigma\sigma\bar{\sigma}$) of the involved orbitals and efficiently analytically calculable 3-body integrals of (5.19), these could be implemented without a major decrease of the performance of the algorithm. In fact the contractions of the 3-body term in (5.19), namely $\mathbf{k} = 0 \veebar \mathbf{k}' = 0 \veebar \mathbf{k} = \mathbf{k}' \veebar \mathbf{q} + \mathbf{k}' = \mathbf{s}$ lead to an $\mathcal{O}(M)$ additional cost of the 2-body matrix element, which have the largest detrimental effect on the performance. (There is an $\mathcal{O}(M^2)$ scaling for the diagonal matrix elements, coming from the $\mathbf{k} = \mathbf{k}' = \mathbf{0}$ contraction, but this has a negligible overall effect, since we store this quantity for each occupied determinant and thus is not computed often). The additional cost for 2-body integrals is similar to the calculation of 1-body integrals in conventional *ab-initio* quantum chemistry calculations and unavoidably hampers the performance, but is manageable. Surprisingly, the actual performance improves with increasing strength of the correlation parameter J, even though the three-body interactions are increasing in magnitude. This is due to the following fact: the performance of the FCIQMC method depends heavily on the "worst-case" $|H_{ij}|/p(i|j)$ ratio, where $p(i|j)$ is the probability to spawn a new walker on determinant $|D_i\rangle$ from $|D_j\rangle$ and $|H_{ij}|$ is the absolute value of the corresponding matrix element $\langle D_i|\hat{H}|D_j\rangle$. The timestep $\Delta\tau$ of the FCIQMC simulation is on-the-fly adapted to ensure the "worst-case" product remains close to unity, $\Delta\tau|H_{ij}|/p(i|j) \approx 1$. An optimal sampling would be achieved, if for every pair $(i,j) : p(i|j) \approx |H_{ij}|$ and thus $\Delta\tau \approx \min(1, E_W^{-1})$. Since $\bar{H}$ is not Hermitian, the off-diagonal matrix elements are not uniform, as in the original Hamiltonian (5.18). We therefore need to ensure an efficient sampling by a more sophisticated choice of $p(i|j)$. Additionally we can separate $p(i|j)$ into a probability to perform a double(triple) excitation $p_D(1-p_D)$ since there are still no single excitations in (5.19), due to momentum conservation. This split into doubles or triples, gives us the flexibility, in addition to $\Delta\tau$, to also adapt p_D during run-time to bring $|H_{ij}|/p(i|j)$ closer to unity. We observed that with increasing correlation parameter J the dynamically adapted probability to create triple excitations increased and thus reducing the detrimental additional cost to calculate 2-body matrix elements.

When we perform the spawning step in FCIQMC we first decide if we perform a double excitation with probability p_D, or a triple excitation with probability $1 - p_D$. Then we pick two or three electrons $mn(l)$ from the starting determinants ($|D_j\rangle$) uniformly, with probability p_{elec}. For a double excitation, due to momentum conservation, we only need to pick one unoccupied orbital, since the second is fixed to fulfil $\mathbf{k}_m + \mathbf{k}_n = \mathbf{k}_a + \mathbf{k}_b$. To guarantee $p(i|j) \sim |H_{ij}|$ we loop over the unoccupied orbitals a in $|D_j\rangle$ and create a cumulative probability list with the corresponding matrix elements $|H_{ij}(mn, ab)|$ and thus pick the specific excitation with $p(i|j) \sim |H_{ij}|$. The cost of the is $\mathcal{O}(M^2)$, due to the loop over the unoccupied orbitals $\sim M$ and the $\mathcal{O}(M)$ cost of the double excitation matrix element calculation. For triple excitations the procedure is similar, except we pick 3 electrons $m_\sigma, n_\sigma, l_{\bar{\sigma}}$ with p_{elec}, then we pick orbital $a_{\bar{\sigma}}$ of the minority spin uniformly with $p_a = 1/n_{holes}$ and pick orbital b_σ weighted from a cumulative probability list proportional to $|H_{ij}|$; the third orbital c_σ is again determined by momentum conservation $\mathbf{k}_m + \mathbf{k}_n + \mathbf{k}_l = \mathbf{k}_a + \mathbf{k}_b + \mathbf{k}_c$. As opposed to double excitations, this is only of cost $\mathcal{O}(M)$, due to the loop over unoccupied orbitals in $|D_j\rangle$ do determine b_σ. We term this procedure as *weighted* excitation generation algorithm.

An alternative and simpler algorithm is to pick the unoccupied orbitals uniformly. This decreases the cost per iteration, but also leads to a "worse worst-case" H_{ij}/p_{ij} ratio leading to a decreased timestep $\Delta\tau$. Fig. 5.2 shows the histogram of the $|\bar{H}_{ij}|/p_{ij}$ ratios for the *weighted* procedure, described above, the *uniform* choice of empty orbitals and a *mixed* method for the half-filled 50-site Hubbard model at $U/t = 4$. In the mixed method, the $\mathcal{O}(M^2)$ scaling double excitations in the weighted scheme, are picked uniformly, while the $\mathcal{O}(M)$ scaling triple excitations are still weighted according to their matrix element $|\bar{H}_{ij}|$. Longer tails in a distribution indicate the need for a lower timestep to ensure $\Delta\tau|\bar{H}_{ij}|/p_{ij} \approx 1$. It is apparent that the *mixed* scheme possesses the optimal combination of favourable $|\bar{H}_{ij}|/p_{ij}$ ratios similar to the *weighted* method, with manageable additional cost per iteration, shown in Table 5.4. Table 5.4 shows the relative difference of the timestep $\Delta\tau$, time per iteration t_{iter}, number of aborted excitations n_{abort} and acceptance rate n_{accept} of the different methods compared to the original $J = 0$ uniform sampled half-filled, 50-site Hubbard model with $U/t = 4$. While there is a sevenfold increase of the time per iteration of the *mixed* scheme com-

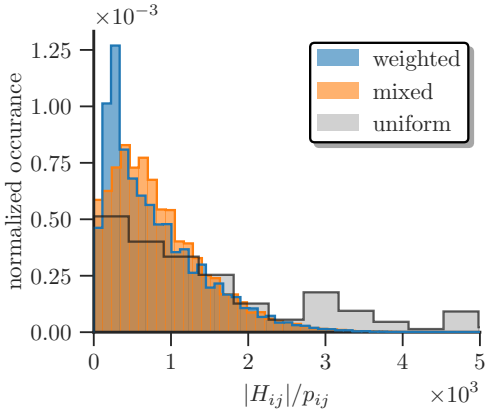

Fig. 5.2: Histogram of $|\bar{H}_{ij}|/p_{ij}$ ratios for the half-filled, 50-site, $U/t = 4$ Hubbard model with periodic boundary conditions for uniform, weighted and mixed generation probabilities.[69]

Tab. 5.4: Ratio of the timestep $\Delta\tau$, time per iteration t_{iter}, aborted n_{abort} and accepted excitations n_{accept} of the different excitation generation probabilities compared to the $J = 0$ uniform reference for the half-filled, 50-site, $U/t = 4$ Hubbard model with periodic boundary conditions.

J	method	$\%\Delta\tau$	$\%t_{iter}$	$\%n_{abort}$	$\%n_{accept}$
0	weighted	100.00	240.12	0.00	100.00
$\neq 0$	uniform	21.02	169.33	93.72	77.31
$\neq 0$	mixed	35.55	719.22	40.14	130.64
$\neq 0$	weighted	45.01	1506.72	0.00	165.29

pared to the original uniform, the timestep is almost a third larger and the accepted rate of spawning events a third higher. n_{abort} indicates those spawning attempts which originally are proposed in the uniform scheme, but are finally rejected, due to zero matrix elements or are Fermi blocked. This quantity is also decreased by more than a half in the mixed method compared to the uniform original scheme. n_{accept} indicates the number of accepted proposed spawning events and is directly related to the p_{spawn} (2.50). The choice of the excitation generator is therefore not straightforward and depends on the interaction strength and J: the *uniform* scheme performs better than expected at small U/t, whilst the mixed scheme performs better at large U/t.

5.4.1 Excited States of non-Hermitian Operators with ST-FCIQMC

The set of right eigenvectors $\bar{H}\left|\Psi_i^R\right\rangle = E_i\left|\Psi_i^R\right\rangle$ of a non-Hermitian operator $\bar{H}$ are in general not orthogonal to each other. Only the set of different left- and right eigenvectors form a biorthogonal basis $\left\langle\Psi_i^L \middle| \Psi_j^R\right\rangle = \delta_{ij}$.[275] Consequently, the approach to obtain excited states in FCIQMC, namely by running multiple independent simulations in parallel and applying a Gram-Schmidt orthogonalization to a chosen number of excited states[22]

$$|\Psi_n(\tau+\Delta\tau)\rangle = \hat{P}_n(\tau+\Delta\tau)\left[\mathbf{1} - \Delta\tau\left(\hat{H} - E_S^{(n)}(\tau)\right)\right]|\Psi_n(\tau)\rangle \tag{5.29}$$

with $E_S^{(n)}$ being the energy shift associated with state n and

$$\hat{P}_n(\tau) = \mathbb{1} - \sum_{m<n}\frac{|\Psi_m(\tau)\rangle\langle\Psi_m(\tau)|}{\langle\Psi_m(\tau)|\Psi_m(\tau)\rangle}, \quad E_m < E_n, \tag{5.30}$$

being the Gram-Schmidt projector, which removes all contributions of lower lying states $|\Psi_m\rangle$ and thus orthogonalises $|\Psi_n\rangle$ to each state with $E_m < E_n$, should in general not be applicable to obtain excited states of non-Hermitian operators. By orthogonalising each eigenvector $\left\langle\Psi_i^L \middle| \Psi_j^R\right\rangle \stackrel{!}{=} 0$ for $i \neq j$ (i and j indicate the excited states), the sampled excited states will in general not be identical to the exact right eigenvectors of the non-Hermitian $\bar{H}$ (5.19). Except, if the excited states belongs to a different spatial or total spin symmetry sectors, the overlap to the ground state is zero, due to symmetry. In this case the excited state approach within the FCIQMC formalism, via orthogonalisation,

correctly samples these orthogonal excited states.

In general, since the set of right eigenvectors $|\Phi_i^R\rangle$ of a non-Hermitian operator are not guaranteed to be orthogonal, we cannot rely on the projected energy estimate (2.52) as an estimate for the excited state energy. It turns out, since the spectrum of $\bar{H}$ does not change due to the similarity transformation (5.6), the shift energy $E_S^{(n)}$ in Eq. (5.29), dynamically adapted to keep the walker number constant, remains a proper estimate for the excited state energy.

To illuminate this fact, the difference to the exact energy, obtained by the projected e_p and shift e_s energy estimator, for the first 10 states of the 1D 6 e^- in 6-site, periodic, $U/t = 4$, $\mathbf{k} = 0$ Hubbard model with a correlation parameter $J = -0.1$ are shown in Fig. 5.3. Also shown is the difference of the sum of the overlap of the i-th excited states to all lower lying states j with $E_j < E_i$, for the exact right eigenvectors obtained by exact diagonalization and the sampled eigenvectors within FCIQMC

$$\Delta O_i = \sum_j \left| \left\langle \Psi_i^{ex} \middle| \Psi_j^{ex} \right\rangle - \left\langle \Psi_i^{qmc} \middle| \Psi_j^{qmc} \right\rangle \right| \quad \forall j : E_j < E_i. \tag{5.31}$$

As mentioned $\left\langle \Psi_i^R \middle| \Psi_j^R \right\rangle \neq 0$ is possible for non-Hermitian operators, and is the case for states $3, 4$ and 5 shown in Fig. 5.3, indicated by a large value of ΔO_i, since within FCIQMC the incorrect $\left\langle \Psi_i^{qmc} \middle| \Psi_j^{qmc} \right\rangle \stackrel{!}{=} 0$ is wrongfully enforced. The incorrect form of the wavefunction is accompanied by a large error in the projected energy e_p compared to the exact result.
Because the i-th excited state is orthogonalised to all the lower lying excited states to converge to the next higher energy governed by the dynamics (2.46) and the spectrum of the Hamiltonian (5.1) is unchanged by the similarity transformation (5.6), the shift energy remains a good energy estimator. This can clearly be seen in Fig. 5.3, as the shift energy remains a good energy estimate of all the targeted eigenstates.

The only exception in Fig. 5.3, which could be misleading, is state number 7, which appears to have a large error in ΔO_i, but the projected energy is still a good estimator for the energy. This comes from the fact that state 6 and 7 are actually degenerate and thus the exact eigenvectors $|\Psi_6^{ex}\rangle$ and $|\Psi_7^{ex}\rangle$ obtained by `Lapack`[4] are an arbitrary linear combination and could be chosen to be both orthogonal to the states $i < 6$.

To see why the shift energy is a valid estimate for the exact excited states energy, let's look at the right eigenvalue equation for a general (Hermitian or non-Hermitian) Hamiltonian $\hat{H}$ for the i-th excited state

$$\hat{H} |\Psi_i\rangle = E_i |\Psi_i\rangle , \tag{5.32}$$

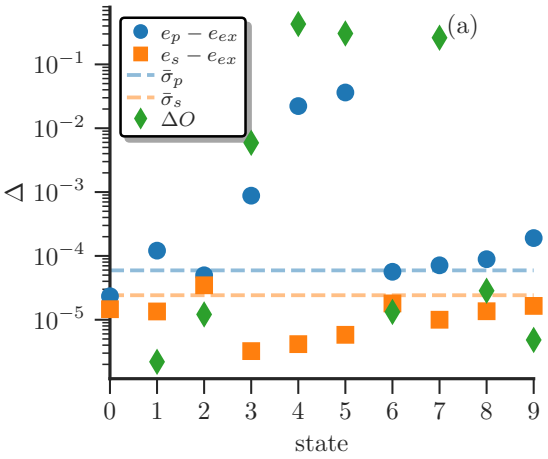

Fig. 5.3: Error of the first 10 eigenstate energies obtained by the projected energy e_p and shift energy e_s for the 6 e^- in 6-site 1D periodic Hubbard model at $U/t = 4$ and $\mathbf{k} = 0$ compared to exact diagonalization results.[69] The horizontal dashed lines indicate the averaged statistical errors. The green pluses show the difference of the exact overlaps to the overlaps obtained within FCIQMC, see Eq. (5.31). A correlation parameter of $J = -0.1$, initiator threshold of $n_{init} = 1.2$ and a maximum walker number of $N_w = 10^5$ were used. (a) Exact overlap is ill-defined due to degeneracy of states 6 and 7.

where $|\Psi_i\rangle$ is the i-th right eigenvector of $\hat{H}$. We now want to show that there exists a vector $|\Phi_i\rangle$, which is an eigenvector of the composite operator $\hat{P}_i\hat{H}$ with the same eigenvalue E_i

$$\hat{P}_i\hat{H}\,|\Phi_i\rangle = E_i\,|\Phi_i\rangle\,, \tag{5.33}$$

where $\hat{P}_i$ is the Gram-Schmidt projector (5.30) and $|\Phi_0\rangle = |\Psi_0\rangle$, which creates an orthonormal basis out of the linearly independent, but not necessarily orthonormal set $\{|\Psi_i\rangle\}$. We assume all states to be normalized. Multiplying eq. (5.32) with $\hat{P}_i$ from the left, we obtain

$$\hat{P}_i\hat{H}\,|\Psi_i\rangle = E_i\hat{P}_i\,|\Psi_i\rangle = E_i\,|\Phi_i\rangle \rightarrow |\Phi_i\rangle = \hat{P}_i\,|\Psi_i\rangle\,. \tag{5.34}$$

And we assume $|\Phi_i\rangle$ to be the desired eigenvector of $\hat{P}_i\hat{H}$. To show that we plug (5.34) into eq. (5.33)

$$\begin{aligned}\hat{P}_i\hat{H}\,|\Phi_i\rangle &= \hat{P}_i\hat{H}\hat{P}_i\,|\Psi_i\rangle = \hat{P}_i\hat{H}\left(|\Psi_i\rangle - \sum_{j<i}\langle\Phi_j\,|\,\Psi_i\rangle\,|\Phi_j\rangle\right)\\ &= E_i\hat{P}_i\,|\Psi_i\rangle - \sum_{j<i} b_{ji}\hat{P}_i\hat{H}\,|\Phi_j\rangle = E_i\,|\Phi_i\rangle - \sum_{j<i} b_{ji}\hat{P}_i\hat{H}\,|\Phi_j\rangle\,,\end{aligned} \tag{5.35}$$

with $b_{ij} = \langle\Phi_j\,|\,\Psi_i\rangle$. We can express $|\Phi_j\rangle$ in eq. (5.35) and all subsequent appearances of $|\Phi_k\rangle$ with $k < i$ as $|\Phi_k\rangle = \hat{P}_k\,|\Psi_k\rangle$ until we reach $|\Psi_0\rangle$. So the remaining thing to show is that $\hat{P}_i\,|\Psi_j\rangle = 0$ for $i > j$.
For $i > j$

$$\hat{P}_i\,|\Phi_j\rangle = |\Phi_j\rangle - \sum_{k<i}\underbrace{\langle\Phi_k\,|\,\Phi_j\rangle}_{\delta_{jk}}|\Phi_k\rangle = 0, \quad \text{with} \quad i > j \tag{5.36}$$

is easy to show since $\{|\Phi_j\rangle\}$ is an orthonormal basis. We prove $\hat{P}_i\,|\Psi_j\rangle = 0, j < i$ by induction. For $i = 1$ we have

$$\hat{P}_1\,|\Psi_0\rangle = |\Psi_0\rangle - \langle\Psi_0\,|\,\Psi_0\rangle\,|\Psi_0\rangle = 0. \tag{5.37}$$

With the assumption $\hat{P}_i |\Psi_j\rangle = 0$ for $i < j$, performing the induction step $i \to i+1$ yields

$$\underline{j < i} : \hat{P}_{i+1} |\Psi_j\rangle = \underbrace{\hat{P}_i |\Psi_j\rangle}_{=0} - \langle\Phi_i | \Psi_j\rangle |\Phi_i\rangle = -\langle\Psi_i| \underbrace{\hat{P}_i^\dagger}_{=\hat{P}_i} |\Psi_j\rangle |\Phi_i\rangle = 0 \tag{5.38}$$

$$\begin{aligned}\underline{j = i} : \hat{P}_{i+1} |\Psi_i\rangle &= \underbrace{\hat{P}_i |\Psi_i\rangle}_{=|\Phi_i\rangle} - \langle\Phi_i | \Psi_i\rangle |\Phi_i\rangle = |\Phi_i\rangle - \langle\Psi_i| \underbrace{\hat{P}_i}_{=\hat{P}_i^2} |\Psi_i\rangle |\Phi_i\rangle \\ &= |\Phi_i\rangle - \langle\Phi_i | \Phi_i\rangle |\Phi_i\rangle = 0,\end{aligned} \tag{5.39}$$

where we used the Hermiticity $\hat{P}_i^\dagger = \hat{P}_i$ and idempotency $\hat{P}_i^2 = \hat{P}_i$ of the projection operator. With $\hat{P}_i |\Psi_j\rangle = 0$ eq. (5.35) gives the desired

$$\hat{P}_i \hat{H} |\Phi_i\rangle = E_i |\Phi_i\rangle . \tag{5.40}$$

And this eigenvector $|\Phi_i\rangle$ of the composite operator $\hat{P}_i \hat{H}$ is the stationary vector we sample in FCIQMC. Since it has the same eigenvalue E_i, we obtain the correct excited state energy estimate from the shift energy $E_S^{(i)}$ in the propagator (2.58). Since the same argument holds for the long-time limit of the projection

$$\hat{Q}_n(E_S^{(n)}) |\Psi_n\rangle = \left(\mathbb{1} - \Delta\tau \left(\hat{H} - E_S^{(n)}(\tau)\right)\right) |\Psi_n\rangle = |\Psi_n\rangle , \tag{5.41}$$

with stationary $|\Psi_n\rangle$ for $E_S^{(n)} = E_n$. There is an eigenvector $|\Phi_n\rangle$ of the composite operator

$$\hat{P}_i \hat{Q}_i(E_S^{(n)}) |\Phi_n\rangle = |\Phi_n\rangle \tag{5.42}$$

for $E_S^{(n)} = E_n$ with

$$|\Phi_n\rangle = P_n |\Psi_n\rangle , \quad \text{since} \quad \hat{P}_n \hat{Q}_n(E_S^{(n)}) |\Psi_n\rangle = \hat{P}_n |\Psi_n\rangle . \tag{5.43}$$

This $|\Phi_n\rangle$ is sampled by the walkers in a FCIQMC simulation and the shift energy $E_S^{(n)}(\tau)$ is adapted to keep the walker population fixed. The projected energy is in general not a good energy estimate, since

$$\begin{aligned}E_P^{(i)} &= \frac{\langle D_i|\hat{H}|\Phi_i\rangle}{\langle D_i | \Phi_i\rangle} = \frac{\langle D_I|\hat{H}\hat{P}_i|\Psi_i\rangle}{\langle D_I|\hat{P}_i|\Psi_i\rangle} = \frac{\langle D_I|\hat{H}\left(\mathbf{1} - \sum_{j<i} |\Phi_j\rangle \langle\Phi_j|\right)|\Psi_i\rangle}{\langle D_I | \Psi_i\rangle - \sum_{j<i} \langle D_I | \Phi_j\rangle\langle\Phi_j | \Psi_i\rangle} \\ &= \frac{E_i c_{I,i} - \sum_{j<i} b_{ij}\langle D_I|\hat{H}|\Phi_j\rangle}{c_{I,i} - \sum_{j<i} d_{I,j} b_{ij}} = \frac{E_i c_{I,i} - \sum_{j<i} b_{ij} d_{I,j} E_P^{(j)}}{c_{I,i} - \sum_{j<i} d_{I,j} b_{ij}}\end{aligned} \tag{5.44}$$

$$\text{with} \quad c_{I,i} = \langle D_I | \Psi_i\rangle, b_{ij} = \langle\Phi_j | \Psi_i\rangle, d_{I,j} = \langle D_I | \Phi_j\rangle \tag{5.45}$$

and $|D_I\rangle$ being the reference determinant of state i. With Eq. (5.44) and knowledge of

the exact eigenfunctions $\{|\Psi_i\rangle\}$ the excited state energy could be calculated as

$$E_i = \left[E_P^{(i)} \left(c_{I,i} - \sum_{j<i} d_{I,j} b_{ij} \right) + \sum_{j<i} b_{ij} d_{I,j} E_P^{(j)} \right] c_{I,i}^{-1}. \tag{5.46}$$

For states where $\langle D_I \,|\, \Phi_i \rangle \approx c_{I,i}$ and $b_{ij} \approx 0$ the projected energy remains a good estimator for the exact E_i. However, especially in cases where the exact right eigenvectors are not orthogonal to all lower lying ones, as demonstrated in Fig. 5.3, the projected energy should not be trusted. Another correction for the projected energy would be

$$\langle D_I \,|\, \Phi_i \rangle E_P^{(i)} = \langle D_I | \hat{H} \hat{P}_i | \Psi_i \rangle = \langle D_I \,|\, \Psi_I \rangle E_i - \sum_{j<i} \langle \Phi_j \,|\, \Psi_i \rangle \underbrace{\langle D_I | \hat{H} | \Phi_j \rangle}_{= \langle D_I \,|\, \Phi_j \rangle E_P^{(j)}} \tag{5.47}$$

$$\rightarrow E_i = \frac{\langle D_I \,|\, \Phi_i \rangle E_P^{(i)}}{+} \sum_{j<i} \langle \Phi_j \,|\, \Psi_i \rangle \langle D_I \,|\, \Phi_j \rangle E_P^{(j)} \langle D_I \,|\, \Psi_i \rangle \tag{5.48}$$

$$\text{with} \quad \langle D_I \,|\, \Psi_i \rangle = \langle D_I \,|\, \Phi_i \rangle + \sum_{j<i} \langle \Phi_j \,|\, \Psi_i \rangle \langle D_I \,|\, \Phi_j \rangle \tag{5.49}$$

$$\rightarrow E_i = \frac{\langle D_I \,|\, \Phi_i \rangle E_P^{(i)} + \sum_{j<i} \langle \Phi_j \,|\, \Psi_i \rangle \langle D_I \,|\, \Phi_j \rangle E_P^{(j)}}{\langle D_I \,|\, \Phi_i \rangle + \sum_{j<i} \langle \Phi_j \,|\, \Psi_i \rangle \langle D_I \,|\, \Phi_j \rangle}. \tag{5.50}$$

Where we can estimate the overlap $\langle \Phi_j \,|\, \Psi_i \rangle$ from the orthogonalisation procedure. Actually for the correct projected energy one needs to calculate

$$\bar{E}_P^{(i)} = \frac{\langle D_I | \hat{P}_i \hat{H} | \Phi_i \rangle}{\langle D_I \,|\, \Phi_i \rangle} = E_i, \quad \text{since} \quad \hat{P}_i \hat{H} \,|\Phi_i\rangle = E_i \,|\Phi_i\rangle \,. \tag{5.51}$$

Unfortunately the numerator of eq. (5.51) takes the following form

$$\langle D_I | \hat{P}_i \hat{H} | \Phi_i \rangle = \langle D_I | \hat{H} | \Phi_i \rangle - \sum_{j<i} \langle D_I \,|\, \Phi_j \rangle \langle \Phi_j | \hat{H} | \Phi_i \rangle. \tag{5.52}$$

To calculate $\langle \Phi_j | \hat{H} | \Phi_i \rangle$ we would need the transition (reduced) density matrices (t-(R)DM) between all states $j < i$. And for the similarity transformed momentum-space Hubbard Hamiltonian even up to the 3-body t-RDM. So we have to rely on the shift energy to yield the correct excited state energy in the ST-FCIQMC method or apply the mentioned *shoelace* technique in 5.6.

5.5 Results of the ST-FCIQMC Method

We assessed the performance of initiator ST-FCIQMC (i-ST-FCIQMC) for different Hubbard lattices, as a function of the Gutzwiller correlation factor J. As a starting guide for J, we use J_{opt} obtained by solving Eq. (5.25) for the specific lattice size M, number of electrons n_{el} and interaction strength U/t, and calculate the ground state and excited

states energies with i-ST-FCIQMC. In particular, we were interested in the rate of convergence of the energy with respect walker number, or in other words, how quickly the initiator error disappeared with increasing walker number. The optimal values of J for each studied system can be found in Table 5.1 in Section 5.3.2. All energies are given per site and in units of the hopping parameter t and the lines in the Figures 5.4 to 5.7 are guides to the eye.

5.5.1 18-site Hubbard Model

We first study the 18-site Hubbard model on a square lattice with tilted boundary conditions (see Fig. 5.8), which can be exactly diagonalised: at half-filling and zero total momentum ($\mathbf{k} = 0$) it has a Hilbert space of $\sim 10^8$ determinants. All the exact reference results were obtained by a Lanczos diagonalization.[121] For this system ST-FCIQMC could be run either in "full" mode or with the initiator approximation, i-ST-FCIQMC. This enables us to assess to two separate questions, namely the performance of i-ST-FCIQMC regarding the initiator error on the one hand, and compactness of the wavefunctions resulting from the similarity transformation (without the complicating effects of the initiator approximation), on the other.

Figure 5.4 shows the error (on a double-logarithmic scale) of the energy per site in the initiator calculation, as a function of walker number. The left panel shows results for the $U/t = 2$ system. As one can see there is a steep decrease in the error and even with only 10^4 walkers, for a correlation parameter of $J = -1/4$ (close to the J_{opt}) the error is below 10^{-4}. At 10^6 walkers it is well below 10^{-6}, almost two orders of magnitude lower than the original (i.e. $J = 0$) Hamiltonian at this value of N_w. This also confirms the assumption that the chosen Ansatz for the correlation function (5.2) is particularly useful in the low U/t regime.

Results for an intermediate strength, $U/t = 4$, are shown in the right panel of Fig. 5.4. Compared to the $U/t = 2$, more walkers are needed to achieve a similar level of accuracy. The two sources for this behaviour are:
Firstly, i-FCIQMC calculations on the momentum-space Hubbard model are expected to become more difficult with increasing interaction strength U/t, due to the enhanced multi-configurational character of the ground state wavefunction. Secondly, the chosen correlation Ansatz (5.2) is proven to be more efficient in the low U/t regime.[155] Nevertheless, the results shown in Fig. 5.4 show a steep decrease in the double logarithmic plot of the error with increasing walker number. The decrease is steeper for $J = -1/2$, close to the analytic result obtained with $J_{opt} = -0.5234470$. For $J = -1/2$, at walker numbers up to $5 \cdot 10^7$ we are, to within error bars, at the exact result. At a walker number of 10^7 there is a two order of magnitude difference in the error of the $J = -1/2$ and $J = 0$ result.

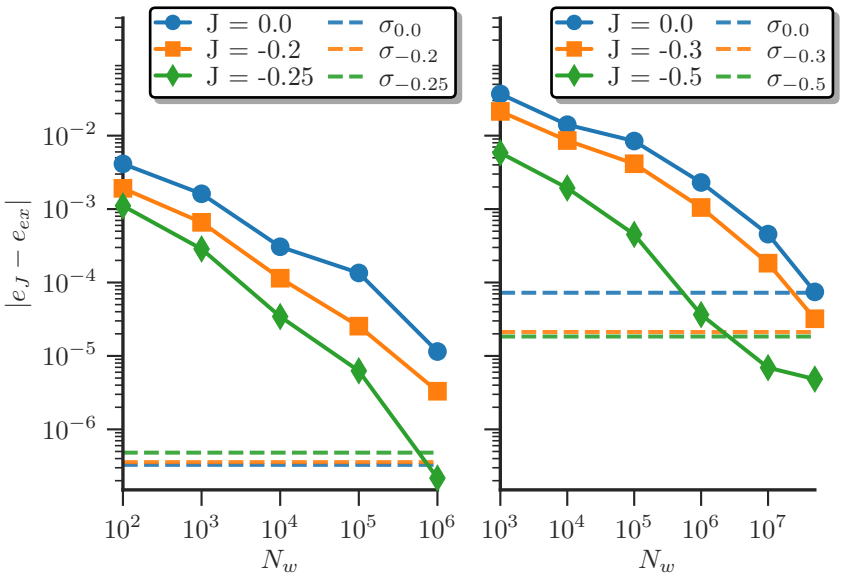

Fig. 5.4: The error of the energy per site $|e_J - e_{ex}|$ for the half-filled 18-site Hubbard model for the original $J = 0$ and different strengths of the correlation parameter J at $\mathbf{k} = 0$ for $U/t = 2$ (left) and $U/t = 4$ (right) versus the walker number N_w.[69] The dashed lines indicate the statistical errors of the $N_w = 10^6$ results with $n_{init} = 1.2$ for $U/t = 2$ and of the $N_w = 5 \cdot 10^7$ with $n_{init} = 2.0$ for $U/t = 4$. The exact reference results were obtained by Lanczos diagonalization.[121]

To confirm the more compact form of the right ground state eigenvector, mentioned in Sec. 5.3.3, we performed two analyses. First was the study of the L^2 norm captured within the HF determinant and double excitations, $L^2_{(0,2)}$, for the ST-FCIQMC wavefunction. In Fig. 5.5 $L^2_{(0,2)}$ of the left and right ground state eigenvector of the half-filled 18-site, $U/t = 4$ Hubbard model as a function of $-J$ is shown. The results were obtained by running full non-initiator ST-FCIQMC calculations to avoid any influence of the initiator error. The left eigenvector was obtained by running with positive J, which corresponds to a conjugation of $\bar{H}$.

$$\bar{H}(J)^\dagger = \left(\mathrm{e}^{-\hat{\tau}}\,\hat{H}\,\mathrm{e}^{\hat{\tau}}\right)^\dagger = \mathrm{e}^{\hat{\tau}}\,\hat{H}\,\mathrm{e}^{-\hat{\tau}} = \bar{H}(-J), \tag{5.53}$$

since $\hat{H}^\dagger = \hat{H}$ and $\hat{\tau}^\dagger = \hat{\tau}$. And

$$\bar{H}^\dagger\,|\Phi_L\rangle = E\,|\Phi_L\rangle\,, \quad \text{with} \quad |\Phi_L\rangle = \mathrm{e}^{-\hat{\tau}}\,|\Psi\rangle\,. \tag{5.54}$$

Similar to the exact results for the 6-site model in Fig. 5.1, the right eigenvector shows a huge compactification compared to the original $J = 0$ result, going from 0.65 to over 0.9. The "optimal" value of $J = J_{max} = -0.57444831$, where $L^2_{(0,2)}$ is maximal, is close to the analytical obtained $J_{opt} = -0.5234470$, indicating that we can simply use J_{opt} without further numerical optimisation of J, and still be close to optimal conditions. The right panel of Fig. 5.6 shows the L^2 norm contained in each excitation level relative to the HF determinant for the half-filled, 18-site, $U/t = 4$ Hubbard model for different values of J.

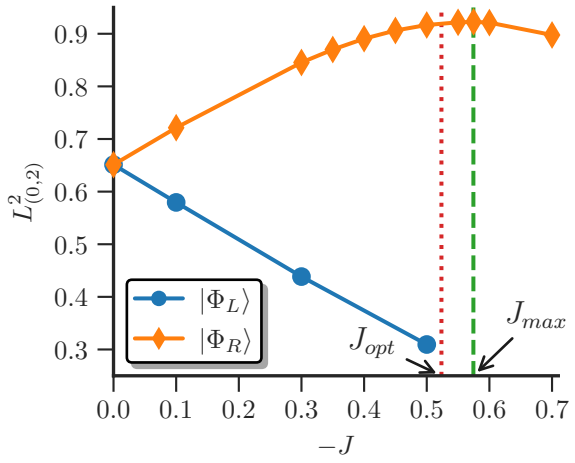

Fig. 5.5: L^2 norm captured within the HF determinant and double excitations, $L^2_{(0,2)}$, for the half-filled 18-site Hubbard model at $U/t = 4$ for the left and right ground state eigenvector of the non-Hermitian similarity transformed Hamiltonian (5.19) as a function of $-J$.[69] The results were obtained by a non-initiator ST-FCIQMC calculation. $|\Phi_L\rangle$ was sampled by running the simulation with positive J, which corresponds to conjugating $\bar{H}$. J_{max} indicates the position of the maximum of $L^2_{(0,2)}$ and J_{opt} is the result of Eq. (5.25).

For $J = -1/2$ there is a huge increase in the L^2 norm of the HF determinant, indicated by an excitation level of 0, while it drops of very quickly for higher excitation levels and remains one order of magnitude lower than the $J = 0$ result above an excitation level of 5.

Our second analysis on the compactness of $|\Phi_0^R\rangle$ consisted of running truncated CI[291] calculations, analogous to the CISD, CISDTQ, etc. methods of quantum chemistry. Here we truncate the Hilbert space by only allowing excitation up to a chosen value n_{trunc} relative to the HF determinant. The left panel of Fig. 5.6 shows the error of the energy per site as a function of n_{trunc} for different J. For $J = -1/2$ we are below 10^{-4} accuracy already at only quintuple excitation, which is two orders of magnitude lower than the original $J = 0$ result at this truncation level. The error bars in the inset of the left panel of Fig. 5.6 are from the $n_{trunc} = 8$ simulations for each value of J, which do not differ much from $n_{trunc} = 5$ to $n_{trunc} = 8$ for each simulation. Already at sextuple excitations we are well within error bars of the exact result for $J = -1/2$, with an error that is two orders of magnitude smaller than the $J = 0$ result.

Off half-filling 14 e^- in 18-sites

We have also investigated the applicability of the i-ST-FCIQMC method to the off-half-filling case, and also to excited states calculations. To this end we calculated the ground, first and second excited states of the 14 e^- in 18-sites, $U/t = 4$, $\mathbf{k} = 0$ system. Such a system can be prepared by removing 4 electrons (2 α and 2 β spins) from the corners of the Fermi-sea determinant, and using this as a starting point for an i-ST-FCIQMC simulation. The calculation of excited states with FCIQMC is explained in Sec. 2.3.6 and the applicability to the non-orthogonal excited states of a non-Hermitian operator is discussed in Sec. 5.4.1.

Figure 5.7 shows the energy per site error of the ground-, first and second excited state of the 14 e^- in 18-site, $U/t = 4$, $\mathbf{k} = 0$ system, compared to exact Lanczos reference

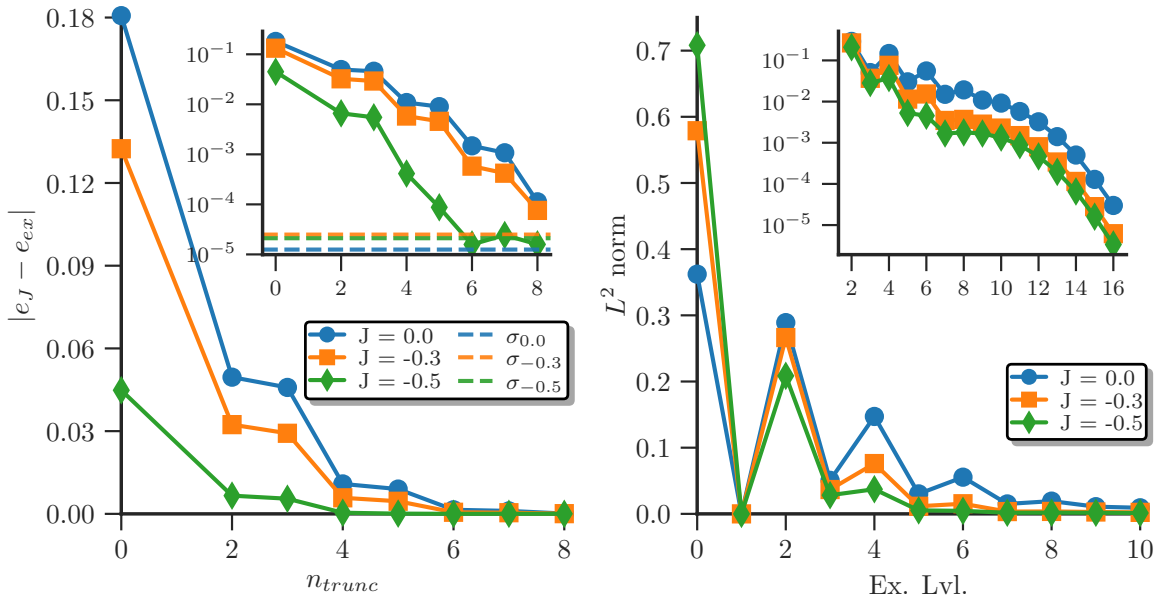

Figure 5.6: (Left) Error of the energy per site versus the excitation level truncation n_{trunc} in the half-filled, 18-site, $U/t = 4$, $\mathbf{k} = 0$ Hubbard model for different values of J.[69] The inset shows the absolute error on a logarithmic scale. The dashed lines in the inset indicate the statistical error for the $n_{trunc} = 8$ results for each value of J. (Right) The L^2 norm contained in each excitation level relative to the HF determinant, indicated by excitation level 0, for the half-filled, 18-site, $U/t = 4$, $\mathbf{k} = 0$ Hubbard model for different values of J. The inset shows the tail of the same data on a logarithmic scale.

results[121] for different values of J versus the walker number N_w, obtained via the shift energy $E_{S,i}$. All states show a similar behaviour of the energy per site error. The closer J gets to the optimal value of $J_{opt} = -0.557941$ for $U/t = 4$, which is determined for E_0, one observes that more than an order of magnitude fewer walkers are necessary to achieve the same accuracy as the $J = 0$ case. This is true for all the states considered. For E_1, the energy difference of the $N_w = 10^7$ and $J = -1/2$ calculation is already within the statistical error of 10^{-5}, hence the non-monotonic behaviour. The size of the absolute error of these states is comparable to the absolute error of the half-filled, 18-site, $U/t = 4$ system, shown in the right panel of Fig. 5.4. Since, without a chemical potential, the total ground state energy per site of the $n_{el} = 14$ system, $e_0^{(14)} = -1.136437$, is lower than the half-filled one, $e_0^{(18)} = -0.958466$, the relative error is in fact smaller off half-filling. As already mentioned above and shown in Table 5.2 and 5.3, the projective solution based on the restricted Hartree-Fock determinant (5.25) also yields smaller relative errors off half-filling. These results give us confidence to also apply the i-ST-FCIQMC method to systems off half-filling and for excited states energy calculations.

Symmetry Analysis

As mentioned in Sec. 5.4.1, the set of right eigenvectors of a non-Hermitian operator are in general not orthogonal, except when they belong to different irreducible repre-

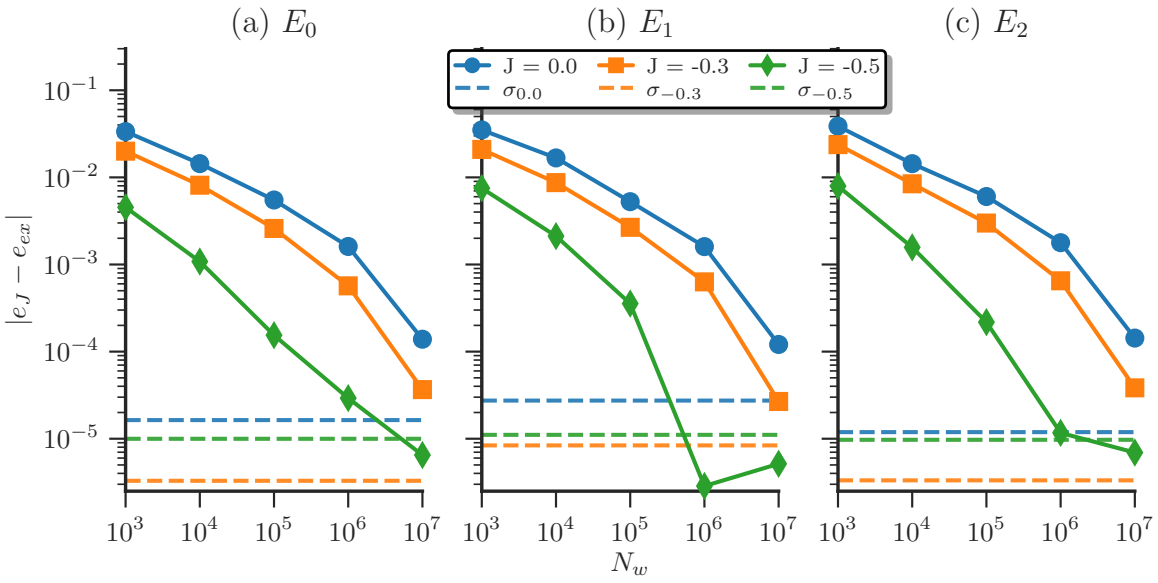

Figure 5.7: Energy per site error compared to exact Lanczos results[121] for the 14 e^- in 18-site, $U/t = 4$, $\mathbf{k} = 0$ Hubbard model for the (a) ground-, (b) first and (c) second excited state as a function of walker number N_w.[69] All three panels share the x and y axes. The dashed lines indicate the statistical errors of the $N_w = 10^7$ for each value of J.

sentations and/or total spin symmetry sectors. Here we investigate the interesting influence of the similarity transformation on the symmetry properties of the truncated low-energy subspace of the $14e^-$ in 18-sites system with total $\mathbf{k} = 0$. There are 8 important low energy determinants with the 5 lowest energy $\mathbf{k}$ points double occupied and 4 e^- distributed among the 4 degenerate orbitals of the corner of the square $\mathbf{k}_1 = (-1,-1), \mathbf{k}_2 = (1,-1), \mathbf{k}_3 = (-1,1)$ and $\mathbf{k}_4 = (1,1)$ to preserve the total $\mathbf{k} = 0$ symmetry. This is illustrated in Fig. 5.8, where red indicates the doubly occupied k-points and green the singly occupied ones. The point group of the square lattice is D_{4h}. There are 2 closed shell determinants in this set, with opposite k-points doubly occupied and 6 open-shell determinants with all 4 corners of the Brillouin zone singly occupied. Without a correlation parameter all these 8 determinants are degenerate in energy, while with $J \neq 0$ this degeneracy is lifted. To study the low energy properties of this system we diagonalized $\bar{H}$ in this subspace. Table 5.5 shows the results. We found that with $J = 0$ the ground state of this subspace has a different spatial and spin symmetry, ${}^5B_{1g}$, than the ground state of the full system, which belongs to ${}^1A_{1g}$. At approximately $J \approx -0.71$ there is a crossover and the subspace ground state changes to ${}^1A_{1g}$ symmetry. The first excited state in the subspace is then the ${}^5B_{1g}$, which is also the symmetry of the first excited state of the full system and the 2nd excited state is of ${}^1B_{2g}$ symmetry, the same as 2nd excited state of the not truncated system. Therefore, the similarity transformation not only ensures a more compact form of the ground- and excited state wavefunctions, but also *correctly orders the states obtained from subspace diagonalization.* The implication is that, in the off half-filling Hubbard model, the structure of ground state has very important contributions arising from high-lying determinants, so much so that they

Tab. 5.5: Irreducible representations and spin symmetry of the ground state E_0 and first two excited states E_1, E_2 of the $U/t = 4$, $\mathbf{k} = 0$, 14 e^- in the 18-site Hubbard model for the full and subspace(subsp.) solutions for different values of J. For a large enough correlation parameter J the ground state of the low-energy subspace resembles the correct symmetry structure as for the full solution.

	E_0	E_1	E_2
Full	${}^1A_{1g}$	${}^5B_{1g}$	${}^1B_{2g}$
$J = 0$ subsp.	${}^5B_{1g}$	${}^1A_{1g}$	${}^1B_{2g}$
$J = -0.72$ subsp.	${}^1A_{1g}$	${}^5B_{1g}$	${}^1B_{2g}$

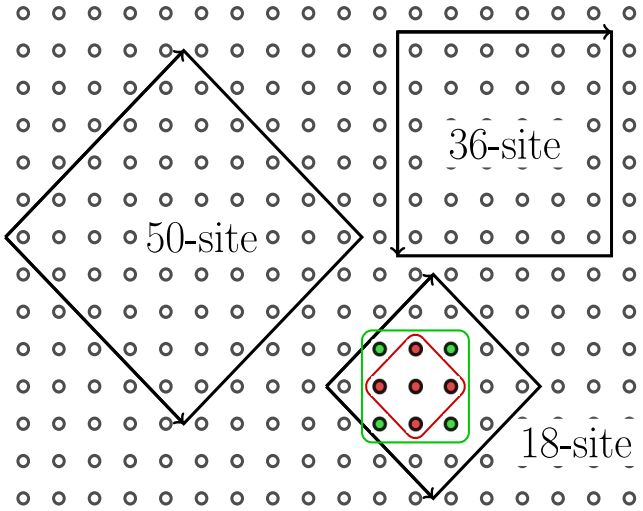

Fig. 5.8: The three different square lattices studied in this paper. Both the 18- and 50-site lattice have tilted periodic boundary conditions with lattice vectors $\mathbf{R}_1 = (3,3), \mathbf{R}_2 = (3,-3)$ and $\mathbf{R}_1 = (5,5), \mathbf{R}_2 = (5,-5)$ respectively; while the 36-site lattice is studied with periodic and mixed, periodic along the x-axis and anti-periodic boundary conditions along the y-axis. The red points in the 18-site lattice indicate the doubly occupied states and the green points the singly occupied states in the sub-space study in 5.5.1.

are necessary to get a qualitatively correct ground state wavefunction (i.e. one with the correct symmetry and spin). With the similarity transformed Hamiltonian this is not the case. Even small subspace diagonalization yield a ground state wavefunction with the same symmetry and spin as the exact one. In other words, the similarity transformation effectively downfolds information from higher lying regions of the Hilbert space to modify the matrix elements between the low-lying determinants. Since the structure of the ground state eigenvector already has the correct symmetry (and therefore signs) in small subspaces, the rate of convergence of the solution with respect to the addition of further determinants is much more rapid. We believe this is a crucial property which leads to the observed greatly improved convergence rate of the i-ST-FCIQMC method in the off half-filling regime.

5.5.2 Results for the 36- and 50-site Hubbard Model

To put the i-ST-FCIQMC method to a stern test, we applied it to two much larger systems, namely 36-site and 50-site lattices, which are well beyond the capabilities of exact diagonalization In the case of the 36-site (6×6) lattice, we considered two boundary conditions, namely fully periodic (PBC) and a mixed periodic-antiperiodic (along the x- and y-axes respectively), the latter being used in some studies to avoid degeneracy of

the noninteracting solution.[365] We considered two fillings, namely half-filling and $24e^-$, at $U/t = 2$ and $U/t = 4$. The optimal J_{opt} was determined by solving Eq. (5.25) and is listed in Table 5.1 in Section 5.3.2. For the 6×6 by lattice we compared our results to AFQMC calculations,[259] which are numerically exact at half-filling.[137] The results are shown in Table 5.6. While the original i-FCIQMC method shows a large error even at walker numbers up to $N_w = 5 \cdot 10^8$ the i-ST-FCIQMC method agrees with the AFQMC reference to within one σ error bars in all but one case (PBC $U/t = 4$ half-filled), where the agreement is within 2σ. Even in that case the energies agree to better than 99.8%. The small discrepancy could be due to this system being strongly open-shell, making equilibration more challenging.

The 50-site Hubbard lattice corresponds to a $5\sqrt{2} \times 5\sqrt{2}$ tilted square, which has been widely investigated using the AFQMC method. We considered half-filling and various off half-filling, $n_{el} = 26, 42, 44, 46$ and 48 cases for $U/t = 1, 2, 3$ and 4 and calculated the ground state energy. The optimal J are listed in Table 5.1 in Section 5.3.2. This system size, especially with increasing U/t and off half-filling, was previously unreachable with the FCIQMC method. We compare our half-filling results to AFQMC[137,308,358] reference values, which do not have a sign problem at half-filling.[137] The remaining sources of error are extrapolation to zero temperature and finite steps, both of which are expected to be very small. Off half-filling, exact AFQMC results are not available, and we compare against constrained-path AFQMC(CP-AFQMC)[46,374] and linearised-AFQMC(L-AFQMC).[305]
Table 5.6 shows the results for various fillings and U/t values the reference calculations, the original i-FCIQMC and the i-ST-FCIQMC method. We converged our results for this system size up to a walker number of $N_w = 10^9$. We can see that the original i-FCIQMC method performs well for the weakly correlated half-filled $U/t = 1$ system, but fails to reproduce the reference results at $U/t = 2$ for this system size, and the discrepancy worsens with increasing interaction. The i-ST-FCIQMC method on the other hand agrees within error bars with the reported reference calculation up to $U/t = 3$ at half-filling. Similar to the half-filled 36-site lattice, the i-ST-FCIQMC results are slightly below the AFQMC reference results at $U/t = 4$, which could be a finite temperature effect of the AFQMC reference results.

We investigated the half-filled 50-site $U/t = 4$ system further by performing the convergence of a truncated CI expansions, similar to the 18-site lattice, shown in Fig. 5.9. The convergence with excitation level truncation shows that convergence occurs from above, and at 6-fold excitations we are converged to statistical accuracy to the fully unconstrained simulation. The energy at 6-fold truncation is indeed slightly below the AFQMC result, although the discrepancy is small (approximately 0.1%). It is intriguing that the CI expansion of the 50-site lattice is converged at 6-fold excitations, which is the same as observed for the 18-site lattice. This suggests that linear solutions to the similarity-transformed Hamiltonian may be size-consistent to a greater degree than simi-

Table 5.6: Zero temperature, $\mathbf{k} = 0$ ground state energy results for the 36-site and 50-site Hubbard model for various interaction strengths U/t, number of electrons n_{el} and periodic (PBC) and mixed (anti-)periodic boundary conditions along the (y-)x-axis, obtained with the initiator FCIQMC and the i-ST-FCIQMC method[69] compared with available (CP-)AFQMC and linearised-AFQMC reference results.[45,259,293,305,307] The differences to the AFQMC reference energies are displayed as ΔE. The correlation parameter J was chosen close to the optimal J_{opt} obtained by solving Eq. (5.25) listed in Table 5.1 of Sec. 5.3.2 for the specific U/t value. An initiator threshold of $n_{init} = 2.0$ was chosen and convergence of the energy up to a walker number of $N_w = 10^9$ was checked.

M	U/t	n_{el}	BC	E_{ref}	iFCIQMC	$\Delta E_{J=0}$	iST-FCIQMC	ΔE_J
36	4	24	APBC		-1.155828(40)		-1.159285(24)	
36	4	24	PBC	-1.18525(4)	-1.182003(57)	0.003247(97)	-1.1852109(52)	0.000039(45)
36	2	36	APBC	-1.208306(56)	-1.2080756(39)	0.000230(60)	-1.2082581(17)	0.000048(58)
36	2	36	PBC	-1.15158(14)	-1.149734(95)	0.00185(24)	-1.151544(18)	0.00004(16)
36	4	36	APBC	-0.87306(56)	-0.847580(84)	0.025480(64)	-0.872612(50)	0.00045(61)
36	4	36	PBC	-0.85736(25)	-0.82807(87)	0.0293(11)	-0.85625(30)	0.00111(55)
50	1	50	PBC	-1.43718(11)	-1.4371801(18)	0.00000(11)	-1.43724130(44)	-0.00006(11)
50	2	50	PBC	-1.22278(17)	-1.220590(16)	0.00219(19)	-1.2228426(80)	-0.00006(18)
50	3	50	PBC	-1.03460(30)	-1.023064(35)	0.01154(34)	-1.034788(18)	-0.00019(32)
50	4	50	PBC	-0.879660(20)	-0.83401(15)	0.04565(17)	-0.880657(60)	-0.000997(80)
50	4	48	PBC	-0.93720(15)	-0.89610(12)	0.04110(27)	-0.93642(40)	0.00078(55)
50	4	46	PBC	-0.9911420(86)	-0.95550(15)	0.03564(24)	-0.990564(89)	0.00058(18)
50	4	44	PBC	-1.037883(59)	-1.006483(38)	0.031400(97)	-1.037458(47)	0.00043(11)
50	4	42	PBC	-1.079276(66)	-1.053756(64)	0.02552(13)	-1.078908(69)	0.00037(14)
50	4	26	PBC	-1.115640(20)	-1.113874(16)	0.001766(36)	-1.1159016(39)	-0.000262(24)

lar truncations to the original untransformed Hamiltonian. However, this question is left for a future study.

For $U/t = 4$ off half-filling the i-ST-FCIQMC energies are consistently slightly above the reference AFQMC results. However, the approximations in the off half-filling AFQMC calculations can lead to energies below the exact ones. For example,[293] CP-AFQMC on a 4×4 lattice with 14 e^- and $U/t = 4$ gives an energy of $-0.9863(1)$ compared to an exact energy of -0.9840, i.e. an overshoot 0.2%. Similar overshoots are observed at other fillings. In the off half-filling regime in the 50-site system at $U/t = 4$, CP-AFQMC overshoots our i-ST-FCIQMC results by similar amounts. Therefore, our results are in line with ED results for smaller lattices, and thus represent a new set of benchmarks for the off half-filling 50-site Hubbard model.

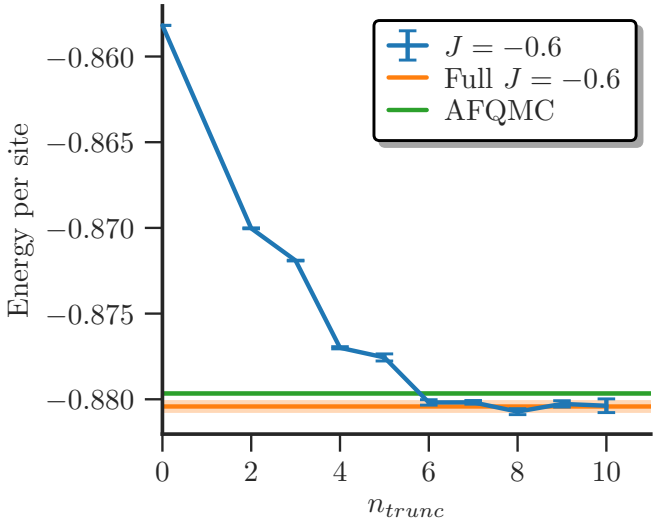

Fig. 5.9: The energy per site versus the excitation level truncation n_{trunc} in the half-filled, 50-site, U/t = 4, k = 0 Hubbard model.[69] AFQMC reference[45] and non-truncated i-ST-FCIQMC results are also shown. Similar to the 18-site system at half-filling (Fig. 4.6), the energies are well-converged at 6-fold excitations.

5.6 Conclusion and Outlook

We have used a projective solution based on the restricted Hartree-Fock determinant to obtain an optimised Gutzwiller correlation parameter. For low to intermediate interaction strength, this method generally recovers over 80% of the ground state energy. Based on this mean-field solution we derived a similarity transformed Hubbard Hamiltonian, generated by the Gutzwiller Ansatz, in a momentum-space basis. We solved for the exact ground- and excited states energy of this non-Hermitian operator with the FCIQMC method. We have shown that the right eigenvector of the non-Hermitian Hamiltonian has a dramatically more compact form, due to suppression of energetically unfavourable double occupancies, via the Gutzwiller Ansatz. This increased compactness of the right eigenvectors allowed us to solve the Hubbard model for system sizes, which were previously unreachable with the i-FCIQMC method. We benchmarked our results with highly accurate AFQMC reference results and find extremely good agreement at and off half-filling up to interaction strengths of $U/t = 4$. We hope this combination of a similarity transformation based on a correlated Ansatz for the ground state wavefunction and subsequent beyond mean-field solution with FCIQMC can aid the ongoing search for the phase diagram of the two-dimensional Hubbard model in the thermodynamic limit.

Outlook

An important extension of the present work will be to compute observables other than the energy. To compute the expectation values of operators $\hat{O}$ which do not commute with the Hamiltonian we need additionally to obtain the left eigenvector of the non-Hermitian $\bar{H}$ with the Ansatz $\langle \Psi_L | = \langle \Phi | \, \mathrm{e}^{-\hat{\tau}}$

$$\langle \Psi | \, \hat{H} = \langle \Phi | \, \mathrm{e}^{-\hat{\tau}} \, H = E \, \langle \Phi | \, \mathrm{e}^{-\hat{\tau}} \, . \tag{5.55}$$

The expectation value of the similarity transformed operator $\bar{O} = \mathrm{e}^{-\hat{\tau}} \, \hat{O} \, \mathrm{e}^{\hat{\tau}}$ with $|\Phi_{R/L}\rangle$ yields the desired

$$\frac{\langle \Phi_L | \bar{O} | \Phi_R \rangle}{\langle \Phi_L \, | \, \Phi_R \rangle} = \frac{\langle \Psi | \mathrm{e}^{\hat{\tau}} \, \mathrm{e}^{-\hat{\tau}} \, \hat{O} \, \mathrm{e}^{\hat{\tau}} \, \mathrm{e}^{-\hat{\tau}} | \Psi \rangle}{\langle \Psi | \mathrm{e}^{\hat{\tau}} \, \mathrm{e}^{-\hat{\tau}} | \Psi \rangle} = \langle \hat{O} \rangle \, . \tag{5.56}$$

As already observed in 5.5.1, applying $\bar{H}$ with $-J$ yields the left eigenvector $|\Phi_L\rangle = \mathrm{e}^{\hat{\tau}} \, |\Psi\rangle$. To perform this in the FCIQMC we only need to run two independent simulations in parallel, as is already done in replica-sampling of reduced density matrices,[228] where the two runs use an opposite sign of the correlation parameter J. Observables, $\hat{O}$, which commute with the chosen Gutzwiller correlator $[\, \hat{\tau}, \hat{O} \,] = 0$, such as the double occupancy $\langle n_\uparrow n_\downarrow \rangle$, can be calculated by the 2-body RDM obtained with the left and right eigenvector

$$\Gamma_{pq,rs} = \langle \Phi_L | c_p^\dagger c_q^\dagger c_s c_r | \Phi_R \rangle, \tag{5.57}$$

with normalized $\langle \Phi_L \, | \, \Phi_R \rangle = 1$ and p, q, r and s denoting spin-orbital labels in the momentum space. Non-commuting observable, $[\, \hat{\tau}, \hat{O} \,]$, have to be similarity transformed $\bar{O} = \mathrm{e}^{-\hat{\tau}} \, \hat{O} \, \mathrm{e}^{\hat{\tau}}$ and might require higher order density matrices.

Simultaneous calculation of the left eigenvectors $|\Phi_L^i\rangle$ also allows us to obtain the correct excited state wavefunctions, in addition to the already correct excited state energy via the shift energy $E_S^{(i)}$ mentioned in Sec. 5.4.1 and 5.5.1, in the following manner: For m excited states we run $2m$ simulations in parallel, where every odd numbered calculation solves for a right eigenstate $|\Phi_R^i\rangle$, which is orthogonalized against all $|\Phi_L^j\rangle$ with $E_j < E_i$. And vice versa, every even numbered simulation solves for a left eigenvector $|\Phi_L^i\rangle$, orthogonalised against each $|\Phi_R^j\rangle$ with $E_j < E_i$. In this *shoelace*-manner m left and right excited state eigenvectors are obtained based on the bi-orthogonal property of left and right eigenvectors of non-Hermitian Operators $\langle \Phi_L^i \, | \, \Phi_R^j \rangle = 0$ for $i \neq j$. Results on observables other than the energy and correct left and right eigenvectors of excited states will be reported in future work.

To perform accurate thermodynamic-limit extrapolations, we also need to reduce the finite size errors of the kinetic term in 5.7. This can be done by twist averaged boundary conditions,[187,250,259,306] which is readily applicable for the similarity transformed Hamiltonian in FCIQMC, and will be reported in future work.

5.6.1 The real-space Hubbard Formulation

To study the Hubbard model in the strong interaction regime, the use of more general two-body[44,219,342] and especially holon-doublon correlators[155,192,344] in the wavefunction Ansatz are necessary. In a momentum space basis, these would lead to N-body excitations in the worst case. There is ongoing work to optimise general two-body correlators with VMC and use the optimised correlation parameters to build a similarity transformed Hamiltonian in real-space, where the correlators only lead to diagonal terms, and solve this model with FCIQMC.

In the large U/t limit the kinetic hopping term in the Hubbard Hamiltonian can be treated as a small perturbation and thus the use of the one-body operator as the correlator

$$\hat{\tau} = J \sum_{\mathbf{i},\mathbf{j},\sigma} a^\dagger_{\mathbf{i},\sigma} a_{\mathbf{j},\sigma} = J \sum_{\mathbf{k},\sigma} \epsilon_{\mathbf{k}}\, n_{\mathbf{k},\sigma} \tag{5.58}$$

is an interesting approach.

The similarity transformation of the momentum-space Hubbard model with the correlator (5.58) yields

$$\tilde{\hat{H}} = -t \sum_{\mathbf{k},\sigma} \epsilon_{\mathbf{k}}\, n_{\mathbf{k},\sigma} + \frac{U}{L} \sum_{\mathbf{p},\mathbf{q},\mathbf{k}} c^\dagger_{\mathbf{p}-\mathbf{k},\uparrow} c^\dagger_{\mathbf{q}+\mathbf{k},\downarrow} c_{\mathbf{q},\downarrow} c_{\mathbf{k},\uparrow}\, \mathrm{e}^{J(\epsilon_{\mathbf{p}}+\epsilon_{\mathbf{q}}-\epsilon_{\mathbf{p}-\mathbf{k}}-\epsilon_{\mathbf{q}+\mathbf{k}})}, \tag{5.59}$$

with an effective two-body potential.

Since in the large U/t regime of the Hubbard model the use of a real-space basis is more beneficial, we can transform Eq. (5.59) back to the real-space* yielding

$$\begin{aligned} \bar{H} = &- t \sum_{\mathbf{i},\mathbf{j},\sigma} a^\dagger_{\mathbf{i},\sigma} a_{\mathbf{j},\sigma} + \frac{U}{2} \sum_{\mathbf{i},\mathbf{j},\mathbf{k},\mathbf{l},\sigma} a^\dagger_{\mathbf{i},\sigma} a^\dagger_{\mathbf{j},\bar{\sigma}} a_{\mathbf{k},\bar{\sigma}} a_{\mathbf{l},\sigma} \\ &\times \sum_{\mathbf{m}} F(J, \mathbf{i}-\mathbf{m}) F(J, \mathbf{j}-\mathbf{m}) F(-J, \mathbf{m}-\mathbf{k}) F(-J, \mathbf{m}-\mathbf{l}), \end{aligned} \tag{5.60}$$

where

$$F(J, \mathbf{l}) = \frac{1}{L} \sum_{\mathbf{p}} e^{i\mathbf{p}\cdot\mathbf{l}}\, \mathrm{e}^{-J\epsilon_{\mathbf{p}}} \tag{5.61}$$

is a Fourier transformation of $\mathrm{e}^{-J\epsilon_{\mathbf{p}}}$.

The similarity transformation with the kinetic hopping correlator (5.58) induces two-body interactions in the real-space Hubbard Hamiltonian, which also include occupation dependent long-range hopping processes for $\mathbf{j} = \mathbf{k}$ and $\mathbf{i} = \mathbf{l}$. This similarity transformed Hamiltonian (5.60) was implemented in our FCIQMC code `NECI`[25] and is currently investigated in the intermediate-to-strong interaction regime of the Hubbard model.

*Derivation omitted

5.6.2 The Heisenberg Model

Similar types of an explicitly correlated wavefunction Ansatz can be applied to the Heisenberg and t-J lattice models.

As discussed in Sec. 4.5 the Heisenberg model can be written as

$$\hat{H}_H = J \sum_{\langle i,j \rangle} \left[\hat{S}_i^z \cdot S_j^z - \frac{1}{2} \left(a_{i\uparrow}^\dagger a_{j\uparrow} a_{j\downarrow}^\dagger a_{i\uparrow} + a_{i\downarrow}^\dagger a_{j\downarrow} a_{j\uparrow}^\dagger a_{i\downarrow} \right) \right] + h \sum_i S_i^z, \tag{5.62}$$

with diagonal contributions proportional $\hat{S}_{i/j}^z$ and spin-flip processes between nearest-neighbour sites i and j.

A possible correlator for the Heisenberg model is

$$\hat{\tau}_s = \frac{g_s}{2} \sum_{\langle i,j \rangle, \sigma} n_{i\sigma} n_{j\bar{\sigma}}, \tag{5.63}$$

which correlates antiparallel spins on nearest-neighbour sites.

The similarity transformation of (5.62) with the correlator (5.63) $\bar{H} = \mathrm{e}^{-\hat{\tau}_s} \, \hat{H} \, \mathrm{e}^{\hat{\tau}_s}$ yields

$$\bar{H}_H = J \sum_{\langle i,j \rangle} \left[\hat{S}_i^z \cdot S_j^z - \frac{\mathrm{e}^{-2g_s}}{2} \left(a_{i\uparrow}^\dagger a_{j\uparrow} a_{j\downarrow}^\dagger a_{i\uparrow} \, \mathrm{e}^{2g_s(\eta_i - \eta_j)} + a_{i\downarrow}^\dagger a_{j\downarrow} a_{j\uparrow}^\dagger a_{i\downarrow} \, \mathrm{e}^{2g_s(\eta_j - \eta_i)} \right) \right] + h \sum_i S_i^z, \tag{5.64}$$

with

$$\eta_i = \sum_{d \in \mathcal{N}(i)} \hat{S}_{i+d}^z = \frac{1}{2} (n_{i+d,\uparrow} - n_{i+d,\downarrow}), \tag{5.65}$$

which modifies the spin-flip term in the Hamiltonian depending on the spin polarization of nearest-neighbour sites d of site i.

5.6.3 The t-J Model

As presented in Sec. 4.5 the Hamiltonian of the t-J model is given by

$$\hat{H}_{t-J} = -t \sum_{\langle i,j \rangle, \sigma} a_{i,\sigma}^\dagger a_{j,\sigma} + J \sum_{\langle i,j \rangle} \left[\hat{S}_i^z \cdot S_j^z - \frac{1}{2} \left(a_{i\uparrow}^\dagger a_{j\uparrow} a_{j\downarrow}^\dagger a_{i\uparrow} + a_{i\downarrow}^\dagger a_{j\downarrow} a_{j\uparrow}^\dagger a_{i\downarrow} \right) - \frac{n_i n_j}{4} \right]. \tag{5.66}$$

Both the correlator based on the number of nearest-neighbour antiparallel spins (5.63) and a general nearest-neighbour density-density correlator

$$\hat{\tau}_d = \frac{g_d}{2} \sum_{\langle i,j \rangle} n_i n_j, \quad \text{with} \quad n_i = n_{i\uparrow} + n_{i\downarrow}, \tag{5.67}$$

can be used as a correlated Ansatz for the ground state wavefunction of the t-J model. Similarity transformation based on the combination of the two correlators (5.63) and (5.67) $\mathrm{e}^{\hat{\tau}_d+\hat{\tau}_s}$, since $[\,\hat{\tau}_s, \hat{\tau}_d\,] = 0$, yields the following transformed t-J Hamiltonian

$$\begin{aligned}\bar{H}_{t-J} = &- t\,\mathrm{e}^{g_d} \sum_{\langle i,j\rangle,\sigma} a^\dagger_{i\sigma} a_{j\sigma}\, \mathrm{e}^{-g_s(\zeta_{j\bar{\sigma}}-\zeta_{i\bar{\sigma}})+g_d(\zeta_j-\zeta_i)} \\ &+ \sum_{\langle i,j\rangle} \left[\hat{S}^z_i \cdot S^z_j - \frac{\mathrm{e}^{-2g_s}}{2} \left(a^\dagger_{i\uparrow} a_{j\uparrow} a^\dagger_{j\downarrow} a_{i\uparrow}\, \mathrm{e}^{2g_s(\eta_i-\eta_j)} + a^\dagger_{i\downarrow} a_{j\downarrow} a^\dagger_{j\uparrow} a_{i\downarrow}\, \mathrm{e}^{2g_s(\eta_j-\eta_i)} \right) \frac{n_i n_j}{4} \right],\end{aligned} \tag{5.68}$$

with

$$\zeta_{i\sigma} = \sum_{d\in\mathcal{N}(i)} n_{i+d,\sigma} \quad \text{and} \quad \zeta_i = \sum_\sigma \zeta_{i\sigma}, \tag{5.69}$$

being sums of nearest-neighbour spins of i.

The similarity transformation of (5.66) based on the correlators (5.63) and (5.67) induces a modified hopping based on the overall and spin-dependent density of nearest-neighbour sites. As in the Heisenberg model, discussed above, the spin-flip terms of (5.68) are modified depending on the spin polarization of nearest-neighbour sites.

Both the t-J and Heisenberg model and the corresponding similarity transformed Hamiltonians mentioned above have been implemented in out FCIQMC code `NECI`,[25] but further studies on the effect of the correlated wavefunction Ansatz need to be conducted.

The method was also applied to the uniform electron gas[197] in the framework of FCIQMC and there is ongoing work to apply this method to ab-initio molecular systems.

6 Discussion and Conclusion

The topic of this thesis was the development of FCIQMC methods for strongly correlated electron systems, to extend their applicability towards increasing size and complexity. In addition to the exponential growing Hilbert space size, due to correlation effects, a (close-to) single-reference description of the wavefunction is not possible, since a multitude of configurations contribute almost equally. The latter defies a compact description within conventional approaches and becomes an obstacle for an efficient sampling with the FCIQMC method, the effectiveness of which depends crucially on the compactness of the wavefunction.

Here, two possible routes to overcome these hurdles, by compressing the information encoded in the wavefunction to enable a more efficient sampling, were systematically investigated; namely the implementation and usage of (i) the total $SU(2)$ spin symmetry of nonrelativistic molecular Hamiltonians, (ii) a correlated wavefunction Ansatz and consequent nonunitary similarity transformation.

Firstly, the efficient usage of a spin-adapted basis in FCIQMC has been made possible within the (graphical) unitary group approach (GUGA) and the severe limitations of previous implementations were overcome. When formulated in such a basis, simulations conserve the total spin quantum number and the Hilbert space size of the problem is reduced. As another consequence, targeting specific many-body subspaces of the Hamiltonian and getting access to their excitation energies is possible, and thus one is able to study phenomena governed by the interplay of different—even degenerate—spin sectors. However, the use of a spin-adapted basis did not improve—as was initially expected—the acceleration of convergence of the projective FCIQMC method.

We benchmarked the spin-adapted FCIQMC method and compare results with other computational approaches, for the nitrogen atom, N_2, the Hubbard model and an one-dimensional hydrogen chain and we find excellent agreement with reference results, when available. In particular for the nitrogen atom we obtain the spin gap of the $^4S^o$ ground- and $^2D^o$ excited state within chemical accuracy to experiment and we demonstrate that the calculation of low-spin eigenstates of systems with up to 30 open-shell orbitals, such as the hydrogen chain, is possible. We apply the method to study, selected 3d-transition metals, cobalt and scandium, targeting properties, which defy a simple single-reference

description. In the cobalt case, the spin-gap of the high-spin ground state (single-reference wavefunction) and low-spin excited state (*multi-reference* wavefunction) was determined within chemical accuracy to experiment. Previous theoretical studies of the electron affinities of the 3d-transition metal series left out scandium, due to the unusual occupation of the 4p orbital of the anion bound states and consequent strong multi-reference character of the wavefunction. In the scandium case, we focus on the electron affinity, a property ignored in previous theoretical studies, mainly due to the unusual occupation of the 4p orbital of its anion bound states that induces a strong multi-reference character in the wavefunction. We find excellent agreement with experimental results and on top we determine from first-principles the order of the anion's bound spin-states.

This spin-adapted implementation brings FCIQMC *en par* with many other quantum chemical methods, which already utilize the inherent total spin conservation of non-relativistic, spin-independent molecular Hamiltonians. To combine the spin-adapted FCIQMC with the stochastic CASSCF method, the final missing piece is the spin-pure implementation of an efficient sampling of reduced density matrices; which would enable us to solve active spaces of unprecedented size in a spin-pure fashion, extending even further the applicability of the method.

Turning our attention to the two-dimensional, repulsive Hubbard model: We investigated an explicitly correlated wavefunction Ansatz, that incorporates part of the correlation effects based on the Gutzwiller correlator, by an exact nonunitary similarity transformation in momentum-space, resulting in a non-Hermitian Hamiltonian with novel three-body interactions. Based on the restricted Hartree-Fock determinant, we optimised the correlation parameter by a simple projective equation, thus obviating the need for an expensive numerical optimisation. We demonstrated that the FCIQMC method, as a projective technique, is well-suited for such non-Hermitian problems, and its stochastic nature can handle the 3-body interactions exactly without undue increase in computational cost. Due to the suppression of energetically unfavourable double occupancies, via the Gutzwiller Ansatz, we observe a dramatically more compact form of the right eigenvector. The latter fact allows a considerably more efficient sampling, which in turn admits the simulation of unprecedented lattice sizes, well beyond the reach of the method applied to the original Hubbard Hamiltonian. However, with increasing interaction strength, due to localisation, the momentum-space basis becomes ill-suited and instead a localised real-space basis should be used. Since our approach is currently formulated in momentum-space, we are limited to the low- to intermediate interaction strength regime.

We studied the resulting non-Hermitian Hamiltonian in the low- to intermediate interaction regime and reproduced the exact results for the 2D 18-site system for the ground- and excited states. Furthermore, due to the extreme compactness of the wavefunction we can handle lattice sizes, unreachable with the standard FCIQMC. In particular, for the

36- and 50-site Hubbard model, our results at and off half-filling are in perfect agreement with more mature methods, i.e. auxiliary field quantum Monte Carlo.

Given the above, together with its flexibility and memory-efficiency, the FCIQMC method is now adequate to study effective lattice models of increasing size, nontrivial geometries, with local or even nonlocal interactions. The extrapolation of results to the thermodynamic limit is now in reach, enabling us to take part in the ongoing research of the underlying mechanisms of the phase diagram of the 2D Hubbard model.

An enormous benefit of FCIQMC, compared to other methods, is the direct availability of a stochastic representation of the ground state wavefunction. However, for the similarity transformed Hamiltonian we will need to sample the different left eigenvector in addition to the right one to be able to correctly sample the reduced density matrices, which in turn will allow us to compute the expectation value of any observable of interest.

A The Graphical Unitary Group Approach

A.1 CSF Excitation Identification

Efficiently identifying the difference between two given CSFs and the type of excitation (generator types) listed in Table 4.3 of Section 4.2 is crucial for an optimized matrix element calculation. However, for CSFs this operation is more involved compared to Slater determinants. This is because not only occupancy differences, but also changes in the singly occupied orbitals (different spin-couplings) have to be taken into account, as they can also lead to non-zero *coupling coefficients*. The defining difference for the excitation is the difference in spatial occupation numbers. The step-values, $d_i = \{0, 1, 2, 3\}$, of the spatial orbitals of a CSF are efficiently encoded by two bits per spatial orbital

$$d_i = 0 : 00, \quad d_i = 1 : 01, \quad d_i = 2 : 10, \quad d_i = 3 : 11,$$

in an integer of length $2n$. This is equivalent to the memory requirement of storing the occupied spin-orbitals of a Slater determinant. The spatial occupation difference, $|\Delta n|$, can be efficiently obtained by shifting all negatively spin-coupled, $d_i = 2 : 10$, to the right, and computing the bit-wise `xor`-operation on two given CSFs and counting the number of set bits in $|\Delta n|$, e.g. by the `Fortran 2008` intrinsic `popcnt`:

$\|m\rangle = \|0, 1, 2, 3\rangle$:	00 01 10 11
$\|m'\rangle = \|1, 2, 1, 2\rangle$:	01 10 01 10
$n(m)$:	00 01 01 11
$n(m')$:	01 01 01 01
$\|\Delta n\|$: `xor`:	01 00 00 01
$\Sigma\|\Delta n\|$: `popcnt`(Δn):	2
$\Delta n = n(m') - n(m)$:	$\|+1, 0, 0, -1\rangle$

With $\Sigma|\Delta n|$ we can identify the excitation level, which would be a single excitation from orbital 4 to 1 in the example above, and Δn gives us information, in which spatial orbitals electrons got removed or added. However, for CSFs the orbital occupation difference alone is not enough to completely identify an excitation between two CSFs, since for excitations

of exchange type, involving $\underline{RL}$ and $\overline{RL}$ generators, there can be a change in the spin-coupling, without an actual change in orbital occupation. So additionally we also need information of the step-vector difference, Δd, which is just obtained by the `xor`-operation on the bit-representation of two given CSFs:

$$\begin{aligned} |m\rangle = |1,1,0,3\rangle: &\quad 01\,01\,00\,11 \\ |m'\rangle = |1,2,1,1\rangle: &\quad 01\,10\,01\,01 \\ \hline |\Delta n|: &\quad 00\,00\,01\,01 \quad \Sigma = 2 \\ \hline \Delta d: &\quad 00\,11\,01\,10 \end{aligned}$$

In this example it can be seen, that the $|\Delta n|$ information alone would lead us again to believe a single excitation connects m and m', but this is not compatible with the change in step-vector at orbital 2. So in addition, we need to determine if there are step-vector changes below the first, Δd_b, or above the last, Δd_a, occupation change in Δn. This can be done efficiently with the `Fortran 2008` intrinsic bit-operations, `leadz(I)` (`trailz(I)`), which give the number of leading(trailing) zeros in integer `I`. The case that there are only step-vector changes, Δd, within, the first and last $\Delta \neq 0$ cases, is encoded by $\Delta d_b = \Delta d_a = 0$.

$\Sigma|\Delta|n > 4$ indicates a higher excitation than double, so the two CSFs are not possibly connected by a single Hamiltonian application and can be disregarded. The non-zero Hamiltonian matrix elements can be identified by following combinations of Δn and Δd:

$\underline{\Sigma|\Delta n| = 0 \;\&\; \Delta d \neq 0}$:
This combination indicates, that there is no difference in the occupation number between two CSFs m and m', but a change in the spin-coupling of the singly occupied orbitals. Only a mixed generator $\underline{RL} \rightarrow \overline{RL}$ generator combination, corresponding to the type (2c) in Table 4.3, can lead to those types of excitations. Details on the matrix element calculation in general can be found in Sec. A.2.

$\underline{\Sigma|\Delta n| = 2 \;\&\; \Delta d_b = \Delta d_a = 0}$:
This combination indicates a regular single excitation and the order of the removed and added electron determines the type of generator $\hat{E}_{ij}$, corresponding to type (0a) in Table 4.3,

$$\begin{aligned} \Delta n = +1 \rightarrow -1: &\quad \underline{R} \rightarrow \overline{R} \\ \Delta n = -1 \rightarrow +1: &\quad \underline{L} \rightarrow \overline{L}. \end{aligned}$$

$\underline{\Sigma|\Delta n| = 2 \;\&\; \Delta d_b \neq 0 \text{ or } d_a \neq 0}$:
This indicates step-vector changes above or below the occupation differences, which identifies a mixed start $\underline{RL}$ or end $\overline{RL}$ segment. Again the order of the orbital occupation

and step-vector changes below or above Δn identifies the type of excitation

$$\begin{aligned}
&(1j) \quad \Delta d_b \to \Delta n_{+1} \to \Delta n_{-1}: \quad \underline{RL} \to \overline{L}R \to \overline{R} \\
&(1i) \quad \Delta d_b \to \Delta n_{-1} \to \Delta n_{+1}: \quad \underline{RL} \to \overline{R}L \to \overline{L} \\
&(1f) \quad \Delta n_{+1} \to \Delta n_{-1} \to \Delta d_a: \quad \underline{R} \to \underline{L}R \to \overline{RL} \\
&(1e) \quad \Delta n_{-1} \to \Delta n_{+1} \to \Delta d_a: \quad \underline{L} \to \underline{R}L \to \overline{RL},
\end{aligned}$$

with $\Delta n_{\pm 1} = \Delta n = \pm 1$ and the reference to the entries of Table 4.3.

$\underline{\Sigma|\Delta n| = 4 \;\&\Delta d_b = \Delta d_a = 0}$:
In this case it is necessary to have $\Delta d_b = \Delta d_a = 0$, otherwise this would indicate more than a double excitation, which would lead to a vanishing Hamiltonian matrix element. Again the order of the occupation differences gives information on the type of generators involved. The following combinations are identifiable only with Δn (with reference to the entries of Table 4.3)

$$\begin{aligned}
&(2b) \quad \Delta n = -2 \to +2: && \underline{LL} \to \overline{LL} \\
&(2a) \quad \Delta n = +2 \to -2: && \underline{RR} \to \overline{RR} \\
&(1h) \quad \Delta n = -2 \to +1 \to +1: && \underline{LL} \to L\overline{L}/\overline{L}L \to \overline{L} \\
&(1g) \quad \Delta n = +2 \to -1 \to -1: && \underline{RR} \to R\overline{R}R \to \overline{R} \\
&(1d) \quad \Delta n = -1 \to -1 \to +2: && \underline{L} \to L\underline{L}/\underline{L}L \to \overline{LL} \\
&(1c) \quad \Delta n = +1 \to +1 \to -2: && \underline{R} \to R\underline{R}/\underline{R}R \to \overline{RR} \\
&(1a) \quad \Delta n = -1 \to +2 \to -1: && \underline{L} \to \overline{L}\underline{R} \to \overline{R} \\
&(1b) \quad \Delta n = +1 \to -2 \to +1: && \underline{R} \to \overline{R}\underline{L} \to \overline{L} \\
&(3b) \quad \Delta n = -1 \to -1 \to +1 \to +1: && \underline{L} \to \underline{L}L/L\underline{L} \to \overline{L}L/L\overline{L} \to \overline{L} \\
&(3a) \quad \Delta n = +1 \to +1 \to +1 \to +1: && \underline{R} \to \underline{R}R/R\underline{R} \to \overline{R}R/R\overline{R} \to \overline{R},
\end{aligned}$$

where, e.g. $\underline{L}L/L\underline{L}$, indicates that the order of indices of equivalent generators, $\hat{e}_{il,jk}/\hat{e}_{ik,jl}$ see Fig. A.1, can not be determined by Δn alone. In the case of alike generators $RR(LL)$ this order does have influence on the sign of the matrix element,[284] see Section A.2 for more details.

There are combinations of occupation differences where additionally the step vector differences have to be checked, since there are multiple two-body operators $\hat{e}_{ij,kl}$ possible,

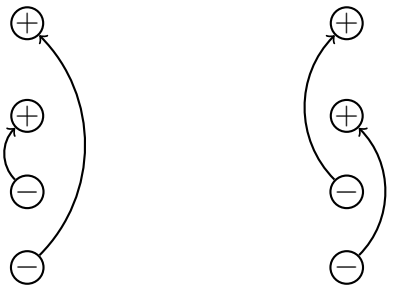

$$\underline{L} \to \underline{L}L \to \overline{L}L \to \overline{L} \qquad \underline{L} \to \underline{L}L \to L\overline{L} \to \overline{L}$$

Figure A.1: Equivalence of the two possible type (3b) double excitations $\hat{e}_{il,jk}$ and $\hat{e}_{ik,jl}$ with $i < j < k < l$. The minus (plus) indicates the removal (addition) of an electron.

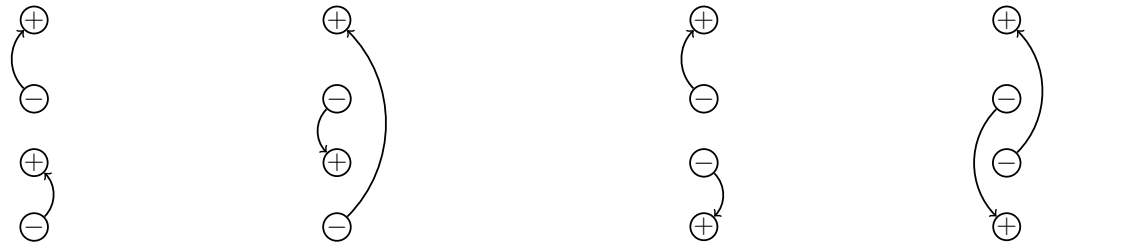

$$\underline{L} \to \overline{L} \to \underline{L} \to \overline{L} \qquad \underline{L} \to \underline{R}L \to \overline{R}L \to \overline{L} \qquad \underline{R} \to \overline{R} \to \underline{L} \to \overline{L} \qquad \underline{R} \to \underline{L}R \to L\overline{R} \to \overline{L}$$

Figure A.2: Equivalence of the $3d_0$ and $3d_1$ (left) and $3e_0$ and $3e_1$ (right) generator combinations leading to the same orbital occupation difference between two CSFs.

which can lead to the same excitation:

$$\Delta n = -1 \to +1 \to \Delta d \to -1 \to +1 : \begin{cases} \underline{L} \to \underline{R}L \to \overline{R}L \to \overline{L} & (3d_1) \\ \underline{L} \to \overline{L} \to \underline{L} \to \overline{L},\ \Delta d \stackrel{!}{=} 0 & (3d_0) \end{cases}$$

$$\Delta n = -1 \to +1 \to \Delta d \to +1 \to -1 : \begin{cases} \underline{L} \to \underline{R}L \to \overline{L}R \to \overline{R} & (3f_1) \\ \underline{L} \to \overline{L} \to \underline{R} \to \overline{R},\ \Delta d \stackrel{!}{=} 0 & (3f_0) \end{cases}$$

$$\Delta n = +1 \to -1 \to \Delta d \to +1 \to -1 : \begin{cases} \underline{R} \to \underline{L}R \to \overline{L}R \to \overline{R} & (3c_1) \\ \underline{R} \to \overline{R} \to \underline{R} \to \overline{R},\ \Delta d \stackrel{!}{=} 0 & (3c_0) \end{cases}$$

$$\Delta n = +1 \to -1 \to \Delta d \to -1 \to +1 : \begin{cases} \underline{R} \to \underline{L}R \to \overline{R}L \to \overline{L} & (3e_1) \\ \underline{R} \to \overline{R} \to \underline{L} \to \overline{L},\ \Delta d \stackrel{!}{=} 0 & (3e_0), \end{cases}$$

where every second case is only possible if there are no step-vector differences, $\Delta d = 0$, between the second and third occupation difference and reference to Table 4.3. The equivalence of these generator combinations can be seen in Fig. A.2. However, even with no Δd difference between the second and third occupation difference both generator combinations still contribute to the Hamiltonian matrix element, see Sec. A.2 for more details.

With this method the distinct excitation types listed in Table 4.3 in Sec. 4.2 can be efficiently identified.

A.2 Detailed Matrix Element Evaluation in the GUGA

In this section we will explain the efficient matrix element calculation in a spin-pure CSF basis based on the GUGA approach in more detail.

A.2.1 Diagonal matrix elements

The diagonal matrix element for a GT state, $|m\rangle$, of the spin-free Hamiltonian (3.8) given in Section 3.3 is given by the sum of the *one-body* matrix elements, $\langle m|\hat{H}_0|m\rangle$, with $\hat{H}_0 = \sum_{ij} t_{ij}\,\hat{E}_{ij}$, and the two-body contribution, $\langle m|\hat{H}_1|m\rangle$, with $\hat{H}_1 = \sum_{ijkl} V_{ijkl}\,\hat{e}_{ij,kl}$. The matrix elements of the *weight* generators, $\hat{E}_{ii}$, are simply just the occupancy of orbital i in state $|m\rangle$

$$\langle m'|\,\hat{E}_{ii}\,|m\rangle = n_i(m)\delta_{m',m}. \tag{A.1}$$

So the one-body contribution is given by

$$\langle m|\,\hat{H}_0\,|m\rangle = \sum_i t_{ii}\,\langle m|\,\hat{E}_{ii}\,|m\rangle = \sum_i t_{ii}\,n(d_i), \tag{A.2}$$

$$\text{with } n(d_i) = \begin{cases} 0 & \text{for } d_i = 0 \\ 1 & \text{for } d_i = 1,2\,, \\ 2 & \text{for } d_i = 3 \end{cases} \tag{A.3}$$

where d_i is step-value of spatial orbital i in $|m\rangle$. The *two-body* contributions are a bit more involved. Let's consider the different cases:

$\underline{i=j=k=l}$: reduces to the sum of doubly occupied orbitals

$$\langle m|\,\hat{H}_1\,|m\rangle = \frac{1}{2}\sum_i V_{iiii}\,\langle m|\,\hat{E}_{ii}^2 - \hat{E}_{ii}\,|m\rangle = \sum_i V_{iiii}\,\delta_{d_i,3}, \tag{A.4}$$

since $\hat{E}_{ii}^2 = \hat{E}_{ii}$ for $d_i = 1,2$.

$\underline{i=j\neq k=l}$: only the $\hat{E}_{ii}\hat{E}_{jj}$ part of $\hat{e}_{ij,kl} = \hat{E}_{ij}\hat{E}_{kl} - \delta_{jk}\hat{E}_{il}$ remains, which reduces to a product of occupation numbers

$$\frac{1}{2}\sum_{i\neq j} V_{iijj}\,\langle d|\,\hat{E}_{ii}\hat{E}_{jj}\,|m\rangle = \frac{1}{2}\sum_{i\neq j} V_{iijj}\sum_{m'}\langle m|\,\hat{E}_{ii}\,|m'\rangle\,\langle m'|\,\hat{E}_{jj}\,|m\rangle = \tag{A.5}$$

$$\frac{1}{2}\sum_{i\neq j} V_{iijj}\,\langle m|\,\hat{E}_{ii}\,|m\rangle\,\langle m|\,\hat{E}_{jj}\,|m\rangle = \frac{1}{2}\sum_{i\neq j} V_{iijj}\,n(d_i)n(d_j) = \sum_{i<j} V_{iijj}\,n(d_i)n(d_j). \tag{A.6}$$

The last relation comes from the fact that the sums are invariant under i, j exchange.

$\underline{i=l\neq j=k}$: Also the exchange integral terms V_{ijji} contribute to the diagonal matrix elements, if the excitation $\langle m|\,\hat{E}_{ij}\hat{E}_{ji}\,|m\rangle$ leads to the same CSF. The calculation of these

Table A.1: Relevant terms of the exchange contribution to diagonal matrix elements.

$d_i \vert d_j$	0	1	2	3
0	0	0	0	0
1	0	$-\frac{1}{2}\left(1+A(b_i,2,0)A(b_j,-1,1)\prod_k f(b_k,d_k)\right)$	$-\frac{1}{2}\left(1-A(b_i,2,0)A(b_j,3,1)\prod_k f(b_k,d_k)\right)$	-1
2	0	$-\frac{1}{2}\left(1-A(b_i,0,2)A(b_j,-1,1)\prod_k f(b_k,d_k)\right)$	$-\frac{1}{2}\left(1+A(b_i,0,2)A(b_j,3,1)\prod_k f(b_k,d_k)\right)$	-1
3	0	-1	-1	-2

matrix elements depends on the step-values between i and j and are obtained by Shavitt's graph rules.[284] As mentioned in Sec. 3.4.1, the matrix elements between two CSFs for a double excitation are given by the product

$$\langle m'|\,\hat{e}_{ij,kl}\,|m\rangle = \prod_{p\in S_2} W(Q_p;d_p,d'_p,\Delta b_p,b_p)\times\sum_{x=0,1}\prod_{p\in S_1} W_x(Q_p;d_p,d'_p,\Delta b_p,b_p) \tag{A.7}$$

with $S_2 = (i,j)\cup(k,l) - S_2$ being the non-overlap range and $S_1 = (i,j)\cap(k,l)$ being the overlap region of the indices of the involved generator $\hat{e}_{ij,kl}$. The one-body segment values $W(Q_p;d_p,d'_p,\Delta b_p,b_p)$ can be found in Table 3.7 of Sec. 3.4.1 and the two-body segment values $W_x(Q_p;d_p,d'_p,\Delta b_p,b_p)$ are listed in Tables A.4 and A.5, which are taken and modified from [284]. In the case relevant for diagonal terms the matrix elements depending on the beginning d_i and end d_j step-values are given in Table A.1 with

$$A(b,x,y) = \sqrt{\frac{b+x}{b+y}} \quad \text{and} \quad f(b,d) = \begin{cases} 1 & \text{for } d=0,3 \\ A(b,2,0)A(b,-1,1) & \text{for } d=1 \\ A(b,0,2)A(b,3,1) & \text{for } d=2 \end{cases} \tag{A.8}$$

Unfortunately this requires the consideration of all step-vector and b-values between i and j to calculate the diagonal matrix element.

$$\sum_{i\neq j}\frac{V_{ijji}}{2}\langle m|\,\hat{e}_{ij,ji}\,|m\rangle = -\sum_{i<j}\frac{V_{ijji}}{2}\Big(n(d_i)n(d_j)+X(i,j)\Big) \tag{A.9}$$

The first term $\frac{1}{2}n(d_i)n(d_j)$ accounts for the first singlet coupled $x=0$ matrix elements in the Table A.1 and $X(i,j)$ accounts for the triplet coupled $x=1$ matrix elements. And only yields a contribution if both d_i and d_j are either 1 or 2

$$X(i,j) = \begin{cases} A(b_i,2,0)\prod_k f(b_k,d_k)A(b_j,-1,1) & d_i=1,d_j=1 \\ -A(b_i,2,0)\prod_k f(b_k,d_k)A(b_j,3,1) & d_i=1,d_j=2 \\ -A(b_i,0,2)\prod_k f(b_k,d_k)A(b_j,-1,1) & d_i=2,d_j=1 \\ A(b_i,0,2)\prod_k f(b_k,d_k)A(b_j,3,1) & d_i=2,d_j=2 \\ 0 & \text{otherwise} \end{cases} \tag{A.10}$$

and the rest gets accounted by the product of occupation numbers $n(d_i)n(d_j)$. In total

the diagonal Hamilton matrix element for a CSF m is given by

$$\langle m|\,\hat{H}\,|m\rangle = \sum_i \left\{ t_{ii}\, n(d_i) + V_{iiii}\,\delta_{d_i,3} + \sum_{j>i} \left[V_{iijj}\, n(d_i)n(d_j) - \frac{1}{2} V_{ijji} \Big(n(d_i)n(d_j) + X(i,j) \Big) \right] \right\}. \tag{A.11}$$

A.2.2 Off-diagonal matrix elements

The off-diagonal matrix element between two CSFs $|m\rangle$ and $|m'\rangle$ is given by

$$\langle m'|\,\hat{H}\,|m\rangle = \sum_{ij} t_{ij}\,\langle m'|\,\hat{E}_{ij}\,|m\rangle + \frac{1}{2}\sum_{ijkl} V_{ijkl}\,\langle m'|\,\hat{e}_{ij,kl}\,|m\rangle \tag{A.12}$$

Similar to the Slater-Condon rules[57,297] for matrix element calculation between Slater determinants, we need to identify the involved orbital indices (i,j,k,l) connecting m' and m and by comparing the *orbital occupation differences* between the two CSFs, $\Delta n_i = n(d_i) - n(d_i')$, already mentioned in Sec. A.1. There are the following possibilities for Δn_i, which yield a possible non-zero matrix element between $|m'\rangle$ and $|m\rangle$:

$\underline{\Delta n_i = 0}$ for all orbitals, but $|m'\rangle$ and $|m\rangle$ differing for some orbitals, implies a full-start $\underline{RL}$ into full-stop $\overline{RL}$ double excitation, type (2c) in Table 4.3, with only changes in the open-shell orbitals. The matrix element can be expressed as

$$\langle m'|\,\hat{H}\,|m\rangle = \frac{1}{2}\sum_{i\neq j} V_{ij,ji}\,\langle m'|\,\hat{e}_{ij,ji}\,|m\rangle + V_{ji,ij}\,\langle m'|\,\hat{e}_{ji,ij}\,|m\rangle = \sum_{i\neq j} V_{ij,ji}\,\langle m'|\,\hat{e}_{ij,ji}\,|m\rangle\,. \tag{A.13}$$

Because these full-start into full-stop excitations are symmetric concerning conjugation of the generator indices and the molecular two-body integrals also, it reduces to

$$\langle m'|\,\hat{H}\,|m\rangle = 2\sum_{i<j} V_{ij,ji}\,\langle m'|\,\hat{e}_{ij,ji}\,|m\rangle\,. \tag{A.14}$$

To yield a non-zero matrix element between m' and m the indices i and j have to engulf all the differing orbitals, yielding a maximum lower index I, and a minimum upper index J. Because full-start into full-stop excitations have the possibility to leave d_i unchanged, basically all combination $i \leq I$ and $j \geq J$ in the summation have to be considered. There has to be at least one difference between m and m', or otherwise it would just be a diagonal matrix element. The singlet coupled x_0 matrix element branch can be discarded, as a change in m implies $\Delta b = \pm 2$ at least at one orbital. Furthermore the integral, $F(I,J)$, between the region of the first to the last change in m ($I \to J$) is the same for all matrix elements. The remaining product terms are given by the triplet coupled x_1

elements for non changing d_i value from orbital i to I and J to j given as

$$\langle m'|\,\hat{H}\,|m\rangle = 2\sum_{\substack{i<I\\ j>J}} F(I,J)\,V_{ij,ji}\prod_{k=i}^{I-1} RL(d_k)\prod_{k'=J+1}^{j} RL(d_j) \quad \text{with} \quad F(I,J)=\prod_{k=I}^{J} RL(d_k), \tag{A.15}$$

where $RL(d_i)$ indicates the triplet-coupled $W_1(Q_i; d_i, d_i', \Delta b_i, b_i)$ matrix elements for a mixed RL generator combination, depending on d and b given in Table A.5. Since we calculate the matrix elements in the excitation generation step of the FCIQMC method, see Sections 4.1, 4.2 and A.3, it is useful to formulate the matrix elements in terms of already calculated terms, i.e. $F(I,J)$, to reduce the computational effort of the spin-adapted FCIQMC implementation.

$\underline{\Delta n_k = \pm 1:}$ for *two* spatial orbitals i, j. This implies a one-body contribution, as well as two-body contributions with two indices being identical, over which has to be summed. However, there is the additional constraint that the double excitation also has to lead to the same orbital occupancy difference Δn, which only leaves following terms:

$$\begin{aligned}\langle m'|\,\hat{H}\,|m\rangle = \; t_{ij}\,\langle m'|\,\hat{E}_{ij}\,|m\rangle + \frac{1}{2}\sum_k \Big(&V_{ij,kk}\,\langle m'|\,\hat{e}_{ij,kk}\,|m\rangle + V_{kk,ij}\,\langle m'|\,\hat{e}_{kk,ij}\,|m\rangle \\ &+V_{ik,kj}\,\langle m'|\,\hat{e}_{ik,kj}\,|m\rangle + V_{kj,ik}\,\langle m'|\,\hat{e}_{kj,ik}\,|m\rangle\Big),\end{aligned} \tag{A.16}$$

where the second line, involving weight generators, due to $V_{ijkk} = V_{kkij}$, reduces to

$$\langle m'|\,\hat{E}_{ij}\,|m\rangle \sum_{k\neq i,j} V_{ij,kk}\,n(d_k). \tag{A.17}$$

For $k \neq (i,j)$ both the remaining terms yield (without the two-particle integrals for clarity and $\hat{e}_{ij,kl} = \hat{E}_{ij}\hat{E}_{kl} - \delta_{jk}\hat{E}_{il}$)

$$\langle m'|\,\hat{E}_{ij}\hat{E}_{ii}\,|m\rangle + \langle m'|\,\hat{E}_{ij}\hat{E}_{jj}\,|m\rangle - \langle m'|\,\hat{E}_{ij}\,|m\rangle = \langle m'|\,\hat{E}_{ij}\,|m\rangle\,\big(n(d_i)+n(d_j)-1\big), \tag{A.18}$$

which in total yields

$$\langle m'|\,\hat{E}_{ij}\,|m\rangle\left(\sum_k V_{ij,kk}\,n(d_k) - V_{ij,jj}\right). \tag{A.19}$$

The third line in Eq. (A.16), due to $V_{ij,kl} = V_{kl,ij}$ and $\hat{e}_{ij,kl} = \hat{e}_{kl,ij}$, reduces to:

$$\sum_k V_{ik,kj}\;\langle m'|\,\hat{e}_{ik,kj}\,|m\rangle \tag{A.20}$$

and is a bit more involved to calculate. Depending on the relation of the index k to (i,j), the two-body integral corresponds to certain sequences of generator combinations

Table A.2: Modified matrix element contributions $\underline{\Delta}(i)$ and $\overline{\Delta}(j)$ necessary for the on-the-fly matrix element calculation during the excitation process in the FCIQMC algorithm.

d'	d	$\underline{R}$	$R\overline{L}$	$\underline{\Delta}(i)$	$\overline{L}$	$\underline{R}L$	$\overline{\Delta}(j)$
1	0	1	-$tA(0,2)$	-$tA(0,2)$	1	$tA(2,0)$	$tA(2,0)$
2	0	1	$tA(2,0)$	$tA(2,0)$	1	-$tA(0,2)$	-$tA(0,2)$
3	1	$A(1,0)$	-$tA(-1,0)$	$tA(-1,1)$	$A(0,1)$	-$tA(2,1)$	-$tA(2,0)$
3	2	$A(1,2)$	-$tA(3,2)$	-$tA(3,1)$	$A(2,1)$	$tA(0,1)$	tA(0,2)

d'	d	$\underline{L}$	$\overline{R}L$	$\underline{\Delta}(i)$	$\overline{R}$	$R\underline{L}$	$\overline{\Delta}(j)$
0	1	1	-t$A(-1,1)$	-$tA(-1,1)$	1	$tA(2,0)$	$tA(2,0)$
0	2	1	$tA(3,1)$	$tA(3,1)$	1	-$tA(0,2)$	-$tA(0,2)$
1	3	$A(2,1)$	$tA(0,1)$	$tA(0,2)$	$A(0,1)$	-$tA(2,1)$	-$tA(2,0)$
2	3	$A(0,1)$	-$tA(2,1)$	-$tA(2,0)$	$A(2,1)$	$tA(0,1)$	$tA(0,2)$

(assuming $i < j$ for now, which is easily generalized):

$\underline{k < i:}$ $\underline{LR} \rightarrow \overline{L}R \rightarrow \overline{R}$: type (1j) excitations in Table 4.3,
without a change in the spin-coupling in the overlap region (k, i) between the two CSFs m and m' . The $\Delta b = 0$ branch matrix elements of the mixed generator RL contribute multiplicatively $-t^2 n(d_k)$ terms, see Table A.5 and the x_1 matrix element contributions are $x_1 = \prod_{l=k}^{i-1} RL(l)$, where $RL(l)$ are just the normal mixed generator x_1 product elements. The product only goes until index $i-1$ to still be able to formulate it in terms of the single excitations $\hat{E}_{ij}$. To formulate it multiplicatively, special factors depending on the step-vector $d(i)$ have to determined, so the semi-stop x_1 elements of $\overline{R}L(i)/\overline{L}R(i)$ have the same elements as the single starts $\underline{R}/\underline{L}$. The formulation in terms of $\hat{E}_{ij}$ enables us to reuse the already calculated one-body elements in the excitation generation of the FCIQMC method, see Sections 4.1, 4.2 and A.3.

The modified values starting $\underline{\Delta}(i)$ and end $\overline{\Delta}(j)$ values for $\underline{RL} \rightarrow R\overline{L} \rightarrow \overline{R}$ and $\underline{RL} \rightarrow \overline{R}L \rightarrow \overline{L}$ type of excitation can be found in Table A.2. The rest of the double excitation overlap matrix elements is the same. So for $k < i$ the two-body matrix elements are given by

$$\sum_{k=1}^{i-1} \left(-t^2\, n(d_k) + \underline{\Delta}(i) \prod_{l=k}^{i-1} RL(d_l, d'_l) \right), \tag{A.21}$$

with $\underline{\Delta}(i)$ from Table A.2 for the corresponding generator combination.

$\underline{k = i:}$ $W\underline{R} \rightarrow \overline{R}$: type (0c) excitations in Table 4.3,
which just reduce to $\langle m'| \hat{E}_{ij} |m\rangle \, (n(d'_i) - 1)$, similarly:
$\underline{k = j:}$
reduces to $\langle m'| \hat{E}_{ij} |m\rangle \, (n(d_j) - 1)$.

$\underline{k > j:}$ $\underline{R} \rightarrow R\underline{L} \rightarrow \overline{RL}$: type (1f) excitations in Table 4.3
As in the $k < i$ case the $x = 0$ contribution is a multiplicative $-t^2\, n(d_k)$ factor. The

Table A.3: Modified two-body terms at the single overlap site k used to formulate the two-body contribution to the single excitations multiplicatively and allow an on-the-fly matrix element calculation thereof.

	Usual value				Modified Value				Multiplicative Factor r_k			
	R		L		$\underline{R}\overline{R}$		$\underline{L}\overline{L}$		$i<j$		$i>j$	
$d'd\|\Delta b$	-1	+1	-1	+1	- 1	+1	-1	+1	-1	+1	-1	+1
00	1	1	1	1	0	0	0	0	0	0	0	0
11	-1	$C(b,0)$	$C(b,1)$	-1	1	0	0	1	-1	0	0	-1
12	-1/$(b+2)$	–	1/$(b+1)$	–	1	–	1	–	-$(b+2)$	–	$(b+1)$	–
21	–	1/b	–	-1/$(b+1)$	–	1	–	1	–	b	–	-$(b+1)$
22	$C(b,2)$	-1	-1	$C(b,1)$	0	1	1	0	0	-1	-1	0
33	-1	-1	-1	-1	1	1	1	1	-1	-1	-1	-1

non-vanishing x_1 overlap matrix elements are again calculated multiplicatively by the use of modified semi-stop segments at j to formulate the matrix element in terms of single excitations for $\underline{R} \rightarrow R\underline{L} \rightarrow \overline{RL}$ and $\underline{L} \rightarrow L\underline{R} \rightarrow \overline{RL}$ generator combinations. The modified terms $\overline{\Delta}(j)$ terms can also be found in Table A.2. Here only the step-vector combinations, which lead to the $\Delta b = 0$ branch in the overlap region are allowed, since there is not step-vector difference above j. The full matrix elements are given by

$$\sum_{k>j}^{n} \left(-t^2\, n(d_k) + \overline{\Delta}(j) \prod_{l=j+1}^{k} RL(d_l, d'_l) \right), \tag{A.22}$$

with $\overline{\Delta}(j)$ from Table A.2 for the specific generator combination.

$\underline{i(j) < k < j(i) : \underline{R} \rightarrow \underline{R}\overline{R} \rightarrow \overline{R}}$ ($\underline{L} \rightarrow \overline{L}\underline{L} \rightarrow \overline{L}$): type (0b) excitations in Table 4.3
These types of generator combinations correspond to one-body terms actually. At index k the usual product term for the $\hat{E}_{ij}$ matrix element calculation takes on a different than usual value. This modification can be applied multiplicatively, but depends on $d_k, d'_k, b_k, \Delta b_k$ and the type of generator($i < j$ or $i > j$). The modified values can be found in Table A.3. By defining r_k as

$$r_k(d'_k, d_k, b_k, \Delta b_k) = \begin{cases} -t^2\, n(d_k) + \underline{\Delta}(i) \prod_{l=k}^{i-1} RL(d_l, d'_l) & \text{for } k < min(i,j) \\ -t^2\, n(d_k) + \overline{\Delta}(j) \prod_{j+1}^{l=k} RL(d_l, d'_l) & \text{for } k > max(i,j) \\ n(d'_i) - 1 & \text{for } k = i \\ n(d_j) - 1 & \text{for } k = j \\ \text{entries from Table A.3} & \text{for } k \in (i,j) \end{cases} \tag{A.23}$$

the total matrix element of a single excitation with one-body and two-body contributions can be expressed as

$$\langle m'|\, \hat{H}\, |m\rangle = \langle m'|\, \hat{E}_{ij}\, |m\rangle \left(t_{ij} - V_{ij,jj} + \sum_k V_{ij,kk}\, n(d_k) + V_{ik,kj}\, r_k(d'_k, d_k, b_k, \Delta b_k) \right) \tag{A.24}$$

in terms of the one-body coupling coefficient. The evaluation requires the calculation of the single excitation matrix element $\langle m'|\,\hat{E}_{ij}\,|m\rangle$ through Shavitt's graphical rules,[283,284] and the summation of terms depending on d'_k and d_k entries of the two CSFs (although in a sequential dependence, since r_k depends on Δb_k). We can calculate the r_k terms similar to Shavitt's matrix product terms with r_k (A.23) in the excitation range given in Table A.3 during excitation generation. This requires an $\mathcal{O}(N)$ effort in calculation of r_k, since only occupied orbitals contribute.

$\underline{\Delta n = \pm 1:}$ at *two orbitals* and *additional step-vector differences* Δd below or above the excitation range, correspond to (1e, 1f, 1i) or (1j) excitations of Table 4.3, depending on the ordering of the remaining indices. These are $d = 1, d' = 2$, and vice versa, step-vector differences outside the range (i, j), corresponding to double excitations with mixed generator full-starts $\underline{RL}$ or full-stops $\overline{RL}$. Similar to the $\Sigma|\Delta n| = 0$ case all possible excitations connecting the two CSFs have to engulf the first step-vector change, I, if it occurs before $\min(i, j)$ or the last step-vector change, J, if it is after $\max(i, j)$. However, all mixed full-starts before I or after J have to be considered too, since there is the possibility of a $\underline{RL}(d = 1, d' = 1)$ or $\underline{RL}(d = 2, d' = 2)$ start with non-zero x_1 matrix element.[284] So the matrix element is given by:

$$\sum_{k<I}^{i-1} \underline{\Delta}(i) F(I,i)\,\langle m'|\,\hat{E}_{ij}\,|m\rangle \prod_{l=k}^{I} RL(d_l) \quad \text{for } I < \min(i,j) \tag{A.25}$$

$$\sum_{k>J} \overline{\Delta}(j) F(j,J)\,\langle m'|\,\hat{E}_{ij}\,|m\rangle \prod_{l>J}^{n} RL(d_l) \quad \text{for } J > \max(i,j), \tag{A.26}$$

with $RL(d_l)$ again being the x_1 matrix elements, $F(I,i)/F(j,J)$ being the always involved x_1 matrix elements engulfing all step-vector changes in the overlap region and $\underline{\Delta}(k)/\overline{\Delta}(k)$ being the modifying terms to express it in terms of single excitation matrix elements $\hat{E}_{ij}$, see Table A.2.

$\underline{\Delta n_i = \pm 2}$ at *two spatial* orbital i and j implies a full-start into full-stop double excitation with two alike generators ($\underline{RR} \rightarrow \overline{RR}$ or $\underline{LL} \rightarrow \overline{LL}$, corresponding to type (2a) and (2b) in Table 4.3). This completely specifies the indices and the full matrix element is just given by

$$\langle m'|\,\hat{H}\,|m\rangle = V_{ij,ij}\,\langle m'|\,\hat{e}_{ij,ij}\,|m\rangle \tag{A.27}$$

and calculated with Shavitt's graphical rules.[284] The order of the orbitals, where electrons are removed and added, determines the type of generators.

$\Delta n \neq 0$ at *three* different orbitals with one $\Delta n = \pm 2$ and two $\Delta n = \mp 1$, corresponds to type (1c, 1d, 1g) or (1h) excitations of Table 4.3. This determines all four indices, with two indices being identical, with $\Delta n_k = \pm 2$ and $\Delta n_i = \Delta n_j = \mp 1$. Leaving the matrix

element to be:

$$\langle m'|\,\hat{H}\,|m\rangle = \begin{cases} V_{ik,jk}\,\langle m'|\,\hat{e}_{ik,jk}\,|m\rangle & \text{if } \Delta n_k = -2 \\ V_{ki,kj}\,\langle m'|\,\hat{e}_{ki,kj}\,|m\rangle & \text{if } \Delta n_k = +2 \end{cases} \tag{A.28}$$

$\underline{\Delta n_i \neq 0}$ at *four* different orbitals with two times $\Delta n = 1$ and two times $\Delta n = -1$ values, corresponds to type (3a, 3b, 3c, 3d, 3e) or (3e) excitations of Table 4.3. This also completely determines all four indices of the excitation, but there are four different combinations of these indices which can lead to the same state, where two of them, however, are equivalent. The relation and ordering of these indices determines the type and combinations of generators, with the total matrix element given by

$$\begin{aligned}\langle m'|\,\hat{H}\,|m\rangle =& \frac{1}{2}\,\langle m'|\,\left(V_{li,kj}\,\hat{e}_{li,kj} + V_{kj,li}\,\hat{e}_{kj,li} + V_{ki,lj}\,\hat{e}_{ki,lj} + V_{lj,ki}\,\hat{e}_{lj,ki}\right)|m\rangle \\ =& \langle m'|\,\left(V_{li,kj}\,\hat{e}_{li,kj} + V_{ki,lj}\,\hat{e}_{ki,lj}\right)|m\rangle\,,\end{aligned} \tag{A.29}$$

where for orbitals l and k, $\Delta n_l = \Delta n_k = +1$ and for i and j, $\Delta n_i = \Delta n_j = -1$. The relative positions of the $\Delta n = +1$ and $\Delta n = -1$ orbitals determines the generator combinations and type of excitations involved, see A.1.

For alike generator combinations, e.g. $\underline{R} \to \underline{R}R \to \overline{R}R \to \overline{R}$, we have to take into account the sign flip due to an exchange of operator indices. Since $\hat{e}_{ik,jl}$ and $\hat{e}_{il,jk}$ $(i < j < k < l)$, both contribute to the same excitation. As already pointed out by Paldus,[33,236] the Coulomb and exchange type contributions can be expressed in terms of the same $x = 0$ and $x = 1$ matrix element contributions with

$$w_0 = \prod_{k\in S_2} W(Q_k; d'_k, d_k, \Delta b_k, b_k) \prod_{k\in S_1} W_1(Q_k; d'_k, d_k, 0, b_k) \tag{A.30}$$

$$w_1 = \prod_{k\in S_2} W(Q_k; d'_k, d_k, \Delta b_k, b_k) \prod_{k\in S_1} W_1(Q_k; d'_k, d_k, \Delta b_k, b_k), \tag{A.31}$$

where $w_0 \neq 0$ only if $\Delta b_k = 0, \forall k \in S_1$. By sticking to the convention to use the standard order of operators, as indicated in Table 4.3, the contribution of an exchange of orbital indices in the generator can be expressed as

$$\langle m'|\,\hat{e}_{jl,ik}\,|m\rangle = w_0 + w_1 \tag{A.32}$$

$$\langle m'|\,\hat{e}_{jk,il}\,|m\rangle = w_0 - w_1, \tag{A.33}$$

with a type (3a) excitation from Table 4.3 as an example. The total matrix element is then given by

$$\langle m'|\,\hat{H}\,|m\rangle = w_0\,(V_{jlik} + V_{jkil}) + w_1\,(V_{jlik} - V_{jkil})\,, \tag{A.34}$$

The case of alternating orbital occupancy differences and $\Delta n = \pm 1 \to \Delta n = \mp 1$ involve no sign change in mixed generator semi-start and semi-stops for the x_1 matrix element. These type (3c-3f) excitations of Table 4.3 also contain non-overlap generator combinations, indicated by the subscript $_0$. Because the non-overlap double excitations are contained

as the $\Delta b_k = 0, \forall k \in S_1$ special case of these mixed generator excitation, we do not treat them explicitly, but stick to the convention to always use the mixed generator combination in the excitation generation, see Sec. A.3. For an excitation, which left the $\Delta b_k = 0$ path at some point in the overlap region, only the $x = 1$ matrix element contributes. If $\Delta b_k = 0, \forall k \in S_1$, the Coulomb type contribution can be obtained by the $x = 0$ term of the exchange matrix element[236]

$$\langle m'| \hat{e}_{il,kj} |m\rangle = -\frac{w_0}{2} + w_1, \quad \langle m'| \hat{e}_{ij,kl} |m\rangle = w_0. \tag{A.35}$$

otherwise $w_0 = 0$. The total matrix element is then given by

$$\langle m'|\hat{H}|m\rangle = w_0 \left(-\frac{V_{ilkj}}{2} + V_{ijkl} \right) + w_1 V_{ilkj}. \tag{A.36}$$

$\underline{\Delta n \neq 0}$ at *more than four* different spatial orbitals or $\underline{\Delta b \neq 0}$ outside of excitation range for $\Sigma|\Delta n| = 4$, yields a zero matrix element, as such excitations cannot be obtained by a single application of the Hamiltonian.

For completeness of this manuscript the extensively used remaining two-body segment value tables, derived by Shavitt,[283,284] are listed here, where the entries are given in terms of the auxiliary functions A and C (3.84) given in Sec. 3.4.1 and the additional (with an implicit dependence on the b value of the given CSF $|m\rangle$)

$$B(p,q) = \sqrt{\frac{2}{(b+p)(b+q)}}, \quad D(p) = \sqrt{\frac{(b+p-1)(p+p+2)}{(b+p)(b+p+1)}} \quad \text{and} \quad t = \frac{1}{\sqrt{2}}. \tag{A.37}$$

The variable μ in the listed Tables A.4 and A.5 is related to the concept of Hamiltonian repartitioninig,[284] which is not discussed in this manuscript, and can be assumed to be zero, $\mu = 0$.

Table A.4: Two-body segment values involving two raising or lowering generator. The $\overline{R}\underline{R}$ and $\overline{L}\underline{L}$ segment types have not been split into the $x = 0, 1$ terms. The segment types marked with an asterisk use lower signs where shown, the others use the upper sign. Taken and modified from [284]. (Permission to reproduce this table has been granted by Springer Nature.)

d'd	$\overline{RR}$, $\underline{LL}$	
	x = 0	x = 1
03	$\sqrt{2}$	0

d'd	$\underline{RR}$, $\overline{LL}$	
	x = 0	x = 1
30	$\sqrt{2}$	0

d'd	$\overline{RR}$, $R\overline{R}$		$\overline{LL}$, $L\overline{L}$	
	Δb = -1	Δb = 1	Δb = -1	Δb = 1
00	$\frac{1}{2}\mu$	$\frac{1}{2}\mu$	$\frac{1}{2}\mu$	$\frac{1}{2}\mu$
11	$1-\frac{1}{2}\mu$	$\frac{1}{2}\mu C(0)$	$\frac{1}{2}\mu C(1)$	$1-\frac{1}{2}\mu$
12	$1-\frac{1}{2}\mu/(b+2)$	-	$1+\frac{1}{2}\mu/(b+1)$	-
21	-	$1+\frac{1}{2}\mu/b$	-	$1-\frac{1}{2}\mu/(b+1)$
22	$\frac{1}{2}\mu C(2)$	$1-\frac{1}{2}\mu$	$1-\frac{1}{2}\mu$	$\frac{1}{2}\mu C(1)$
33	$1-\frac{1}{2}\mu$	$1-\frac{1}{2}\mu$	$1-\frac{1}{2}\mu$	$1-\frac{1}{2}\mu$

d'd	$R\overline{R}$, $\overline{R}R^*$				$L\underline{L}$, $\underline{L}L^*$			
	Δb = -1		Δb = 1		Δb = -2	Δb = 0		Δb = 2
	x = 0	x = 1	x = 0	x = 1	x = 1	x = 0	x = 1	x = 1
01	0	±1	tA(1,0)	∓tA(-1,0)	-	tA(0,1)	±tA(2,1)	±1
02	tA(1,2)	±tA(3,2)	0	±1	±1	tA(2,1)	∓tA(0,1)	-
13	-t	∓tA(0,2)	0	±A(-1,0)	±A(3,2)	-t	±tA(2,0)	-
23	0	±A(3,2)	-t	±tA(2,0)	-	-t	∓tA(0,2)	±A(-1,0)

d'd	$\underline{RR}$, $\underline{RR}^*$				$\overline{LL}$, $\overline{LL}^*$			
	Δb = -2	Δb = 0		Δb = 2	Δb = -1		Δb = 1	
	x = 1	x = 0	x = 1	x = 1	x = 0	x = 1	x = 0	x = 1
10	±1	tA(0,1)	±tA(2,1)	-	tA(2,1)	∓tA(0,1)	0	±1
20	-	tA(2,1)	∓tA(0,1)	±1	0	±1	tA(0,1)	±tA(2,1)
31	-	-t	±tA(2,0)	±A(1,0)	0	±A(0,1)	-t	∓tA(-1,1)
32	±A(1,2)	-t	∓tA(0,2)	-	-t	±tA(3,1)	0	±A(2,1)

d'd	RR				LL			
	Δb = -2	Δb = 0		Δb = 2	Δb = -2	Δb = 0		Δb = 2
	x = 1	x = 0	x = 1	x = 1	x = 1	x = 0	x = 1	x = 1
00	1	1	1	1	1	1	1	1
11	1	-1	-D(0)	D(-1)	D(1)	-1	-D(0)	1
12	B(2,3)	0	B(1,2)	-	B(1,2)	0	B(0,1)	-
21	-	0	B(0,1)	B(-1,0)	-	0	B(1,2)	B(0,1)
22	D(2)	-1	-D(1)	1	1	-1	-D(1)	D(0)
33	1	1	1	1	1	1	1	1

Table A.5: Two-body segment values involving one raising and one lowering generator. The $\overline{R}\underline{L}$ and $\underline{R}\overline{L}$ segment types have not been split into the $x = 0, 1$ terms. The relative sign of the contribution is independent of order of the generators for two mixed contributions. Taken and modified from [284]. (Permission to reproduce this table has been granted by Springer Nature.)

d'd	$\overline{RL}$	
	Δb = -1	Δb = 1
03	A(2,1)	A(0,1)

d'd	$\underline{RL}$	
	Δb = -1	Δb = 1
30	A(1,2)	A(1,0)

d'd	$\overline{RL}$		$\underline{RL}$	
	x = 0	x = 1	x = 0	x = 1
00	-tμ	0	tμ	0
11	t(1-μ)	-tA(-1,1)	t(μ-1)	tA(2,0)
12	0	1	0	C(2)
21	0	1	0	C(0)
22	t(1-μ)	tA(3,1)	t(μ-1)	-tA(0,2)
33	t(2-μ)	0	t(μ-2)	0

d'd	$\overline{RL}$				$\underline{RL}$			
	Δb = -1		Δb = 1		Δb = -2	Δb = 0		Δb = 2
	x = 0	x = 1	x = 0	x = 1	x = 1	x = 0	x = 1	x = 1
01	0	1	t	-tA(-1,1)	-	-t	tA(2,0)	C(0)
02	t	tA(3,1)	0	1	C(2)	-t	-tA(0,2)	-
13	tA(2,1)	tA(0,1)	0	-A(0,1)	-A(3,2)	-tA(0,1)	-tA(2,1)	-
23	0	-A(2,1)	tA(0,1)	-tA(2,1)	-	-tA(2,1)	tA(0,1)	-A(-1,0)

d'd	$\underline{RL}$				$\underline{R}\overline{L}$			
	Δb = -2	Δb = 0		Δb = 2	Δb = -1		Δb = 1	
	x = 1	x = 0	x = 1	x = 1	x = 0	x = 1	x = 0	x = 1
10	C(2)	-t	tA(2,0)	-	t	-tA(0,2)	0	1
20	-	-t	-tA(0,2)	C(0)	0	1	t	tA(2,0)
31	-	-tA(0,1)	-tA(2,1)	-A(1,0)	0	-A(1,2)	tA(1,0)	tA(-1,0)
32	-A(1,2)	-tA(2,1)	tA(0,1)	-	tA(1,2)	-tA(3,2)	0	-A(1,0)

d'd	RL			
	Δb = -2	Δb = 0		Δb = 2
	x = 1	x = 0	x = 1	x = 1
00	1	1	1	1
11	-C(2)	1	D(0)	-C(0)
12	$-\sqrt{2}/(b+2)$	0	-B(0,2)	-
21	-	0	-B(0,2)	$-\sqrt{2}/b$
22	-C(2)	1	D(1)	-C(0)
33	1	1	1	1

A.3 Weighted Orbital Choice with GUGA Restrictions

A note on the weighting of the integral contribution to the orbital picking process: As one can see in Eq. (A.32) and (A.35) it is not as easy as in a SD based implementation to weight an integral contribution of orbitals by the exact matrix element, V_{ikjl} for spin-opposite and $V_{ikjl} - V_{iklj}$ for spin parallel excitations, as it is done in the current FCIQMC implementation. Since the relative sign of the w_0 and w_1 contribution (A.30, A.31) depends on the chosen excitation $|m'\rangle$ and can not be easily predetermined and there is no notion of a m_s quantum number in a spin-adapted calculation. Our choice was to weight the integral contribution by the magnitude of the integrals $|V_{ikjl}| + |V_{iklj}|$ to capture the strongest couplings at least. This leads to some inefficiencies in the excitation generation of the CSF based implementation. See Sec. 4.3 for a study on the effect.

A.3.1 Restrictions on the Orbital Choice for Single Excitations

To ensure at least one possible non-zero excitation, $\hat{E}_{ij}\,|m\rangle$, we have to place some additional restriction on the choice of orbital (i, j) compared to a SD-based implementation. The idea is to first pick an electron in an occupied spatial orbital j at random with $p(j) = 1/N$. Depending on the step-value d_j certain restriction on the to-be-picked orbital i are placed. A general restriction is that i must not be doubly occupied $d_i \neq 3$.

If $d_j = 3$, since both Δb branches can end at d_j for raising generators R ($i < j$) and also both branches can start for a lowering generator L ($i > j$) there are no additional restrictions on the orbital i, except $d_i \neq 3$.

For $d_j = 1$ there is only a $\Delta b_j = +1$ start $\underline{L}$ and a $\Delta b_{j-1} = -1$ end $\overline{R}$ possible. So there is the restriction, that d_i must be 0, which allows both Δb branches to start or to end, or $d_i = 2$, which would lead to the correct $\Delta b_i = -1$ start for $\underline{R}$ or would allow the $\Delta b_{i-1} = +1$ end for $\overline{L}$. A $d_i = 1$ value is only allowed, if there is a valid switch possibility $d_k = 2$ in the range (i, j). For a chosen $d_j = 2$ electron orbital the restrictions are similar with $d_i = \{0, 1\}$ being valid in general, and $d_i = 2$ only if a switch possibility $d_k = 1$ for $k \in (i, j)$. The actual restriction is implemented by finding the adjacent opposite spin-coupled orbitals i_{lower} and i_{upper} for a $d_j = \{1, 2\}$ and only allowing $d_i = d_j$ to be picked if $i < i_{lower}$ or $i > i_{upper}$. A flow-chart of this decision-making process is given in Fig. A.3.

If we want to make use of point group symmetry it is much easier than suggested in the literature,[39] to just restrict the choice of orbital i from the symmetry allowed orbitals n_j corresponding to the picked electron orbital j.

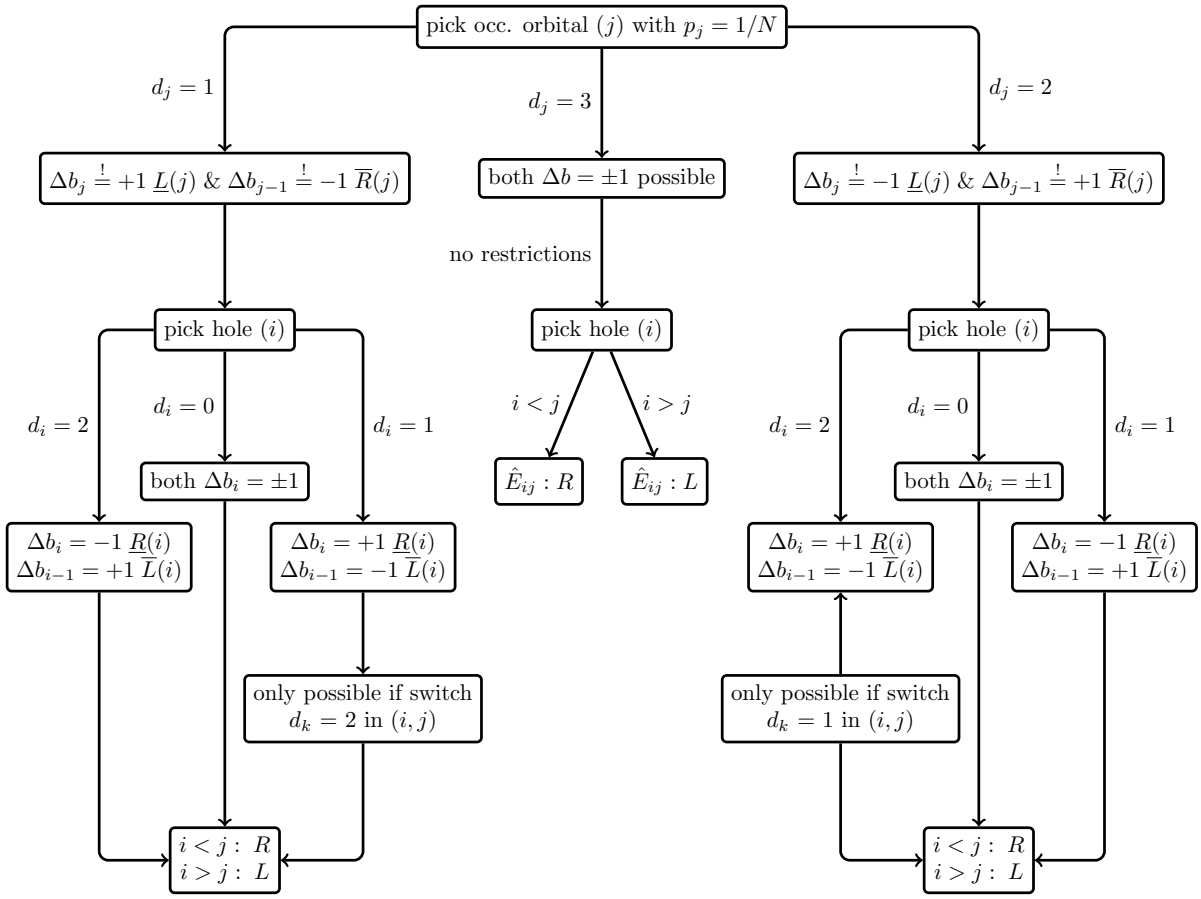

Figure A.3: Flow-chart of the decision-making process to find a valid index combination (i, j) to ensure at least one non-zero single excitation $\hat{E}_{ij}\,|m\rangle$ and determine the type of generator, R or L, depending on the order of i and j.

A.3.2 Restriction on the Orbital Choice for Double Excitations

The excitation generation for doubles is a bit more involved, but due to the product structure of the matrix elements (3.98). We follow the same approach as for single excitations to pick the four orbitals of $\hat{e}_{ij,kl}$ in such a manner to have the probability $p(ijkl)$ be related to the integral contribution of the Hamiltonian matrix element and at the same time ensure that at least one valid excitation can be reached.

We first pick the ordered electron pair ($j < l$) at random with a probability $p(jl) = 1/N_{pairs}$, where N_{pairs} is the number of electron pairs in the simulation. The first orbital (i) to excite to is then picked out of all, non-doubly occupied $d_i \neq 3$ orbitals, weighted with the Cauchy-Schwarz inequality based approximation[139,300] of the integral contribution V_{ijkl}, see Sec. 2.3.8

The major change, compared to SD based implementation, now comes only in the choice of the second orbital (k) to excite to. Here we place the restrictions depending on the possible used spatial symmetry and the additional restriction, due to the UGA to obtain non-zero excitations. Additionally, we restrict the picking of orbital (k) in such a way that we do not pick *quasi*-single excitations, which are already taken account of in the single excitation matrix elements, explained in Section A.2.2. The overall restriction $d_k \neq 3$ remains of course.

To formulate the conditions for a valid orbital index choice, (i, j, k, l), we have to look at the properties of the non-zero two-body segment shapes. The *semi-start* segments, $\underline{L}L, \underline{R}R$, behave similar to single segment shapes concerning the restrictions on the in-coming and out-going Δb values of an excitation and are listed in Table A.6. And similar to the end of a single excitation there are certain restriction for non-zero two-body elements at the end of the overlap range, depending on the type of the two alike generators, see Table A.7. As one can see in these tables these segments behave like a single-excitation starts for an in-going $\Delta b_{k-1} = 0$ branch and like a single excitation end segment for the approaching $\Delta b_{k-1} = \pm 2$ branches.

For two-body generators with identical starting indices, $\hat{e}_{ij,ik}$, only the $\Delta b_k = 0$ branch contributes, due to a zero $x = 1$ matrix element in the overlap region.[284] In addition only a $\Delta b_k = 0$ branch leads to a non-zero matrix element with two coinciding upper indices, $\hat{e}_{ij,kj}$. This means that for the $\underline{R}R$ or $\underline{L}L$ segments only the $\Delta b_k = 0$ branch can be chosen. So these type of double excitations can be treated very similar to single excitations, since the $x = 0$ contribution is very easy to compute, (-1^{n_2}, with n_1 being the number of singly occupied orbitals in the overlap region) and are only non-zero if $d'_k = d_k$ in the overlap range. So no switch decisions have to be made in the excitation generation.

The case of mixed generators $R+L$ is a bit more involved. A simultaneous start $e_{ij,ki}$ acts similar to an usual double intermediate segment value, except that a $d_i = 0$ value leads to a zero matrix element, see Tables A.8 and A.5. And similar to intermediate segment

Table A.6: $L\underline{L}, \underline{L}L^*$ and $\underline{R}R, R\underline{R}^*$ contributions at the overlap range start. * indicates the sign change of the $x = 1$ matrix element, depending on the order of operators. $N'_k = N_k - 2$ for two lowering generators and $N'_k = N_k + 2$ for two raising generators. And RR and LL intermediate segments in the overlap region of a double excitation, depending on Δb_{k-1}.

$L\underline{L}/\underline{L}L^*$				$\underline{R}R/R\underline{R}^*$				$RR\,/\,LL$				
Δb_{k-1} :		-1	+1			-1	+1			0	-2	+2
d'	d	Δb_k		d'	d	Δb_k		d'	d	Δb_k		
0	1	0	+2	1	0	-2	0	0	0	0	-2	+2
0	2	-2	0	2	0	0[a]	+2[b]	1	1	0	-2	+2
1	3	-2	0	3	1	0	+2	2	1	+2[b]	0[a]	−
2	3	0[a]	+2[b]	3	2	-2	0	1	2	-2	−	+2[b]
								2	2	0	-2[a]	+2[b]
								3	3	0	-2	+2

[a] No b_k restriction, since $\Delta b_{k-1} = -1$ or $\Delta b_{k-1} = -2$.
[b] This path is only possible if $b_k > 1$, otherwise $S_k < 0$.

Table A.7: Segment value restriction for the end of the overlap range for two lowering generators $\overline{L}L, L\overline{L}^*$, and two raising generators $R\overline{R}, \overline{R}R^*$, depending on Δb_{k-1} value. $N'_k = N_k \pm 1$ depending on the generator type. * indicated that the $x = 1$ matrix element contribution has opposite sign for exchanged order of generators.

$\overline{L}L\,/\,L\overline{L}^*$				$R\overline{R}\,/\,\overline{R}R^*$			
d'	d	Δb_{k-1}	Δb_k	d'	d	Δb_{k-1}	Δb_k
1	0	0	-1	0	1	0	+1
		+2	+1			-2	-1
2	0	0	+1[a]	0	2	0	-1
		-2	-1			+2	+1
3	1	0	+1	1	3	0	-1
		-2	-1			+2	+1
3	2	0	-1	2	3	0	+1[a]
		+2	+1			-2	-1

[a] Only possible if $b_k > 0$, otherwise $S_k < 0$.

Table A.8: $\underline{RL}$ starting segments, where there is no change in the orbital occupation number $N'_k = N_k$. And $\overline{RL}$ end segment restrictions, depending on the Δb_{k-1} value.

		$\underline{RL}$	$\overline{RL}$
d'	d	Δb_k	Δb_{k-1}
1	1	0	0
2	1	+2[a]	-2
1	2	-2	+2
2	2	0	0
3	3	0[b]	0[b]

[a] Only for $b_k > 1$.
[b] $x = 1$ matrix element is zero.

values of alike generators in the overlap region, the $x = 0$ matrix elements are zero for the $\Delta b_k = \pm 2$ branches.

As one can see in Table A.5 of the mixed two-body segment values, the $x = 1$ contribution is zero for $d_i = 3$, but not for the $\Delta b_k = 0$ branches of $d_i = \{1, 2\}$. This leads to a major complication in the implementation of CSFs in the FCIQMC algorithm through the GUGA approach. These contributions with no change in step-value with a non-zero matrix element correspond to an exchange type contribution to double excitations. Since in the FCIQMC excitation generation it is necessary to uniquely assign a definite probability $p(m'|m)$, different starting orbitals $i' < I$, with I indicating the first step-value change Δd_I, can contribute to an excitation with a $\underline{RL}$ start. The matrix element influence was mentioned in Section A.2, but also the probabilities, $p(i')$, for all possible other starting orbitals $i' < I$ have to be accounted for. Similarly for an $\overline{RL}$ end, all other possible $j' > J$, with J indicating the last step-value change Δd_J, ending orbitals have to taken into account. And for a pure exchange type excitation (type 2c in Table 4.3) $\underline{RL} \rightarrow \overline{RL}$ all combinations ($i' < I, j' > J$) of possibly contributing orbitals have to be considered in the matrix element and generation probability computation. See A.2 for more details on the matrix element calculation of these excitations.

Otherwise a $R\underline{L}$ segment behaves similar to an $L\underline{L}$ and $\underline{R}L$ to an $\underline{R}R$ in terms of d'_k, b_k and Δb_{k-1} restrictions, except the number of electrons in $N'_k = N_k$. Also the intermediate RL segments behave as LL and RR and the $R\overline{L}$ is equivalent to $L\overline{L}$ and $L\overline{R}$ to $R\overline{R}$ respectively. Except the electron number difference becomes the corresponding value $N'_k = N_k \pm 1$ of the ongoing excitation (R in the case of $R\overline{L}$ and L for $L\overline{R}$). It should also be noted, that a $\Delta b_k = 0$ branch can end at any $d_j \neq 0$ value, whereas $\Delta b_k = -2$ is restricted to $d_j = 1$ and $\Delta b_k = +2$ to $d_j = 2$, to be able to align the S_k value of $|m'\rangle$ and $|m\rangle$, so they coincide outside of the range of the generator $\hat{e}_{ij,jl}$. Since $\Delta b_k = 0$ already indicates $|m'\rangle = |m\rangle$ in the overlap range, this issue is no problem in a direct CI calculation with CSFs, but is burdensome to implement in FCIQMC, since we want to be able to get one out of all possible excitations for a given CSF $|m\rangle$ and assign it a unique generation probability. So we also have to take into account all other possible

index combinations, which would be able to lead to this excitation and sum their matrix elements of course, but also recompute the probability.

Due to the uniqueness for most type of excitations, this is no problem, but only in the case of these exchange type excitations with coinciding indices and a RL generator combination. Unfortunately we have not yet found a more elegant way to treat these cases, except implement it in the most efficient way. With a heavy re-usage of terms to avoid an $\mathcal{O}(N^2)$ or even $\mathcal{O}(n^2)$ computational cost of these excitations.

A.3.3 Orbital Picking and Excitation Identification

In the following, the work flow of picking a valid index combination (i, j, k, l) for a non-zero double excitation of a CSF $|m\rangle$ in the FCIQMC method is presented. A flow-chart of the decision-making process is shown in Fig. A.4.

Both electron indices ($j < l$) and the first hole index (i) are picked with uniform or a weighted probability. If both picked electrons are in the same spatial orbital $\underline{j = l \rightarrow d_j = 3}$, similar restrictions as for *single excitations* apply, for the remaining orbitals i and k. Of course both orbitals i and k have to be non-doubly occupied. This applies in general, independent of the relation of electron orbitals j and l and their step-value d_j, d_l. And $i = k$ is only possible if $d_k = 0$, since both electrons will be excited to the same spatial orbital. Since both electrons get removed from the same orbital the only possible excitation types are (1b,1c,1d,2a,2b) of Table 4.3. If $i = k$ the type of excitation is (2a) if $i > j$, or (2b) if $i < j$, requiring $d_i = 0$. For $i \neq k$ the same restrictions as for single excitations apply, that $d_i = d_k = 1$ is only possible if a switch possibility $d_m = 2$ in the range (i, k) and vice versa for $d_i = d_k = 2$. The type of excitation only depends on the order of the involved indices. As already mentioned, all these excitations require $\Delta b_m = 0$ in the overlap range. With the trivial case of type (1b) excitation with a single orbital overlap range. Which make the calculation of the excitation very similar to single excitations.

If the electron indices are not equal $j \neq l$, the picking of the remaining orbitals k and i depends more strongly on the step-values of the already chosen orbitals (j, l).
If $\underline{d_j = d_l = 3}$ there is no additional restriction on orbital k, since in except of b value restrictions on starts of a doubly occupied orbital ($\Delta b = +1$ branch forbidden due to $b = 0$, e.g.) all restrictions mentioned in the previous Section A.3.2 can be accounted for, due to the flexibility of the $d_j = d_l = 3$ step-values.

If $i = k$, depending on the order of the indices this leads to excitations of type (1a,1d) or (1g), since $i \neq j, l$ due to $d_j = d_l = 3$. These excitations again can be easily treated, due to the single overlap region (1a) or a necessary $\Delta b_m = 0$ in the overlap region.

If $i \neq k$ all 4 indices are different, leading to a type (3*) excitation depending on the order of the indices. Where again, the exchange type excitation is chosen by definition and not

a possibly non-overlap double excitation ($3c_0$,$3d_0$,$3e_0$,$3f_0$).

If $\underline{d_j = 3, d_l = \{1,2\}}$: Depending on if the already picked first orbital to excite to $i = l$, orbital k must be restricted to $k < l$. This is because $k > l$ would lead to an exchange contribution to a single excitation, which is already taken into account for in the singles matrix elements. This leads to excitations of type (1e) or (1f) depending on the order of k and j. If $i > l$ orbital $k \neq l$ since this again would lead to an already accounted exchange contribution to a single excitation. If $i = k$ it is an (1d) excitation otherwise it is one of the type (3*) depending on the relation of the indices. If $i < l$ there is no restriction on the indices for k and this can lead to a variety of excitations.

If $\underline{d_j = \{1,2\}, d_l = 3}$: There are similar restrictions considering the already picked orbitals. If $i = j$, k must be picked $k > j$ to avoid choosing already accounted for exchange contributions to single excitations. And if $i < j$ k must not be j, otherwise there are no additional restrictions.

If both $\underline{d_j = \{1,2\}}$ and $\underline{d_l = \{1,2\}}$ are singly occupied the most stringent restrictions apply. If $i = l$ there should be a possible switch between the already picked j and l if both have the same step-value $d_j = d_l$, since otherwise it would not be possible to fulfil the Δb criteria at the end of an excitation to lead to a non-zero excitation. Additionally, orbital k has to be lower than i, otherwise it is again an exchange contribution to a single excitation. Depending on the order of the orbitals, this leads to type (1e,1f,2c) excitation, which, already mentioned, needs additional re-computation of matrix element and generation probability contribution.

If $i = j$, there also must be a switch possibility for $d_j = d_l$ between $jandl$ and $k > j$. This leads to type (1i,1j,2c) excitations. With the necessity of recalculation of matrix element and generation probability contributions.

If $i > j$ orbital k must not be l to avoid an exchange contribution to singles and similarly if $i < j$, k must not be j. And k can only coincide with j for $i > j$, if there is a switch possibility between j and l, if $d_j = d_l$. And similar for $i < j$, $k = l$ is only possible if $d_j \neq d_l$ or there is a switch possibility between j and l. Otherwise no restrictions are place on the picking of orbital k and the type of excitation depends on the order of the indices and can lead to all sort of excitation types in Table 4.3.

In the whole picking process, since we allow the empty orbitals to be picked in any order, in addition to $p(i|jkl)$ we also have to recompute $p(k|ijl)$ of having picked the orbitals in the opposite order, since they lead to the same possible excitation. This increases the generation probability by 2 in general, but introduces the effort to recompute. We could, similar to the electron orbitals j and l, decide to pick only orbitals $i < l$, which would also make the identification of the excitation type easier.

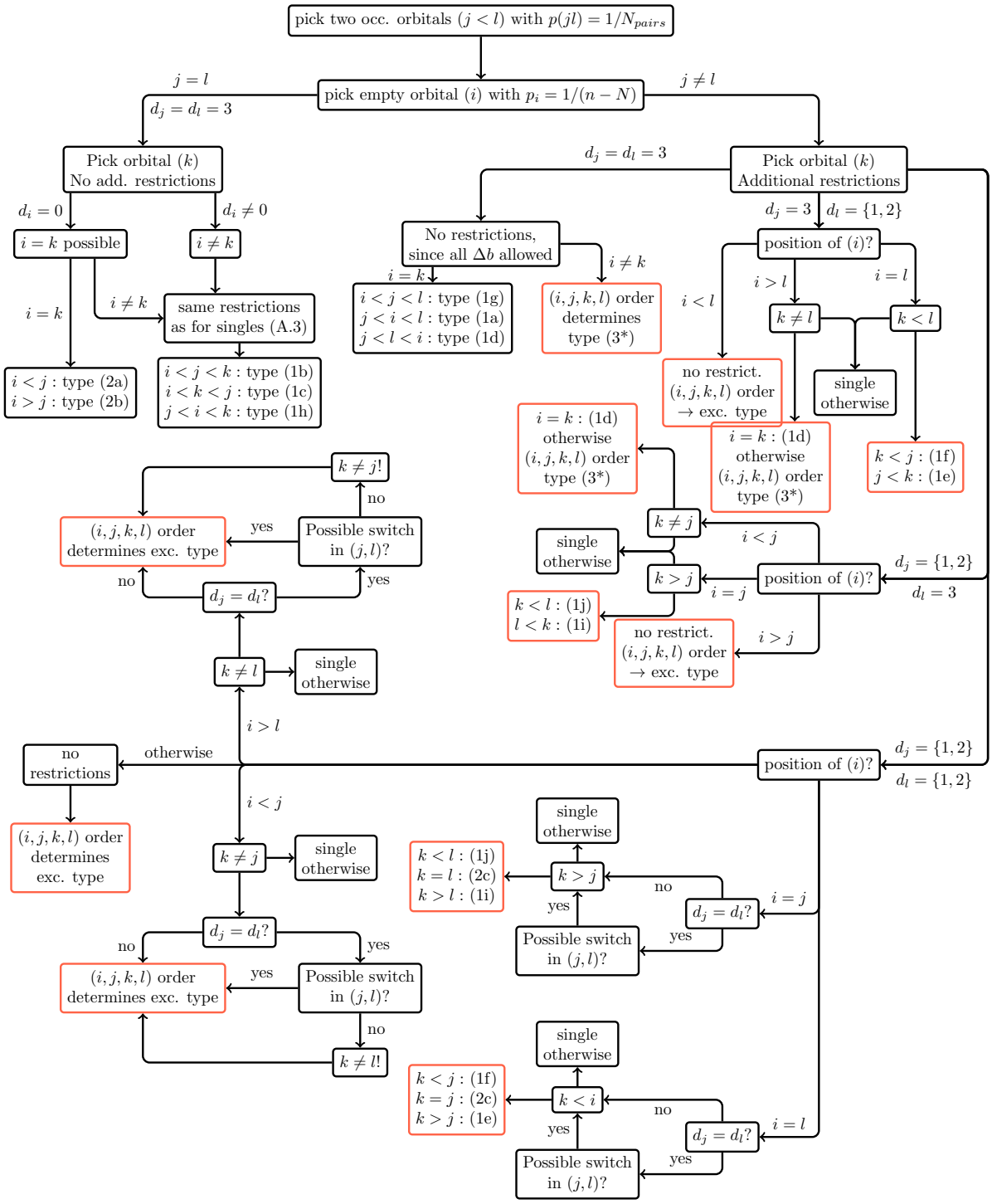

Figure A.4: Flow-chart of the decision-making process to find a valid index combination (i, j, k, l) to ensure at least one non-zero double excitation $\hat{e}_{ij,kl}\,|m\rangle$ and identify the excitation type based on these indices.

B

The Similarity Transformed Hamiltonian

B.1 Analytic Optimization of J in the Thermodynamic Limit at Half-Filling

The results in this chapter were obtained in collaboration with Hongjun Luo and Ali Alavi and parts of the remaining chapter are included in the published article:[69]
Compact numerical solutions to the two-dimensional repulsive Hubbard model obtained via nonunitary similarity transformations. Werner Dobrautz, Hongjun Luo and Ali Alavi, Phys. Rev. B **99**, 075119 (2019)

For an infinite system at half-filling, we define

$$T_0(\mathbf{k}) = \frac{1}{M}\sum_{\mathbf{q}} \Theta(\epsilon_F - \epsilon_{\mathbf{q}})\Theta(\epsilon_{\mathbf{q}+\mathbf{k}} - \epsilon_F), \tag{B.1}$$

$$T_1(\mathbf{k}) = \frac{1}{M}\sum_{\mathbf{p}} \Theta(\epsilon_F - \epsilon_{\mathbf{p}})\Theta(\epsilon_{\mathbf{p}-\mathbf{k}} - \epsilon_F)\sum_{\mathbf{d}} e^{i(\mathbf{p}-\mathbf{k})\cdot\mathbf{d}}, \tag{B.2}$$

$$T_2(\mathbf{k}) = \frac{1}{M}\sum_{\mathbf{p}} \Theta(\epsilon_F - \epsilon_{\mathbf{p}})\Theta(\epsilon_{\mathbf{p}-\mathbf{k}} - \epsilon_F)\sum_{\mathbf{d}} e^{i\mathbf{p}\cdot\mathbf{d}}. \tag{B.3}$$

The 2-body contributions of Eq. (5.25) in Section 5.3.2 can be expressed as

$$\frac{U}{2}\frac{1}{M}\sum_{\mathbf{k}} T_0^2(\mathbf{k}) - \frac{t}{M}\left((e^J - 1)\sum_{\mathbf{k}} T_0(\mathbf{k})T_1(\mathbf{k}) + (e^{-J} - 1)\sum_{\mathbf{k}} T_0(\mathbf{k})T_2(\mathbf{k})\right) = 0. \tag{B.4}$$

In the thermodynamic limit ($M \to \infty$) the summation in the expression of the T_m factors (B.1-B.3) become integrals

$$\frac{1}{M}\sum_{\mathbf{q}} \longrightarrow \frac{1}{(2\pi)^d}\int d^d q.$$

For an unpolarized system at half filling, the factor $\Theta(\epsilon_F - \epsilon_{\mathbf{q}})$ leads to a square region in the $k_x - k_y$ plane and $T_m(\mathbf{k})$ integrals can be easily calculated after a rotation of coordinates

$$k'_x = \frac{1}{\sqrt{2}}(k_x - k_y), \quad k'_y = \frac{1}{\sqrt{2}}(k_x + k_y). \tag{B.5}$$

With this rotation, T_0 is found to be symmetric with respect to $k'_x \to -k'_x$ and $k'_y \to -k'_y$, so it reduces to a function of $|k_x|$ and $|k_y|$

$$T_0(\mathbf{k}) = \frac{1}{(2\pi)^2}\int \Theta(\epsilon_F - \epsilon_{\mathbf{q}})\Theta(\epsilon_{\mathbf{q}+\mathbf{k}} - \epsilon_F) d^2q \tag{B.6}$$

$$= \frac{1}{(2\pi)^2}\left(\int_{-\pi/\sqrt{2}}^{-\pi/\sqrt{2}+|k'_x|}\int_{-\pi/\sqrt{2}+|k'_y|}^{\pi/\sqrt{2}} dq'_x dq'_y + \int_{-\pi/\sqrt{2}+|k'_x|}^{\pi/\sqrt{2}}\int_{-\pi/\sqrt{2}}^{-\pi/\sqrt{2}+|k'_y|} dq'_x dq'_y\right) \tag{B.7}$$

$$= \frac{1}{(2\pi)^2}\left(\sqrt{2}\pi(|k'_x| + |k'_y|) - 2|k'_x k'_y|\right) \tag{B.8}$$

$$= \frac{1}{(2\pi)^2}\left(\pi(|k_x - k_y| + |k_x + k_y|) - |k_x^2 - k_y^2|\right). \tag{B.9}$$

With the coordinate rotation (B.5), the integrand of T_1 can be factorized as

$$\begin{aligned}\sum_{\mathbf{d}} e^{i(\mathbf{p}-\mathbf{k})\cdot\mathbf{d}} &= \cos(p_x - k_x) + \cos(p_y - k_y)\\ &= \cos\left(\frac{1}{\sqrt{2}}(p'_x - k'_x) + \frac{1}{\sqrt{2}}(p'_y - k'_y)\right) + \cos\left(\frac{1}{\sqrt{2}}(p'_x - k'_x) - \frac{1}{\sqrt{2}}(p'_y - k'_y)\right)\\ &= 2\cos\left(\frac{1}{\sqrt{2}}(p'_x - k'_x)\right)\cos\left(\frac{1}{\sqrt{2}}(p'_y - k'_y)\right),\end{aligned}$$

and T_1 can also be found as a function of $|k_x|$ and $|k_y|$

$$T_1(\mathbf{k}) = \frac{16}{(2\pi)^2}\left[\cos\left(\frac{k_x - k_y}{2}\right)\cos\left(\frac{k_x + k_y}{2}\right) - 1\right]. \tag{B.10}$$

Similarly T_2 can be calculated as

$$T_2(\mathbf{k}) = \frac{16}{(2\pi)^2}\left[1 - \cos\left(\frac{k_x - k_y}{2}\right)\cos\left(\frac{k_x + k_y}{2}\right)\right] = -T_1(\mathbf{k}). \tag{B.11}$$

The exchange part of the three body contribution in (5.25) to the correlation energy can be calculated as (using here again the rotation (B.5) for $\mathbf{p}$)

$$\begin{aligned}&\frac{1}{M^2}\sum_{\mathbf{pqk}\sigma}\left(n_{\mathbf{p},\sigma}n_{\mathbf{q}+\mathbf{k},\bar{\sigma}}n_{\mathbf{q},\bar{\sigma}}\sum_{\mathbf{d}}\cos(\mathbf{p}\cdot\mathbf{d})e^{i\mathbf{k}\cdot\mathbf{d}}\right)\\ &= \frac{1}{M}\sum_{\mathbf{pk}\sigma}\left(n_{\mathbf{p},\sigma}(\frac{1}{2} - T_0(\mathbf{k}))\sum_{\mathbf{d}}\cos(\mathbf{p}\cdot\mathbf{d})e^{i\mathbf{k}\cdot\mathbf{d}}\right)\\ &= \frac{2M}{(2\pi)^4}\int\int_{-\pi/\sqrt{2}}^{\pi/\sqrt{2}} dp'_x dp'_y \int\int_{-\pi}^{\pi} dk_x dk_y \times \left(\frac{1}{2} - \frac{1}{(2\pi)^2}\left(\pi(|k_x - k_y| + |k_x + k_y|) - |k_x^2 - k_y^2|\right)\right)\\ &\times\left(\cos(\frac{p'_x + p'_y}{\sqrt{2}})\cos(k_x) + \cos(\frac{p'_x - p'_y}{\sqrt{2}})\cos(k_y)\right) = \frac{32M}{\pi^6}.\end{aligned} \tag{B.12}$$

The final results are

$$T_0(\mathbf{k}) = \frac{1}{(2\pi)^2}\left(\pi(|k_x - k_y| + |k_x + k_y|) - |k_x^2 - k_y^2|\right), \tag{B.13}$$

$$T_1(\mathbf{k}) = \frac{16}{(2\pi)^2}\left[\cos\left(\frac{k_x - k_y}{2}\right)\cos\left(\frac{k_x + k_y}{2}\right) - 1\right], \tag{B.14}$$

$$T_2(\mathbf{k}) = -T_1(\mathbf{k}), \tag{B.15}$$

and the summations can also be calculated as integrals

$$\frac{1}{M}\sum_{\mathbf{k}} T_0^2(\mathbf{k}) = \frac{5}{72}, \tag{B.16}$$

$$\frac{1}{M}\sum_{\mathbf{k}} T_0(\mathbf{k})T_1(\mathbf{k}) = -\frac{16+\pi^4}{\pi^6}. \tag{B.17}$$

J_{opt}^{TDL} can be obtained by solving

$$\frac{5U}{144} + t\frac{16+\pi^4}{\pi^6}\left((e^J - e^{-J}\right) = 0, \tag{B.18}$$

which, for small U/t, can be approximated as

$$J_{opt}^{TDL} = \text{argsinh}(-\frac{5U}{288t} \times \frac{\pi^6}{16+\pi^4}) \approx -0.14717\frac{U}{t}. \tag{B.19}$$

At half-filling Hartree-Fock energy of the original Hubbard Hamiltonian (5.18), with $\mathbf{k} = 0$ in the two-body term,

$$E_{HF}^{J=0} = \left\langle -t\sum_{\mathbf{k},\sigma}\epsilon_{\mathbf{k}} n_{\mathbf{k},\sigma}\right\rangle_{HF} + \frac{U}{2}\left\langle \frac{1}{M}\sum_{\mathbf{p},\mathbf{q},\sigma} n_{\mathbf{p},\sigma} n_{\mathbf{q},\bar{\sigma}}\right\rangle_{HF} \tag{B.20}$$

results to

$$E_{HF}^{J=0} = M\left(-t\frac{64}{(2\pi)^2} + \frac{U}{4}\right) \tag{B.21}$$

in the thermodynamic limit (TDL). The additional contributions arising due to the similarity transformation

$$E_{HF}^{J} = \left\langle -2t\frac{\cosh(J-1)}{M}\sum_{\mathbf{p},\mathbf{q},\sigma}\epsilon_{\mathbf{p}} n_{\mathbf{p},\sigma} n_{\mathbf{q},\bar{\sigma}}\right\rangle_{HF} - \left\langle 2t\frac{\cosh(J-1)}{M^2}\sum_{\mathbf{p},\mathbf{q},\mathbf{k},\sigma}\epsilon_{\mathbf{p}+k} n_{\mathbf{p},\sigma} n_{\mathbf{q}+\mathbf{k},\bar{\sigma}} n_{\mathbf{q},\bar{s}}\right\rangle_{HF} \tag{B.22}$$

can be estimated, with $\cosh(J-1) \approx J^2$ for small J and Eq. (B.12), as

$$E_{HF}^{J} \approx -tJ^2 M\left(\frac{16}{(2\pi)^2} + \frac{64}{\pi^6}\right). \tag{B.23}$$

Hence, the energy per site in the TDL for an unpolarized system at half-filling is given

by

$$E_{opt}^{TDL} = -t\frac{64}{(2\pi)^2} + \frac{U}{4} - tJ^2\left(\frac{16}{(2\pi)^2} + \frac{64}{\pi^6}\right). \tag{B.24}$$

Bibliography

[1] W. A. Al-Saidi, H. Krakauer, and S. Zhang. A study of H+H_2 and several H-bonded molecules by phaseless auxiliary-field quantum Monte Carlo with plane wave and Gaussian basis sets. *J. Chem. Phys.*, 126(19):194105, 2007.

[2] J. Almlöf, B. J. Deleeuw, P. R. Taylor, C. W. Bauschlicher, and P. Siegbahn. The dissociation energy of N_2. *Int. J. Quantum Chem.*, 36(S23):345, 2009.

[3] J. Almlöf and P. R. Taylor. Atomic Natural Orbital (ANO) Basis Sets for Quantum Chemical Calculations. In P.-O. Löwdin, J. R. Sabin, and M. C. Zerner, editors, *Advances in Quantum Chemistry*, volume 22, page 301. Academic Press, 1991.

[4] E. Anderson, Z. Bai, C. Bischof, S. Blackford, J. Demmel, J. Dongarra, J. Du Croz, A. Greenbaum, S. Hammarling, A. McKenney, and D. Sorensen. *LAPACK Users' Guide*. Society for Industrial and Applied Mathematics, Philadelphia, PA, third edition, 1999.

[5] J. B. Anderson. Diffusion and Greens Function Quantum Monte Carlo Methods. In A. M. J. Grotendorst, D. Marx, editor, *Quantum Simulations of Complex Many-Body Systems: From Theory to Algorithms*, volume 10, page 25. John von Neumann Institute for Computing, Jülich, Germany, 2002.

[6] P. Anderson and N. Ong. Theory of asymmetric tunneling in the cuprate superconductors. *J. Phys. Chem. Solids*, 67(1):1, 2006.

[7] P. W. Anderson. Localized Magnetic States in Metals. *Phys. Rev.*, 124:41, 1961.

[8] P. W. Anderson. The Resonating Valence Bond State in La_2CuO_4 and Superconductivity. *Science*, 235(4793):1196, 1987.

[9] K. Andersson, P.-Å. Malmqvist, and B. O. Roos. Second-order perturbation theory with a complete active space self-consistent field reference function. *J. Chem. Phys.*, 96(2):1218, 1992.

[10] F. Aquilante, J. Autschbach, R. K. Carlson, L. F. Chibotaru, M. G. Delcey, L. De Vico, I. Fdez. Galvn, N. Ferr, L. M. Frutos, L. Gagliardi, M. Garavelli, A. Giussani, C. E. Hoyer, G. Li Manni, H. Lischka, D. Ma, P.-Å. Malmqvist,

T. Mller, A. Nenov, M. Olivucci, T. B. Pedersen, D. Peng, F. Plasser, B. Pritchard, M. Reiher, I. Rivalta, I. Schapiro, J. Segarra-Mart, M. Stenrup, D. G. Truhlar, L. Ungur, A. Valentini, S. Vancoillie, V. Veryazov, V. P. Vysotskiy, O. Weingart, F. Zapata, and R. Lindh. Molcas 8: New capabilities for multiconfigurational quantum chemical calculations across the periodic table. *J. Comput. Chem.*, 37(5):506, 2016.

[11] N. B. Balabanov and K. A. Peterson. Systematically convergent basis sets for transition metals. I. All-electron correlation consistent basis sets for the 3d elements Sc-Zn. *J. Chem. Phys.*, 123(6):064107, 2005.

[12] N. B. Balabanov and K. A. Peterson. Basis set limit electronic excitation energies, ionization potentials, and electron affinities for the 3d transition metal atoms: Coupled cluster and multireference methods. *J. Chem. Phys.*, 125(7):074110, 2006.

[13] R. J. Bartlett. Many-Body Perturbation Theory and Coupled Cluster Theory for Electron Correlation in Molecules. *Annu. Rev. Phys. Chem.*, 32(1):359, 1981.

[14] C. W. Bauschlicher, S. R. Langhoff, and P. R. Taylor. On the electron affinities of the Ca, Sc, Ti and Y atoms. *Chem. Phys. Lett.*, 158(3):245, 1989.

[15] F. Becca, M. Capone, and S. Sorella. Spatially homogeneous ground state of the two-dimensional Hubbard model. *Phys. Rev. B*, 62:12700, 2000.

[16] J. G. Bednorz and K. A. Müller. Possible high-T_c superconductivity in the Ba-La-Cu-O system. *Z. Phys. B*, 64(2):189, 1986.

[17] R. Bellman, R. Corporation, and K. M. R. Collection. *Dynamic Programming*. Rand Corporation research study. Princeton University Press, 1957.

[18] J. Bernoulli. *Ars conjectandi, opus posthumum. Accedit Tractatus de seriebus infinitis, et epistola gallice scripta de ludo pilae reticularis.* Basileae: impensis Thurnisiorum, fratrum, 1713.

[19] G. Berthier. Extension de la methode du champ moleculaire self-consistent a l'etude des couches incompletes [Extension of the method of molecular self-consistent field to the study of incomplete layers] (in French). *C. r. hebd. sances Acad. sci.*, 238:91, 1954.

[20] R. Blankenbecler, D. J. Scalapino, and R. L. Sugar. Monte Carlo calculations of coupled boson-fermion systems. I. *Phys. Rev. D*, 24:2278, 1981.

[21] N. S. Blunt, T. W. Rogers, J. S. Spencer, and W. M. C. Foulkes. Density-matrix quantum Monte Carlo method. *Phys. Rev. B*, 89:245124, 2014.

[22] N. S. Blunt, S. D. Smart, G. H. Booth, and A. Alavi. An excited-state approach within full configuration interaction quantum Monte Carlo. *J. Chem. Phys.*, 143(13):134117, 2015.

[23] N. S. Blunt, S. D. Smart, J. A. F. Kersten, J. S. Spencer, G. H. Booth, and A. Alavi. Semi-stochastic full configuration interaction quantum Monte Carlo: Developments and application. *J. Chem. Phys.*, 142(18):184107, 2015.

[24] N. Bohr. I. On the constitution of atoms and molecules. *Philos. Mag.*, 26(151):1, 1913.

[25] G. H. Booth and A. Alavi et. al. Standalone `NECI` codebase designed for FCIQMC and other stochastic quantum chemistry methods. `https://github.com/ghb24/NECI_STABLE`, 2013.

[26] G. H. Booth, D. Cleland, A. Alavi, and D. P. Tew. An explicitly correlated approach to basis set incompleteness in full configuration interaction quantum Monte Carlo. *J. Chem. Phys.*, 137(16):164112, 2012.

[27] G. H. Booth, D. Cleland, A. J. W. Thom, and A. Alavi. Breaking the carbon dimer: The challenges of multiple bond dissociation with full configuration interaction quantum Monte Carlo methods. *J. Chem. Phys.*, 135(8):084104, 2011.

[28] G. H. Booth et al. Full Configuration Interaction Quantum Monte Carlo: A Game of Life, Death and Annihilation. In *Advanced Methods and Applications in Quantum Chemistry 2012: An international workshop with hands-on exercises using Molpro*, 2012. (Poster).

[29] G. H. Booth, S. D. Smart, and A. Alavi. Linear-scaling and parallelisable algorithms for stochastic quantum chemistry. *Mol. Phys.*, 112(14):1855, 2014.

[30] G. H. Booth, A. J. W. Thom, and A. Alavi. Fermion Monte Carlo without fixed nodes: A game of life, death, and annihilation in Slater determinant space. *J. Chem. Phys.*, 131(5):054106, 2009.

[31] M. Born and J. R. Oppenheimer. Quantum Theory of Molecules. *Ann. Phys.*, 84(20):457, 1927.

[32] Bose. Planck's Gesetz und Lichtquantenhypothese. *Z. Phys.*, 26(1):178, 1924.

[33] M. J. Boyle and J. Paldus. Particle-hole formulation of the unitary group approach to the many-electron correlation problem. II. Matrix element evaluation. *Phys. Rev. A*, 22:2316, 1980.

[34] S. Boys and N. Handy. A calculation for the energies and wavefunctions for states of neon with full electronic correlation accuracy. *Proc. Royal Soc. A*, 310(1500):63, 1969.

[35] S. Boys and N. Handy. A condition to remove the indeterminacy in interelectronic correlation functions. *Proc. Royal Soc. A*, 309(1497):209, 1969.

[36] S. Boys and N. Handy. The determination of energies and wavefunctions with full electronic correlation. *Proc. Royal Soc. A*, 310(1500):43, 1969.

[37] S. F. Boys. Electronic wave functions - I. A general method of calculation for the stationary states of any molecular system. *Proc. Royal Soc. A*, 200(1063):542, 1950.

[38] W. F. Brinkman and T. M. Rice. Application of Gutzwiller's Variational Method to the Metal-Insulator Transition. *Phys. Rev. B*, 2:4302, 1970.

[39] B. R. Brooks, W. D. Laidig, P. Saxe, N. C. Handy, and H. F. S. III. The Loop-Driven Graphical Unitary Group Approach: A Powerful Method for the Variational Description of Electron Correlation. *Phys. Scr.*, 21(3):312, 1980.

[40] B. R. Brooks and H. F. Schaefer. The graphical unitary group approach to the electron correlation problem. Methods and preliminary applications. *J. Chem. Phys.*, 70(11):5092, 1979.

[41] R. J. Buenker and S. D. Peyerimhoff. CI method for the study of general molecular potentials. *Theor. Chem. Acc.*, 12(3):183, 1968.

[42] J. Bünemann, W. Weber, and F. Gebhard. Multiband Gutzwiller wave functions for general on-site interactions. *Phys. Rev. B*, 57:6896, 1998.

[43] L. Bytautas and K. Ruedenberg. Correlation energy extrapolation by intrinsic scaling. IV. Accurate binding energies of the homonuclear diatomic molecules carbon, nitrogen, oxygen, and fluorine. *J. Chem. Phys.*, 122(15):154110, 2005.

[44] M. Capello, F. Becca, M. Fabrizio, S. Sorella, and E. Tosatti. Variational Description of Mott Insulators. *Phys. Rev. Lett.*, 94:026406, 2005.

[45] G. Carleo, F. Becca, S. Moroni, and S. Baroni. Reptation quantum Monte Carlo algorithm for lattice Hamiltonians with a directed-update scheme. *Phys. Rev. E*, 82:046710, 2010.

[46] J. Carlson, J. E. Gubernatis, G. Ortiz, and S. Zhang. Issues and observations on applications of the constrained-path Monte Carlo method to many-fermion systems. *Phys. Rev. B*, 59:12788, 1999.

[47] D. Ceperley. Ground state of the fermion one-component plasma: A Monte Carlo study in two and three dimensions. *Phys. Rev. B*, 18:3126, 1978.

[48] D. Ceperley, G. V. Chester, and M. H. Kalos. Monte Carlo simulation of a many-fermion study. *Phys. Rev. B*, 16:3081, 1977.

[49] D. M. Ceperley and M. H. Kalos. Quantum Many-Body Problems. In *Monte Carlo Methods in Statistical Physics*, page 145. Springer Berlin Heidelberg, 1986.

[50] G. K.-L. Chan and M. Head-Gordon. Highly correlated calculations with a polynomial cost algorithm: A study of the density matrix renormalization group. *J. Chem. Phys.*, 116(11):4462, 2002.

[51] G. K.-L. Chan, M. Kállay, and J. Gauss. State-of-the-art density matrix renormalization group and coupled cluster theory studies of the nitrogen binding curve. *J. Chem. Phys.*, 121(13):6110, 2004.

[52] G. K.-L. Chan and S. Sharma. The Density Matrix Renormalization Group in Quantum Chemistry. *Annu. Rev. Phys. Chem.*, 62(1):465, 2011.

[53] C.-C. Chang and S. Zhang. Spatially inhomogeneous phase in the two-dimensional repulsive Hubbard model. *Phys. Rev. B*, 78:165101, 2008.

[54] C.-C. Chang and S. Zhang. Spin and Charge Order in the Doped Hubbard Model: Long-Wavelength Collective Modes. *Phys. Rev. Lett.*, 104:116402, 2010.

[55] W. Cheney. *Linear Algebra: Theory And Applications*. Jones & Bartlett Learning, 2008.

[56] D. Cleland, G. H. Booth, and A. Alavi. Communications: Survival of the fittest: Accelerating convergence in full configuration-interaction quantum Monte Carlo. *J. Chem. Phys.*, 132(4):041103, 2010.

[57] E. U. Condon. The Theory of Complex Spectra. *Phys. Rev.*, 36(7):1121, 1930.

[58] S. Cook. The P versus NP problem. In *Clay Mathematical Institute; The Millennium Prize Problem*, 2000.

[59] S. A. Cook. The Complexity of Theorem-proving Procedures. In *Proceedings of the Third Annual ACM Symposium on Theory of Computing*, STOC '71, page 151, New York, NY, USA, 1971. ACM.

[60] A. C. Cosentini, M. Capone, L. Guidoni, and G. B. Bachelet. Phase separation in the two-dimensional Hubbard model: A fixed-node quantum Monte Carlo study. *Phys. Rev. B*, 58:R14685, 1998.

[61] E. Dagotto. Correlated electrons in high-temperature superconductors. *Rev. Mod. Phys.*, 66:763, 1994.

[62] C. Dahnken, M. Aichhorn, W. Hanke, E. Arrigoni, and M. Potthoff. Variational cluster approach to spontaneous symmetry breaking: The itinerant antiferromagnet in two dimensions. *Phys. Rev. B*, 70:245110, 2004.

[63] E. R. Davidson. The iterative calculation of a few of the lowest eigenvalues and corresponding eigenvectors of large real-symmetric matrices. *J. Comput. Phys.*, 17(1):87, 1975.

[64] H. De Raedt and A. Lagendijk. Monte Carlo Calculation of the Thermodynamic Properties of a Quantum Model: A One-Dimensional Fermion Lattice Model. *Phys. Rev. Lett.*, 46:77, 1981.

[65] P. A. M. Dirac. On the Theory of Quantum Mechanics. *Proc. Royal Soc. A*, 112(762):661, 1926.

[66] P. A. M. Dirac. The Quantum Theory of the Electron. *Proc. Royal Soc. A*, 117(778):610, 1928.

[67] P. A. M. Dirac. The Quantum Theory of the Electron. Part II. *Proc. Royal Soc. A*, 118(779):351, 1928.

[68] P. A. M. Dirac. *The Principles of Quantum Mechanics (International Series of Monographs on Physics).* Clarendon Press, 1982.

[69] W. Dobrautz, H. Luo, and A. Alavi. Compact numerical solutions to the two-dimensional repulsive Hubbard model obtained via nonunitary similarity transformations. *Phys. Rev. B*, 99:075119, 2019.

[70] W. Dobrautz, H. Luo, P. Rios, and A. Alavi. Combining VMC and similarity tranformed FCIQMC for the real-space Hubbard model. to be published.

[71] M. J. Downward and M. A. Robb. The computation of the representation matrices of the generators of the unitary group. *Theor. Chem. Acc.*, 46(2):129, 1977.

[72] G. W. F. Drake and M. Schlesinger. Vector-coupling approach to orbital and spin-dependent tableau matrix elements in the theory of complex spectra. *Phys. Rev. A*, 15:1990, 1977.

[73] W. Duch and G. H. F. Diercksen. Size-extensivity corrections in configuration interaction methods. *J. Chem. Phys.*, 101(4):3018, 1994.

[74] W. Duch and J. Karwowski. Symmetric group graphical approach to the direct configuration interaction method. *Int. J. Quantum Chem.*, 22(4):783, 1982.

[75] J. J. Duistermaat and J. A. C. Kolk. *Lie Groups.* Springer Berlin Heidelberg, 2000.

[76] T. H. Dunning. Gaussian basis sets for use in correlated molecular calculations. I. The atoms boron through neon and hydrogen. *J. Chem. Phys.*, 90(2):1007, 1989.

[77] R. H. Eade and M. A. Robb. Direct minimization in MC SCF theory. The quasi-Newton method. *Chem. Phys. Lett.*, 83(2):362, 1981.

[78] B. Edegger, N. Fukushima, C. Gros, and V. N. Muthukumar. Particle number renormalization in nearly half-filled Mott Hubbard superconductors. *Phys. Rev. B*, 72:134504, 2005.

[79] D. Eichenberger and D. Baeriswyl. Superconductivity and antiferromagnetism in the two-dimensional Hubbard model: A variational study. *Phys. Rev. B*, 76:180504, 2007.

[80] J. Eisert, M. Cramer, and M. B. Plenio. Colloquium: Area laws for the entanglement entropy. *Rev. Mod. Phys.*, 82:277, 2010.

[81] V. J. Emery. Theory of high-T_c superconductivity in oxides. *Phys. Rev. Lett.*, 58:2794, 1987.

[82] K. B. S. Eriksson and J. E. Pettersson. New Measurements in the Spectrum of the Neutral Nitrogen Atom. *Phys. Scr.*, 3(5):211, 1971.

[83] S. B. Fahy and D. R. Hamann. Positive-projection Monte Carlo simulation: A new variational approach to strongly interacting fermion systems. *Phys. Rev. Lett.*, 65:3437, 1990.

[84] M. Fannes, B. Nachtergaele, and R. F. Werner. Finitely correlated states on quantum spin chains. *Comm. Math. Phys.*, 144(3):443, 1992.

[85] P. Fazekas. Improved Gutzwiller Ansatz and Gutzwiller approximation for strongly correlated electron systems. *Physica C*, 153:1283, 1988.

[86] C. Feigerle, Z. Herman, and W. Lineberger. Laser photoelectron spectrometry of Sc^- and Y^-: A determination of the order of electron filling in transition-metal anions. *J. Electron Spectrosc. Relat. Phenom.*, 23(3):441, 1981.

[87] D. Feller and J. A. Sordo. Performance of CCSDT for diatomic dissociation energies. *J. Chem. Phys.*, 113(2):485, 2000.

[88] D. L. Feng, A. Damascelli, K. M. Shen, N. Motoyama, D. H. Lu, H. Eisaki, K. Shimizu, J.-i. Shimoyama, K. Kishio, N. Kaneko, M. Greven, G. D. Gu, X. J. Zhou, C. Kim, F. Ronning, N. P. Armitage, and Z.-X. Shen. Electronic Structure of the Trilayer Cuprate Superconductor $Bi_2Sr_2Ca_2Cu_3O_{10+\delta}$. *Phys. Rev. Lett.*, 88:107001, 2002.

[89] E. Fermi. Zur Quantelung des idealen einatomigen Gases. *Z. Phys.*, 36(11):902, 1926.

[90] A. Fick. On liquid diffusion. *J. Membr. Sci.*, 100(1):33, 1995.

[91] C. Filippi and C. J. Umrigar. Multiconfiguration wave functions for quantum Monte Carlo calculations of firstrow diatomic molecules. *J. Chem. Phys.*, 105(1):213, 1996.

[92] H. Flyvbjerg and H. G. Petersen. Error estimates on averages of correlated data. *J. Chem. Phys.*, 91(1):461, 1989.

[93] V. Fock. Näherungsmethode zur Lösung des quantenmechanischen Mehrkörperproblems. *Z. Phys.*, 61(1):126, 1930.

[94] P. Fulde. *Electron Correlations in Molecules and Solids*. Springer Berlin Heidelberg, 1995.

[95] J. Gallagher and C. Moore. *Tables of Spectra of Hydrogen, Carbon, Nitrogen, and Oxygen Atoms and Ions*. CRC series in evaluated data in atomic physics. Taylor & Francis, 1993.

[96] R. J. Gdanitz and R. Ahlrichs. The averaged coupled-pair functional (ACPF): A size-extensive modification of MR CI(SD). *Chem. Phys. Lett.*, 143(5):413, 1988.

[97] F. Gebhard and D. Vollhardt. Correlation functions for Hubbard-type models: The exact results for the Gutzwiller wave function in one dimension. *Phys. Rev. Lett.*, 59:1472, 1987.

[98] F. Gebhard and D. Vollhardt. Correlation functions for interacting fermions in the Gutzwiller ansatz. *Phys. Rev. B*, 38:6911, 1988.

[99] I. M. Gel'fand. The center of an infinitesimal group ring. *Mat. Sb.*, 26(68):103, 1950.

[100] I. M. Gel'fand and M. L. Cetlin. Finite-dimensional representations of the group of orthogonal matrices. *Dokl. Akad. Nauk*, 71:1017, 1950. Amer. Math. Soc. Transl. 64, 116 (1967).

[101] I. M. Gel'fand and M. L. Cetlin. Finite-dimensional representations of the group of unimodular matrices. *Dokl. Akad. Nauk*, 71:825, 1950.

[102] A. Georges and G. Kotliar. Hubbard model in infinite dimensions. *Phys. Rev. B*, 45:6479, 1992.

[103] W. Gerlach and O. Stern. Der experimentelle Nachweis der Richtungsquantelung im Magnetfeld. *Z. Phys.*, 9(1):349, 1922.

[104] T. Giamarchi and C. Lhuillier. Phase diagrams of the two-dimensional Hubbard and t-J models by a variational Monte Carlo method. *Phys. Rev. B*, 43:12943, 1991.

[105] G. Gidofalvi, S. R. Brozell, and R. Shepard. Wave function analysis with Shavitt graph density in the graphically contracted function method. *Theor. Chem. Acc.*, 133(9):1512, 2014.

[106] G. Gidofalvi and R. Shepard. Computation of determinant expansion coefficients within the graphically contracted function method. *J. Comput. Chem.*, 30:2414, 2009.

[107] F. R. Gilmore. Potential energy curves for N_2, NO, O_2 and corresponding ions. *J. Quant. Spectrosc. Radiat. Transf.*, 5(2):369, 1965.

[108] F. R. Gilmore, R. R. Laher, and P. J. Espy. Franck-Condon Factors, r-entroids, Electronic Transition Moments, and Einstein Coefficients for Many Nitrogen and Oxygen Band Systems. *J. Phys. Chem. Ref. Data*, 21(5):1005, 1992.

[109] J. Goldstone. Derivation of the Brueckner Many-Body Theory. *Proc. Royal Soc. A*, 239(1217):267, 1957.

[110] G. Golub and C. V. Loan. *Matrix Computations*. John Hopkins Univ. Press, Baltimore, MD, second edition, 1989.

[111] M. S. Gordon and M. W. Schmidt. Advances in electronic structure theory: `GAMESS` a decade later. In C. E. Dykstra, G. Frenking, K. S. Kim, and G. E. Scuseria, editors, *Theory and Applications of Computational Chemistry*, chapter 41, page 1167. Elsevier, Amsterdam, 2005.

[112] M. D. Gould and J. S. Battle. Spindependent unitary group approach. II. Derivation of matrix elements for spindependent operators. *J. Chem. Phys.*, 99(8):5961, 1993.

[113] M. D. Gould and G. S. Chandler. A spin-dependent unitary group approach to many-electron systems. *Int. J. Quantum Chem.*, 26(4):441, 1984.

[114] M. D. Gould and J. Paldus. Spin-dependent unitary group approach. I. General formalism. *J. Chem. Phys.*, 92(12):7394, 1990.

[115] M. D. Gould, J. Paldus, and G. S. Chandler. Unitary group approach to reduced density matrices. *J. Chem. Phys.*, 93(6):4142, 1990.

[116] C. Gros. Superconductivity in correlated wave functions. *Phys. Rev. B*, 38:931, 1988.

[117] C. Gros. Physics of projected wavefunctions. *Ann. Phys.*, 189(1):53, 1989.

[118] C. Gros, R. Joynt, and T. M. Rice. Antiferromagnetic correlations in almost-localized fermi liquids. *Phys. Rev. B*, 36:381, 1987.

[119] C. Gros, R. Joynt, and T. M. Rice. Superconducting instability in the large-U limit of the two-dimensional Hubbard model. *Z. Phys. B*, 68(4):425, 1987.

[120] A. Grüneis, S. Hirata, Y.-y. Ohnishi, and S. Ten-no. Perspective: Explicitly correlated electronic structure theory for complex systems. *J. Chem. Phys.*, 146(8):080901, 2017.

[121] O. Gunnarsson. personal communication, 2018.

[122] M. C. Gutzwiller. Effect of Correlation on the Ferromagnetism of Transition Metals. *Phys. Rev. Lett.*, 10:159, 1963.

[123] M. C. Gutzwiller. Correlation of Electrons in a Narrow s Band. *Phys. Rev.*, 137:A1726, 1965.

[124] J. Hachmann, W. Cardoen, and G. K.-L. Chan. Multireference correlation in long molecules with the quadratic scaling density matrix renormalization group. *J. Chem. Phys.*, 125(14):144101, 2006.

[125] W. G. Harter and C. W. Patterson. *A Unitary Calculus for Electronic Orbitals (Lecture Notes in Physics)*. Springer, 1976.

[126] D. R. Hartree. The Wave Mechanics of an Atom with a Non-Coulomb Central Field. Part I. Theory and Methods. *Math. Proc. Camb. Philos. Soc.*, 24(1):89, 1928.

[127] M. B. Hastings. An area law for one-dimensional quantum systems. *J. Stat. Mech.: Theory Exp.*, 2007(08):P08024, 2007.

[128] W. K. Hastings. Monte Carlo sampling methods using Markov chains and their applications. *Biometrika*, 57(1):97, 1970.

[129] C. Hättig, W. Klopper, A. Köhn, and D. P. Tew. Explicitly Correlated Electrons in Molecules. *Chem. Rev.*, 112(1):4, 2012.

[130] Y. He and D. Cremer. Spin-projected coupled-cluster theory with single and double excitations. *Theor. Chem. Acc.*, 105:132, 2000.

[131] D. Hegarty and M. A. Robb. Application of unitary group methods to configuration interaction calculations. *Mol. Phys.*, 38(6):1795, 1979.

[132] W. J. Hehre, R. F. Stewart, and J. A. Pople. Self-Consistent Molecular-Orbital Methods. I. Use of Gaussian Expansions of Slater-Type Atomic Orbitals. *J. Chem. Phys.*, 51(6):2657, 1969.

[133] T. Helgaker, P. Jørgensen, and J. Olsen. *Molecular Electronic-Structure Theory*. John Wiley & Sons, Chichester, 2000.

[134] M. H. Hettler, A. N. Tahvildar-Zadeh, M. Jarrell, T. Pruschke, and H. R. Krishnamurthy. Nonlocal dynamical correlations of strongly interacting electron systems. *Phys. Rev. B*, 58:R7475, 1998.

[135] J. E. Hirsch. Discrete Hubbard-Stratonovich transformation for fermion lattice models. *Phys. Rev. B*, 28:4059, 1983.

[136] J. E. Hirsch. Erratum: Discrete Hubbard-Stratonovich transformation for fermion lattice models. *Phys. Rev. B*, 29:4159, 1984.

[137] J. E. Hirsch. Two-dimensional Hubbard model: Numerical simulation study. *Phys. Rev. B*, 31:4403, 1985.

[138] J. O. Hirschfelder. Removal of Electron-Electron Poles from Many-Electron Hamiltonians. *J. Chem. Phys.*, 39(11):3145, 1963.

[139] A. A. Holmes, H. J. Changlani, and C. J. Umrigar. Efficient Heat-Bath Sampling in Fock Space. *J. Chem. Theory Comput.*, 12(4):1561, 2016.

[140] P. Horsch and T. A. Kaplan. Exact and Monte Carlo studies of Gutzwiller's state for the localised-electron limit in one dimension. *J. Phys. Condens. Matter*, 16(35):L1203, 1983.

[141] H.-X. Huang, Y.-Q. Li, and F.-C. Zhang. Charge-ordered resonating valence bond states in doped cuprates. *Phys. Rev. B*, 71:184514, 2005.

[142] J. Hubbard. Electron Correlations in Narrow Energy Bands. *Proc. Royal Soc. A*, 276(1365):238, 1963.

[143] J. Hubbard. Electron correlations in narrow energy bands III. An improved solution. *Proc. Royal Soc. A*, 281(1386):401, 1964.

[144] K. Huber and G. Herzberg. *Molecular Spectra and Molecular Structure: IV. Constants of Diatomic Molecules*. Springer, 2013.

[145] E. A. Hylleraas. Über den Grundzustand des Heliumatoms. *Z. Phys.*, 48(7):469, 1928.

[146] E. A. Hylleraas. Neue Berechnung der Energie des Heliums im Grundzustande, sowie des tiefsten Terms von Ortho-Helium. *Z. Phys.*, 54(5):347, 1929.

[147] F. Iachello. Algebraic methods in quantum mechanics with applications to nuclear and molecular structure. *Nucl. Phys. A*, 560(1):23, 1993.

[148] R. Jastrow. Many-Body Problem with Strong Forces. *Phys. Rev.*, 98(5):1479, 1955.

[149] F. Jensen. *Introduction to Computational Chemistry*. Wiley, 1998.

[150] G. Jeung. Electron affinities of Sc. *Phys. Lett. A*, 113(2):73, 1985.

[151] H. Kahn. Modifications of the Monte Carlo method. In *Seminar on Scientific Computation*, page 2027, New York, 1950. International Business Machines Corporation.

[152] M. H. Kalos, D. Levesque, and L. Verlet. Helium at zero temperature with hard-sphere and other forces. *Phys. Rev. A*, 9:2178, 1974.

[153] M. H. Kalos and P. A. Whitlock. *Monte Carlo Methods*. Wiley-VCH, Weinheim, 2008.

[154] J. Kanamori. Electron Correlation and Ferromagnetism of Transition Metals. *Prog. Theor. Phys.*, 30(3):275, 1963.

[155] T. A. Kaplan, P. Horsch, and P. Fulde. Close Relation between Localized-Electron Magnetism and the Paramagnetic Wave Function of Completely Itinerant Electrons. *Phys. Rev. Lett.*, 49:889, 1982.

[156] T. Kato. On the eigenfunctions of many-particle systems in quantum mechanics. *Commun. Pure Appl. Math.*, 10(2):151, 1957.

[157] N. Kawashima, J. E. Gubernatis, and H. G. Evertz. Loop algorithms for quantum simulations of fermion models on lattices. *Phys. Rev. B*, 50:136, 1994.

[158] R. Kent, M. Schlesinger, and G. Drake. Calculations of atomic spin-orbit matrix elements in the unitary group approach. *J. Comput. Phys.*, 40(2):430, 1981.

[159] R. D. Kent and M. Schlesinger. Unitary-group approach to spin-dependent operators. *Phys. Rev. A*, 42:1155, 1990.

[160] R. D. Kent and M. Schlesinger. Spin-dependent operators in the unitary-group approach. *Phys. Rev. A*, 50:186, 1994.

[161] J. A. F. Kersten, G. H. Booth, and A. Alavi. Assessment of multireference approaches to explicitly correlated full configuration interaction quantum Monte Carlo. *J. Chem. Phys.*, 145(5):054117, 2016.

[162] D. Kleima, W. Holman, and L. Biedenharn. The Algebras of Lie Groups and Their Representations. In E. M. Loebl, editor, *Group Theory and its Applications*, page 1. Academic Press, 1968.

[163] W. Klopper, F. R. Manby, S. Ten-No, and E. F. Valeev. R12 methods in explicitly correlated molecular electronic structure theory. *Int. Rev. Phys. Chem.*, 25(3):427, 2006.

[164] P. Knowles and N. Handy. A new determinant-based full configuration interaction method. *Chem. Phys. Lett.*, 111(4):315, 1984.

[165] P. J. Knowles, C. Hampel, and H. Werner. Coupled cluster theory for high spin, open shell reference wave functions. *J. Chem. Phys.*, 99(7):5219, 1993.

[166] P. J. Knowles, C. Hampel, and H.-J. Werner. Erratum: Coupled cluster theory for high spin, open shell reference wave functions [J. Chem. Phys. 99, 5219 (1993)]. *J. Chem. Phys.*, 112(6):3106, 2000.

[167] P. J. Knowles and N. C. Handy. Unlimited full configuration interaction calculations. *J. Chem. Phys.*, 91(4):2396, 1989.

[168] P. J. Knowles and H.-J. Werner. An efficient second-order MC SCF method for long configuration expansions. *Chem. Phys. Lett.*, 115(3):259, 1985.

[169] M. Kotani and A. Amemiya. *Table of Molecular Integrals*. Maruzen Company, 1955.

[170] G. Kotliar, S. Y. Savrasov, G. Pálsson, and G. Biroli. Cellular Dynamical Mean Field Approach to Strongly Correlated Systems. *Phys. Rev. Lett.*, 87:186401, 2001.

[171] A. Kramida, Yu. Ralchenko, J. Reader, and NIST ASD Team. NIST Atomic Spectra Database (ver. 5.6.1), [Online]. Available: `https://physics.nist.gov/asd` [2018, December 5]. National Institute of Standards and Technology, Gaithersburg, MD., 2018.

[172] R. Krishnan and J. A. Pople. Approximate fourth-order perturbation theory of the electron correlation energy. *Int. J. Quantum Chem.*, 14(1):91, 1978.

[173] D. P. Kroese, T. Brereton, T. Taimre, and Z. I. Botev. Why the Monte Carlo method is so important today. *Wiley Interdiscip. Rev. Comput. Mol. Sci.*, 6(6):386, 2014.

[174] H. Kurzweil and B. Stellmacher. *The Theory of Finite Groups: An Introduction (Universitext)*. Springer, 2010.

[175] W. Kutzelnigg and J. D. Morgan. Rates of convergence of the partial-wave expansions of atomic correlation energies. *J. Chem. Phys.*, 96(6):4484, 1992.

[176] C. Lanczos. An iteration method for the solution of the eigenvalue problem of linear differential and integral operators. *J. Res. Natl. Bur. Stand. (U. S.)*, 45:225, 1950.

[177] S. R. Langhoff and E. R. Davidson. Configuration interaction calculations on the nitrogen molecule. *Int. J. Quantum Chem.*, 8(1):61, 1974.

[178] J. P. F. LeBlanc, A. E. Antipov, F. Becca, I. W. Bulik, G. K.-L. Chan, C.-M. Chung, Y. Deng, M. Ferrero, T. M. Henderson, C. A. Jiménez-Hoyos, E. Kozik, X.-W. Liu, A. J. Millis, N. V. Prokof'ev, M. Qin, G. E. Scuseria, H. Shi, B. V. Svistunov, L. F. Tocchio, I. S. Tupitsyn, S. R. White, S. Zhang, B.-X. Zheng, Z. Zhu, and E. Gull. Solutions of the Two-Dimensional Hubbard Model: Benchmarks and Results from a Wide Range of Numerical Algorithms. *Phys. Rev. X*, 5:041041, 2015.

[179] T. K. Lee and S. Feng. Doping dependence of antiferromagnetism in La_2CuO_4: A numerical study based on a resonating-valence-bond state. *Phys. Rev. B*, 38:11809, 1988.

[180] X. Li and J. Paldus. Unitary group approach to the many-electron correlation problem: spin-dependent operators. *Theor. Chem. Acc.*, 133(5):1467, 2014.

[181] Y. M. Li and N. d'Ambrumenil. A new expansion for generalized Gutzwiller wave functions: Antiferromagnetic case. *J. Appl. Phys.*, 73(10):6537, 1993.

[182] Z. Li and G. K.-L. Chan. Spin-Projected Matrix Product States: Versatile Tool for Strongly Correlated Systems. *J. Chem. Theory Comput.*, 13(6):2681, 2017.

[183] G. Li Manni and A. Alavi. Understanding the Mechanism Stabilizing Intermediate Spin States in Fe(II)-Porphyrin. *J. Phys. Chem. A*, 122(22):4935, 2018.

[184] G. Li Manni, S. D. Smart, and A. Alavi. Combining the Complete Active Space Self-Consistent Field Method and the Full Configuration Interaction Quantum Monte Carlo within a Super-CI Framework, with Application to Challenging Metal-Porphyrins. *J. Chem. Theory Comput.*, 12(3):1245, 2016.

[185] A. I. Lichtenstein and M. I. Katsnelson. Antiferromagnetism and d-wave superconductivity in cuprates: A cluster dynamical mean-field theory. *Phys. Rev. B*, 62:R9283, 2000.

[186] E. H. Lieb and F. Y. Wu. Absence of Mott Transition in an Exact Solution of the Short-Range, One-Band Model in One Dimension. *Phys. Rev. Lett.*, 20:1445, 1968.

[187] C. Lin, F. H. Zong, and D. M. Ceperley. Twist-averaged boundary conditions in continuum quantum Monte Carlo algorithms. *Phys. Rev. E*, 64:016702, 2001.

[188] H. Lischka, T. Müller, P. G. Szalay, I. Shavitt, R. M. Pitzer, and R. Shepard. `Columbus` - a program system for advanced multireference theory calculations. *Wiley Interdiscip. Rev. Comput. Mol. Sci.*, 1(2):191, 2011.

[189] H. Lischka, R. Shepard, F. B. Brown, and I. Shavitt. New implementation of the graphical unitary group approach for multireference direct configuration interaction calculations. *Int. J. Quantum Chem.*, 20:91, 1981.

[190] H. Lischka, R. Shepard, R. M. Pitzer, I. Shavitt, M. Dallos, T. Müller, P. G. Szalay, M. Seth, G. S. Kedziora, S. Yabushita, and Z. Zhang. High-level multireference methods in the quantum-chemistry program system COLUMBUS: Analytic MR-CISD and MR-AQCC gradients and MR-AQCC-LRT for excited states, GUGA spin-orbit CI and parallel CI density. *Phys. Chem. Chem. Phys.*, 3:664, 2001.

[191] H. Lischka, R. Shepard, I. Shavitt, R. M. Pitzer, M. Dallos, T. Müller, P. G. Szalay, F. B. Brown, R. Ahlrichs, H. J. Böhm, A. Chang, D. C. Comeau, R. Gdanitz, H. Dachsel, C. Ehrhardt, M. Ernzerhof, P. Höchtl, S. Irle, G. Kedziora, T. Kovar, V. Parasuk, M. J. M. Pepper, P. Scharf, H. Schiffer, M. Schindler, M. Schüler, M. Seth, E. A. Stahlberg, J.-G. Zhao, S. Yabushita, Z. Zhang, M. Barbatti, S. Matsika, M. Schuurmann, D. R. Yarkony, S. R. Brozell, E. V. Beck, , J.-P. Blaudeau, M. Ruckenbauer, B. Sellner, F. Plasser, J. J. Szymczak, R. F. K. Spada, and A. Das. `COLUMBUS`, an *ab-initio* electronic structure program, release 7.0, 2017. see https://www.univie.ac.at/columbus/.

[192] J. Liu, J. Schmalian, and N. Trivedi. Pairing and Superconductivity Driven by Strong Quasiparticle Renormalization in Two-Dimensional Organic Charge Transfer Salts. *Phys. Rev. Lett.*, 94:127003, 2005.

[193] A. Lofthus and P. H. Krupenie. The spectrum of molecular nitrogen. *J. Phys. Chem. Ref. Data*, 6(1):113, 1977.

[194] J. D. Louck. Recent progress toward a theory of tensor operators in the unitary groups. *Am. J. Phys.*, 38:3, 1970.

[195] P.-O. Löwdin. Quantum Theory of Many-Particle Systems. III. Extension of the Hartree-Fock Scheme to Include Degenerate Systems and Correlation Effects. *Phys. Rev.*, 97:1509, 1955.

[196] H. Luo. Transcorrelated calculations of homogeneous electron gases. *J. Chem. Phys.*, 136(22):224111, 2012.

[197] H. Luo and A. Alavi. Combining the Transcorrelated Method with Full Configuration Interaction Quantum Monte Carlo: Application to the Homogeneous Electron Gas. *J. Chem. Theory Comput.*, 14(3):1403, 2018.

[198] P.-Å. Malmqvist, A. Rendell, and B. O. Roos. The restricted active space self-consistent-field method, implemented with a split graph unitary group approach. *J. Phys. Chem.*, 94(14):5477, 1990.

[199] R. S. Mangina, J. M. Ajello, R. A. West, and D. Dziczek. High-resolution Electron-impact Emission Spectra and Vibrational Emission Cross Sections from 330-1100nm for N_2. *Astrophys. J. Suppl. S.*, 196(1):13, 2011.

[200] N. H. March. Spatially dependent generalization of Kato's theorem for atomic closed shells in a bare Coulomb field. *Phys. Rev. A*, 33:88, 1986.

[201] A. Markov. *Theory of Algorithms.* TT 60-51085. Academy of Sciences of the USSR, 1954.

[202] F. Matsen. Spin-Free Quantum Chemistry. In *Advances in Quantum Chemistry*, page 59. Elsevier, 1964.

[203] F. A. Matsen. The unitary group formulation of the N-particle problem. *Int. J. Quantum Chem.*, 8(S8):379, 1974.

[204] L. F. Mattheiss. Electronic band properties and superconductivity in $La_{2-y}X_yCuO_4$. *Phys. Rev. Lett.*, 58:1028, 1987.

[205] M. Mazhdrakov, D. Benov, and N. Valkanov. *The Monte Carlo Method: Engineering Applications.* ACMO Academic Press, 2018.

[206] I. P. McCulloch and M. Gulácsi. The non-Abelian density matrix renormalization group algorithm. *Europhys. Lett.*, 57(6):852, 2002.

[207] A. Messiah. *Quantum Mechanics, Volume II.* North Holland, 1981.

[208] N. Metropolis, A. W. Rosenbluth, M. N. Rosenbluth, A. H. Teller, and E. Teller. Equation of State Calculations by Fast Computing Machines. *J. Chem. Phys.*, 21(6):1087, 1953.

[209] N. Metropolis and S. Ulam. The Monte Carlo Method. *J. Am. Stat. Assoc.*, 44(247):335, 1949.

[210] W. Metzner and D. Vollhardt. Ground-state properties of correlated fermions: Exact analytic results for the Gutzwiller wave function. *Phys. Rev. Lett.*, 59:121, 1987.

[211] W. Metzner and D. Vollhardt. The Hubbard Model in Infinite Dimensions. In D. Baeriswyl and D. K. Campbell, editors, *Interacting Electrons in Reduced Dimensions*, page 129. Springer US, Boston, MA, 1989.

[212] C. Møller and M. S. Plesset. Note on an Approximation Treatment for Many-Electron Systems. *Phys. Rev.*, 46:618, 1934.

[213] M. Moshinsky. *Group theory and the many-body problem.* N.Y. : Gordon and Breach, 1968.

[214] M. Motta, D. M. Ceperley, G. K.-L. Chan, J. A. Gomez, E. Gull, S. Guo, C. A. Jiménez-Hoyos, T. N. Lan, J. Li, F. Ma, A. J. Millis, N. V. Prokof'ev, U. Ray, G. E. Scuseria, S. Sorella, E. M. Stoudenmire, Q. Sun, I. S. Tupitsyn, S. R. White, D. Zgid, and S. Zhang. Towards the Solution of the Many-Electron Problem in Real Materials: Equation of State of the Hydrogen Chain with State-of-the-Art Many-Body Methods. *Phys. Rev. X*, 7:031059, 2017.

[215] M. Motta and S. Zhang. Ab initio computations of molecular systems by the auxiliary-field quantum Monte Carlo method. *Wiley Interdiscip. Rev. Comput. Mol. Sci.*, 8(5):e1364, 2018.

[216] R. S. Mulliken. The Energy Levels of the Nitrogen Molecule. In M. Zelikoff, editor, *The Threshold of Space*, page 169, 1957.

[217] H. Nakatsuji and K. Hirao. Cluster expansion of the wavefunction. Pseduo-orbital theory applied to spin correlation. *Chem. Phys. Lett.*, 47(3):569, 1977.

[218] H. Nakatsuji and K. Hirao. Cluster expansion of the wavefunction. Symmetry-adaptedcluster expansion, its variational determination, and extension of open-shell orbital theory. *J. Chem. Phys.*, 68(5):2053, 1978.

[219] E. Neuscamman, H. Changlani, J. Kinder, and G. K.-L. Chan. Nonstochastic algorithms for Jastrow-Slater and correlator product state wave functions. *Phys. Rev. B*, 84:205132, 2011.

[220] E. Noether. Invariante Variationsprobleme. *Nachrichten von der Gesellschaft der Wissenschaften zu Göttingen, Mathematisch-Physikalische Klasse*, 1918:235, 1918.

[221] T. Ogawa, K. Kanda, and T. Matsubara. Gutzwiller Approximation for Antiferromagnetism in Hubbard Model. *Prog. Theor. Phys.*, 53(3):614, 1975.

[222] Y. Öhrn, J. R. Sabin, R. Shepard, G. Gidofalvi, and P. D. Hovland. An efficient recursive algorithm to compute wave function optimization gradients for the graphically contracted function method. *Int. J. Quantum Chem.*, 110:2938, 2010.

[223] Y. Ohtsuka, P. Piecuch, J. R. Gour, M. Ehara, and H. Nakatsuji. Active-space symmetry-adapted-cluster configuration-interaction and equation-of-motion coupled-cluster methods for high accuracy calculations of potential energy surfaces of radicals. *J. Chem. Phys.*, 126(16):164111, 2007.

[224] Y. Ohtsuka and S. Ten-no. Explicitly correlated projector Monte Carlo method based on Slater determinants (PMC-SD-F12 method). *AIP Conf. Proc.*, 1456(1):97, 2012.

[225] J. Olsen. The CASSCF Method: A Perspective and Commentary. *Int. J. Quantum Chem.*, 111:3267, 2011.

[226] J. Olsen. A direct method to transform between expansions in the configuration state function and Slater determinant bases. *J. Chem. Phys.*, 141(3):034112, 2014.

[227] S. Östlund and S. Rommer. Thermodynamic Limit of Density Matrix Renormalization. *Phys. Rev. Lett.*, 75:3537, 1995.

[228] C. Overy, G. H. Booth, N. S. Blunt, J. J. Shepherd, D. Cleland, and A. Alavi. Unbiased reduced density matrices and electronic properties from full configuration interaction quantum Monte Carlo. *J. Chem. Phys.*, 141(24):244117, 2014.

[229] R. T. Pack and W. B. Brown. Cusp Conditions for Molecular Wavefunctions. *J. Chem. Phys.*, 45(2):556, 1966.

[230] J. Paldus. Group theoretical approach to the configuration interaction and perturbation theory calculations for atomic and molecular systems. *J. Chem. Phys.*, 61(12):5321, 1974.

[231] J. Paldus. A pattern calculus for the unitary group approach to the electronic correlation problem. *Int. J. Quantum Chem.*, 9(S9):165, 1975.

[232] J. Paldus. Unitary-group approach to the many-electron correlation problem: Relation of Gelfand and Weyl tableau formulations. *Phys. Rev. A*, 14:1620, 1976.

[233] J. Paldus. The Unitary Group for the Evaluation of Electronic Energy Matrix Elements. In J. Hinze, editor, *Unitary Group Approach to Many-Electron Correlation Problem*, page 1. Springer Berlin Heidelberg, Berlin, Heidelberg, 1981.

[234] J. Paldus. Dynamical Groups. In G. Drake, editor, *Springer Handbook of Atomic, Molecular, and Optical Physics*, page 87. Springer New York, New York, NY, 2006.

[235] J. Paldus. Many-Electron Correlation Problem A Group Theoretical Approach. In H. Eyring, editor, *Theoretical Chemistry Advances and Perspectives*. Elsevier Science, 2012.

[236] J. Paldus and M. J. Boyle. Unitary Group Approach to the Many-Electron Correlation Problem via Graphical Methods of Spin Algebras. *Phys. Scr.*, 21(3):295, 1980.

[237] J. Paldus and J. Čížek. Time-Independent Diagrammatic Approach to Perturbation Theory of Fermion Systems. In *Advances in Quantum Chemistry Volume 9*, page 105. Elsevier, 1975.

[238] J. Paldus and M. D. Gould. Unitary group approach to reduced density matrices. *Theor. Chem. Acc.*, 86(1):83, 1993.

[239] A. Paramekanti, M. Randeria, and N. Trivedi. Projected Wave Functions and High Temperature Superconductivity. *Phys. Rev. Lett.*, 87:217002, 2001.

[240] R. Pariser and R. G. Parr. A Semi-Empirical Theory of the Electronic Spectra and Electronic Structure of Complex Unsaturated Molecules. I. *J. Chem. Phys.*, 21(3):466, 1953.

[241] R. Pariser and R. G. Parr. A Semi-Empirical Theory of the Electronic Spectra and Electronic Structure of Complex Unsaturated Molecules. II. *J. Chem. Phys.*, 21(5):767, 1953.

[242] W. Pauli. Über den Zusammenhang des Abschlusses der Elektronengruppen im Atom mit der Komplexstruktur der Spektren. *Z. Phys.*, 31(1):765, 1925.

[243] W. Pauli. The Connection Between Spin and Statistics. *Phys. Rev.*, 58:716, 1940.

[244] W. Pauli. *General Principles of Quantum Mechanics*. Springer, 1990.

[245] R. Pauncz. *Spin Eigenfunctions: Construction and Use*. Springer, 1979.

[246] R. Pauncz. *The Symmetric Group in Quantum Chemistry*. Mathematical Chemistry. Taylor & Francis, 1995.

[247] P. W. Payne. Matrix element factorization in the unitary group approach for configuration interaction calculations. *Int. J. Quantum Chem.*, 22(6):1085, 1982.

[248] F. R. Petruzielo, A. A. Holmes, H. J. Changlani, M. P. Nightingale, and C. J. Umrigar. Semistochastic Projector Monte Carlo Method. *Phys. Rev. Lett.*, 109:230201, 2012.

[249] J. C. Pickering and A. P. Thorne. The Spectrum and Term Analysis of Co I. *Astrophys. J. Suppl. S.*, 107(2):761, 1996.

[250] D. Poilblanc. Twisted boundary conditions in cluster calculations of the optical conductivity in two-dimensional lattice models. *Phys. Rev. B*, 44:9562, 1991.

[251] I. Polyak, M. J. Bearpark, and M. A. Robb. Application of the unitary group approach to evaluate spin density for configuration interaction calculations in a basis of S^2 eigenfunctions. *Int. J. Quantum Chem.*, 118(12):e25559, 2018.

[252] J. Pople and D. Beveridge. *Approximate molecular orbital theory*. McGraw-Hill series in advanced chemistry. McGraw-Hill, 1970.

[253] J. A. Pople. Electron interaction in unsaturated hydrocarbons. *Trans. Faraday Soc.*, 49:1375, 1953.

[254] J. A. Pople and R. K. Nesbet. Self-Consistent Orbitals for Radicals. *J. Chem. Phys.*, 22(3):571, 1954.

[255] J. A. Pople, D. P. Santry, and G. A. Segal. Approximate SelfConsistent Molecular Orbital Theory. I. Invariant Procedures. *J. Chem. Phys.*, 43(10):S129, 1965.

[256] M. Potthoff, M. Aichhorn, and C. Dahnken. Variational Cluster Approach to Correlated Electron Systems in Low Dimensions. *Phys. Rev. Lett.*, 91:206402, 2003.

[257] D. Prendergast, M. Nolan, C. Filippi, S. Fahy, and J. C. Greer. Impact of electron-electron cusp on configuration interaction energies. *J. Chem. Phys.*, 115(4):1626, 2001.

[258] W. H. Press, S. A. Teukolsky, W. T. Vetterling, and B. P. Flannery. *Numerical Recipes 3rd Edition: The Art of Scientific Computing*. Cambridge University Press, 2007.

[259] M. Qin, H. Shi, and S. Zhang. Benchmark study of the two-dimensional Hubbard model with auxiliary-field quantum Monte Carlo method. *Phys. Rev. B*, 94:085103, 2016.

[260] Y. Qiu, T. M. Henderson, J. Zhao, and G. E. Scuseria. Projected coupled cluster theory. *J. Chem. Phys.*, 147(6):064111, 2017.

[261] K. Raghavachari, J. A. Pople, E. S. Replogle, and M. Head-Gordon. Fifth order Møller-Plesset perturbation theory: comparison of existing correlation methods and implementation of new methods correct to fifth order. *J. Phys. Chem.*, 94(14):5579, 1990.

[262] J. Rayleigh. *The Theory of Sound*. Number Bd. 1 in The Theory of Sound. Macmillan, 1877.

[263] C. M. Reeves. An Algorithm for Generating Projective Reduction Formulas for Matrix Elements of Many-electron Wavefunctions. *Commun. ACM*, 9(4):276, 1966.

[264] M. Reiher. Douglas–Kroll–Hess Theory: a relativistic electrons-only theory for chemistry. *Theor. Chem. Acc.*, 116(1):241, 2006.

[265] P. L. Rios. personal communication, 2018.

[266] M. A. Robb and U. Niazi. The unitary group approach in Configuration Interaction (CI) methods. *Comp. Phys. Rep.*, 1(3):127, 1984.

[267] C. Robert and G. Casella. *Monte Carlo Statistical Methods (Springer Texts in Statistics)*. Springer, 2005.

[268] C. C. J. Roothaan. Self-Consistent Field Theory for Open Shells of Electronic Systems. *Rev. Mod. Phys.*, 32:179, 1960.

[269] K. Ruedenberg. Expectation Values of Many-Fermion Spin Eigenstates. *Phys. Rev. Lett.*, 27:1105, 1971.

[270] G. Rumer. Zur Theorie der Spinvalenz. *Nachrichten von der Gesellschaft der Wissenschaften zu Göttingen, Mathematisch-Physikalische Klasse*, 1932:337, 1932.

[271] W. I. Salmon and K. Ruedenberg. Many-Electron Wavefunctions Expanded in Spin-Adapted Antisymmetrized Products, and Their Expectation Values. *J. Chem. Phys.*, 57(7):2776, 1972.

[272] D. J. Scalapino. Numerical Studies of the 2D Hubbard Model. In J. R. Schrieffer and J. S. Brooks, editors, *Handbook of High-Temperature Superconductivity: Theory and Experiment*, page 495. Springer New York, New York, NY, 2007.

[273] D. J. Scalapino and S. R. White. Numerical Results for the Hubbard Model: Implications for the High-T_C Pairing Mechanism. *Found. Phys.*, 31(1):27, 2001.

[274] M. W. Schmidt, K. K. Baldridge, J. A. Boatz, S. T. Elbert, M. S. Gordon, J. H. Jensen, S. Koseki, N. Matsunaga, K. A. Nguyen, S. Su, T. L. Windus, M. Dupuis, and J. A. Montgomery Jr. General atomic and molecular electronic structure system. *J. Comput. Chem.*, 14(11):1347, 1993.

[275] H. Schneider and G. Barker. *Matrices and Linear Algebra*. Dover Books on Mathematics Series. Dover Publications, 1989.

[276] U. Schollwöck. The density-matrix renormalization group. *Rev. Mod. Phys.*, 77:259, 2005.

[277] U. Schollwöck. The density-matrix renormalization group in the age of matrix product states. *Ann. Phys.*, 326(1):96, 2011. January 2011 Special Issue.

[278] E. Schrödinger. Quantisierung als Eigenwertproblem. *Ann. Phys.*, 385(13):437, 1926.

[279] R. Serber. Extension of the Dirac Vector Model to Include Several Configurations. *Phys. Rev.*, 45:461, 1934.

[280] S. Sharma and G. K.-L. Chan. Spin-adapted density matrix renormalization group algorithms for quantum chemistry. *J. Chem. Phys.*, 136(12):124121, 2012.

[281] S. Sharma, T. Yanai, G. H. Booth, C. J. Umrigar, and G. K.-L. Chan. Spectroscopic accuracy directly from quantum chemistry: Application to ground and excited states of beryllium dimer. *J. Chem. Phys.*, 140(10):104112, 2014.

[282] I. Shavitt. Graph theoretical concepts for the unitary group approach to the many-electron correlation problem. *Int. J. Quantum Chem.*, 12(S11):131, 1977.

[283] I. Shavitt. Matrix element evaluation in the unitary group approach to the electron correlation problem. *Int. J. Quantum Chem.*, 14 S12(S12):5, 1978.

[284] I. Shavitt. The Graphical Unitary Group Approach and Its Application to Direct Configuration Interaction Calculations. In J. Hinze, editor, *The Unitary Group for the Evaluation of Electronic Energy Matrix Elements*, page 51. Springer Berlin Heidelberg, Berlin, Heidelberg, 1981.

[285] I. Shavitt and R. J. Bartlett. *Many-Body Methods in Chemistry and Physics: MBPT and Coupled-Cluster Theory (Cambridge Molecular Science)*. Cambridge University Press, 2010.

[286] R. Shepard. A General Nonlinear Expansion Form for Electronic Wave Functions. *J. Phys. Chem. A*, 109:11629, 2005.

[287] R. Shepard. Hamiltonian Matrix and Reduced Density Matrix Construction with Nonlinear Wave Functions. *J. Phys. Chem. A*, 110(28):8880, 2006.

[288] R. Shepard, G. Gidofalvi, and S. R. Brozell. The multifacet graphically contracted function method. I. Formulation and implementation. *J. Chem. Phys.*, 141(6):064105, 2014.

[289] R. Shepard, G. Gidofalvi, and S. R. Brozell. The multifacet graphically contracted function method. II. A general procedure for the parameterization of orthogonal matrices and its application to arc factors. *J. Chem. Phys.*, 141(6):064106, 2014.

[290] R. Shepard and J. Simons. Multiconfigurational wavefunction optimization using the unitary group method. *Int. J. Quantum Chem.*, 18:211, 1980.

[291] C. D. Sherrill and H. F. Schaefer. The Configuration Interaction Method: Advances in Highly Correlated Approaches. In P.-O. Löwdin, J. R. Sabin, M. C. Zerner, and E. Brändas, editors, *Advances in Quantum Chemistry*, volume 34 of *Advances in Quantum Chemistry*, pages 143 – 269. Academic Press, 1999.

[292] O. B. Sheynin. S. D. Poisson's Work in Probability. *Arch. Hist. Exact Sci.*, 18(3):245, 1978.

[293] H. Shi and S. Zhang. Symmetry in auxiliary-field quantum Monte Carlo calculations. *Phys. Rev. B*, 88:125132, 2013.

[294] T. Shiozaki and H.-J. Werner. Multireference explicitly correlated F12 theories. *Mol. Phys.*, 111(5):607, 2013.

[295] M. Simonetta, E. Gianinetti, and I. Vandoni. Valence-Bond Theory for Simple Hydrocarbon Molecules, Radicals, and Ions. *J. Chem. Phys.*, 48(4):1579, 1968.

[296] J. C. Slater. Central Fields and Rydberg Formulas in Wave Mechanicsb. *Phys. Rev.*, 31:333, 1928.

[297] J. C. Slater. The Theory of Complex Spectra. *Phys. Rev.*, 34(10):1293, 1929.

[298] J. C. Slater. Atomic Shielding Constants. *Phys. Rev.*, 36:57, 1930.

[299] J. C. Slater. Note on Hartree's Method. *Phys. Rev.*, 35:210, 1930.

[300] S. Smart, G. Booth, and A. Alavi. Excitation generation in full configuration interaction quantum Monte Carlo based on Cauchy-Schwarz distributions. unpublished.

[301] S. D. Smart. *The use of spin-pure and non-orthogonal Hilbert spaces in Full Configuration Interaction Quantum Monte-Carlo.* PhD thesis, University of Cambridge, 2013.

[302] Y. G. Smeyers and L. Doreste-Suarez. Half-Projected and Projected Hartree-Fock Calculations for Singlet Ground States. I. four-Electron Atomic Systems. *Int. J. Quantum Chem.*, 7(4):687, 1973.

[303] A. Sommerfeld. Zur Quantentheorie der Spektrallinien. *Ann. Phys.*, 356(17):1, 1916.

[304] V. Sonnad, J. Escher, M. Kruse, and R. Baker. An Informal Overview of the Unitary Group Approach. Technical report, Lawrence Livermore National Lab. (LLNL), 2016.

[305] S. Sorella. Linearized auxiliary fields Monte Carlo technique: Efficient sampling of the fermion sign. *Phys. Rev. B*, 84:241110, 2011.

[306] S. Sorella. Finite-size scaling with modified boundary conditions. *Phys. Rev. B*, 91:241116, 2015.

[307] S. Sorella. personal communication, 2016.

[308] S. Sorella, S. Baroni, R. Car, and M. Parrinello. A Novel Technique for the Simulation of Interacting Fermion Systems. *Europhys. Lett.*, 8(7):663, 1989.

[309] J. S. Spencer, N. S. Blunt, and W. M. Foulkes. The sign problem and population dynamics in the full configuration interaction quantum Monte Carlo method. *J. Chem. Phys.*, 136(5):054110, 2012.

[310] J. S. Spencer and W. M. C. Foulkes. Evaluation of expectation values in full configuration interaction quantum monte carlo. In *APS Meeting Abstracts*, page W24.006, 2013.

[311] R. L. Stratonovich. On a Method of Calculating Quantum Distribution Functions. *Dokl. Phys.*, 2:416, 1957.

[312] M. Suewattana, W. Purwanto, S. Zhang, H. Krakauer, and E. J. Walter. Phaseless auxiliary-field quantum Monte Carlo calculations with plane waves and pseudopotentials: Applications to atoms and molecules. *Phys. Rev. B*, 75:245123, 2007.

[313] J. Sugar and C. Corliss. *Atomic Energy Levels of the Iron-period Elements, Potassium Through Nickel*. Journal of physical and chemical reference data: Supplement. American Chemical Society and the American Institute of Physics, 1985.

[314] M. Suzuki. Generalized Trotter's formula and systematic approximants of exponential operators and inner derivations with applications to many-body problems. *Comm. Math. Phys.*, 51(2):183, 1976.

[315] A. Szabo and N. S. Ostlund. *Modern Quantum Chemistry: Introduction to Advanced Electronic Structure Theory*. Dover, Mineola, 1996.

[316] W. Tatsuaki. Interaction-round-a-face density-matrix renormalization-group method applied to rotational-invariant quantum spin chains. *Phys. Rev. E*, 61:3199, 2000.

[317] P. R. Taylor. Coupled-cluster Methods in Quantum Chemistry. In B. O. Roos, editor, *Lecture Notes in Quantum Chemistry II: European Summer School in Quantum Chemistry*, page 125. Springer Berlin Heidelberg, Berlin, Heidelberg, 1994.

[318] S. Ten-no. A feasible transcorrelated method for treating electronic cusps using a frozen Gaussian geminal. *Chem. Phys. Lett.*, 330(1):169, 2000.

[319] S. Ten-no. Three-electron integral evaluation in the transcorrelated method using a frozen Gaussian geminal. *Chem. Phys. Lett.*, 330(1):175, 2000.

[320] S. Ten-no. Initiation of explicitly correlated Slater-type geminal theory. *Chem. Phys. Lett.*, 398(1):56, 2004.

[321] S. Ten-no. New implementation of second-order Møller-Plesset perturbation theory with an analytic Slater-type geminal. *J. Chem. Phys.*, 126(1):014108, 2007.

[322] D. P. Tew. Explicitly correlated coupled-cluster theory with Brueckner orbitals. *J. Chem. Phys.*, 145(7):074103, 2016.

[323] L. F. Tocchio, F. Becca, A. Parola, and S. Sorella. Role of backflow correlations for the nonmagnetic phase of the t–t' Hubbard model. *Phys. Rev. B*, 78:041101, 2008.

[324] N. Trivedi and D. M. Ceperley. Green-function Monte Carlo study of quantum antiferromagnets. *Phys. Rev. B*, 40:2737, 1989.

[325] N. Trivedi and D. M. Ceperley. Ground-state correlations of quantum antiferromagnets: A Green-function Monte Carlo study. *Phys. Rev. B*, 41:4552, 1990.

[326] H. F. Trotter. On the product of semi-groups of operators. *Proc. Am. Math. Soc.*, 10(4):545, 1959.

[327] M. Troyer and U.-J. Wiese. Computational Complexity and Fundamental Limitations to Fermionic Quantum Monte Carlo Simulations. *Phys. Rev. Lett.*, 94:170201, 2005.

[328] T. Tsuchimochi and S. L. Ten-no. Orbital-invariant spin-extended approximate coupled-cluster for multi-reference systems. *J. Chem. Phys.*, 149(4):044109, 2018.

[329] T. Tsuchimochi and S. L. Ten-no. Extending spin-symmetry projected coupled-cluster to large model spaces using an iterative null-space projection technique. *J. Comput. Chem.*, 40(1):265, 2019.

[330] S. Tsuneyuki. Transcorrelated Method: Another Possible Way towards Electronic Structure Calculation of Solids. *Prog. Theor. Phys. Supp.*, 176:134, 2008.

[331] G. E. Uhlenbeck and S. Goudsmit. Ersetzung der Hypothese vom unmechanischen Zwang durch eine Forderung bezüglich des inneren Verhaltens jedes einzelnen Elektrons. *Die Naturwissenschaften*, 13(47):953, 1925.

[332] C. J. Umrigar. Observations on variational and projector Monte Carlo methods. *J. Chem. Phys.*, 143(16):164105, 2015.

[333] C. J. Umrigar, M. P. Nightingale, and K. J. Runge. A diffusion Monte Carlo algorithm with very small time-step errors. *J. Chem. Phys.*, 99(4):2865, 1993.

[334] H. J. M. van Bemmel, D. F. B. ten Haaf, W. van Saarloos, J. M. J. van Leeuwen, and G. An. Fixed-Node Quantum Monte Carlo Method for Lattice Fermions. *Phys. Rev. Lett.*, 72:2442, 1994.

[335] J. H. Van Vleck and A. Sherman. The Quantum Theory of Valence. *Rev. Mod. Phys.*, 7:167, 1935.

[336] C. N. Varney, C.-R. Lee, Z. J. Bai, S. Chiesa, M. Jarrell, and R. T. Scalettar. Quantum Monte Carlo study of the two-dimensional fermion Hubbard model. *Phys. Rev. B*, 80:075116, 2009.

[337] J. Čížek. On the Correlation Problem in Atomic and Molecular Systems. Calculation of Wavefunction Components in UrsellType Expansion Using QuantumField Theoretical Methods. *J. Chem. Phys.*, 45(11):4256, 1966.

[338] J. Čížek and J. Paldus. Correlation problems in atomic and molecular systems III. Rederivation of the coupled-pair many-electron theory using the traditional quantum chemical methods. *Int. J. Quantum Chem.*, 5(4):359, 1971.

[339] F. Verstraete, J. J. García-Ripoll, and J. I. Cirac. Matrix Product Density Operators: Simulation of Finite-Temperature and Dissipative Systems. *Phys. Rev. Lett.*, 93:207204, 2004.

[340] D. Vollhardt. Normal ^{3}He: an almost localized Fermi liquid. *Rev. Mod. Phys.*, 56:99, 1984.

[341] W. von der Linden. A quantum Monte Carlo approach to many-body physics. *Phys. Rep.*, 220(2):53, 1992.

[342] J. M. Wahlen-Strothman, C. A. Jiménez-Hoyos, T. M. Henderson, and G. E. Scuseria. Lie algebraic similarity transformed Hamiltonians for lattice model systems. *Phys. Rev. B*, 91:041114, 2015.

[343] J. M. Wahlen-Strothman and G. E. Scuseria. Biorthogonal projected energies of a Gutzwiller similarity transformed Hamiltonian. *J. Phys.: Condens. Matter*, 28(48):485502, 2016.

[344] T. Watanabe, H. Yokoyama, Y. Tanaka, and J.-i. Inoue. Superconductivity and a Mott Transition in a Hubbard Model on an Anisotropic Triangular Lattice. *J. Phys. Soc. Jpn.*, 75(7):074707, 2006.

[345] H.-J. Werner and P. J. Knowles. A second order multiconfiguration SCF procedure with optimum convergence. *J. Chem. Phys.*, 82(11):5053, 1985.

[346] H.-J. Werner and P. J. Knowles. An efficient internally contracted multiconfiguration-reference configuration interaction method. *J. Chem. Phys.*, 89(9):5803, 1988.

[347] H.-J. Werner and P. J. Knowles. A comparison of variational and non-variational internally contracted multiconfiguration-reference configuration interaction calculations. *Theor. Chem. Acc.*, 78(3):175, 1990.

[348] H.-J. Werner and P. J. Knowles. Accurate multireference configuration interaction calculations of the potential energy function and the dissociation energy of N_2. *J. Chem. Phys.*, 94(2):1264, 1991.

[349] H.-J. Werner, P. J. Knowles, G. Knizia, F. R. Manby, and M. Schütz. `Molpro`: a general-purpose quantum chemistry program package. *Wiley Interdiscip. Rev. Comput. Mol. Sci.*, 2:242, 2012.

[350] H.-J. Werner, P. J. Knowles, G. Knizia, F. R. Manby, M. Schütz, et al. MOLPRO, version 2015.1, a package of *ab initio* programs, 2015. see http://www.molpro.net.

[351] H. Weyl. *The Theory of Groups and Quantum Mechanics*. Dover, New York, 1931.

[352] H. Weyl. *The Classical Groups, Their Invariants and Representations*. Princeton U. P, Princeton, 1946.

[353] H. Weyl, G. Rumer, and E. Teller. Eine für die Valenztheorie geeignete Basis der binären Vektorinvarianten. *Nachrichten von der Gesellschaft der Wissenschaften zu Göttingen, Mathematisch-Physikalische Klasse*, 1932:499, 1932.

[354] S. R. White. Density matrix formulation for quantum renormalization groups. *Phys. Rev. Lett.*, 69:2863, 1992.

[355] S. R. White. Density-matrix algorithms for quantum renormalization groups. *Phys. Rev. B*, 48:10345, 1993.

[356] S. R. White and D. J. Scalapino. Phase separation and stripe formation in the two-dimensional $t - J$ model: A comparison of numerical results. *Phys. Rev. B*, 61:6320, 2000.

[357] S. R. White and D. J. Scalapino. Stripes on a 6-Leg Hubbard Ladder. *Phys. Rev. Lett.*, 91:136403, 2003.

[358] S. R. White, D. J. Scalapino, R. L. Sugar, E. Y. Loh, J. E. Gubernatis, and R. T. Scalettar. Numerical study of the two-dimensional Hubbard model. *Phys. Rev. B*, 40:506, 1989.

[359] E. P. Wigner. On the Matrices Which Reduce the Kronecker Products of Representations of S. R. Groups. In A. S. Wightman, editor, *The Collected Works of Eugene Paul Wigner: Part A: The Scientific Papers*, page 608. Springer Berlin Heidelberg, Berlin, Heidelberg, 1993.

[360] S. Yabushita. Applications of Spin-dependent GUGA, Time-reversal and Double Point Group Symmetries to an Efficient Direct Spin-Orbit CI Method. *J. Comput. Chem., Jpn.*, 13(1):43, 2014.

[361] K. Yamaji, T. Yanagisawa, T. Nakanishi, and S. Koike. Variational Monte Carlo study on the superconductivity in the two-dimensional Hubbard model. *Physica C*, 304(3):225, 1998.

[362] T. Yanai and G. K.-L. Chan. Canonical transformation theory from extended normal ordering. *J. Chem. Phys.*, 127(10):104107, 2007.

[363] T. Yanai, Y. Kurashige, E. Neuscamman, and G. K.-L. Chan. Multireference quantum chemistry through a joint density matrix renormalization group and canonical transformation theory. *J. Chem. Phys.*, 132(2):024105, 2010.

[364] T. Yanai and T. Shiozaki. Canonical transcorrelated theory with projected Slater-type geminals. *J. Chem. Phys.*, 136(8):084107, 2012.

[365] H. Yokoyama and H. Shiba. Variational Monte-Carlo Studies of Hubbard Model. I. *J. Phys. Soc. Jpn.*, 56(4):1490, 1987.

[366] H. Yokoyama and H. Shiba. Variational Monte-Carlo Studies of Superconductivity in Strongly Correlated Electron Systems. *J. Phys. Soc. Jpn.*, 57(7):2482, 1988.

[367] A. Young. On Quantitative Substitutional Analysis. *P. Lond. Math. Soc.*, s1-33(1):97, 1900.

[368] J. Yu, A. J. Freeman, and J. H. Xu. Electronically driven instabilities and superconductivity in the layered $La_{2-x}Ba_xCuO_4$ perovskites. *Phys. Rev. Lett.*, 58:1035, 1987.

[369] D. Zgid and M. Nooijen. On the spin and symmetry adaptation of the density matrix renormalization group method. *J. Chem. Phys.*, 128(1):014107, 2008.

[370] F. C. Zhang, C. Gros, T. M. Rice, and H. Shiba. A renormalised Hamiltonian approach to a resonant valence bond wavefunction. *Supercond. Sci. Technol.*, 1(1):36, 1988.

[371] F. C. Zhang and T. M. Rice. Effective Hamiltonian for the superconducting Cu oxides. *Phys. Rev. B*, 37:3759, 1988.

[372] S. Zhang, J. Carlson, and J. E. Gubernatis. Constrained Path Quantum Monte Carlo Method for Fermion Ground States. *Phys. Rev. Lett.*, 74:3652, 1995.

[373] S. Zhang, J. Carlson, and J. E. Gubernatis. Constrained path Monte Carlo method for fermion ground states. *Phys. Rev. B*, 55:7464, 1997.

[374] S. Zhang, J. Carlson, and J. E. Gubernatis. Pairing Correlations in the Two-Dimensional Hubbard Model. *Phys. Rev. Lett.*, 78:4486, 1997.

[375] S. Zhang and M. H. Kalos. Exact Monte Carlo calculation for few-electron systems. *Phys. Rev. Lett.*, 67:3074, 1991.

[376] S. Zhang and H. Krakauer. Quantum Monte Carlo Method using Phase-Free Random Walks with Slater Determinants. *Phys. Rev. Lett.*, 90:136401, 2003.

[377] B.-X. Zheng, C.-M. Chung, P. Corboz, G. Ehlers, M.-P. Qin, R. M. Noack, H. Shi, S. R. White, S. Zhang, and G. K.-L. Chan. Stripe order in the underdoped region of the two-dimensional Hubbard model. *Science*, 358(6367):1155, 2017.

Acknowledgements

First and foremost I would like to thank my supervisor Ali Alavi for his excellent support, guidance, enthusiasm and seemingly never-ending spring of ideas. His warm and guiding presence made the work in the past four years a really enjoyable experience.

I would also like to express my deepest gratitude to my current and past group members and colleagues at the institute:
Simon Smart —with his geeky presence and mismatching socks—who introduced me to this area of research and programming in general. I am very grateful and indebted to him for his help in implementation and optimization of my projects.
I would like to thank my first office mates, Tal Levy and Alexander "just call me Sasha" Lozovoi for the warm welcome to the group. Sashas Russian "jokes" and Tals charming presence and optimistic (although he tries to hide it, hard) and experience-ridden world view made working here in Stuttgart an enjoyable experience from day one.
I am not sure if it is common to meet so many great people and develop deep friendships on the journey to ones PhD. Sandeep Sharma, Guillaume "Chatoun" Jeanmairet and Emanuel Giner are just some of the many examples. I would like to thank them for their guidance and support and especially for the enjoyable common time.
I would like to thank Olle Gunnarsson for his excellent insights in physics, talks about Swedish politics and on top providing me helpful reference results used in this thesis.
I would like to thank Giovanni Li Manni for his never ending trying to bash chemistry in my stubborn physics head (in the end you managed, to some degree at least). In addition I would like to thank him for his help in understanding basic concepts and importance of symmetry and for helping and providing me with results obtained with Molcas.

Additionally I want to thank:
Pablo Lopez Rios, Hongjun Luo, David Tew, Kai Guther, Nikolay Bogdanov, Eugenio Vitale, Pradipta Samantha, Aron Cohen, Filip Podjaski, Pinar Kaya, Ke Liao, Felix Hummel, Theodoros Tsatsoulis and Alejandro Gallo
for there support, feedback, fruitful scientific discussions, teachings, guidance, friendship or for just being awesome and without whom my scientific journey of the last four years would have been way less enjoyable.

As a special mention I would like to express my deepest gratitude to Daniil "Danny" Mantadakis for his excellent —albeit very critical —feedback and proofreading and in general for helping me finish this thesis. My work would not have this quality without your critical thoughts dude!

I would also like to express my gratitude to the people outside of the institute, who made my stay in Stuttgart so damn enjoyable: My first two roommates Damaris Brenner and Johannes Nagel for the warm welcome in Stuttgart and an amazing time in our shared flat.
Matthias “Matze” Mayerle and Marc Wiedenmann for all the great times enjoying our shared passion of basketball, going out and our home-office sessions. Dunja Reichart and Monika Gabernig for many enjoyable conversations and support.

My family, especially my oldest sister Marianne, for there never-ending support, especially in hard times and my mother Kerstin—without here I would not be here.

And last but most definitely not least, I would like to thank the love of my life Jennifer Barucha, for being there for me, in good and in bad times. Without you I would have not managed to finish this!

Thank you!

So long, and thanks for all the fish.

–*Douglas Adams*